Animal Hide Processing: Impact on Collagen Structure

Clark Alexander Maxwell

Submitted in partial fulfilment of the requirements of the degree of

Doctor of Philosophy

School of Optometry and Vision Sciences, Cardiff University

December 2007

ProQuest LLC
789 East Eisenhower Parkway
P.O. Box 1346
Ann Arbor, MI 48106-1346

DECLARATION

This work has not previously been accepted in substance for any degree and is not concurrently submitted in candidature for any degree.

Signed ..... (candidate) Date 14/12/07

STATEMENT 1

This thesis is being submitted in partial fulfillment of the requirements for the degree of PhD.

Signed ..... (candidate) Date 14/12/07

STATEMENT 2

This thesis is the result of my own independent work/investigation, except where otherwise stated.
Other sources are acknowledged by explicit references.

Signed ..... (candidate) Date 14/12/07

STATEMENT 3

I hereby give consent for my thesis, if accepted, to be available for photocopying and for inter-library loan, and for the title and summary to be made available to outside organisations.

Signed ..... (candidate) Date 14/12/07

Abstract

The manufacture of parchment and leather from animal skin involves processes that remove hair, fats, and other macromolecules. Although it is well understood that the collagen fibres "open up" during processing, the study in this thesis used small and wide-angle X-ray diffraction to measure quantitatively the changes induced at the nanoscopic and microscopic levels.

Collagen axial rise per residue is unaffected by salting, liming and drying of animal hide. The intermolecular lateral packing distance between the hydrated collagen molecules (1.4 nm) increases after salting (1.5 nm) and liming (1.55 nm); drying causes a reduction to 1.2 nm in all samples. The axial D-period is reduced by 1 nm after liming and is unaffected by drying. The average fibril diameter increased from 103.2 nm to 114.5 nm following liming, and the fibril-to-fibril distance increased from 122.6 to 136.1 nm.

Furthermore, the effects of the solvents propan-2-one and 2-ethoxy ethanol on collagen structure were investigated. The D-period of the treated collagen was reduced by approximately 3 nm. Wide angle X-ray diffraction displayed clear peaks brought about by the presence of calcite, residual from the liming process. The presence of calcium carbonate was confirmed by Fourier transform Infrared spectroscopy. It was shown to differentiate between caprine and ovine samples, and the flesh and grain layers of the hide. Principal components analysis inferred from the differences in the calcite peaks that calcium carbonate uptake varies between animal species in the liming process. The solvent treatments did not appear to affect the Fourier transform infrared spectra.

Efforts were made to investigate a treatment process of a fibrous collagen material for the leather industry that produces minimum effluents. Bovine collagen treated with tanning

agents at chromium concentrations of (1, 3, 5, 7, 9, 11%), resulted in changes in the molecular packing within the collagen fibrils.

Acknowledgements

I would like to acknowledge many people for their help during my thesis. I would like to thank Professor Tim Wess (Cardiff University, PhD Supervisor) for his supervision, guidance, advice and support over the past 4 years. I would also like to thank Dr Carlo Knupp (Cardiff University, PhD Advisor) for his assistance, advice and support throughout this work.

I am grateful to Wim Visscher of William Cowley, Parchment works, Newport Pagnell for supplying samples and images taken from the manufacturing process of parchment. Also, thanks to Chris Clarkson, for providing samples of parchment treated with acetone and 2-ethoxy ethanol. Thanks to Krzysztof Smiechowski, Jan Zarlok (Radom Technical University), and to Alina Sionkowska (Nicholas Copernicus University, Torun), for the chromium treated leather samples and advice.

Thanks to Nancy Bell and Kostas Ntanos (National Archives, London) for use of the FT-IR, images, advice and support. Also thanks to Linda Ramsey (National Archives of Scotland) for the supply of images, and advice over the years.

Thank you to past and present members of the research group: Jen Hiller, Craig Kennedy, Graeme Cameron, Donna Lammie, Christian Pinali, Veronique Siegler, Kate Thomas, Lee Gonzalez, Joanna Glab, Linda Wess for their friendship and support. Also, I would like to thank the support staff for their help and advice throughout my time at Cardiff University.

A major proportion of this work was undertaken at synchrotron radiation sources; therefore, I would like to thank the following people for their help: Dr. Günter Grossmann, Dr. Kalotina Geraki (Station 2.1, SRS, Daresbury), Dr. Manfred Burghammer (ID13, ESRF) and the staff at station ID02 (ESRF).

Thank you to my friends and family for their love and support throughout my academic career. To my son, Finlay Maxwell, and to my brother Steven Maxwell; friends, Ross Berwick, Ben Dixon, Yoshan Moodley, Sharon Obrzud, Andrew Stopford and to my partner Kirsten Hamilton.

Table of Contents

List of Figures

List of Tables

Chapter 1: Introduction

1.1: Background knowledge and objectives

The aim of this thesis is to examine how an important collagen based tissue such as skin can be used *post mortem,* and how its integrity as a useful material can be prolonged even after the natural repair mechanisms within a living organism are removed.

The areas of interest were the structural change in collagen architecture due to the manufacturing processes involved in converting living collagen based tissue (animal hide) into parchment and leather. Although these were the processes studied, it should be noted that the early stages of these processes are often generic and are important for many different product preparation processes, for example in drug delivery systems, photography and the food industry [1, 2]. Examples of animal hide uses are shown in Figure 1.1.

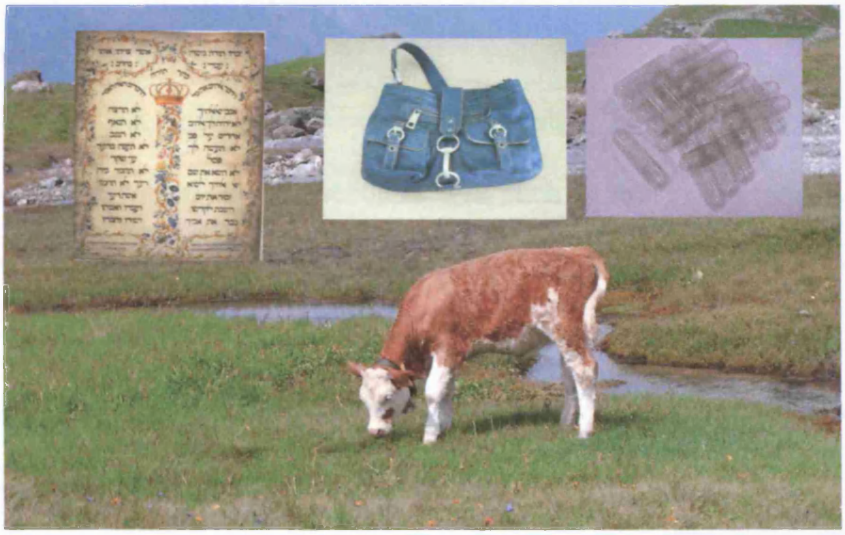

Figure 1.1: Image representing the uses of animal hides. Background image of calf. Inserts (left to right): Parchment, Leather bag, gelatine drug capsule.

A term used often in literature to describe the effects that these processes have on collagen is that of "opening up" of the fibres [3]; however, this is a qualitative description without quantitative information. The work presented in this thesis quantitatively measured the structural features of the collagen hierarchy after different treatments using X-ray diffraction and scattering techniques. Furthermore, some manufacturing processes are adjusted to suit the uses of the product with little knowledge of the effects on the nano-and mesostructure of the material. These treatments and adjustments were examined using X-ray diffraction/scattering and Fourier transform infrared (FT-IR) spectroscopy to determine if the processes were possibly predisposing the end-products to degradation.

In order to add value and put into context any investigation into animal hide, it is beneficial to cover a brief introduction into skin structure and hierarchy.

1.2: Introduction to skin

The skin is the largest organ in the body and arguably the most complex. Its primary function is as a barrier from environmental factors, such as viruses, bacteria, chemicals and UV radiation [4]. It prevents rapid loss of water and is involved in thermo-regulation [5]. Furthermore, it resists physical stresses and continually repairs itself [6]. The repair mechanisms vary depending on the type and the depth of injury but are typically as shown in Figure 1.2.

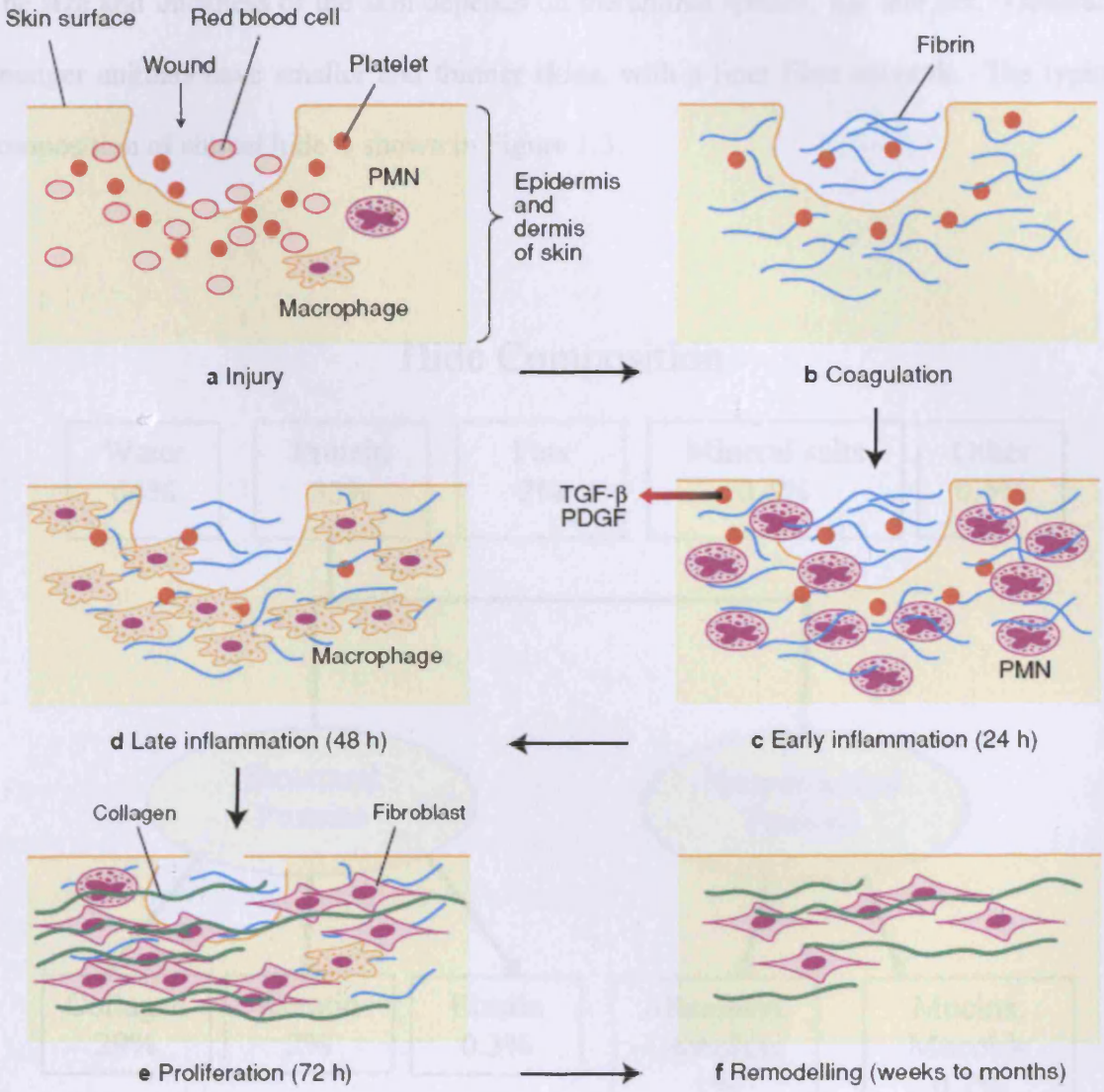

Figure 1.2: The phases of skin wound healing taken from the review paper by Beanes *et al* [7]: a) After injury blood elements extravagate into the wound, including polymorphonuclear neutrophils (PMNs) and platelets. b) Platelets and fibrin aggregate together as part of coagulation. c) Early inflammation occurs as platelets release growth factors (PDGF) attracting PMNs to the wound. d) Late inflammation as macrophages remove debris, produce PDGFs (attracting fibroblasts) and begin re-organising extracellular matrix. e) Proliferation begins as fibroblast cells produce collagen. f) Remodelling phase is when collagen cross-linking and re-organisation occurs.

The size and thickness of the skin depends on the animal species, age and sex. Generally younger animals have smaller and thinner skins, with a finer fibre network. The typical composition of animal hide is shown in Figure 1.3.

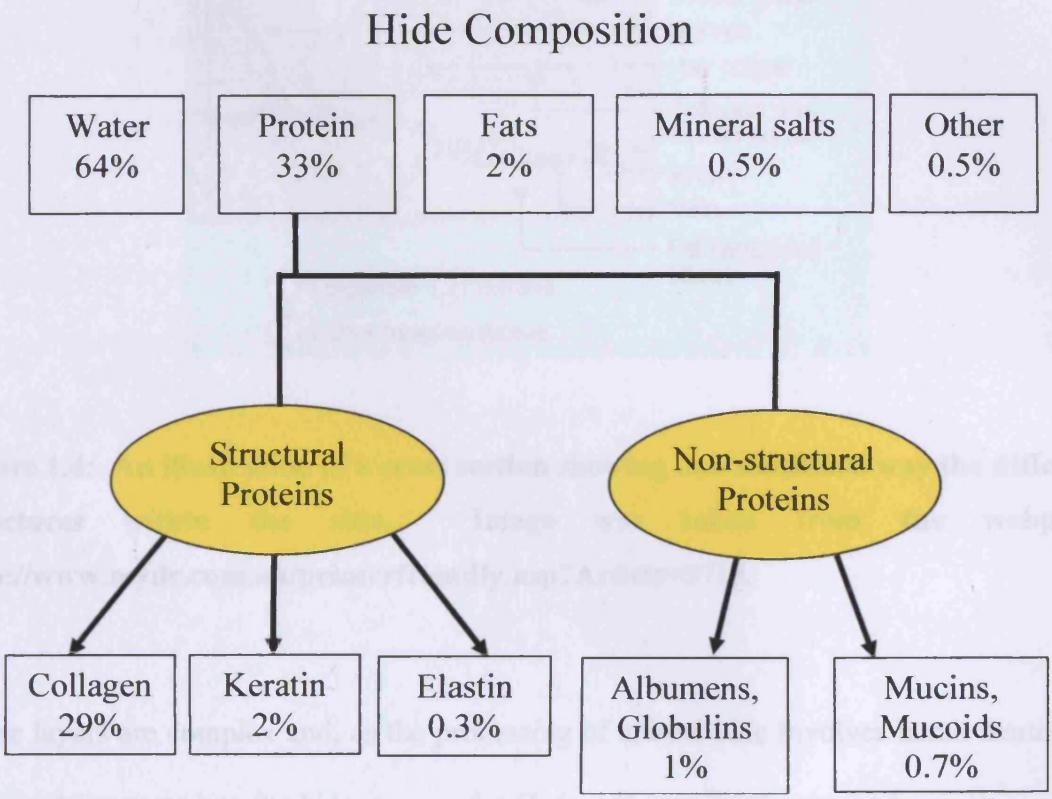

Figure 1.3: The approximate composition of animal hide, adapted from the *LEATHER TECHNICIANS HANDBOOK* [8].

Skin in general terms is a multilayered structure, which can be simplified into the outer epidermal layer, the central dermal layer and the inner subcutaneous tissue (hypodermal layer), as shown in Figure 1.4.

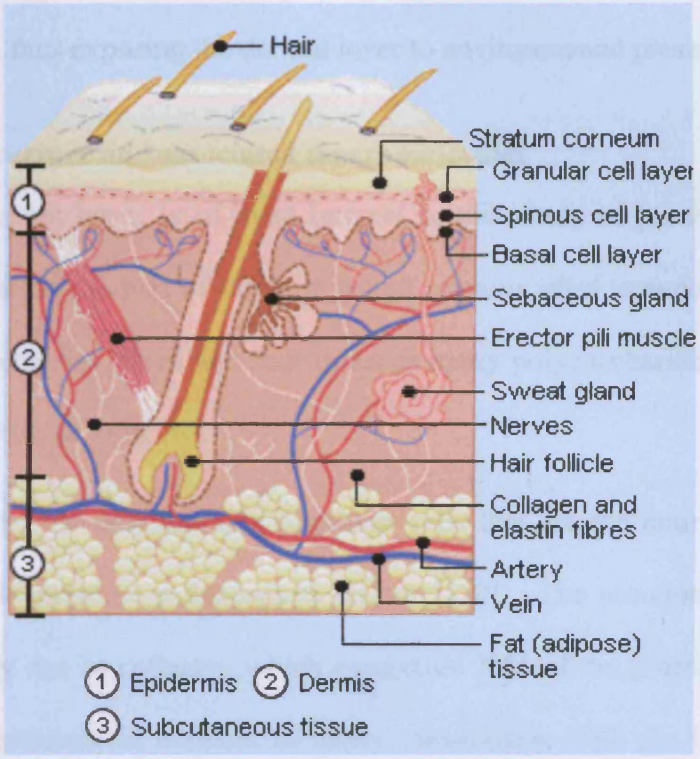

Figure 1.4: An illustration of a cross section showing in a simplified way the different structures within the skin. Image was taken from the webpage. http://www.mydr.com.au/printerfriendly.asp?Article=3718.

These layers are complex and, as the processing of animal hide involves harsh treatments that must penetrate into the hide, a more detailed understanding is required.

1.2.1: The layers of the epidermis

The epidermis is the outer layer of the skin and is composed of four layers of varying cell thicknesses. The stratum corneum is the surface aspect of the epidermis and consists of several layers of dead cells full of the insoluble protein keratin [9], which varies in thickness depending on age [10]. The next layer, is the stratum granulosum, then the

stratum spinosum and the stratum basale [6, 11, 12]. The epidermal layer is removed during processing, thus exposing the dermal layer to environmental pressures.

1.2.2: Dermal structure and associated macromolecules

The dermis, or central layer, is of most interest in this study of parchment and leather manufacture, as this is the part of the hide which remains after treatment. The papillary layer (grain) contains fine fibres and four times as many polysaccharides than the coarser fibre containing reticular layer [6].

The dermal layer of the skin contains fibroblast cells that are the main producers of the extracellular matrix proteins collagen and elastin [10]. The structural strength of the dermis is primarily due to collagen, which comprises 70% of the protein component and forms a specific hierarchical network of fibres. Association with the finer elastin fibres gives the skin its elasticity and suppleness (Figure 1.5).

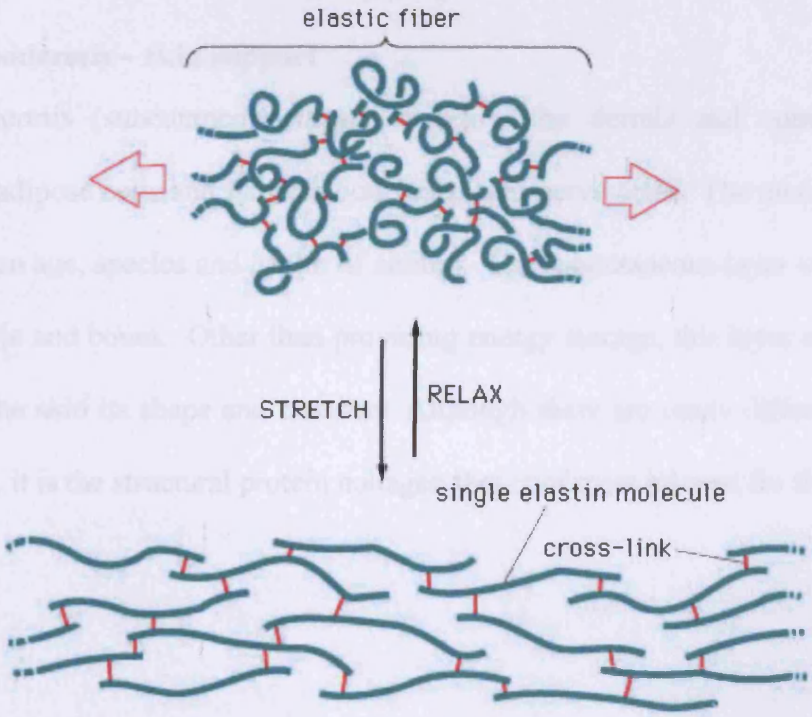

Figure 1.5: An illustration of elastin elasticity. Image taken from Essential Cell Biology [13]

Water accounts for about 80% of the dermal content, with the remaining 20% composed of macromolecules, such as collagen and elastin suspended in a glycoprotein gel rich in hyaluronic acid (see Subsection 1.3.4) [6]. As well as being vascularised, the dermis contains the hair root, which is encased in an epithelial sheath forming the hair follicle. Within this follicle there are melanocytes that produce and transfer pigment molecules, or melanin, to the keratin producing cells, the keratinocytes. The production of keratin and melanin form the hair shaft and colour respectively. Associated with the hair shaft is the sebaceous gland, which produces sebum and secretes it as the hair extends outwards [10]. The reticular dermis also contains structures such as ruffinian corpuscles, which are penetrated by nerves that branch out and react to external stimuli on the skin. It is worth mentioning these various structures, to emphasise the heterotrophic nature of skin and also to highlight possible sources of minerals, lipids and macromolecules that may be observed during analysis. The dermis as shown in Figure 1.4 sits on top of the hypodermis.

1.2.3: Hypodermis – skin support

The hypodermis (subcutaneous layer) is below the dermis and contains fat (lipid) containing adipose cells and larger blood vessel and nerve cells. The amount of fat varies depending on age, species and health of animal. The subcutaneous layer connects the skin to the muscle and bones. Other than providing energy storage, this layer acts as a cushion and gives the skin its shape and contour. Although there are many different components within skin, it is the structural protein collagen that is of most interest for this project.

1.3: Collagens - General introduction

As discussed in Subsection 1.2.2, skin contains an extracellular matrix fibre network that is primarily composed of collagen. The collagen fibres within the extracellular matrix confer specific mechanical and biochemical properties to tissues [14-16]. For example, in tendon, the collagen fibres are preferentially aligned to accommodate the direction of strain, as shown in Figure 1.6. However, the collagen fibres in skin are randomly orientated as a feltwork perpendicular to the plane of the skin allowing the collagen, and subsequently the skin to resist strain in multiple directions within the plane of the skin [17-19].

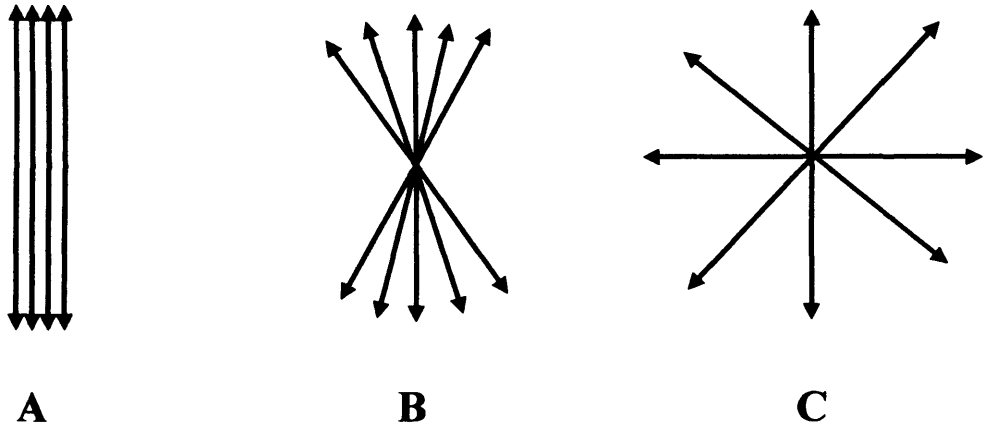

Figure 1.6: Images representing collagen fibre orientation in different tissues. A) Tendon has preferred orientation; B) Skin alignment has some preferential orientation along spine. C) Skin randomly orientated perpendicular to the plane of the tissue.

The collagens are the most abundant proteins found in the extracellular matrix; there are more than 29 different types [14]. Depending on the collagen structure and hierarchical organisation, they can be grouped into two sets: the fibril forming collagens and the non fibril forming collagens. This thesis will concentrate on the fibril forming collagens (see

Table 1.1) as these are the type that is predominantly found in the skin and therefore in parchment and leather. A fibre is composed of tightly packed fibrils.

Collagen Type	Molecular composition	Tissue distribution
Fibril-forming		
I	$[\alpha1(I)]_2\alpha2(I)$	bone, dermis, tendons, ligaments, cornea, skin
II	$[\alpha1(II)]_3$	cartilage, vitreous body,
III	$[\alpha1(III)]_3$	skin, vessel wall, reticular fibres of most tissues (lungs, liver, spleen. etc)
V	$\alpha1(V),\alpha2(V),\alpha3(V)$	lung, cornea, bone, foetal membranes: together with type I collagen
XI	$\alpha1(XI),\alpha2(XI),\alpha3(XI)$	cartilage, vitreous body
Adapted from Table 1 Gelse et al [14]		

Table 1.1: List of the fibril forming collagens, molecular composition and tissue distribution.

Of the 29 known collagen types I, II, III, V, and XI are capable of forming fibrils. The collagen molecules are orientated into a microfibrillar structure which then forms larger cylindrical fibrillar objects (fibril) as shown in Figure 1.7, with diameters ranging between 10 and 500 nm [20]. The microfibrils are composed of axially aligned triple helical collagen molecules, which are formed by polypeptide chains (Figure 1.8). Each molecule contains three polypeptide chains. These chains can have the same polypeptide sequence, hence forming homotrimer molecules, or have different sequences forming heterotrimer molecules, depending on the collagen type as shown in Table 1.1.

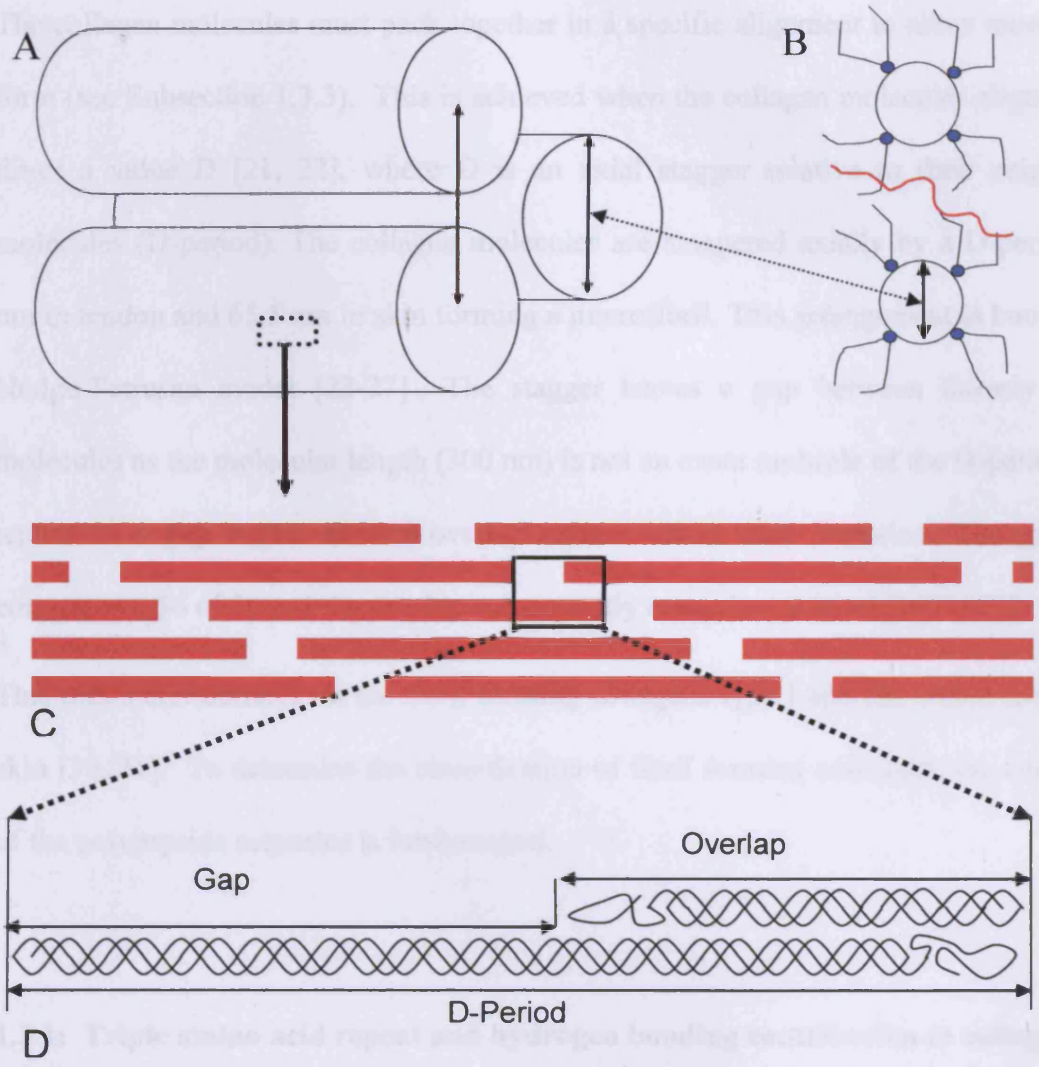

Figure 1.7: Representation of collagen fibril packing and collagen molecule arrangement within a fibril. A) A schematic representation of collagen fibril diameter and lateral packing. B) An axial view of collagen fibrils (large circles), with associated proteoglycans highlighted (see section 1.3.4 for details of proteoglycans (PGs), and glycosaminoglycans (GAGs), Blue circle is the proteoglycan protein core and the outward facing lines represent the GAG chains [12]. The red line represents the hyaluronic acid (HA) chain which is not covalently bonded to a protein core. C) Each block represents a collagen molecule in the staggered array conformation found within a fibril. D) The D-period of the collagen molecules represented by a gap and overlap area within the staggered array. This is representative of the electron density profile, which gives the characteristic step function of the collagen fibril.

The collagen molecules must pack together in a specific alignment to allow cross-links to form (see Subsection 1.3.3). This is achieved when the collagen molecules alignment is 4 times a value D [21, 22], where D is an axial stagger relative to their neighbouring molecules (D-period). The collagen molecules are staggered axially by a D-period of 67 nm in tendon and 65.5 nm in skin forming a microfibril. This arrangement is known as the Hodge-Petruska model [23-27] The stagger leaves a gap between linearly adjacent molecules as the molecular length (300 nm) is not an exact multiple of the D-period, which results in a gap region and an overlap region within each D-period. The gap region comprises 0.54 of D, and the overlap subsequently comprises 0.46 of D [28, 29] .

This thesis concentrates on the fibril forming collagens type I and III, which are found in skin [30, 31]. To determine the classification of fibril forming collagens, the composition of the polypeptide sequence is fundamental.

1.3.1: Triple amino acid repeat and hydrogen bonding contribution to collagen stability

The primary characterisation of fibril forming collagen is determined by a typical triple amino acid repeat (Gly-X-Y)n [14, 32, 33], with the X and Y positions usually occupied by proline, lysine or by the post translationally modified versions, hydroxyproline or hydroxylysine, depending on the collagen type. The resulting polypeptide chain has a glycine residue, which contains only one hydrogen atom on its side chain, which confers a smaller steric hindrance when compared with the cyclic nature of the imino acids. This, when combined in a polypeptide chain induces the formation of a left handed helical conformation. These polypeptide chains associate together forming a triple helix with a supercoiled right handed conformation [14, 34] shown in Figure 1.8.

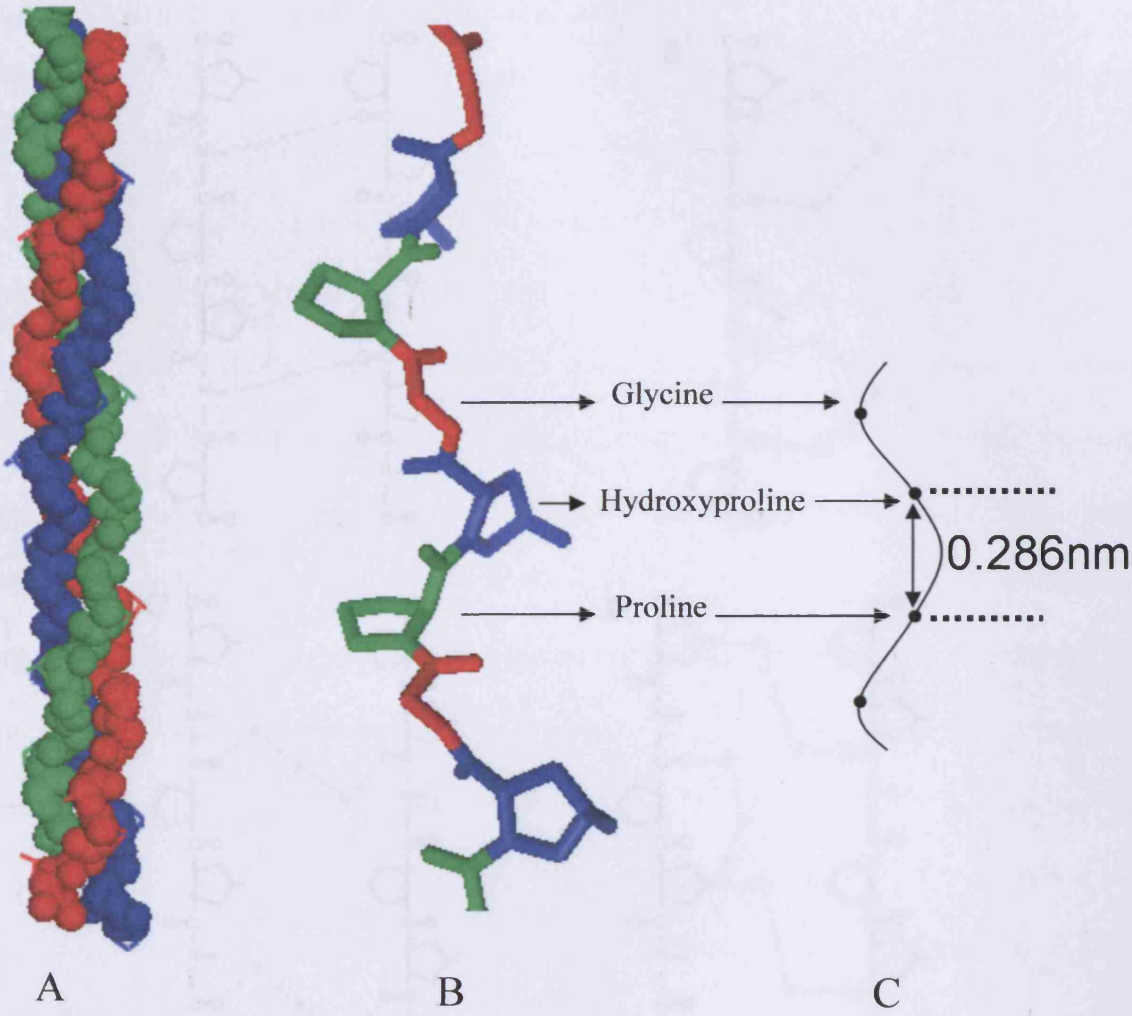

Figure 1.8: Illustration of collagen polypeptide and molecular structure. A) Collagen triple helix; B) Collagen polypeptide chain with the [Gly-X-Y] repeating unit; C) A schematic interpretation of the collagen helical rise per residue distance 0.286nm [35] highlighted. Images adapted using PYMOL of a collagen like peptide 1CAG [36] on the Protein Data Bank.

The post translationally modified 4-hydroxyproline in the Y position is essential for intra- and intermolecular hydrogen bond formation, contributing to helical stability [14]. The positions of the X and Y residues expose them to solvent and are thus available for self association and binding to other molecules [37]. The amount of association and binding is limited by the availability of solvent, which is reduced in the dehydrated samples compared to the hydrated ones. Examples of both direct and water-mediated hydrogen bonding types are shown in Figure 1.9.

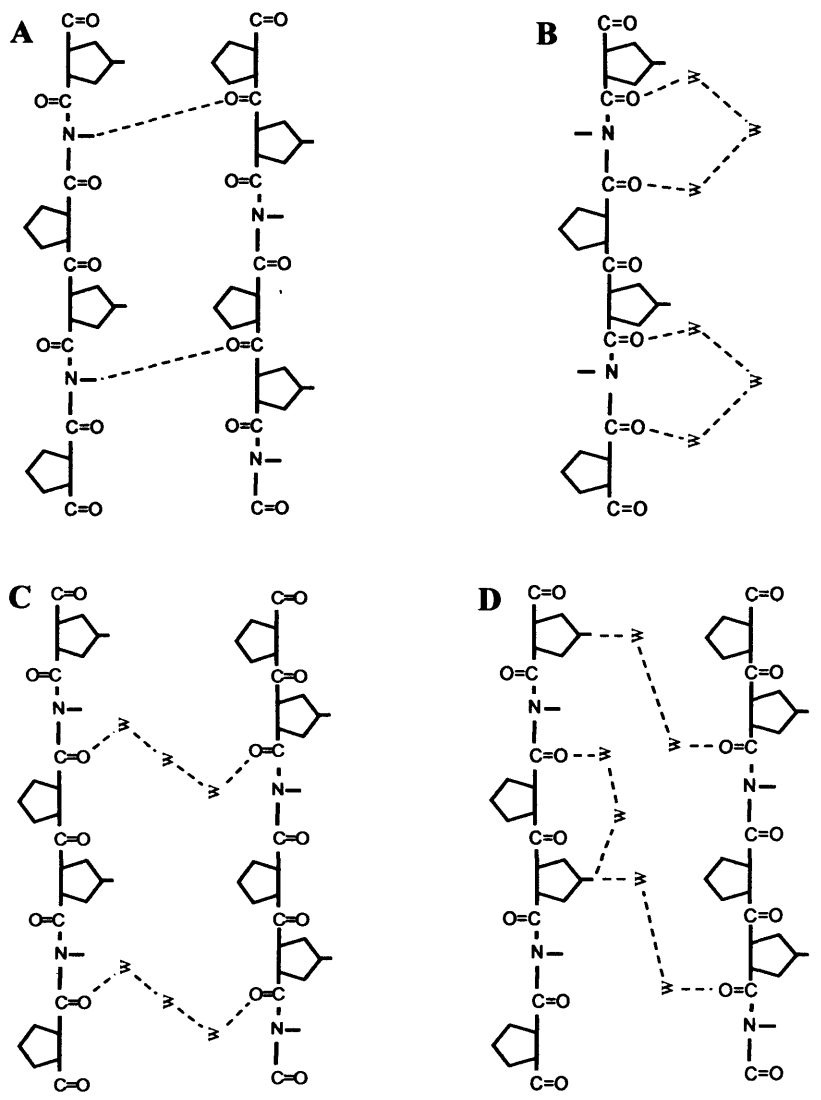

Figure 1.9: A schematic drawing illustrating the hydrogen bonding types found in the collagen triple helix adapted from Brodsky and Ramshaw (1997) [38]. A) Interchain hydrogen bond between peptide groups; B) carbonyl group intrachain water mediated hydrogen bond; C) carbonyl group interchain water mediated hydrogen bond; D) Hydroxyproline (OH group) and carbonyl group inter and intra water mediated hydrogen bonds.

1.3.2: Collagen molecules and the hydration shell

Water mediated hydrogen bonding is involved in the linking between the collagen triple helical molecules. The collagen triple helix is surrounded by three water shells. The fundamental residue involved in connecting the triple helix to this hydration shell is hydroxyproline [37], although other amino acid carbonyl groups are used. The 1st level hydration shell contains water molecules that are directly hydrogen bonded to amino acid groups within the groove of the triple helix. The 2nd shell water molecules are connected by hydrogen bonds to the water molecules in the first shell. The 3rd outer shell contains water molecules that are then bonded to the inner 2nd shell, thus completing the hydration shells. It has been suggested that the relationship of the hydration shell with the different amino acids (water to hydrophobic compared with water to hydrophilic amino acids) along the peptide chain may contribute to the positions that the collagen molecules take in relation to one another as packing takes place [37]. An example of the hydration shell surrounding a collagen triple helix and the intermolecular packing conformation is shown in Figure 1.10.

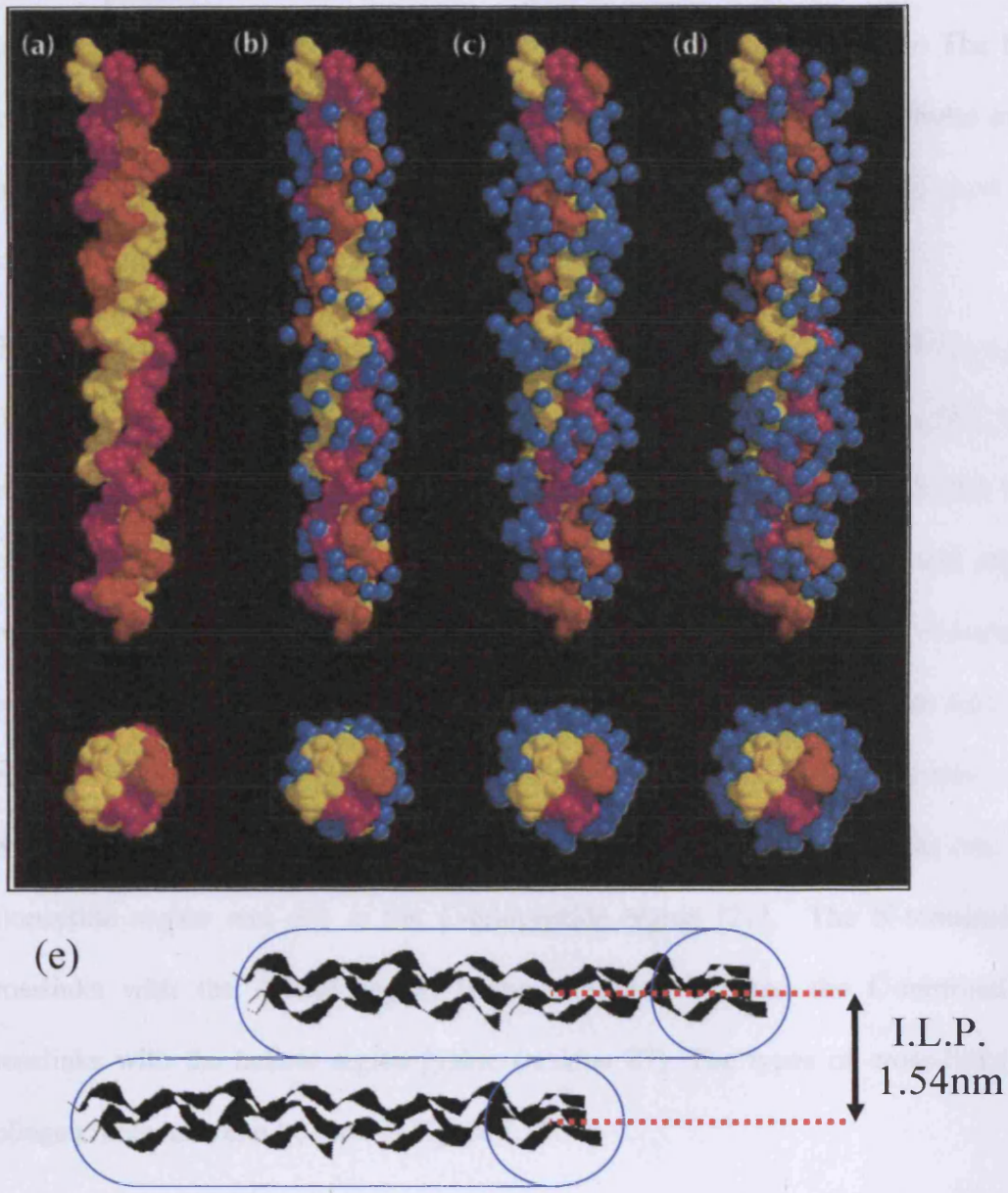

Figure 1.10: Illustration of collagen molecular packing and hydration shells. Images, a to d, space filling representations of increasing hydration levels of a collagen like polypeptide, taken from Bella *et al*, 1995 [37]. Both axial and parallel images shown; (a) Collagen triple helix, (b) 1st water hydration shell, (c) 2nd water hydration shell bonded to 1st, (d) 3rd hydration shell bonded to 2nd, (e) Schematic interpretation of the collagen intermolecular lateral packing. Hydration sphere highlighted in blue. Intermolecular lateral packing (I.L.P.) shown; typically 1.54 nm in hydrated state for skin.

1.3.3: Intermolecular covalent cross-links

As shown in Figure 1.10 the collagen molecules pack together laterally. The hydrogen bonding network, which occurs within and between the molecules, contributes to a stable structure. Further stabilisation of the molecules is gained with the formation of covalent bonds, which form at specific points on the collagen molecules.

The length of the collagen molecules vary depending on collagen type, but for types I and III, which contain about 1000 amino acids; the helical length is 300 nm [39, 40]. The helical region is flanked by non helical regions (telopeptides), at both the N and C terminus which do not conform to the typical collagen triple amino acid repeat, and comprise about 2% of the molecule [41]. These non-helical regions are essential for the formation of covalent cross-links. Collagen molecules contain two lysine rich crosslink regions within the helical portion. There are also two allysine (6-oxonorleucine: aldehyde forms of lysine after the action of lysyl oxidase [42]) containing crosslinks one at the N-telopeptide region and one at the C-telopeptide region [21]. The N-terminal allysine crosslinks with the helical region lysine (residue 930) and the C-terminal allysine crosslinks with the helical region lysine (residue 87). The types of cross-links between collagen molecules can be seen in Figure 1.11.

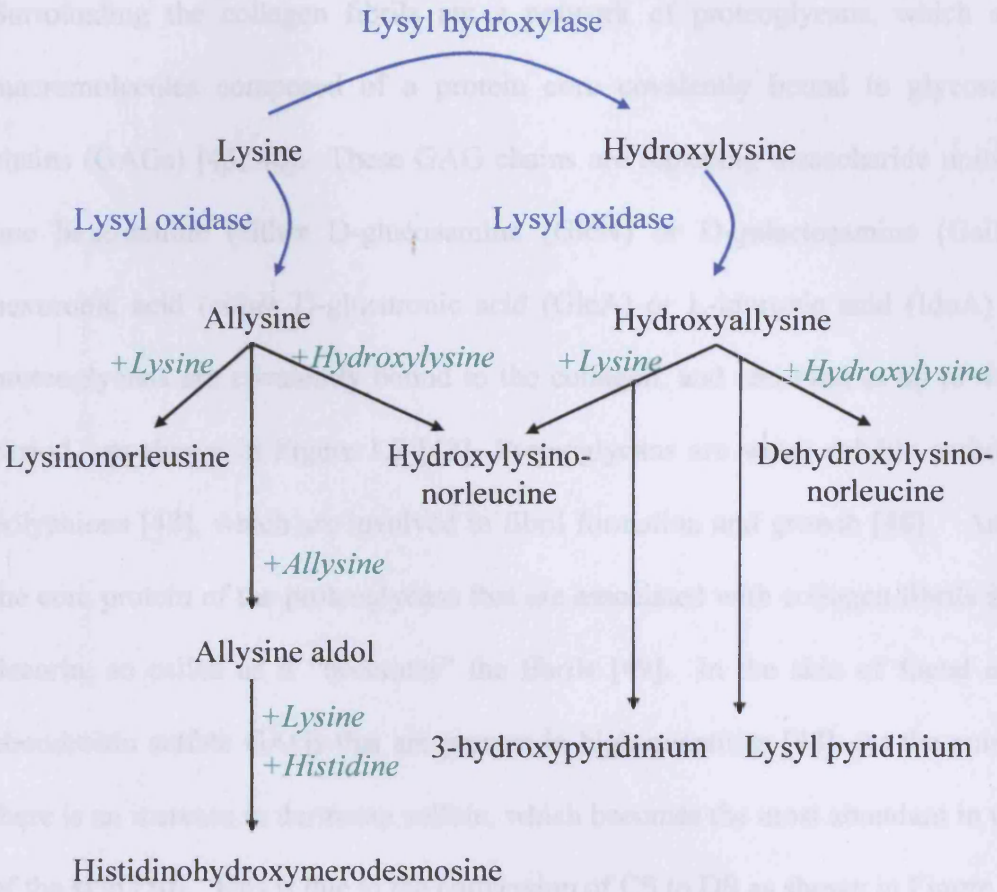

Figure 1.11: Reactions of lysine and hydroxylysine in the biosynthesis of collagen cross-links. Blue represents enzyme mediated reactions. Green represents non enzyme mediated reactions.

The lysine aldehyde pathway is the primary one for adult skin, sclera and cornea collagens [43]; for embryonic skin, bone, cartilage, ligaments and tendons, the hydroxylysine aldehyde pathway predominates [44].

1.3.4: Proteoglycan interactions with collagen fibrils

Surrounding the collagen fibrils are a network of proteoglycans, which are complex macromolecules composed of a protein core covalently bound to glycosaminoglycan chains (GAGs) [45, 46]. These GAG chains are repeating disaccharide units, containing one hexosamine (either D-glucosamine (GlcN) or D-galactosamine (GalN) and one hexuronic acid (either D-glucuronic acid (GlcA) or L-iduronic acid (IdoA) [46]. The proteoglycans are covalently bound to the collagen, and can bind at up to 4 sites per D-period, as shown in Figure 1.7 [47] Proteoglycans are water soluble carbohydrate rich polyanions [48], which are involved in fibril formation and growth [48]. An example of the core protein of the proteoglycans that are associated with collagen fibrils is the 36 kDa decorin, so called as it "decorates" the fibrils [49]. In the skin of foetal animals, it is chondroitin sulfate GAGs that are present in high quantities [48]. As the animal matures, there is an increase in dermatan sulfate, which becomes the most abundant in the collagens of the skin [50]. This is due to the conversion of CS to DS as shown in Figure 1.12.

Another important GAG is hyaluronic acid, (HA) (Figure 1.12) which is not covalently bonded to a protein core and as such is not classified as a proteoglycan. This repeating disaccharide can form chains of up to 25000 units and is capable of occupying large volumes [45]. The combination of the proteoglycans and the HA contributes to maintaining skin structure and shape and resistance to physical compression stresses.

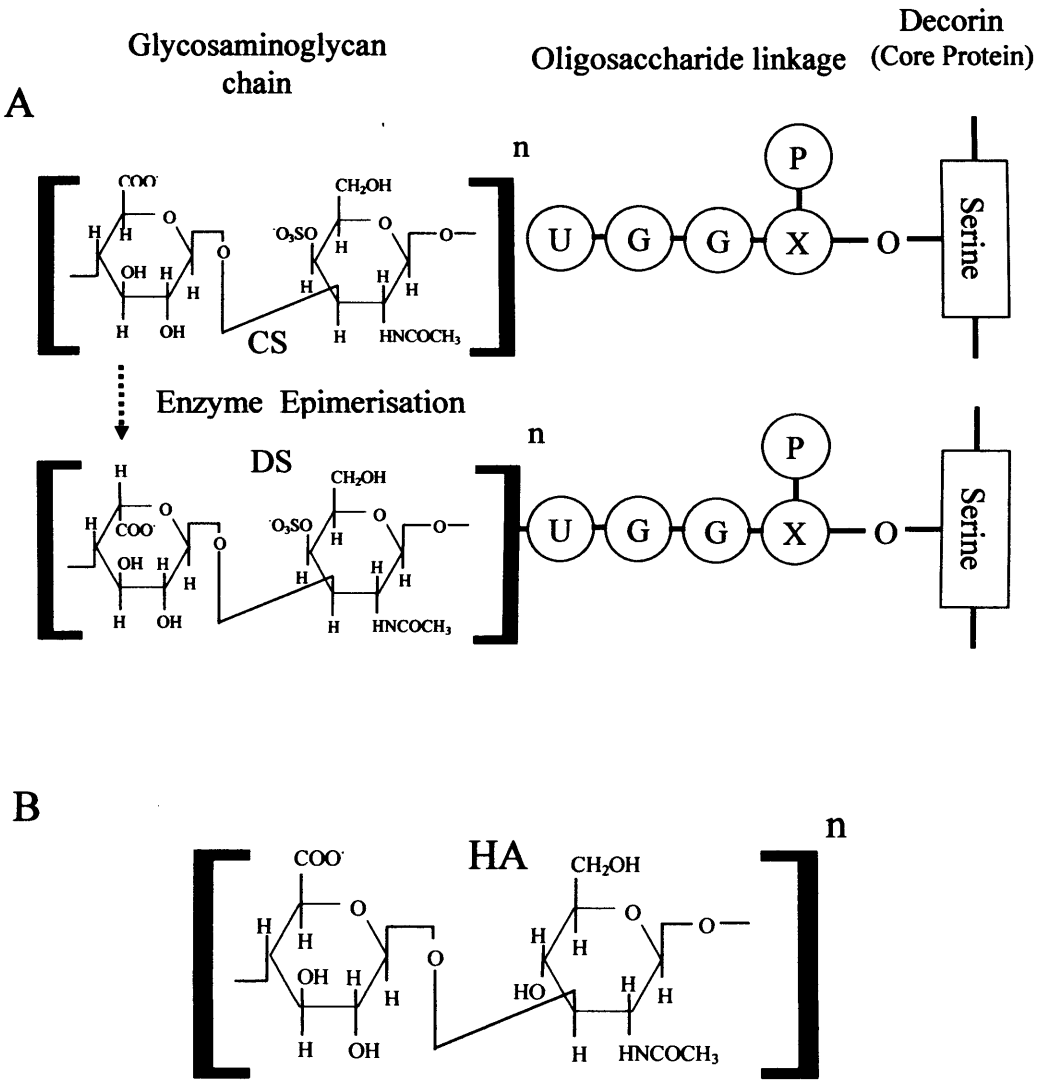

Figure 1.12: A diagrammatical representation of proteoglycan and glycosaminoglycan macromolecules: A) Representation of proteoglycan structure, P is phosphate, X is xylose, G is galactose, and U is glucoronic acid. CS is chrondoitin sulfate and DS is dermatan sulphate; B) The repeating hyaluronic acid (HA) chain. Images adapted from [12, 45].

In summation, animal hide is a complex organ containing cells and many different macromolecules that give the skin its strength and flexibility, and are responsible for

repairing damage to the tissue. Over the centuries many uses have been found for this by-product of the meat industry, with the driving force behind the methods used being the end product and what was required to achieve this aim. It is now understood that these processes removed the macromolecules associated with the collagen fibres and enhanced the stability of the fibres. Details of these processes are given in the following sections.

1.4: Animal *post mortem* uses

Animal hide was and is used for a wide range of purposes, including clothing, armour, kayaks, thread, bookbinding, shoes, whips, and as a writing material. There are many stages and problems to overcome when converting raw animal hide into a useful end product. Firstly the animal species, age and condition are considerations which are of the utmost importance. Depending on the purpose of the animal hide, the species is of importance due to the differences in fibre density and weave. Age affects fibre weave and density, but the older an animal is, the more likely that the hide will be damaged by scarring or attack by pests.

1.4.1: Removal of animal hide from the flesh (flaying) and preservation

The way in which an animal is flayed has an effect, where care is generally taken to ensure quality of the meat and to a lesser extent to the animal hide. This is when careless cuts may gouge into the dermis of the hide, thereby weakening the fibre weave. The flayed animal hide, Figure 1.13, is susceptible to environmental attack from pollutants and from bacterial action leading to putrefaction.

Figure 1.13: Flayed calfskins, salted and stacked together ready for processing into parchment. Images supplied by Linda Ramsay of the National Archives of Scotland. Authorised for publication by Wim Visscher of William Cowley, Parchment works, Newport Pagnell.

Depending on the climate, methods of preservation vary, ranging from the simplest method of drying, then wet (brine solution) and dry salting, through to the more expensive freezing. The method used depends on the country of origin and cost considerations, including energy, transport and materials. A consequence of the salting process, other than preservation, is the removal of HA and plasma proteins held within the hide [51]. After transportation to the tannery, the animal hides are then washed to restore to the pre-cured condition and to remove dirt, blood and other particles, such as the plasma proteins and HA, that have been dissociated from collagen fibrils.

1.4.2: Methods of hair removal and loosening of the collagen fibres

To obtain a useful material, the removal of hair and other non-collagenous macromolecules is required. Early methods of hair removal were to simply tread on the skins or to beat them with sticks [51]. More sophisticated methods were to soak the skins in enzymatic solutions made from vegetable matter (mulberry or bryony) or from human or animal excrement [52]. Vegetable matter is known to contain carbohydrase or mucopolysaccharidase enzymes, which depolymerise HA [53], thus releasing the plasma proteins. In addition to the fermenting solution, minerals such as sodium chloride or aluminium ammonium sulfate were added [54].

The most widely used method today is that of placing the hides into a lime solution (i.e. roasted limestone (calcium carbonate), forming quicklime (calcium oxide), which reacts with water (slaking) to form calcium hydroxide as shown in Figure 1.14 [2].

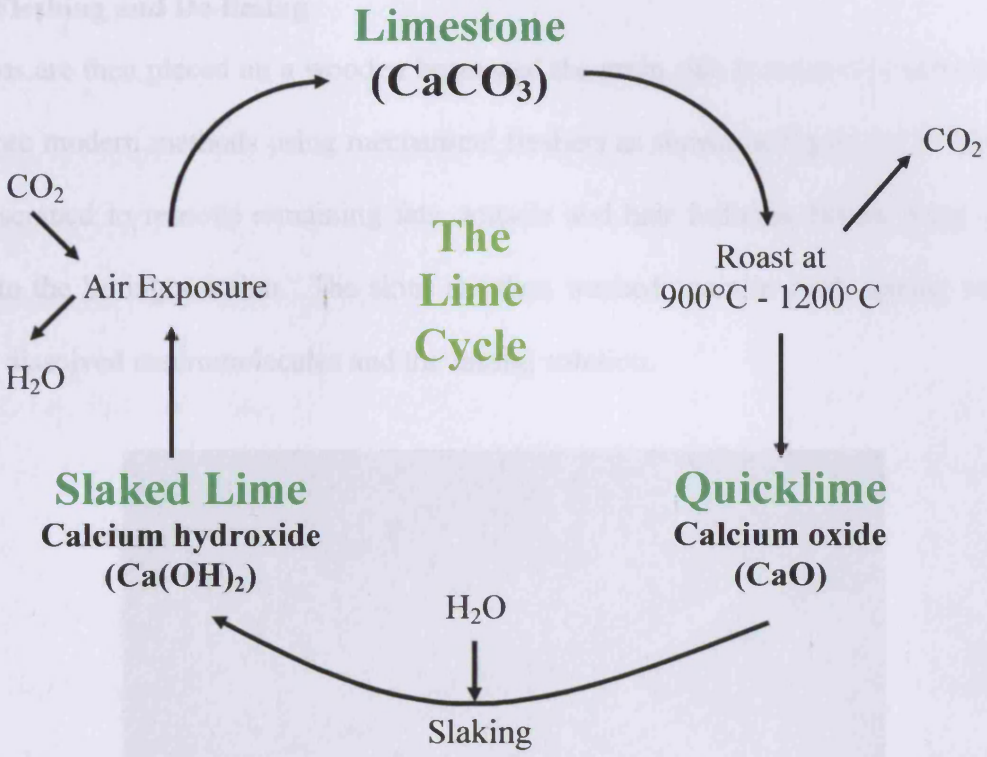

Figure 1.14: An illustration of the lime cycle.

The high alkalinity (pH 12.6) of the liming solution dissolves the hair root and keratin, which aids hair removal. Furthermore, the decomposition of the keratin produces sulfur compounds that accelerate the keratin breakdown, thus making old liming liquor a more effective solution for dehairing animal hide [8]. If, as in the case of sheepskin, the hair or wool is required, then the application of a liming paste to the flesh side is used to aid removal of the wool before the hide is soaked in the liming solution.

1.4.3: Fleshing and De-liming

The skins are then placed on a wooden beam and the grain side is scraped to remove hair, with more modern methods using mechanical fleshers as shown in Figure 1.15. The flesh side is scraped to remove remaining fats, muscle and hair follicles, before being placed back into the liming solution. The skins are then washed again in cold running water to remove dissolved macromolecules and the liming solution.

Figure 1.15: Images from the manufacturing process of parchment. Top) Hide placed on wooden beam and hair removed by scraping. Bottom) Mechanical flesher to remove fats, muscle and hair follicles. Images supplied by Linda Ramsay of the National Archives of Scotland. Authorised for publication by Wim Visscher of William Cowley, Parchment works, Newport Pagnell.

Prolonged exposure to the liming solution will decompose the collagen fibres, and it is imperative to prevent this from happening. Deliming of the animal hide can be achieved by prolonged exposure to water, but the process can be accelerated by adding acids or acid producing salts to the water bath. The deliming stage is where the processes diverge depending on the end product required, in this case parchment or leather.

1.4.4: Parchment finishing

Parchment is primarily a writing material made from animal hide using the above methods, although there are some variations due to regions, historical period and religious restrictions. The main aim of parchment manufacture is to make a smooth, high contrast and adsorptive writing surface. To achieve this, treatments applied to the hide must prevent the processed animal hide becoming hard and brittle; therefore, the skins are put under constant tension and allowed to air dry slowly to retain flexibility and to stop contraction (Figure 1.16).

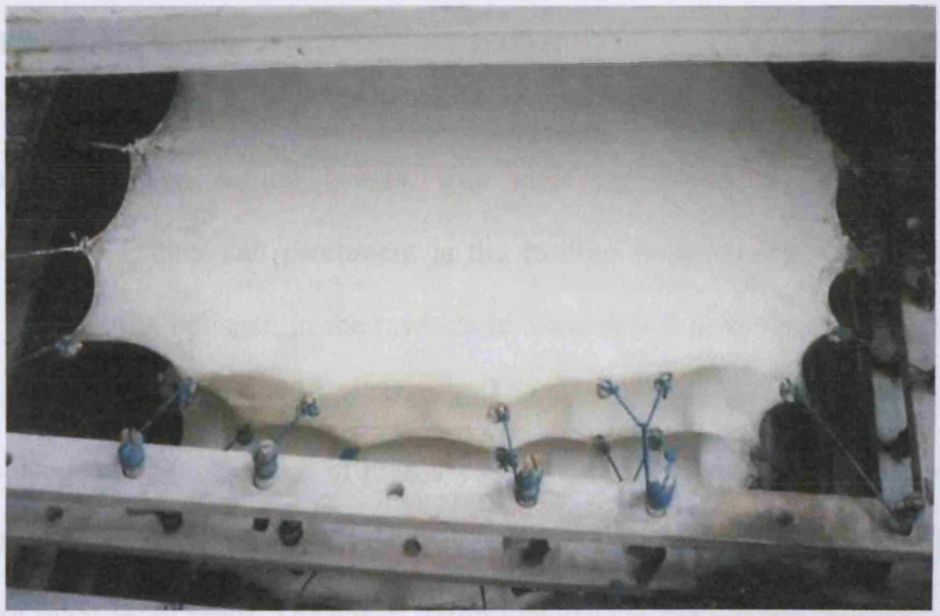

Figure 1.16: Drying stage of the parchment process. Images supplied by Linda Ramsay of the National Archives of Scotland. Authorised for publication by Wim Visscher of William Cowley, Parchment works, Newport Pagnell.

The dried skin is then scraped with the sharp edge of a half moon knife to give a smooth writing surface. The addition of chalk using a pumice stone and further scraping is used until a smooth surface is achieved. Sometimes the application of aldehyde and alcohols are used to provide a better finished material; the effects of these treatments on the collagen structure are shown in Chapter 5.

There are various uses of parchment and some of them contain important historical information, both within the text written on them and in their structural composition, with examples dating back thousands of years. The Dead Sea Scrolls, perhaps the most famous example of historical parchment, have been dated between 300BC and 70AD [52]. Documents of such antiquity indicate the crucial role of the pre-retrieval environment (conditions that parchment were exposed to before discovery), as well as conservation and storage following their recovery.

1.4.5: Processing of animal hide to make leather

Leather is made from animal skins or hides which have been chemically treated to preserve quality and natural beauty. The most significant difference between the manufacture of leather and parchment is the tanning process after the deliming stage. During tanning, the collagen in the rawhide is cross-linked to make it stronger and more durable, and to keep it from rotting. Raw animal skins go through several steps during the process. Depending on the type of hide used and the desired end-product, the steps taken during tanning can vary greatly. Tanning is essentially the reaction of collagen fibres in the hide with the tanning agent. The use of chromium salts as the tanning agent has dominated the tanning industry in recent decades and this remains the most widespread method of tanning today, although there is growing pressure in many countries for replacement by materials with a lower environmental impact [55, 56]. For example chromium has been

shown to have links with cell death of human lymphocyte cells [57] and cancer [58, 59]. Leather waste usually contains 3-7% Cr (III), obtained in the chromic tanning and production of shoes and leather goods.

Research has been dedicated to the improvement of leather quality, and to extend leather durability by developing new technologies for the tanning of collagenous materials. This can be achieved in several ways: by judicious selection of parameters for leather drying to promote retention of the proper content of water, by improving the UV and heat resistance of automotive upholstery leather, and by developing in-line monitoring of the mechanical properties of leather during its manufacture. Research programmes are aimed at minimising the environmental impact of leather production, through the development of new tanning processes and the utilization of solid tannery waste [56, 60, 61]. Central to the success of leather production is the degree of modification to the hierarchical structures formed by collagen molecules, fibrils and fibres during the conversion from rawhide to leather [62-64].

A study by Maeser [65] indicated that intra-hide variability of tensile stiffness depended upon the preferred direction of fibres in different regions of the hide. Kronick and Beuchler [17] showed that stretching untanned hide can produce changes in the orientation and distribution of its collagen fibres. Furthermore, studies into the effects on mechanical strength and collagen orientation of tanned leathers have been investigated [66-69]. A broad objective of research in leather technology is to provide knowledge of the collagen fibrillar and molecular integrity necessary for the development of effective low chromium tanning systems. Approaches are generally through a correlation of biophysical experiments [62, 63] of bovine skin treatment with different concentrations of chromium salt. X-ray diffraction studies covering length scales from ~100 to 0.2 nm spacing enables

rapid assessment of interactions between amino acid residues in the helix and inter-helical interactions within the fibrils [70].

1.5: Conclusion

The processing of animal hide removes important macromolecules from the complex structure of animal hide. The harshness of these treatments may cause damage to the collagen network that remains in the finished product. This damage is permanent, as the repair mechanisms of the skin are no longer functioning in *post mortem* tissue. Furthermore, the removal of the epidermis and the hypodermis leaves the dermis exposed to environmental pressures that would not exist *in vivo*.

The processes used to preserve the tissue and to make a useful material will be investigated here using the techniques of X-ray diffraction and FT-IR spectroscopy, as these will give structural information and limit damage to the samples. Principles of these techniques will be discussed in Chapter 2. Specifically, the treatments of liming (Chapter 4), alcohol and ketone finishing (Chapter 5), and chromium tanning (Chapter 6).

Chapter 2: X-ray principles

2.1: General introduction to X-rays

X-rays are electromagnetic waves with similar properties to visible light, first discovered by the German physicist Wilhelm Röntgen in 1895. X-ray wavelengths (λ) are typically in the range 0.5-2.5Å, (Cu k^{α} is 1.54Å) compared to visible light which has wavelengths in the order of 6000Å. The unit of measurement in X-ray regions is often given as the Angstrom (Å), which is equal to 10^{-8} m; however the SI unit is the nanometre (nm), which is equal to 10^{-9} m. The SI unit of nm will be the unit used throughout this thesis.

The wavelength of X-rays makes them useful for measuring internal structures in the order of 0.1nm. The types of matter that can be investigated at the atomic and molecular levels using X-rays include gases, liquids, amorphous solids and crystalline solids. The X-ray techniques used in this thesis are scattering and diffraction. This chapter will give a general background to the theory of scattering and diffraction, highlighting the differences between them. First a brief description of wave parameters will be explained. This will be followed by a practical description of X-ray images in relation to collagen molecules in rat tail tendon, which is the preferred reference standard in this thesis.

2.1.1: Wave parameters of light

Before beginning to define the theory behind X-ray scattering and diffraction it is necessary to understand the parameters of a wave. The parameters of interest are shown in Figure 2.1.

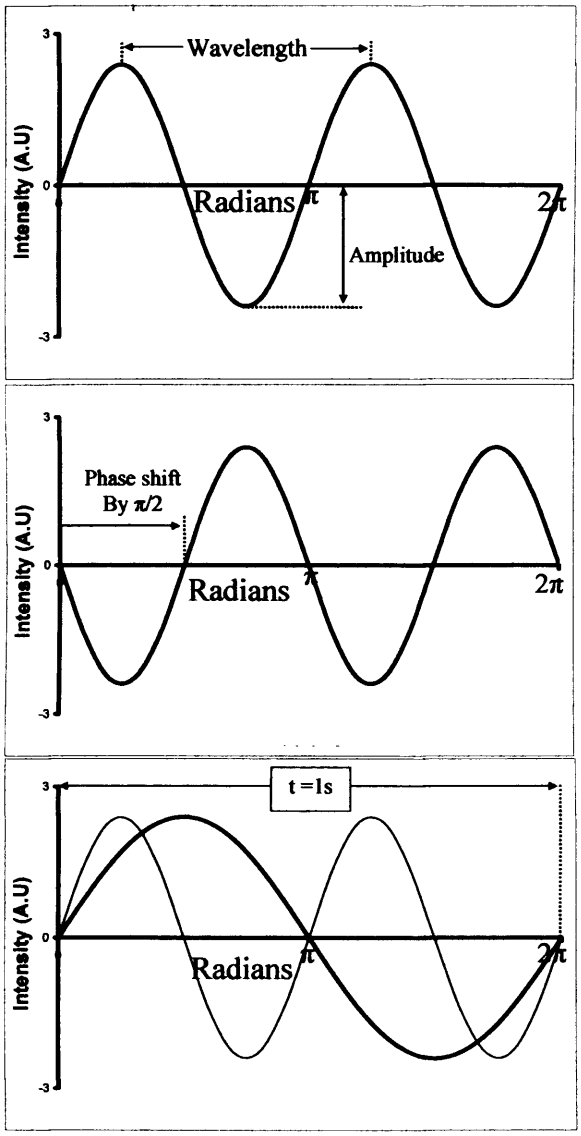

Figure 2.1: Parameters of a wave: Top, wavelength is the distance between one point on a wave, to the corresponding longitudinal repeat of that point. The amplitude is the maximum displacement of the wave. Middle, An example of a shift in phase by π/2 compared to the top wave, where the phase is defined as an arbitrary point selected on the wave. Bottom, Frequency is wave repeats per second (hertz Hz). Here is an example of waves at 1Hz and 2Hz. AU = arbitrary units.

Figure 2.1 illustrates the features of waves, which are wavelength, amplitude, frequency and phase. These features of waves are fundamental to X-ray scattering and diffraction principles. In order to understand why X-rays are more useful at determining structural information than visible light, the wavelength has to be considered, as well as how wavelength affects penetrative power of the wave and absorption of the wave by the sample.

2.2: X-ray penetrative power and absorption

The first parameter to examine is the wavelength of a light wave and why this determines penetrative power. As illustrated in Equation 2.1 the wavelength of light has a reciprocal relationship with the energy (E) of the light wave.

$$\lambda = \frac{hc}{E} \qquad (2.1)$$

where, h is Planck's constant (4.135×10^{-15} eV.sec) and c is the speed of light (3×10^{10}cm/s), also a constant. Electromagnetic radiation with shorter wavelengths has more penetrative power than the longer wavelengths; therefore, as X-rays have a shorter wavelength than visible light, they are able to penetrate further/deeper into the sample. This is of fundamental importance when considering which wavelength to use when accounting for the properties of the sample and the information that has to be obtained, i.e. sample resistance to heat and size of the internal structures. This knowledge of waves gives a platform to explain the fundamentals of X-rays and their interaction with matter.

2.3: X-ray interaction with matter

There are many sources that provide a more in-depth description on the interaction of X-rays with matter, for example by Hukins[71] and Cullity[72]. The way X-ray waves interact with matter depends on the type of matter. This interaction causes the X-rays to scatter. In the case of an ideal gas, where the molecules are sufficiently far apart, there are no interactions (electrostatic forces) between the molecules and therefore it is intra-molecular or atomic interference, which affects the X-rays. The closer the molecules are to each other, as in a liquid, the more that interference between them comes into play; this is termed inter-molecular interference. The level of inter-molecular interference between the molecules in a liquid depends primarily on the concentration. However, the interactions between molecules of a weakly concentrated liquid are still relatively random compared to solids, and thus weakly concentrated liquids behave more like gases. The more regularly spaced molecules in solids produce a cumulative effect reinforcing scattering in specific directions; this is termed diffraction. The theory behind scattering and diffraction will be discussed in sections 2.4 and 2.5 respectively.

2.4: X-ray scattering theory

When X-rays interact with matter, they are scattered at different angles depending on the tissue or material. The angle at which the X-rays are deflected gives internal structural information on the sample at different size scales, i.e. wide angles give information on smaller molecular spacings/structures, and the small angles relate to the size, shape and distribution of larger structures within the sample. The scattering can be either coherent or incoherent, which are defined in the following subsection (2.4.1).

2.4.1: Coherent scatter of X-rays

X-ray beams exhibit electromagnetic wave characteristics of an electric field. When this electric field interacts with tightly bound electrons of the sample, they oscillate: continually accelerating and decelerating, releasing energy, and therefore emitting an electromagnetic wave. This is the scattered X-ray beam, which has the same wavelength and frequency as the incident beam. If the X-rays were to interact with a single particle they would scatter in all directions. However, as discussed before, if the X-rays were to interact with a solid crystalline material, some X-rays will scatter in the same direction, reinforcing each other and giving diffracted beams. The cumulative effect of coherent scatter is so much stronger than incoherent for the biological systems studied in this thesis that the effect of incoherent scatter, which relates to free or loosely bound electrons, is negligible.

To understand scattering from biological systems, it is useful to study the scattering from a perfect crystal and then to examine the deviations from this for the more disordered biological systems.

2.5: Crystals and Diffraction theory

A comprehensive review of crystal structures can be found in the book by Glazer[73]. Essentially, a perfect crystal is composed of regularly spaced atoms, and the interaction of X-rays with crystals, although still scattering, is more specifically termed X-ray diffraction. The rules for determining diffraction can be illustrated by the simple mathematical equation of Bragg's law.

2.5.1: Bragg's Law

The interaction of X-rays with matter causes the incident beam to be scattered in all directions. In some cases the scattered beams are in phase and reinforce each other (constructive interference), giving diffracted beams as shown in Figure 2.2.

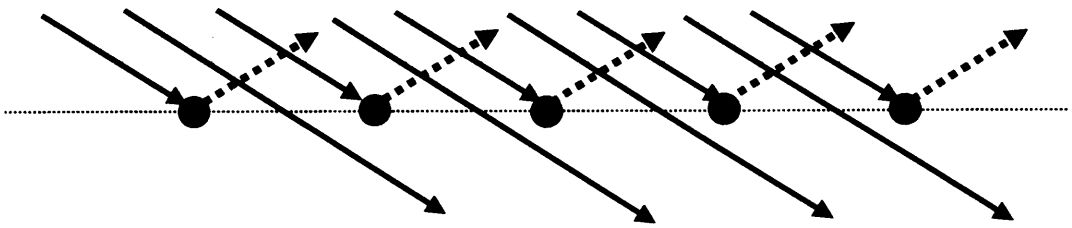

Figure 2.2: An illustration of coherent interference of scattered X-rays on a single layer of atoms. Incident beam = solid black lines, scattered X-rays = dashed blue lines.

Where the angle of incoming rays equals the angle of the outgoing rays relative to the plane of the atoms, then diffraction is achieved. However, three dimensional crystals have more than one layer, and therefore determining whether outgoing rays are diffracting is more complex. In 1912, Bragg stated a mathematical law to determine the geometry of diffraction, Equation 2.2, when applied to crystals which have more than one layer.

$$n\lambda = 2d \sin \theta \qquad (2.2)$$

Where d is the distance between the atomic planes, Bragg's law can be derived from Figure 2.3 by applying principles of trigonometry to the interaction of incoming incident rays with the outgoing scattered rays.

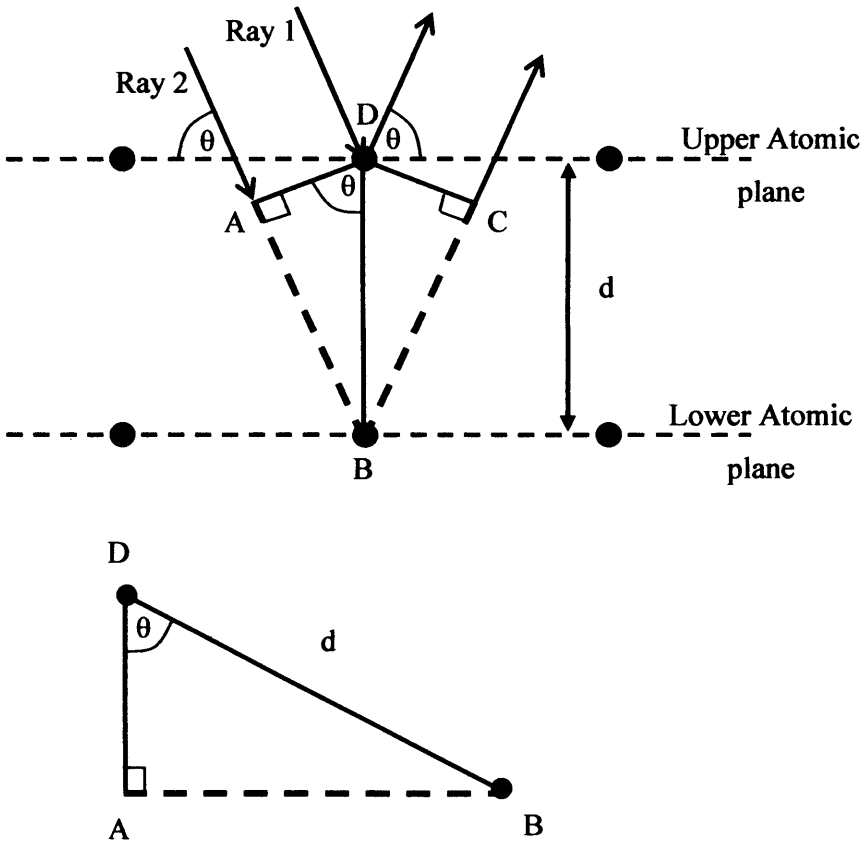

Figure 2.3: Diagrammatic representation of X-ray scatter by two planes of atoms to aid the derivation of Bragg's law. Rays 1 and 2 are from the incoming X-ray incident beam.

In Figure 2.3, Ray 1 deflects off the upper atomic plane at an angle θ, which is equal to the angle of the incoming incident beam. Ray 2 is parallel to ray 1, but it travels through the crystal to the lower atomic plane and is deflected again at angle θ. However, ray 2 travels a distance of AB + AC further than ray 1. If this distance is equal to an integral of the incoming wavelength, then the rays are in phase and constructive interference is obtained. The distance d can be obtained, when d is recognised as the hypotenuse of the triangle ABD. When the rays are in phase, ie; $n\lambda = AB + BD$ and $AB=BD= d \sin \theta$.

$$n\lambda = AB + BD \tag{2.3}$$

Therefore as $AB = BD = d\sin\theta$, Equation 2.3 becomes Bragg's law in Equation 2.4:

$$n\lambda = 2AB = 2d \sin \theta \tag{2.4}$$

For each set of λ and d there may be several angles θ that diffraction can occur. To gain a practical understanding of the applications of Bragg's law and diffraction of X-rays the concept of reciprocal space must be introduced.

2.5.2: Reciprocal space

X-rays interact with matter and are deflected at different θ angles. These scattered X-rays are collected on a detector as shown in Figure 2.4.

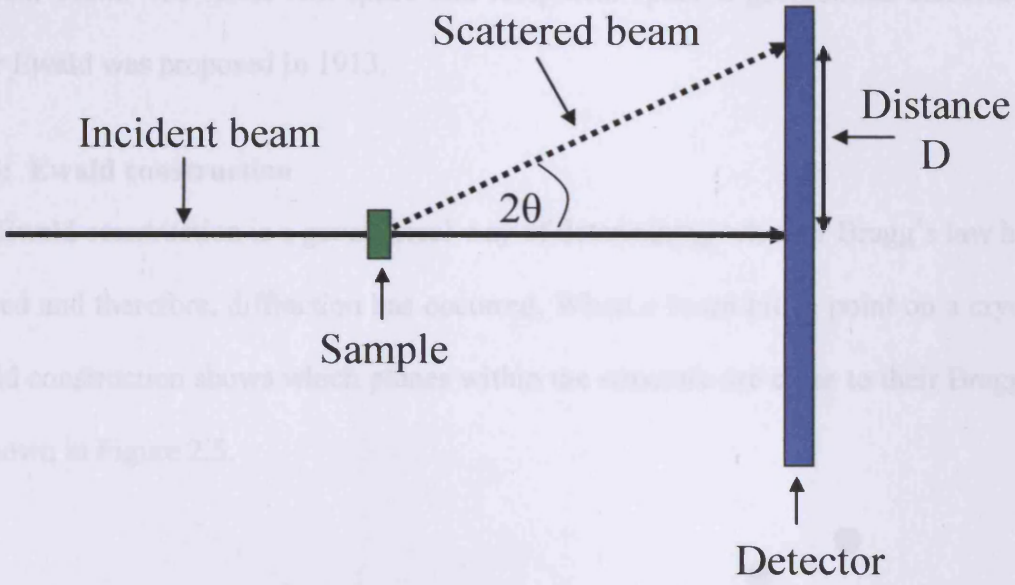

Figure 2.4: An illustration showing an incident X-ray beam scattered at an angle of 2θ onto a detector. Detector image D is reciprocal of d from Bragg's law (equation 2.4). Application of Equation 2.5 gives a direct relationship of D with 2θ.

A useful terminology to help aid the interpretation of the data on a diffraction pattern is reciprocal space. This is achieved by rearranging Bragg's law (Equation 2.2) to 1/d as shown in Equation 2.5.

$$D = \frac{1}{d} = \frac{2}{n\lambda} \sin \theta \qquad (2.5)$$

The distance D in Figure 2.4 can be measured and by the application of Equation 2.5 it is possible to determine the diffraction angle if the wavelength is known. This equation is of fundamental importance when interpreting diffraction images. It should be noted that the interactions of X-rays with matter will produce diffracted waves that are reciprocal to the incident beam. To relate real space and reciprocal space a geometrical construction by Peter Ewald was proposed in 1913.

2.5.3: Ewald construction

The Ewald construction is a geometrical way of determining whether Bragg's law has been obeyed and therefore, diffraction has occurred. When a beam hits a point on a crystal, the Ewald construction shows which planes within the structure are close to their Bragg angle, as shown in Figure 2.5.

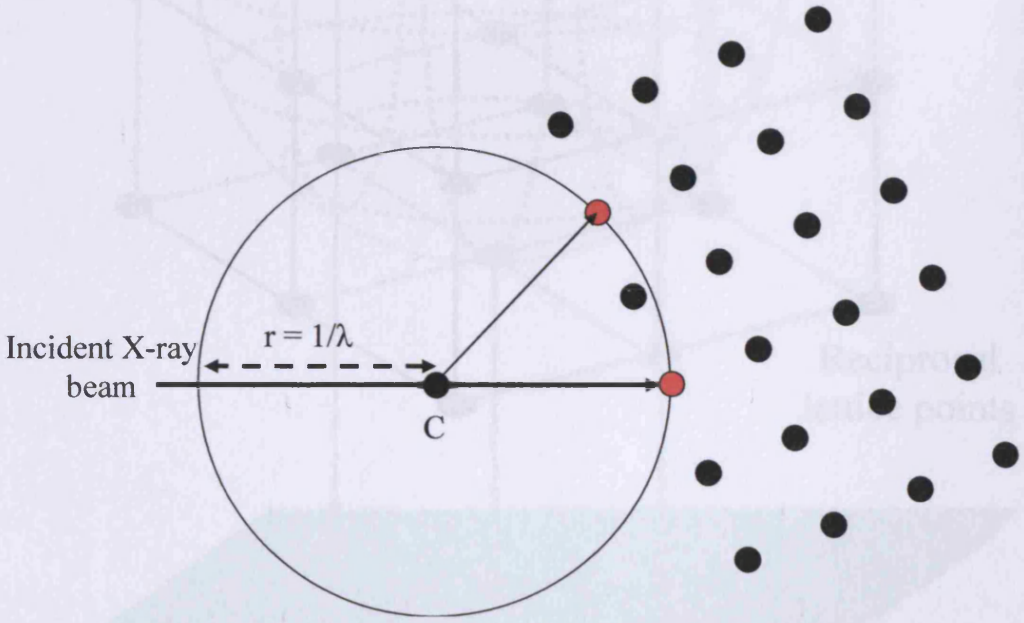

Figure 2.5: 2D Ewald constructions: incoming incident beam passes through crystal real lattice point, C. A circle of radius (r) = 1/λ of incoming beam is drawn. Red circles are the reciprocal space lattice points which touch the Ewald circle and are the points at which Bragg's law is obeyed, i.e. the path difference leads to constructive interference and the scattered X-rays are in phase and reinforce each other, resulting in diffraction.

However, crystals are 3D structures and therefore Ewald constructions must be illustrated as a 3D sphere as shown in Figure 2.6, where the radius of the sphere is $1/\lambda$.

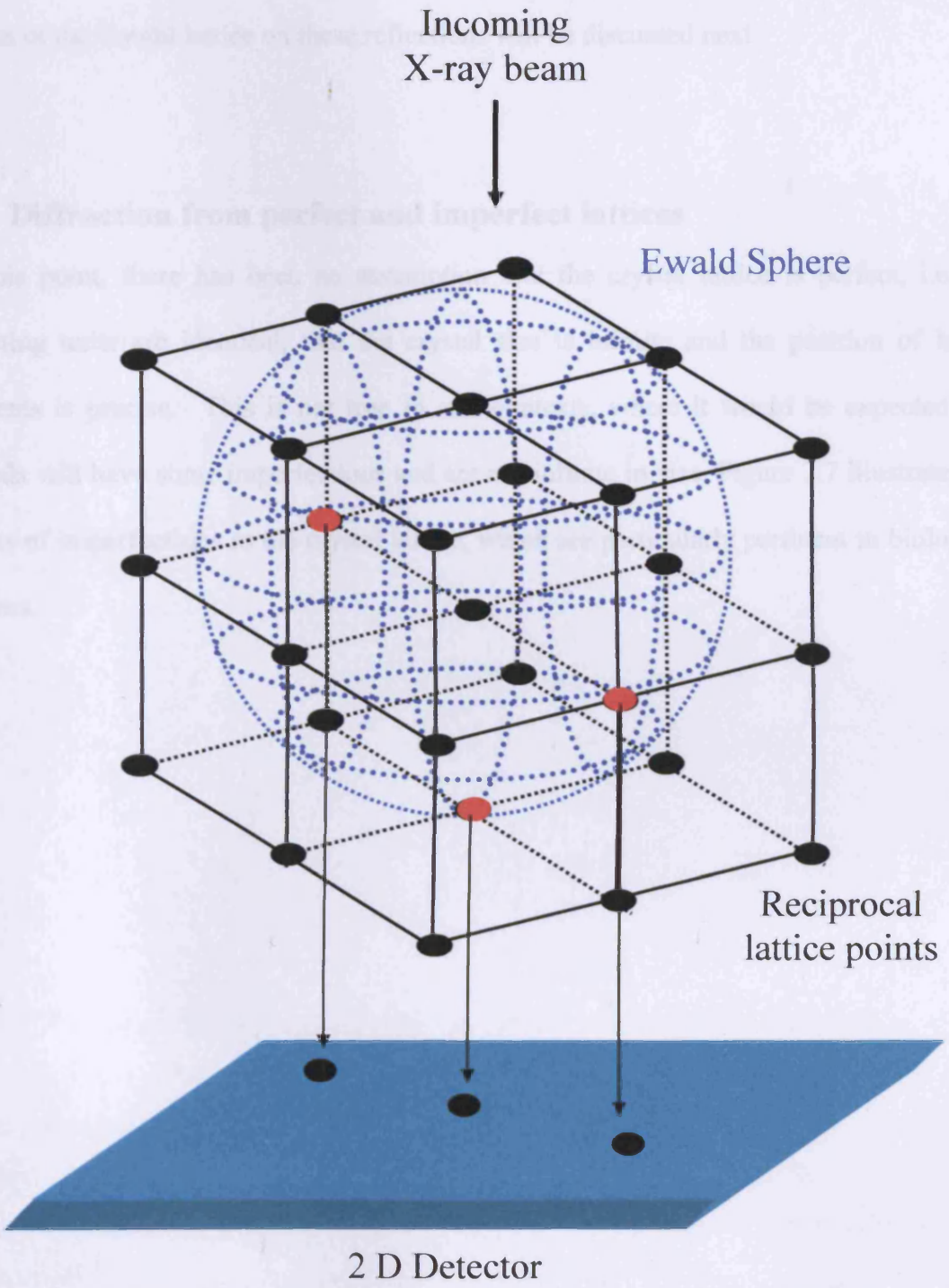

Figure 2.6: Ewald construction as a 3D sphere (blue) to account for the 3D nature of a crystal lattice. Reciprocal lattice points are in black, with the exception of the red points which represent where Bragg's law is obeyed and thus diffraction occurs. The 3D lattice points that diffract are captured by a 2D detector.

Figure 2.6 gives an illustration of the Ewald sphere and how these reciprocal lattice points which obey Bragg's law and diffract, appear on a 2D detector. These images are converted to a 1D linear profile, which will be discussed later in Subsection 3.2, and the effects of the crystal lattice on these reflections will be discussed next.

2.6: Diffraction from perfect and imperfect lattices

To this point, there has been an assumption that the crystal lattice is perfect, i.e. the repeating units are identical, that the crystal size is infinite and the position of lattice elements is precise. This is not true in real contexts, where it would be expected that crystals will have some imperfections and are not infinite in size. Figure 2.7 illustrates the effects of imperfections in the crystal lattice, which are particularly pertinent to biological systems.

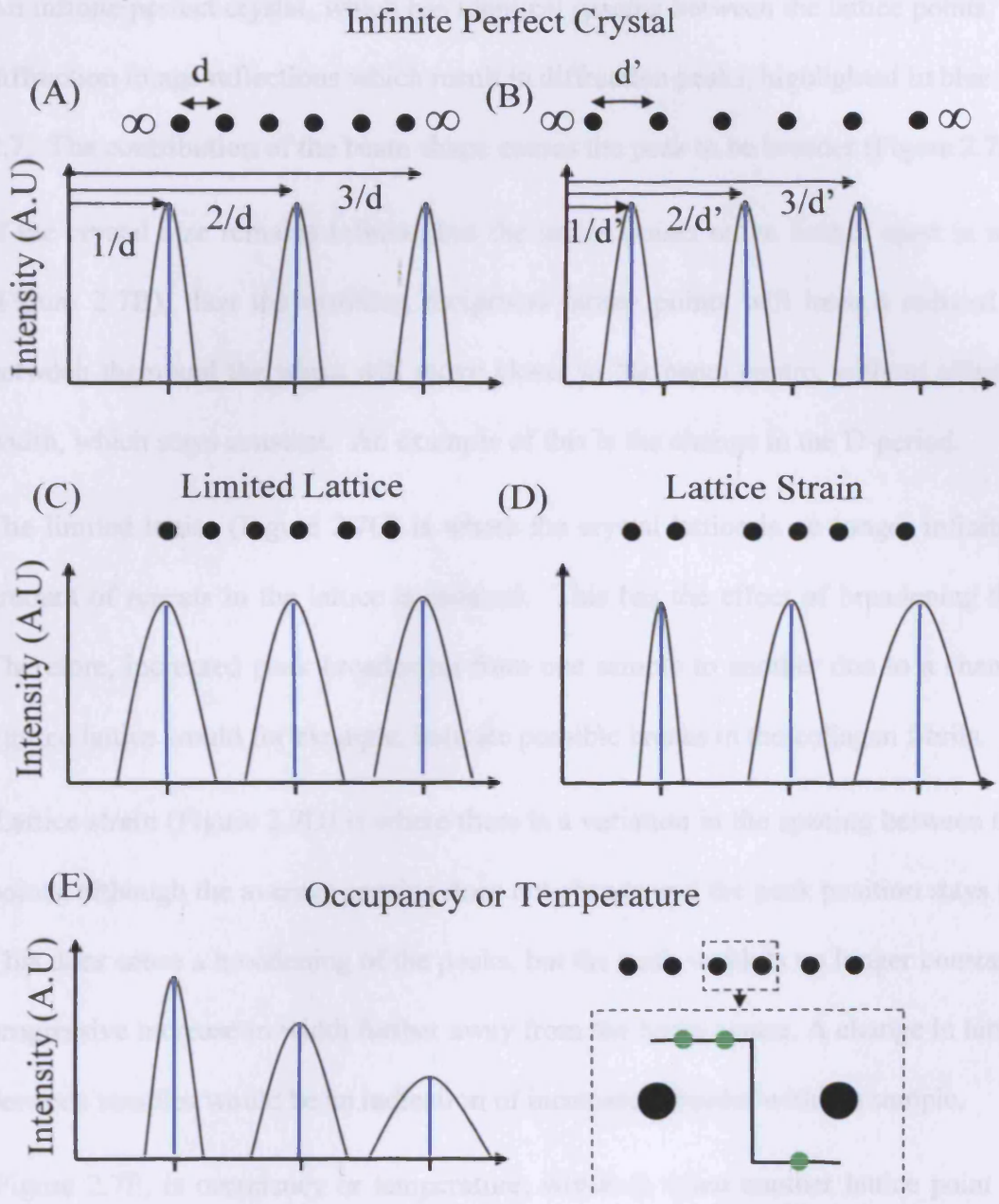

Figure 2.7: The effects of variations in the 1D crystal lattice on peak profiles; A) and B) Infinite perfect crystal lattice points of real space d and d'; Reciprocal peak positions and shape highlighted in blue, with peak widening due to beam profile. C) Limited crystal lattice points and reciprocal d peak profiles. D) Lattice strain, where d space varies, but d mean does not change. E) Occupancy or temperature; where for example chromium ions (green) enter into the lattice space.

An infinite perfect crystal, which has identical spacing between the lattice points, will give diffraction image reflections which result in diffraction peaks, highlighted in blue in Figure 2.7. The contribution of the beam shape causes the peak to be broader (Figure 2.7A).

If the crystal size remains infinite, but the lattice points move further apart in real space (Figure 2.7B), then the resulting reciprocal lattice points will have a reduced distance between them and the peaks will move closer to the beam centre, without affecting peak width, which stays constant. An example of this is the change in the D-period.

The limited lattice (Figure 2.7C) is where the crystal lattice is no longer infinite and the amount of repeats in the lattice is reduced. This has the effect of broadening the peaks. Therefore, increased peak broadening from one sample to another due to a change in the limited lattice would for example, indicate possible breaks in the collagen fibrils.

Lattice strain (Figure 2.7D) is where there is a variation in the spacing between the lattice points, although the average spacing does not change and the peak position stays the same. This does cause a broadening of the peaks, but the peak width is no longer constant, with a progressive increase in width further away from the beam centre. A change in lattice strain between samples would be an indication of increased disorder within a sample.

Figure 2.7E, is occupancy or temperature, which is when another lattice point has been introduced between the original crystal points, which is the case when chromium ions are introduced into the collagen lattice (Chapter 6). This looks similar to lattice strain; the difference is that peak height also reduces as peaks move out from beam centre. The effect of the beam profile has been discussed, and shown to have an effect on the shape of the reflection profiles.

2.7: Shape and the convolution theory

So far changes in lattice points and crystal size have been discussed, without the complication of the shape of the lattice point being taken into account. Lattice points are not dimensionless, but can be made up of a number of atoms and in some cases repeating structures several nm in size; such as, the collagen D-period. The mathematical interpretation of this is the convolution theory, which is described in the context of diffraction by Glazer[73]. Essentially the shape causes the infinite crystal reciprocal lattice points to broaden.

2.8: Scattering from a cylinder

For cylinders of uniform electron density and equal diameter in a parallel array, the total equatorial scatter, I(q), is given by the product of two factors [74] as shown in equation 2.6:

$$I(q) = [F(q)^2]G(q) \qquad (2.6)$$

where F(q) is the structure factor or scattered amplitude for a single crystal, G(q) is the interparticle interference function of the cylindrical lattice arrangement, and q is $4\pi/\lambda\sin\theta$, where 2θ relates to the equatorial plane scattering angle.

For an infinitely long cylinder with uniform electron density, the scattered amplitude F(q) of the X-rays is shown in Equation 2.7 [75]:

$$F(q_r) = 2Max\,1(q_r)/q_r \qquad (2.7)$$

where r is the fibril radius and Max1 relates to the 1st Bessel function maximum. When the scattered amplitude is of a cylinder with axis normal to the direction of the X-ray beam, then the normalised scattered intensity is given by $F^2(q_r)$ [28]. Plotting I(q), which is equal to $F^2(q_r)$, against q as shown in Figure 2.8, gives the radius of the cylinder.

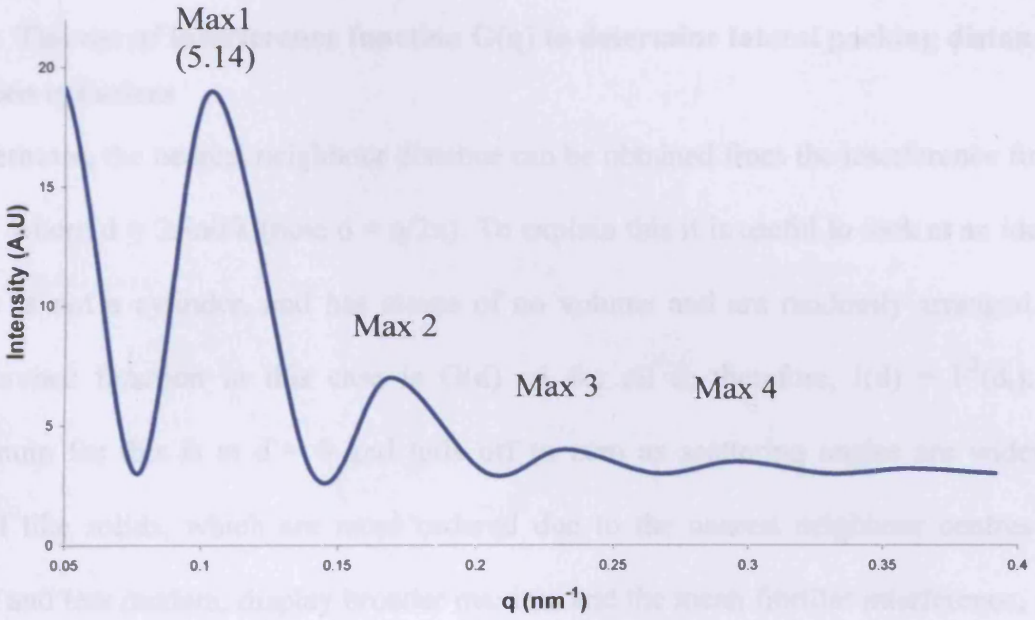

Figure 2.8: A 1D linear trace of an imaginary Bessel function for a cylinder of diameter equal to 100nm. Bessel function has maxima at $q_{(r)}$ 0.0, 5.14. 8.42, 11.6, and 14.8 nm^{-1}, where $q = (4\pi/\lambda) \sin\theta$ (λ= X-ray wavelength and θ = half of the scattering angle) and r is the cylinder radius.

The 1st order Bessel function has a maximum at 5.14 (Max1), which is a dimensionless quantity that can be used (Equation 2.8), to give the radius of the cylinder and therefore, the diameter.

$$cylinder\ diameter = 2r = 2(Max1(q)/q) \quad (2.8)$$

If, for example, the 5.14 1st order Bessel function maximum, (Max 1), is at q = 0.1028 nm^{-1}, Equation 2.8 yields a cylinder diameter value equal to 2r =2(5.14/0.1028) =100 nm.

2.8.1: The use of interference function G(q) to determine lateral packing distance between cylinders

Furthermore, the nearest neighbour distance can be obtained from the interference function G(d), where $d = 2\sin\theta/\lambda$ (note $d = q/2\pi$). To explain this it is useful to look at an ideal gas which is not a cylinder, and has atoms of no volume and are randomly arranged. The interference function in this case is G(d) =1 for all d; therefore, $I(d) = F^2(d_r)$. The maximum for this is at d = 0 and tails off to zero as scattering angles are wider [28]. Liquid like solids, which are more ordered due to the nearest neighbour centres being closer and less random, display broader maxima and the mean fibrillar interference, can be obtained from Equation 2.9:

$$i = 1.12 \,/\, Pm\,(d) \quad (2.9)$$

where, i, is the mean interfibrillar distance, and Pm(d) is the position of the peak maxima on the d axis in reciprocal space. The value of 1.12 was proposed [76] to account for the liquid like structures found in biological systems for example collagen. So far lattice

points and cylinders have been discussed, but many biological systems contain helical structures and the next section will address the implications of this.

2.9: Helical parameters

A common motif in biological systems is the helix, for example the double helix of DNA and the triple helical motif in collagen. Comprehensive reviews of X-rays fibre diagram analysis from helical structures were written by Ramachandran [77] and Squire [78]. To relate the helical structure in X-ray diffraction terms, then the following helical parameters are required as shown in Figure 2.9.

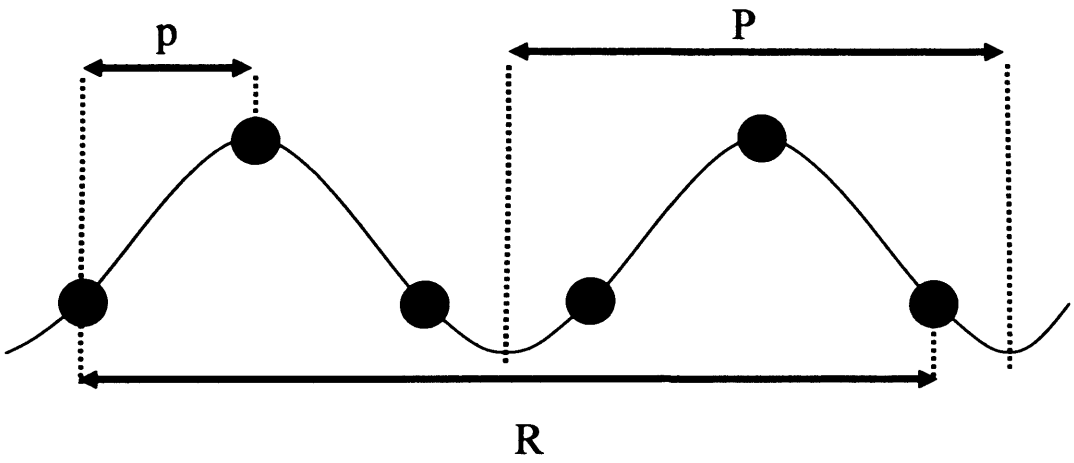

Figure 2.9: Parameters of a simplified 2D representation of a helical repeating structure. Black circles represent repeating subunit. P is the helical pitch. Subunit axial translation is p, and R is the axial repeat.

Assuming that the repeating subunits are identical, the height difference between individual monomers next to each other along the helix is termed the axial translation, p (axial rise per residue). The height shift required to complete one full turn of the helix is

termed the pitch, P, and the axial repeat distance, R, is the distance required for two monomers to repeat on the helix, so as to be located exactly over each other.

The practical applications of X-ray diffraction due to helical structure and X-ray scattering due to cylindrical structures will be discussed in the fibre diffraction section (2.10).

2.10: Fibre diffraction

The generic principles of X-ray scattering and diffraction, as described previously, can be applied to the description of scatter and diffraction of X-rays by collagen molecules of rat tail tendon, as shown in Figure 2.10. This is useful because orientation of the molecules allows the helical and molecular interactions to be distinguished.

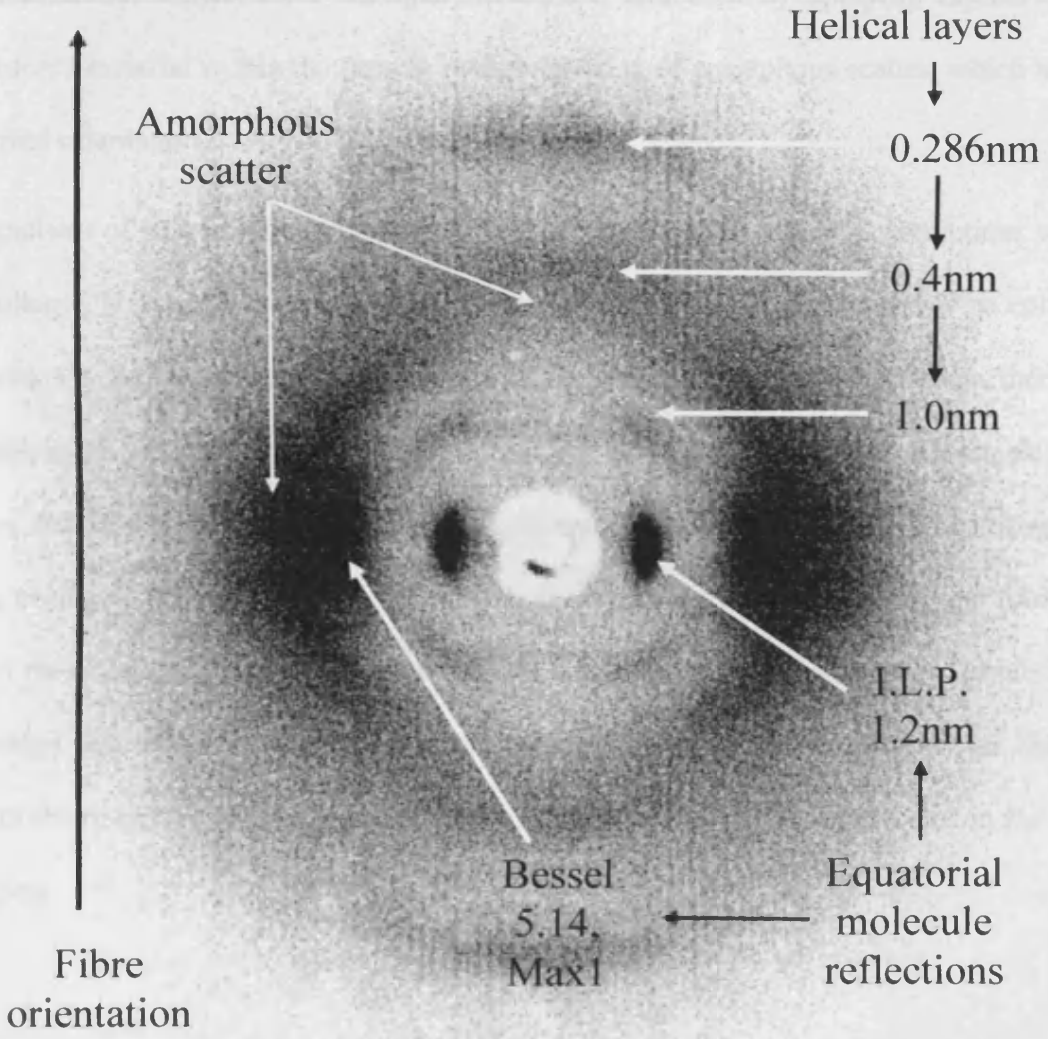

Figure 2.10: 2D diffraction pattern of rat tail tendon obtained on a Bruker AXS Nanostar at Cardiff University at a sample to detector distance of 4cm. The fibre was orientated perpendicular to the X-ray beam. Image shows diffraction reflections due to the collagen helix and scattering from the collagen molecules. Collagen intermolecular lateral packing (I.L.P.) is the interference between collagen molecules. A Bessel function maxima at 5.14, (Max1), is due to the cylindrical diameter of the collagen molecules.

Figure 2.10 shows a typical wide angle diffraction/scattering image due to collagen interactions with X-rays. The reflections from the collagen helix are shown by the helical layer lines, and it is the reflection at 0.286 nm that is a result of the axial translation, (Figure 2.9). Intermolecular lateral packing (I.L.P.) between the collagen molecules (Figure 1.8C) can be obtained by measuring the position of the reflection which is due to the interference between the collagen molecules, and then by applying Equation 2.9. Disordered material within the sample results in a ring of amorphous scatter, which has no preferred orientation.

The analysis of structural information in fibre diagrams pertains to larger structures within the collagen hierarchy, for example the fibrils can be treated in the same way as collagen molecules. They cause equatorial scatter of X-rays and are cylindrical in shape, therefore by applying Equation 2.8 and Equation 2.9 the fibril diameter and lateral packing distance can be obtained respectively. Furthermore, interactions of X-rays with the repeating unit of the collagen gap and overlap (Figure 1.7), gives rise to meridional reflections similar to that of the collagen helix. In this case it is not due to the repeating monomers of the helix, but rather the orders of Bragg reflections (Figure 2.11), which represents the electron density distribution of the gap and overlap interactions of collagen molecules in the axial direction.

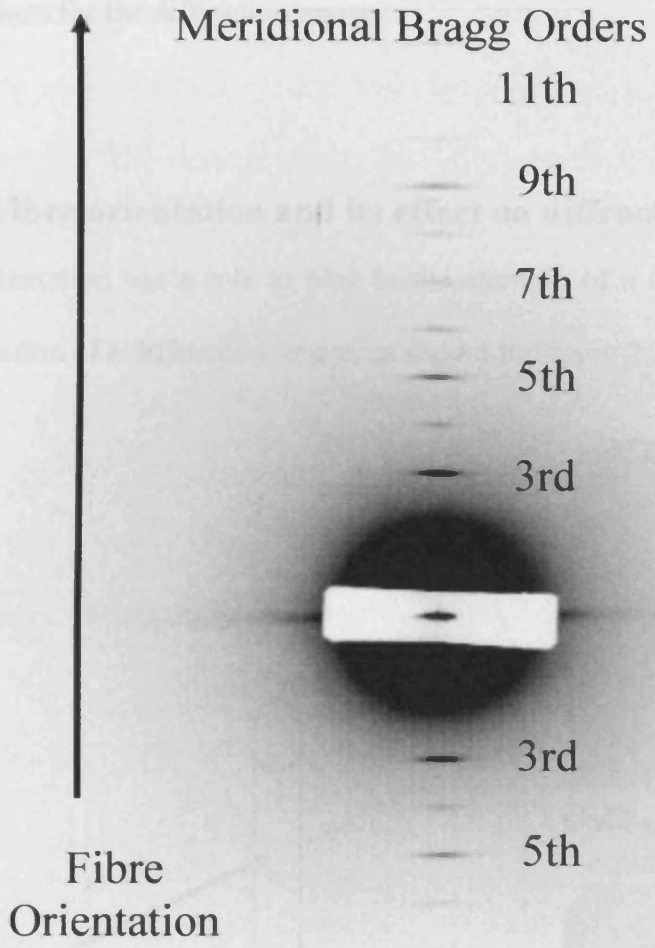

Figure 2.11: A SAXS pattern obtained at SRS Daresbury station 2.1 of hydrated rat tail tendon (reference standard). The meridional 3rd to 11th order axial Bragg reflections and collagen fibre orientation have been highlighted.

Figure 2.11 shows the Bragg orders of the collagen gap and overlap region, known as the D-period. Rat tail tendon collagen (Type I) has a D-period of 67nm in the hydrated state and is commonly used as a calibration standard. The diffraction image is the reciprocal of the real space structures. Therefore, the position of the reflection due to the 1st order Bragg reflection is at 1/67nm in reciprocal space. The position of the second is at 2/67nm, 3rd at 3/67nm and so on for all of the increasing order numbers. Figures 2.10 and 2.11 are scattering images for a single fibre orientation. However, skin, leather and parchment

have fibres of more than one orientation, as shown in Figure 1.6, and this has important implications for the diffraction image.

2.11: Fibre orientation and its effect on diffraction image

Fibre orientation has a role to play in the strength of a tissue, but it can complicate the interpretation of a diffraction image, as shown in Figure 2.12.

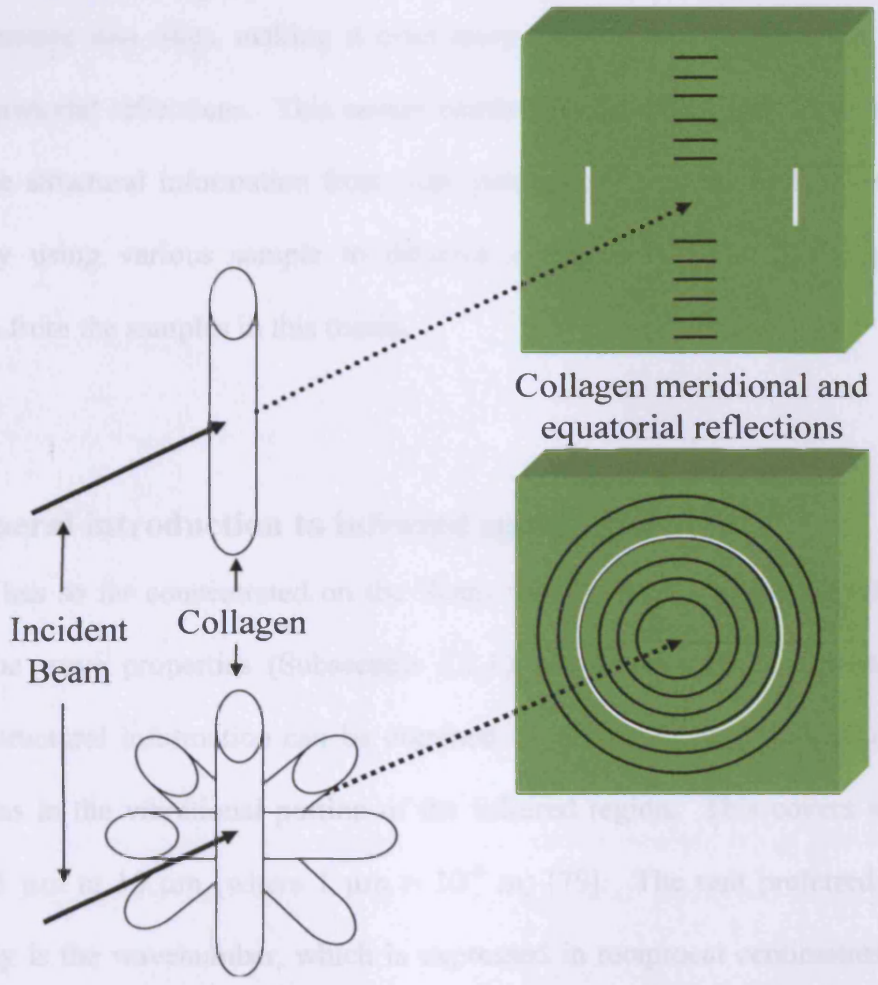

Figure 2.12: Illustration of how fibre orientation affects the diffraction image. (Top) Scattering from a single fibril, showing preferred orientation. (Bottom) Random orientation of fibrils in a plane perpendicular to the incident beam. For display purposes the meridional reflections are in black and equatorial reflections are in white.

Figure 2.12 shows that the orientation of the collagen fibrils has a direct effect on the diffraction image observed. The single fibril displays meridional reflections and equatorial reflections at 90° to each other. With the exception of the amorphous scatter in Figure 2.10, it is possible to identify clearly the different reflections resulting from meridional and equatorial scatter. It is however, difficult to identify clearly the Bessel function for the collagen molecules.

When there is more than one fibril as shown in Figure 2.12, the meridional and equatorial reflections merge into rings, making it even more difficult to distinguish the meridional from the equatorial reflections. This causes restrictions on which reflections can be used to determine structural information from skin, parchment and leather samples. It is still possible, by using various sample to detector distances (Chapter 3), to gain useful information from the samples in this thesis.

2.12: General introduction to infrared spectroscopy (IR)

This thesis has so far concentrated on the X-ray region of the electromagnetic spectrum and how the wave properties (Subsection 2.1.1) can be utilised in a practical sense. However, structural information can be obtained by using longer wavelengths, which in this case was in the vibrational portion of the infrared region. This covers wavelengths between 2.5 μm to 15 μm (where 1 μm = 10^{-6} m) [79]. The unit preferred in infrared spectroscopy is the wavenumber, which is expressed in reciprocal centimetres (cm^{-1}). A wavenumber is essentially the reciprocal of the wavelength in centimetres [79]. From Equation 2.1, it is clear that energy has a reciprocal relationship with wavelength; therefore, wavenumber has a direct relationship with energy. The absorption of various

frequencies of electromagnetic radiation in the infrared region by compounds which have covalent bonds was utilised in chapter 5.

2.12.1: Interaction of Infrared electromagnetic radiation with molecules

The absorption of infrared radiation by molecules is the same as with other types of radiation in that it increases the energy of the molecules to a higher state. An energy increase of between 8 to 40 kJ/mole occurs after absorption of IR radiation and corresponds to the bending and stretching frequencies (Figure 2.13) of most covalent bonds [79].

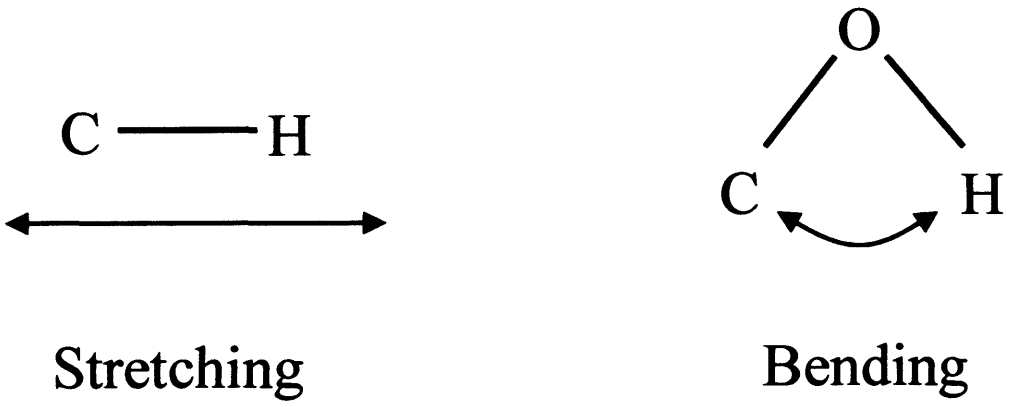

Figure 2.13: Illustrations of the simplest vibrational motion types (stretching and bending) in a molecule that absorbs infrared radiation. Adapted from Pavia *et al* [79].

Similar to X-rays, the IR radiation, must be in phase, with a matching frequency (Subsection 2.4.1) before energy can be absorbed (energy transfer). However, not all

molecules, will absorb IR radiation, as the molecules must have a changing electrical dipole moment, which is in frequency and phase matching that of the incoming IR electromagnetic field [79].

2.12.2: Practical applications of IR spectroscopy

Practical applications of spectroscopy can be obtained in the books by Pavia *et al* [79] and Hollas [80]. Essentially, every bonding mode in a molecule that is IR active will have a specific frequency. This frequency will depend on the type of mode and also the surrounding atoms. The locations of these modes are then compared with a known correlation chart, which then gives information that relates to specific molecules. Examples of this are shown in chapter 5.

Chapter 3: Experimental description and data reduction

3.1: Introduction

Application of the principles outlined in Chapter 2 can be used to gain useful structural information in the nanoscopic scale. This chapter provides details regarding the utilisation of these principles, and a description of the instrumentation used for data collection throughout this thesis. The main sources of data collection were the NanoStar, an in-house bench filament source (Subsection 3.2) and at two different synchrotron radiation sources (SRS, Daresbury, 2.1; ESRF, stations ID02 and ID13). Variation in scattering angle can be used to analyse different structural information within a given sample; therefore, this is the reason for using different X-ray sources and stations. This can be achieved by adjusting the distance between the sample and the detector as shown in Figure 3.1. Experimental set-ups are optimised for different measurements.

Data reduction was achieved using FibreFix software and peak fitting was obtained using PeakFit4 software (Subsection 3.4). Fourier transforms infrared spectroscopy (Subsection 3.5) and PCA data reduction (Subsection 3.6) will also be explained.

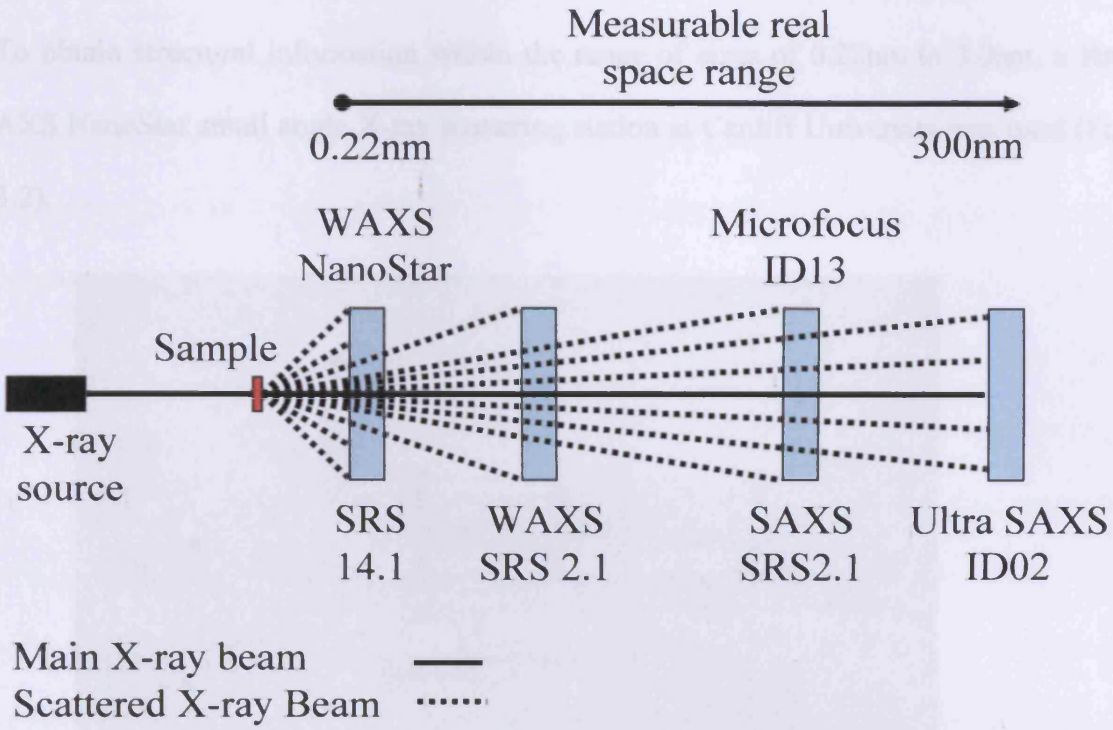

Figure 3.1: Illustration of variation in scattering angle, and the subsequent X-ray stations used to measure the different real space structural information. The measurable real space range relates to the particular set up parameters used in these experiments and not the complete range for all beam lines and set-ups.

The following chapters will give details on the X-ray stations used for the accumulation of scattering images for the samples analysed in this thesis; the individual experimental set-up of each station will be outlined. The structural information that is obtainable from the samples due to each station set-up will be explained. The smallest scales were obtained at Cardiff University on a Bruker AXS NanoStar bench X-ray source.

3.2: Bruker NanoStar - small angle X-ray scattering station (Filament source)

To obtain structural information within the range of sizes of 0.22nm to 3.0nm, a Bruker AXS NanoStar small angle X-ray scattering station at Cardiff University was used (Figure 3.2).

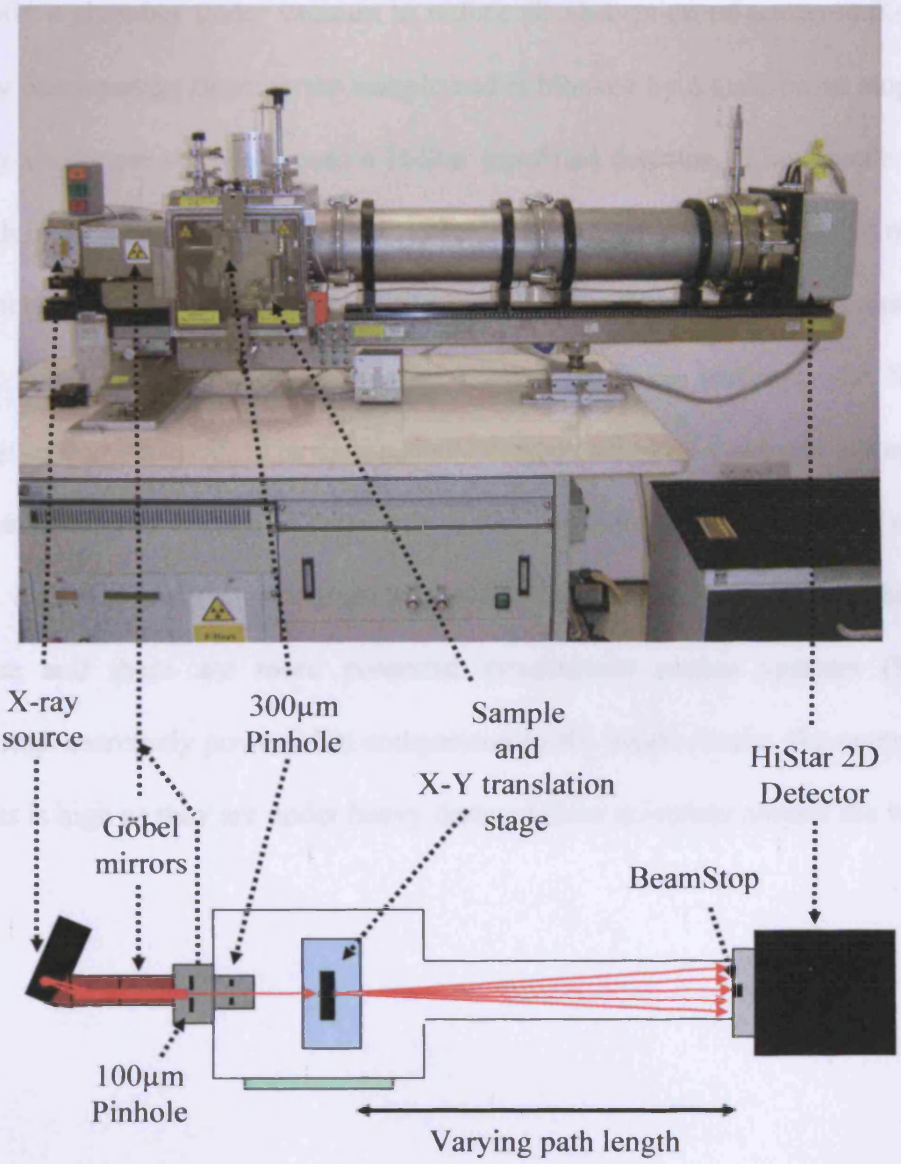

Figure 3.2: Bruker AXS NanoStar small angle X-ray scattering station. (top) Image of the NanoStar small angle scattering station at Cardiff University. (bottom) Schematic diagram of the Nanostar.

The X-ray beam is produced by a Kristalloflex 760 X-ray generator (Bruker AXS, Germany). The beam is doubly diffracted (split into 4) using 2 Göbel mirrors. The intensely focused beam is reduced in size by inclusion of the 100μm pinhole, which also blocks out all of the other diffracted beams. A 300μm pinhole is positioned after the 100μm pinhole to remove pinhole scatter. The sample is placed on an X-Y translation stage in a chamber under vacuum to reduce air absorption of scattered X-rays. The main X-ray beam passes through the sample and is blocked by a gold beam stop. The scattered X-ray waves are collected onto a HiStar gas filled detector. The sample to detector path length is variable between 4cm and 107cm, but was set at 4cm for the set of experiments in chapters 4, 5 and 6. This allowed the axial rise per residue characteristics of the collagen helix and the contributions of collagen and amorphous matter to the X-ray diffraction image to be measured. The calibration reference standard used was silver behenate. The Bruker NanoStar system is extremely stable and allows for comparison of data collected from different experimental sessions, which can be years apart. It is, however, a bench source and there are more powerful synchrotron source systems (Subsection 3.3). Although extremely powerful in comparison to the bench source, the competition to obtain access is high as they are under heavy demand from scientists around the world.

3.3: Synchrotron radiation

Synchrotron radiation is a high brilliance source of electromagnetic radiation, including X-rays. The X-rays produced are orders of magnitude more intense than the previously described bench X-ray source. Of the many synchrotron sources throughout the world the ones used for these experiments were the Synchrotron Radiation Source (SRS), Daresbury science and innovation campus, Daresbury, UK (http://www.srs.ac.uk/srs) and the European Synchrotron Radiation Source (ESRF), Grenoble, France (http://www.esrf.eu). Details of synchrotron radiation can be found at both webpages for these synchrotrons. The purpose of using these types of sources for this thesis was twofold: first, the increased range of structural sizes to be obtained and second, that sample exposure time can be reduced. For example, the Bruker NanoStar station requires 3 hours for data collection, whereas the synchrotron typically requires 3mins at SRS and 30s at ESRF for these samples.

3.3.1: SRS Daresbury Station 2.1, Experimental setup and technical details

An overview of station 2.1 at the SRS Daresbury is represented in Figure 3.3 and the complete technical details of this beam line can be found in the paper by Grossmann [81].

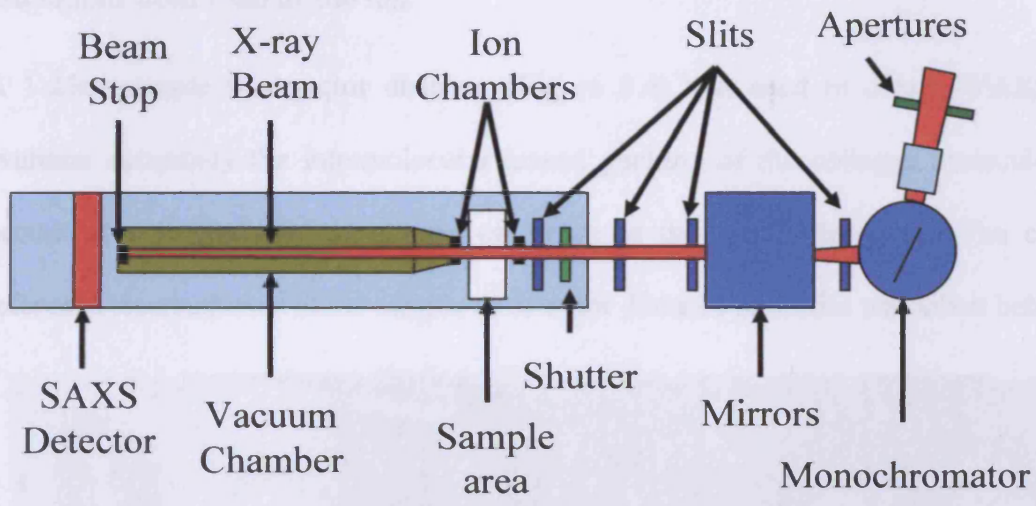

Figure 3.3: An overview of station 2.1 at SRS Daresbury. Adapted from the beamline webpage floorplan (http://srs.dl.ac.uk/ncd/station21/2.1_floorplan.html)

The synchrotron source from dipole magnet 2 delivers from the centre tangent point 32mrad of horizontal aperture. Station 2.1 accepts 17mrad of horizontal aperture, which is limited to 15-1.5mrad on the horizontal and 1.5-0mrad on the vertical by water cooled pre-monochromator apertures. Selection of the 0.154nm X-ray wavelength is obtained by a monochromator, which has a Ge111 bent triangular crystal, accepting up to 15mrad of horizontal aperture. The crystal has a Fankuchen cut of 11.6° causing a beam compression of ~11 times. The beam size is defined by a series of horizontal and vertical slits before

and after the mirror preceding the sample. The beam path is under vacuum, with the exception of the sample area distance, which is kept to a minimum to reduce background air scatter. The sample holder has a computer controlled X-Y elevation stage for movement of the sample in specific and measurable directions. Station 2.1 has a variable sample to camera (multiwire 2D area detector) length of 0.9 to 8.0 m giving spatial resolutions from 1 nm to 200 nm.

A 1.25m sample to detector distance (Figure 3.4) was used to obtain WAXS data to evaluate accurately the intermolecular lateral packing of the collagen molecules, which occurs in real space in the region of ~1nm in the dehydrated state. The calibration reference standard used at the sample to detector distance of 1.25m was silver behenate.

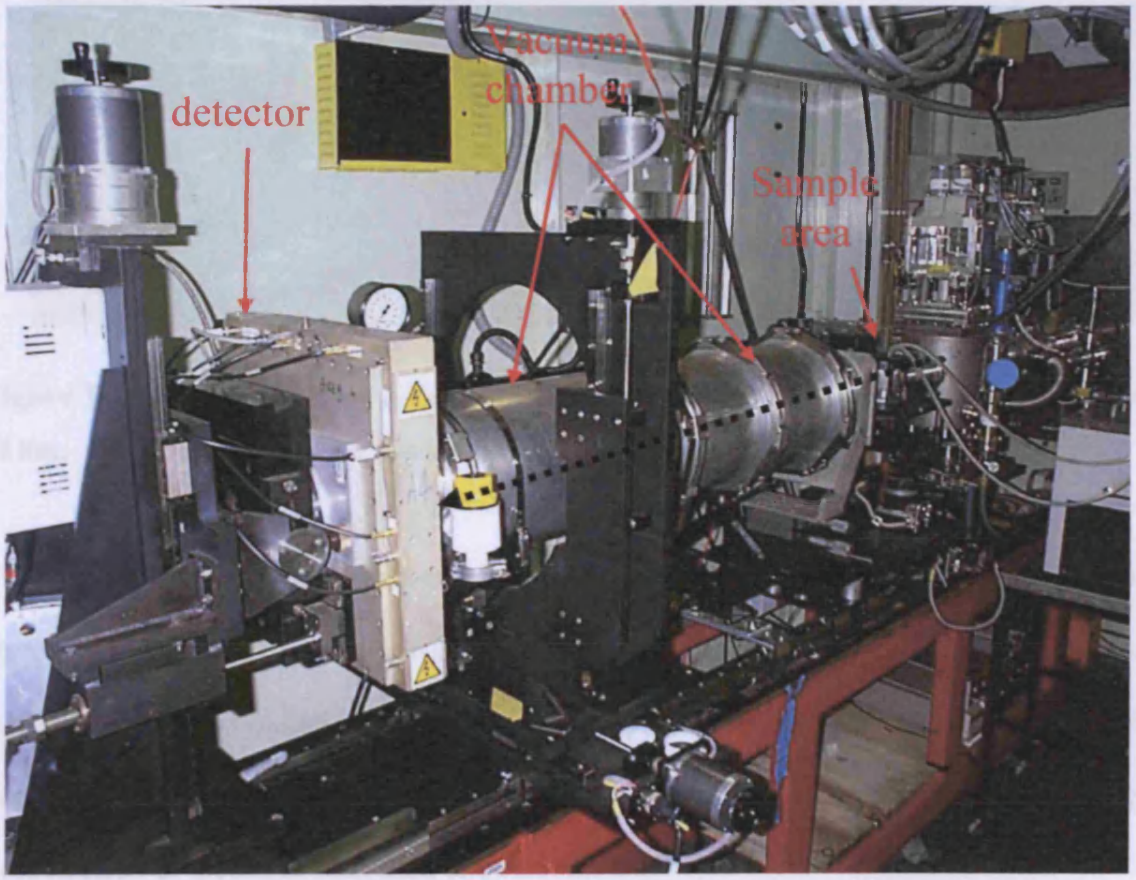

Figure 3.4: Image of station 2.1 at SRS Daresbury, with a sample to detector distance of 1.25m. Beam path = black broken arrow.

To obtain structural dimensions at larger scales it was possible to continue using station 2.1, but with the sample to detector distance increased to 8m (Figure 3.5).

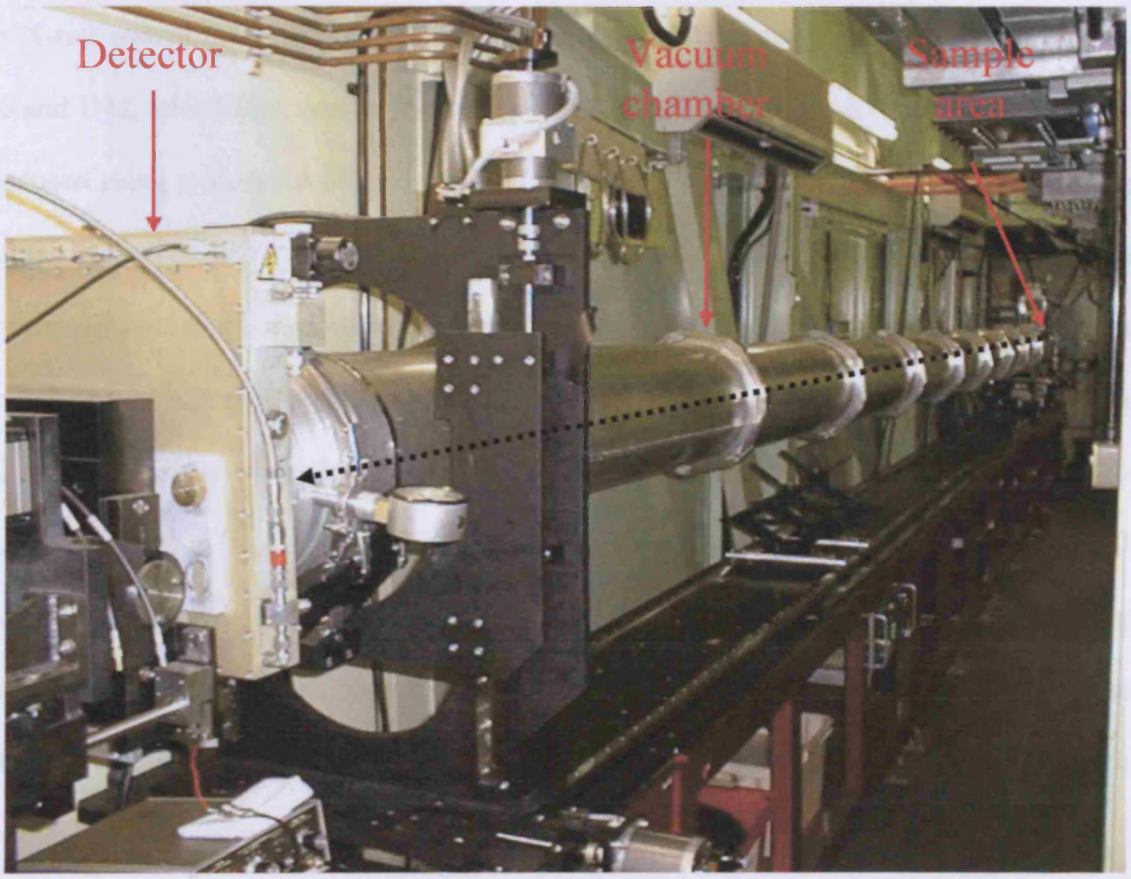

Figure 3.5: Image of station 2.1 at SRS Daresbury, with a sample to detector distance of 8m. Beam path = black broken arrow.

This allowed SAXS experiments to observe long-range interactions of collagen resulting from axial order (D-period). Calibration standard used at 8m was hydrated rat tail tendon. Although the set-up at station 2.1 will allow structural information of the samples at spatial resolutions of up to 200nm, the beam stop begins to influence the scattering image. Station ID02 at the ESRF was used to overcome this problem.

3.3.2: ESRF Station ID02- Ultra small angle X-ray scattering station set-up

Ultra small angle X-ray scattering (USAXS) experiments were carried out on station ID02 at the European Synchrotron Radiation Facility (ESRF, Grenoble, France).

The X-ray source is provided from the synchrotron storage ring by the undulators U24, U26 and U42, undulators, which give a high photon flux with a low divergence. The beam is focused using a cryogenically cooled Si-111 channel cut monochromator and a focusing toroidal mirror system. The standard beam size is 200μm vertically and 400μm horizontally, with a divergence of 20μrad by 40μrad. Optimised wavelength for this beam line is 0.1nm. Data was recorded on a XRII-FReLoN CCD area detector. At a wavelength of 0.1 nm and a sample to detector distance of 10 m, structural information up to 300 nm is obtained from a beam size and detector resolution of 100nm [82]. Hydrated rat tail tendon was used as a calibration reference standard. The ultra small-angle X-ray scattering patterns of bovine hide obtained at station ID02 gave a sufficient resolution to determine scattering features due to the cylindrical nature of collagen fibrils and the interference between fibril structures.

3.3.3: ESRF station ID13 - Microfocus beamline technical details

Station ID13 has a Microfocus beam, which provides small focal spots for diffraction and small angle X-ray scattering experiments. This station is used for scanning diffraction and single crystal experiments. Details for this station can be obtained from the ESRF website at www.esrf.fr, but a simple outline is as follows.

The beamline X-ray source uses an 18mm (U18) period vacuum undulator optimised for 13 keV and a 46 mm period tunable undulator for different energies. The incident photon energy is variable between 5 keV and 17 keV, with higher energies accessible without focusing. Monochromators used are liquid nitrogen cooled Si(111) double crystal or channel cut Si(111) in series. Micron beam of 2 μm is obtained using a Kirkpatrick-Baez (KB) [83] mirror and capillary optics, with an exit beam divergence of 2.3 mrad at 13keV.

Sample stage offers an x/y/z translation, rotation and tilt. The detector is a 2D Mar165-CCD with 2048 by 2048 pixels image.

3.4: Data reduction and analysis software

To obtain useful information from the diffraction images, it is necessary to perform data reduction and to use specialist analysis software. The data reduction is achieved by using FibreFix software from the Collaborative Computational Project for fibre diffraction and solution scattering, CCP13.

3.4.1: FibreFix - the CCP13 data reduction software

Although it was common practice for individual groups to write their own data reducing software, in 1992 the formation of the CCP13 project attempted to combine computational knowledge for data reduction of X-ray fibre diffraction and solution scattering images. A

key software outcome in data reduction was the program FibreFix, (Figure 3.6), which can be downloaded from the CCP13 webpage (http://www.ccp13.ac.uk).

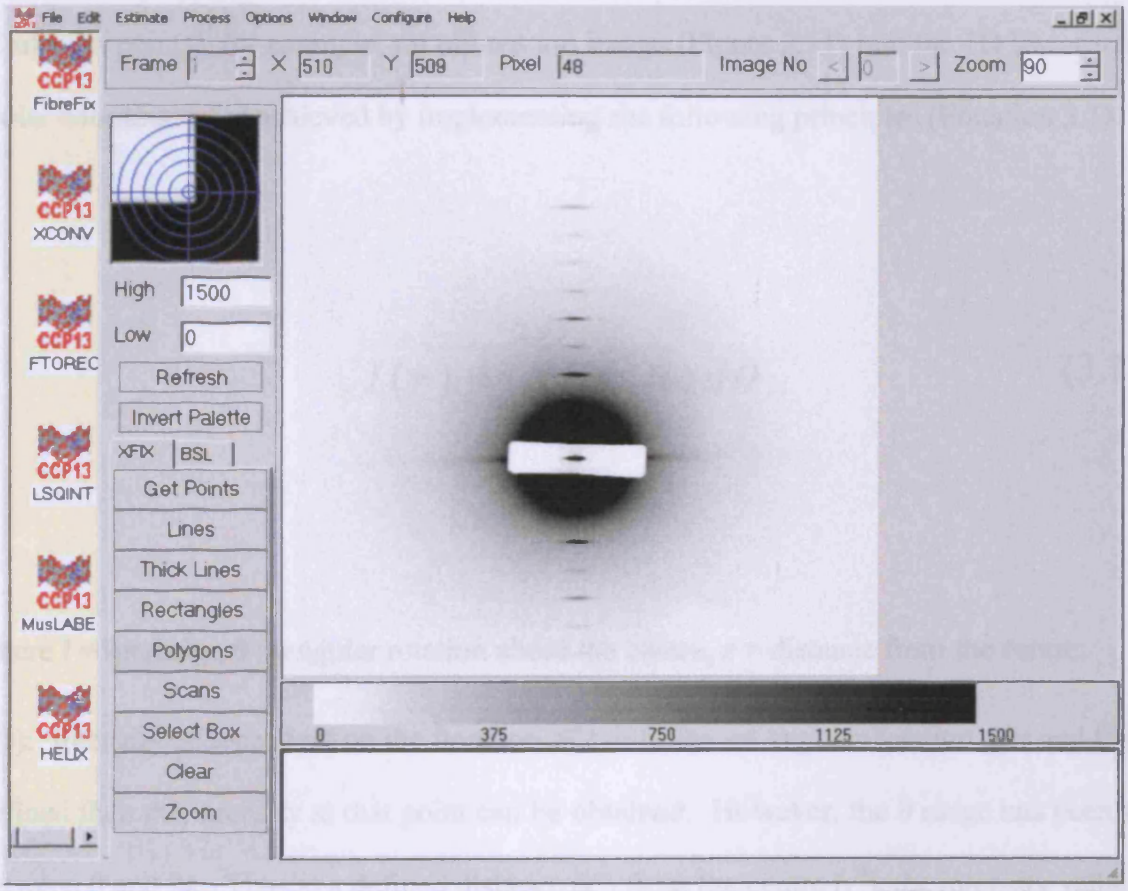

Figure 3.6: Interactive GUI for FibreFix software from CCP13. An X-ray diffraction image of hydrated rat tail tendon obtained at station 2.1 at SRS Daresbury at a sample to detector distance of 4.5m.

Multiple X-ray patterns can be loaded into FibreFix; usually one would be a calibration standard. The mathematical principle behind the data reduction of the 2D X-ray images into 1D linear profiles is explained in Subsection 3.4.2.

3.4.2: Principles of data reduction

Data analysis of diffraction images is difficult in the 2D form; therefore, it is useful to convert the 2D image into a 1D linear trace form. Conversion of the 2D diffraction image (Cartesian points), for example, rat tail tendon image (Figure 2.11) into the 1D linear trace (polar coordinates) is achieved by implementing the following principles (Equation 3.1).

$$I(r) = \int_0^{2\pi} I(r,\theta)\,d\theta \qquad (3.1)$$

where I = intensity, θ = angular rotation about the centre, r = distance from the centre.

I (r): Intensity is dependent on the function of r over the set angular rotation. If r and θ are defined then the intensity at that point can be obtained. However, the θ range has been set between 0 and 2π. Thus at a defined distance (r') from the centre (r^0), the intensity value is the sum of intensities at r' over the set θ range. Then at a distance r'', the intensity value is the sum of intensities at r'' over the set θ range and so on.

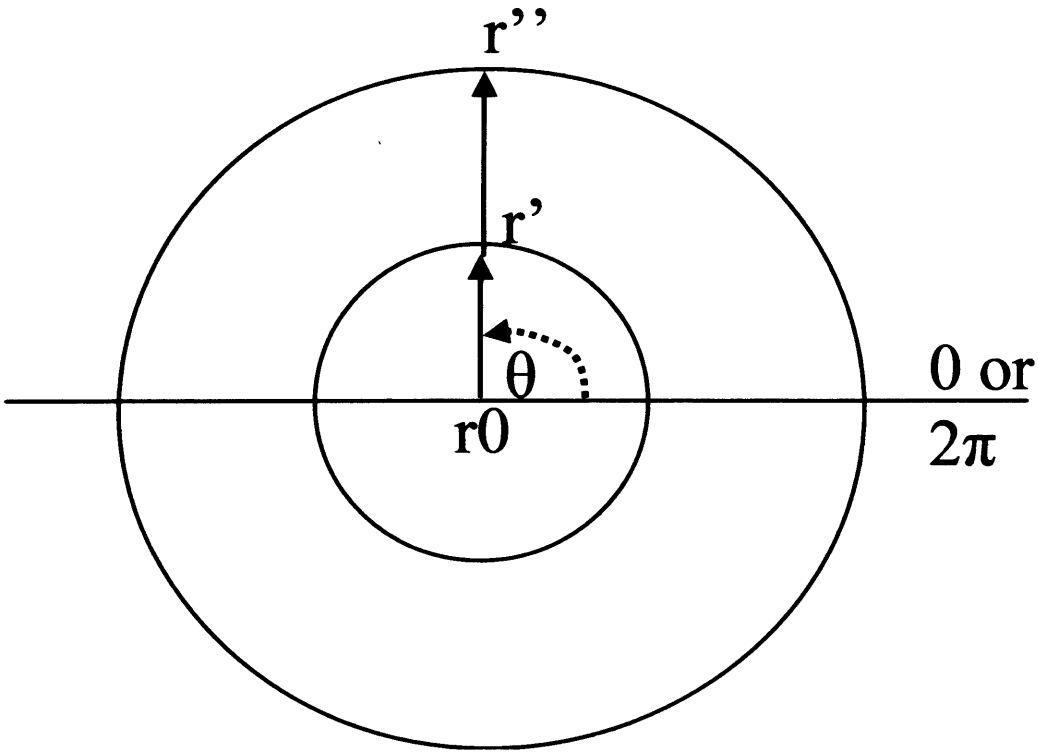

Figure 3.7: Illustration of the mathematical conversion of Cartesian co-ordinates to polar co-ordinates. (Data reduction of 2D X-ray images into 1D linear traces).

In Figure 3.7 the range is the distance from the centre (r' to r''). Therefore, the intensity of a particular reflection can be highlighted and by moving through the angular rotation θ, orientation can be determined (Equation 3.2).

$$I(\theta) = \int_{r'}^{r''} I(r,\theta)dr \qquad (3.2)$$

The resulting data points can be plotted as a 1D linear trace as shown in Figure 3.8:

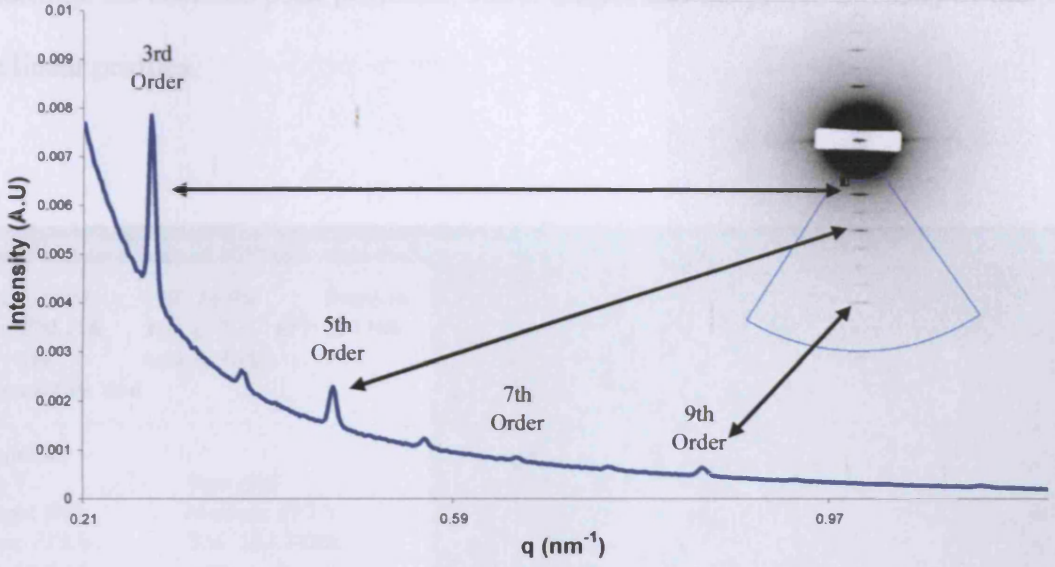

Figure 3.8: 1D linear trace converted from a 2D X-ray diffraction image of hydrated rat tail tendon (insert; blue sector is the area of the scan that was selected). Graph has been calibrated to a q axis, where $q = 4\pi/\lambda\sin\theta$.

The 1D linear trace can now be used to determine structural information about the sample, by analysing peak positions and peak shapes as discussed before. To do this accurately then it is necessary to use peak fitting software. Peak fitting for this thesis was done with PeakFit4 software.

3.4.3: Peak fitting

PeakFit4 (AISL software) the one-dimensional peak fitting program (Figure 3.9) was used to determine the accurate peak positions, sizes, shapes and integrated intensity of the peaks in the linear profiles.

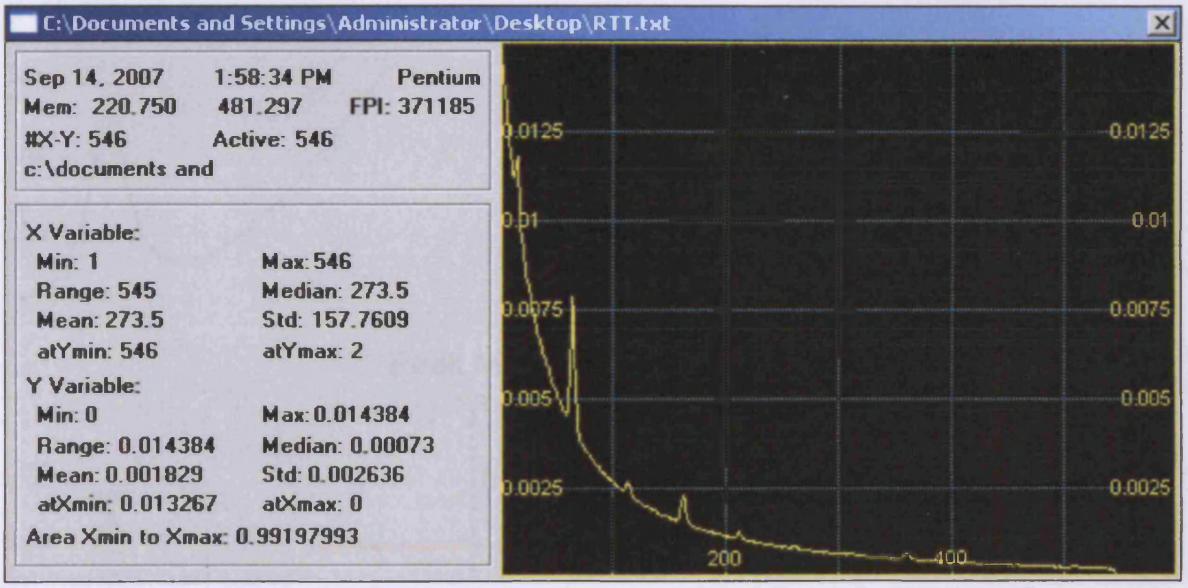

Figure 3.9: Image of PeakFit4 (AISL software) GUI. Linear trace of an X-ray image of hydrated rat tail tendon.

PeakFit4 software was used to remove background scatter, and to accurately measure the peak positions in pixels, which are then calibrated using a known standard. In the case of Figure 3.9, the hydrated rat tail tendon image is the calibration standard. In chapter 2, it was shown that peak profiles can be used to indicate structural information about the sample. The full width half maxima (FWHM) and integrated intensity are parameters of interest and these will be explained next.

3.4.3.1: Peak full width half maxima and integrated intensity

A useful parameter of a peak profile is that of the full width half maximum (FWHM), as the width of a peak can give information on lattice type (section 2.6). An example of FWHM measurements are shown in Figure 3.10.

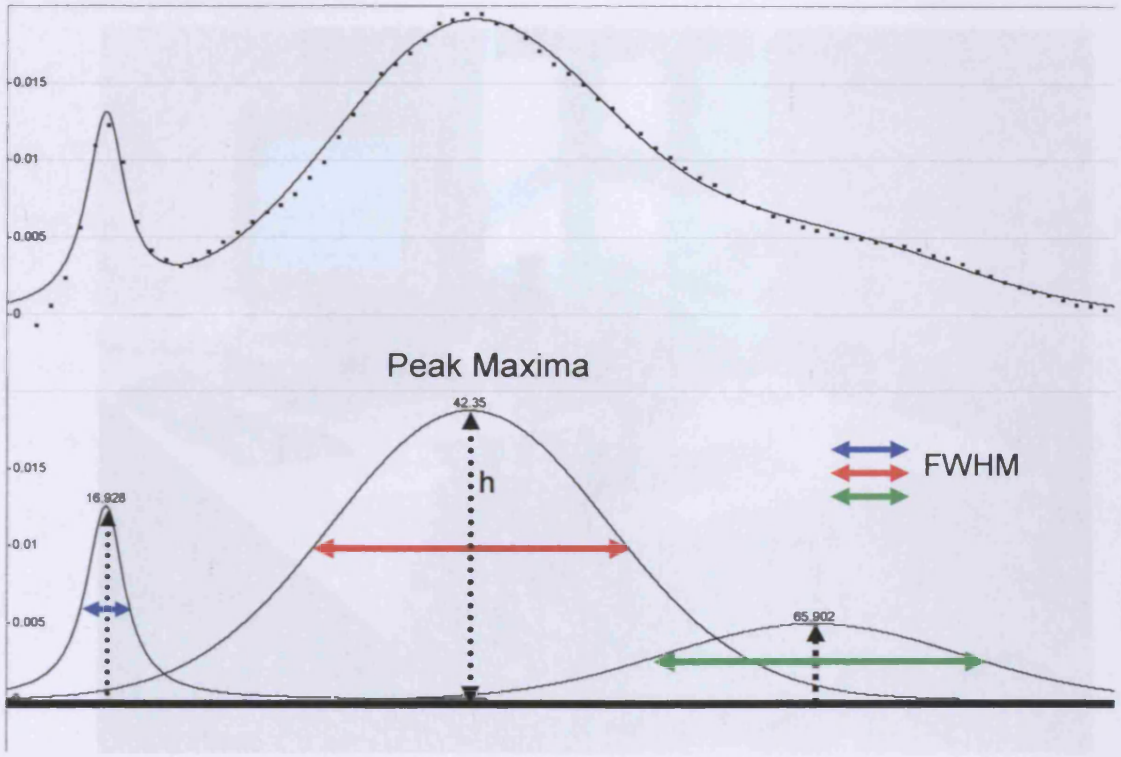

Figure 3.10: An example of peak fitting using PeakFit4. The blue, red, and green arrows indicate the full width half maxima of each peak respectively.

Another useful parameter of the peak is the integrated intensity, which is the total value of the intensity values that make up a peak. This is particularly useful to determine the collagen/amorphous ratio, described in chapter 6.

3.5: Fourier transform infrared spectroscopy

Fourier transform infrared (FT-IR) spectra were obtained using a Nicolet 380FT-IR spectrometer (Figure 3.11) at The National Archives, London. All spectra were recorded by absorption mode at 4 cm^{-1} intervals and 32-times scanning over a wavelength range from 400 cm^{-1} up to 4000 cm^{-1}. Data reduction was obtained by OMNIC software.

Figure 3.11: Picture of a FT-IR system at the National Archives, London, kindly supplied by Kostas Ntanos and Nancy Bell.

The FT-IR system was used to determine changes in samples treated with ketones and alcohols in Chapter 5. Further data analysis was carried out using the mathematical data reduction technique of principal components analysis (PCA).

3.6: Principal Components Analysis (PCA)

To explain better the differences present in the FT-IR spectra between samples, principal components analysis (PCA) was performed (Subsection 5.3.3) using in-house software. PCA is a data reduction technique that aims to reduce the dimensionality of any given data set, and to identify new underlying variables in the data set. The mathematical basis for PCA has been well documented [84, 85]. PCA rotates the original data into a new set of axes, such that the first few axes reflect most of the variations within the data. By plotting the data on these axes, major underlying structures may be spotted more easily. PCA generates basis functions that explain the nature of the variance in the data. There are as many basis functions as there are initial variables, and they are sorted in decreasing order of importance, as dictated by their associated eigenvalues. For each original variable, PCA generates coefficients that describe how much that variable contributes to the basis functions. Plotting the coefficients can determine if there is any correlation or trend in the variables.

3.7: Conclusions

This chapter has provided a background to the experimental techniques used throughout this thesis. The requirements for using different X-ray sources, i.e. filament and synchrotron radiation, was explained. The technical differences and set-ups of the X-ray stations used for the samples in this thesis were provided. Furthermore, the benefits of using various set-ups to gain structural information at different length scales were highlighted. The data reduction software and mathematical principles behind the conversion of raw data into useable information was shown. The peak fitting software used in this thesis was shown, with examples of methods used in this thesis. The practical uses and data reduction methods applied to FT-IR spectroscopy has been outlined.

In the next chapter, all of the X-ray techniques were used to determine structural changes brought about by the treatments of animal hide with salt solutions, liming solutions and also the effects of drying.

Chapter 4: X-ray Diffraction Study into the Effects of Liming on the Structure of Collagen

4.1: Introduction

Collagen based tissues, such as skin, are hierarchically organized materials, with an intimate relationship and connectivity between the molecular structure relating to the helical organization within individual collagen molecules. The combination of well-defined nanoscopic axial and lateral organization of locally associated collagen molecules and the organization of discrete fibrillar structures produces a functional tissue. The subsequent processing of a collagenous tissue such as skin, into parchment or leather can involve treatments with salt and liming solutions.

To date, the changes in collagen and associated molecules at the molecular, nanoscopic, and microscopic levels brought about by these hide treatments are not well described in the literature. Terms such as "opening up" of the collagen fibres are often used to describe the effects of the processes such as liming and salting without a firm structural basis [86]. The purpose of the data presented here is to describe quantitatively the alterations to collagen structure in the processes of salting, liming, and drying that are used in parchment manufacture, but which are also representative of many other collagen treatments.

4.2: Experimental

4.2.1: Sample parameters

A selection of bovine and ovine treated skins was supplied by W. Visscher (William Cowley parchment and vellum works, Newport Pagnell, U.K). The samples selected were treated in a traditional parchment liming manufacturing process. The exact methods are subject to proprietary control, and a detailed description of the manufacturing process can not be disclosed, but typically salting is used for preservation before processing, followed by soaking the skin in slaked lime for up to 2 weeks for dehairing and removal of proteoglycans and other non-collagenous macromolecules. Deliming of skins involves washing in water and the addition of neutralizing salts [87].

As an in-house control, fresh rat hide was soaked in a salt solution (NaCl) for three days followed by seven days in a liming solution (CaOH). Figure 4.1 shows images of a representative sample and Table 4.1 contains a list of the samples used including the dry samples, which were obtained by slowly air drying a portion of the hydrated samples at room temperature over a 7 day period.

The control samples used were untreated, mechanically dehaired skin (scraped using a blunt knife; the presence of hair keratin was not observed in X-ray diffraction images and therefore was discounted as a possible cause of interference) and parchment representing the start and end products of the process.

Figure 4.1: Images of animal hide samples used in chapter 4 representing the processing of animal hide into parchment. Bovine and ovine hide samples supplied by W. Visscher from Newport Pagnell vellum work. Rat hide was treated in-house at Cardiff University. Complete sample list is shown in Table 4.1.

Newport Pagnell Samples		In-house Samples
Bovine	**Ovine**	**Rat**
Untreated (w/d)	**Untreated (w/d)**	**Untreated (w/d)**
Salted (w/d)	**N/A**	**Salted (w/d)**
Limed (w/d)	**Limed (w/d)**	**Limed (w/d)**
Delimed (w/d)	**Split-limed (w/d)**	**N/A**
Parchment (d)	**Parchment (d)**	**N/A**

Table 4.1: A list of the samples used in chapter 4 for data analysis. The treated bovine and ovine samples were supplied by Newport Pagnell by W. Visscher and the rat hide was treated in-house at Cardiff University. (w/d) signifies that samples were both hydrated and dehydrated for analysis- (d) are samples that were only in the dehydrated state.

4.2.2: Sample set-up on the Bruker AXS NanoStar small angle scattering X-ray station

Animal hides (including an untreated control) were dissected into 1cm squares and loaded onto the NanoStar sample holder to allow multiple samples to be analysed in an efficient way, without changing the sample environment. The samples were loaded into the NanoStar chamber holder perpendicular to beam (from grain to flesh side) at a sample distance of 4cm from the detector. The sample chamber and beam path was evacuated to reduce air scatter of X-rays. NanoStar technical details are found in chapter 3.2.

4.2.3: SRS Daresbury station 2.1 WAXS and SAXS

Treated animal hides were dissected as in section 4.2.2 and loaded perpendicular to the beam onto a multiple sample holder as supplied at station 2.1. The WAXS images were obtained at a sample to detector distance of 1.25m and the SAXS images at 8m. Hydrated rat tail tendon was used at both sample to detector distances as the calibrating standard. Daresbury station 2.1 technical details are shown in subsection 3.3.1.

4.2.4: ESRF station IDO2 Ultra SAXS setup

The ultra small angle X-ray scattering images (USAXS) of bovine hide obtained at station ID02 of the European Synchrotron Radiation Facility (ESRF), Grenoble, France, (details in subsection 3.3.2) gave a sufficient resolution to determine scattering features due to the cylindrical nature of collagen fibrils and the interference between fibril structures. Hydrated rat tail tendon was used as a calibration standard.

4.2.5: ESRF station ID13 Microfocus beamline

The small beam size obtained on station ID13 was used to measure structural changes that occur from the grain side through the sample to the flesh side. As such the samples were cut into a wedge shape and rotated by 90° compared to all other sample in this thesis. ESRF station ID13 technical details are shown in subsection 3.1.4

4.3: Results - Evaluation of Diffraction Data

X-ray diffraction data was obtained for treated animal hides. Using the benefits of different set-up parameters and characteristics of the different stations, it was possible to investigate the various hierarchies of the collagen molecules and to obtain quantitative structural packing information.

4.3.1: Effects of processing at the molecular level

To determine the effects of the parchment manufacturing process on the animal hide and in particular the collagen fibrous network, it seems prudent to start at the molecular level. An examination of structures within the collagen molecule can be achieved using WAXS techniques. Figure 1.6 shows the axial rise distance (helical rise per residue) between the amino acid residues along the collagen molecular triple helices.

To determine the changes in the collagen triple helix WAXS images were obtained on the Bruker NanoStar at Cardiff University for the sample set of treated animal hides. An example of the typical isotropy of a WAXS pattern from bovine hide can be seen in Figure 4.2.

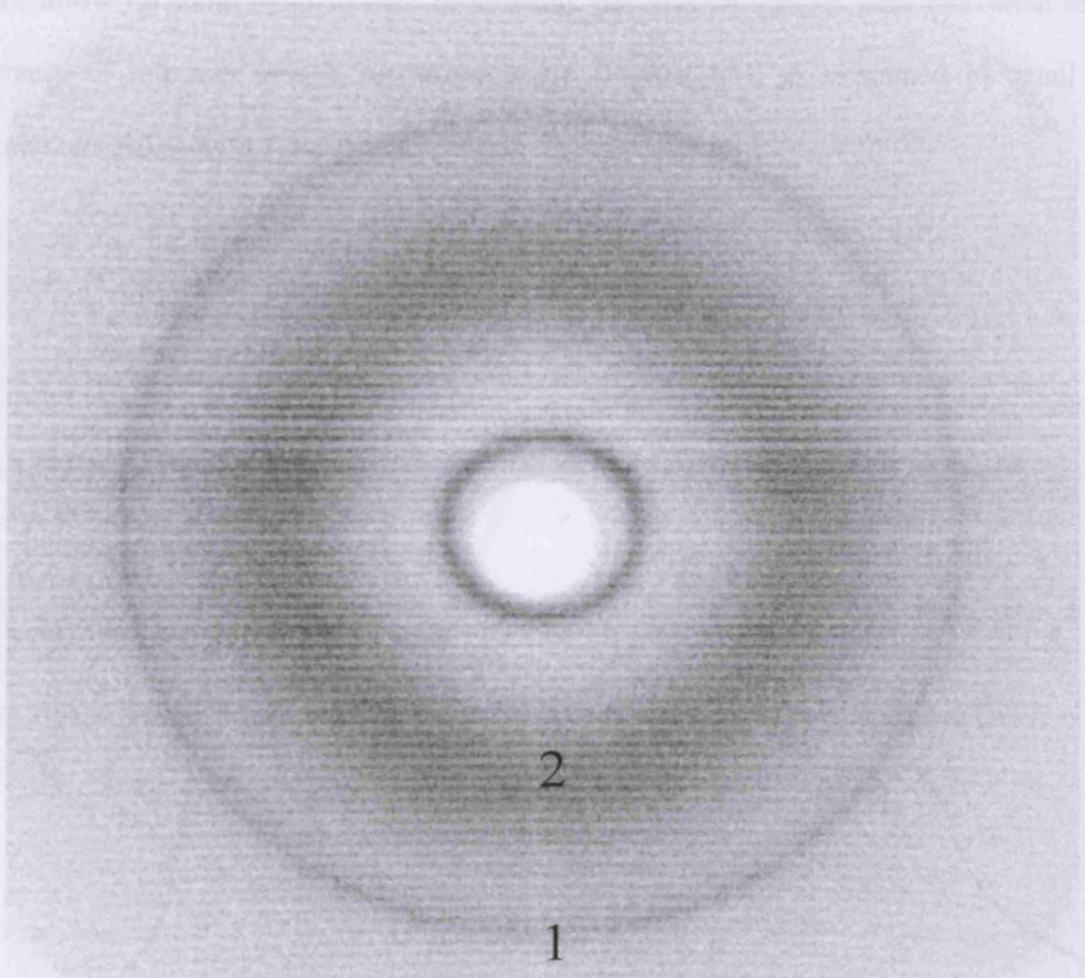

Figure 4.2: WAXS pattern obtained on the NanoSTAR at Cardiff University of salted bovine hide at a sample to detector distance of 4 cm. Allowing dimensions in the region of 10-0.2 nm to be resolved. 1) Helical rise per residue; 2) Amorphous scatter.

X-ray diffraction patterns of collagen obtained by WAXS, display diffraction series corresponding to axial repeating structures. The position of the strong reflection at approximately 0.29nm [88] shown in Figure 4.2 position 1, relates to the axial rise distance (helical rise per residue) between the amino acid residues along collagen molecular triple helices.

To allow for more detailed data processing, the WAXS images were converted to linear traces of intensity versus scattering angle (Figure 4.3), as explained in detail in the methods Subsection 3.4.2.

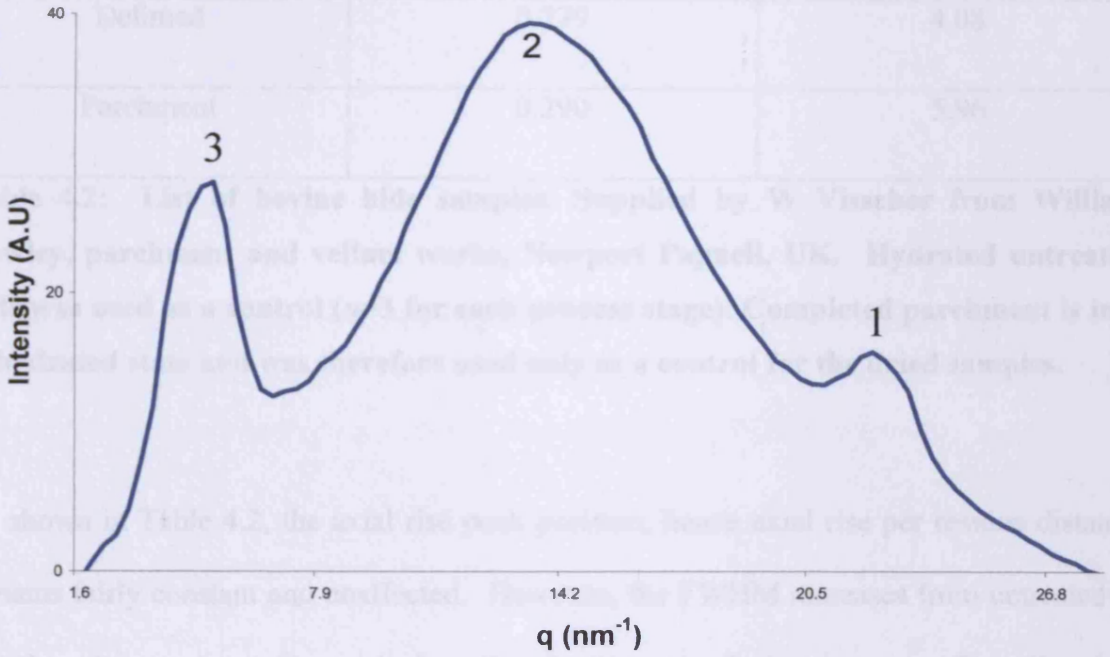

Figure 4.3: Linear intensity profile of the 2D image. Peak 3 is representative of the scatter related to the intermolecular lateral packing of the collagen molecules. Peak 2 contains the amorphous scatter. Peak 1 corresponds to the periodicity of the axial rise per residue.

Peaks 2 and 3 will be discussed later, but for the moment the significant peak is 1, which relates to the helical rise per residue dimension. Peak fitting software PeakFit4 was used to determine the position of peak 1 and also the FWHM value of the peak (Subsection 3.4.3). The result of the peak fitting for the treated bovine hide sample set is shown in Table 4.1.

Bovine Hide	Axial rise per residue (nm) (± 0.022nm)	Full width half maxima (nm^{-1})
Untreated	0.278	3.23
Salted	0.277	3.95
Limed	0.279	4.89
Delimed	0.279	4.08
Parchment	0.290	5.96

Table 4.2: List of bovine hide samples. Supplied by W Visscher from William Cowley, parchment and vellum works, Newport Pagnell, UK. Hydrated untreated hide was used as a control (n=3 for each process stage). Completed parchment is in a dehydrated state and was therefore used only as a control for the dried samples.

As shown in Table 4.2, the axial rise peak position, hence axial rise per residue distance remains fairly constant and unaffected. However, the FWHM increases from untreated to salted, and even more from salted to limed and again further increases from limed to parchment.

4.3.2: Collagen / Amorphous ratio

Gelatinization is caused by a loss of structural order within collagen due to unfolding of the molecules. [89] Dividing the integrated intensity of the peak 3 (Subsection 3.4.3), that accounts for the intermolecular lateral packing of the collagen molecules, by the peak 2 arising from a combination of both collagen and amorphous scatter (gelatin and other non-collagenous materials), it is possible to determine a ratio of collagen to amorphous content within the samples (Table 4.3) [89, 90].

Bovine Hide	I.L.P. Integrated Intensity (peak 3)	Amorphous Integrated Intensity (peak 2)	Collagen/ Amorphous Ratio
Untreated	123.36	872.62	0.14
Salted	206.63	1229.72	0.17
Limed	215.85	1231.38	0.18
Delimed	242.33	1430.99	0.17
Parchment	145.75	803.66	0.18

Table 4.3: Collagen/amorphous ratio of treated bovine hide samples. Calculated by dividing the integrated intensity of the peaks which represent collagen intermolecular lateral packing and amorphous scatter obtained from WAXS images.

Table 4.3 shows that the ratio of collagen to amorphous material increases as the untreated skin is treated with sodium chloride and then slaked lime. This ratio is a comparison of a portion of the collagen scatter compared to almost the entire scatter from the amorphous material. This is not a measurement of the amount of collagen or gelatin in the sample, but is a way of comparing changes between samples.

4.3.3: Molecule to molecule lateral packing

The next step is to examine how the processing affects the interactions between the collagen molecules. It is known that collagen molecules pack together laterally, as shown in Figure 1.10. The rod like shell surrounding the collagen molecules represents the space

between the collagen molecules and contains typically water molecules, which can be associated with the collagen molecules. An X-ray diffraction image displaying the collagen molecule-molecule interactions (I.L.P) observable at 1.2nm [24] is shown in Figure 4.4.

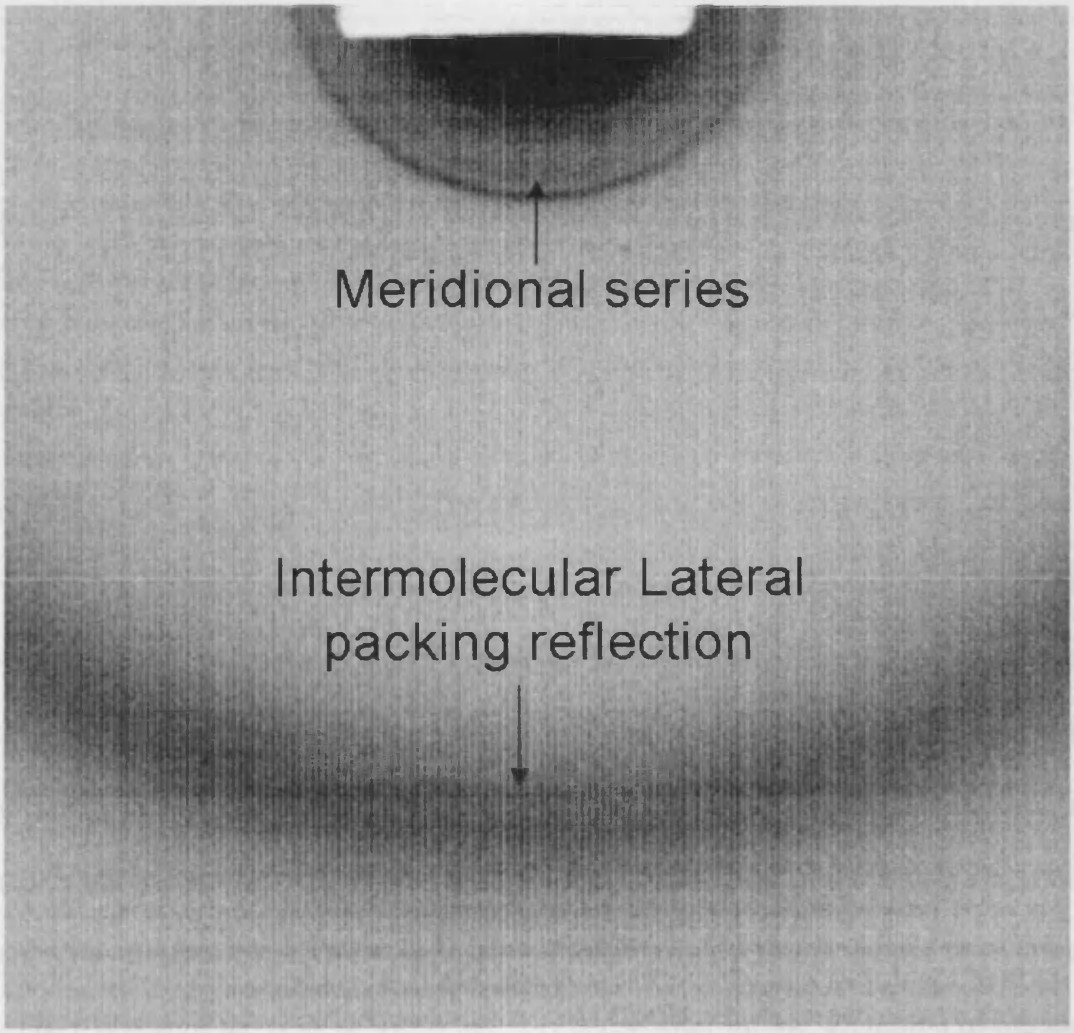

Figure 4.4: A WAXS pattern obtained at SRS Daresbury station 2.1 of limed bovine hide at a sample to detector distance of 1.25m. Allowing dimensions as small as 1nm to be resolved.

Bovine Hide (wet)	Intermolecular lateral packing (nm) (± 0.012nm)	Full width half maxima (nm^{-1})
Untreated	1.40	1.83
Salted	1.49	1.70
Limed	1.55	1.57
Delimed	1.57	1.61

Table 4.4: Collagen intermolecular lateral packing and peak full width half maxima (FWHM) measurements of bovine hide in its hydrated state.

From Table 4.4 it is shown that salting of bovine hide induces an increase from 1.4 to ~1.5nm in the intermolecular lateral packing distance between the collagen molecules in the hydrated state, compared to untreated skin. The FWHM of the intermolecular lateral packing reflection of the diffraction pattern in Figure 4.4 is reduced slightly by salting. These results show that salting induces a greater average distance between collagen molecules but has a minimal effect on the collagen crystallinity. Liming of the bovine hide increases the distance between the collagen molecules by ~0.15 nm compared to untreated skin. The FWHM of the peak at ~1.55 nm is reduced after liming. Deliming of the sample does not appear to have an effect on the intermolecular lateral packing distance, indicating that the liming stage has induced a permanent change in the collagen hierarchical stability.

The samples were dried and the effect on I.L.P. after drying are presented in Table 4.5.

Bovine Hide (dry)	Intermolecular lateral packing (nm) (± 0.051nm)	Full width half maxima (nm^{-1})
Untreated	1.20	1.01
Salted	1.20	1.05
Limed	1.17	1.01
Delimed	1.18	1.02
Parchment	1.16	1.04

Table 4.5: Collagen intermolecular lateral packing and peak full width half maxima (FWHM) measurements of bovine hide in its dehydrated state. Wet samples were air dried.

Table 4.5 shows that after dehydration the collagen molecule-to-molecule distance reduces to ~1.2 nm for all samples and that there is little variation in the FWHM of the intermolecular lateral packing peak.

4.3.4: Quarter Staggered Array (D-period)

Collagen exhibits a number of long-range interactions resulting from axial order and possible substructures within the fibril. One of these substructures is the stagger in the axial direction of the laterally packed collagen molecules. This conformation as shown in Figure 1.7 is known as the quarter staggered array and for simplicity will be termed the D-period. These large scale features can be observed by X-ray diffraction, using small angle scattering. The electron density profile of the D-period produces a diffraction series of sharp reflections on the small angle scattering image as shown in Figure 4.5, panels A and B [91].

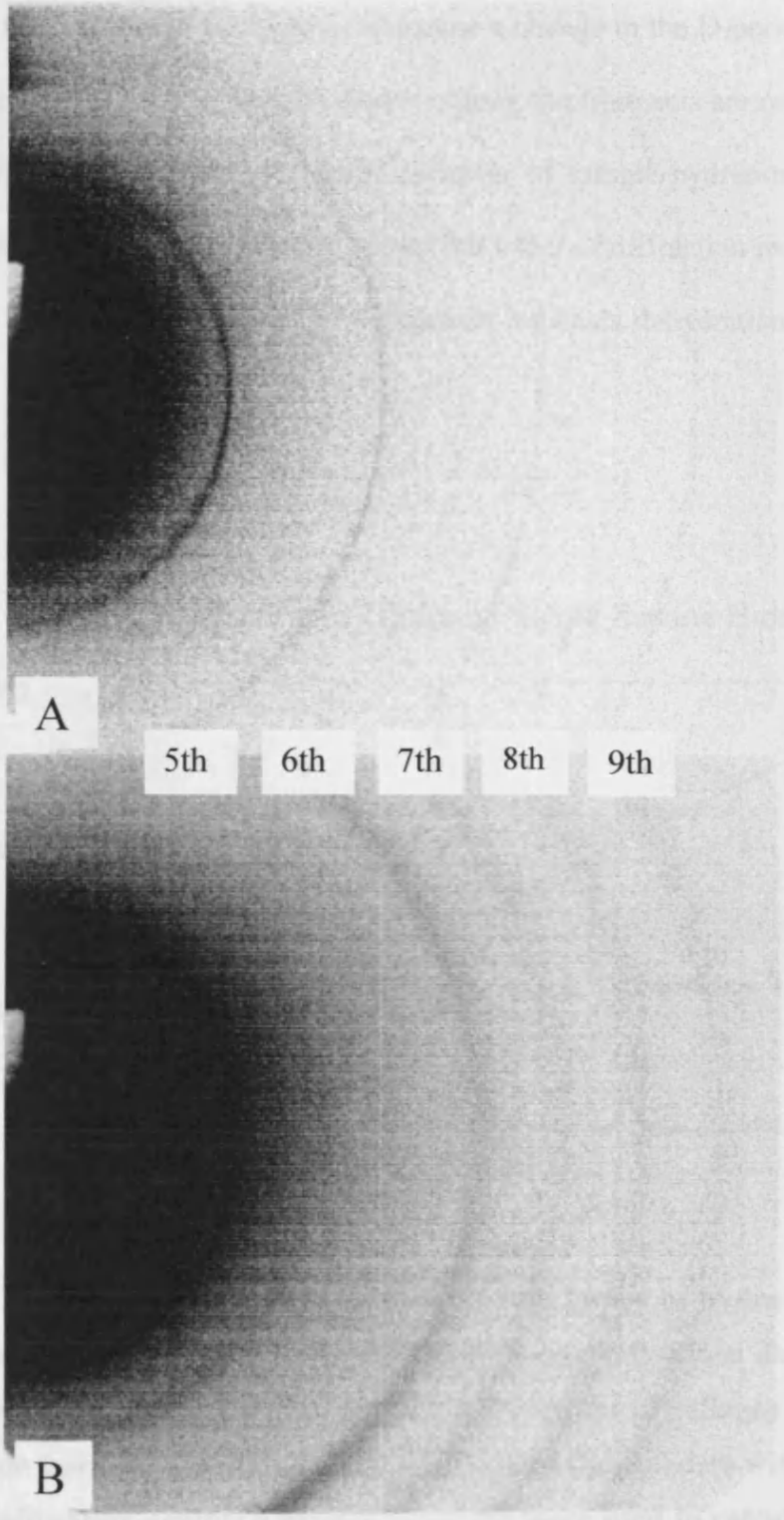

Figure 4.5: A SAXS pattern obtained at SRS Daresbury station 2.1 of bovine hide at a sample to detector distance of 8m. Allowing dimensions in the region of 200nm to be resolved. A) Wet untreated hide; B) Dry parchment. The 5th to 9th axial Bragg reflections have been highlighted.

These sharp reflections can be used to determine a change in the D-period of the collagen molecules as the alteration in electron density along the fibre axis are reflected in changes to the intensity of these peaks. A useful indicator of sample hydration can be obtained from the reflection intensities, where a strong 5th order of diffraction indicates high levels of hydration and a strong 6th order of diffraction indicates dehydration [92] as shown in Figure 4.6.

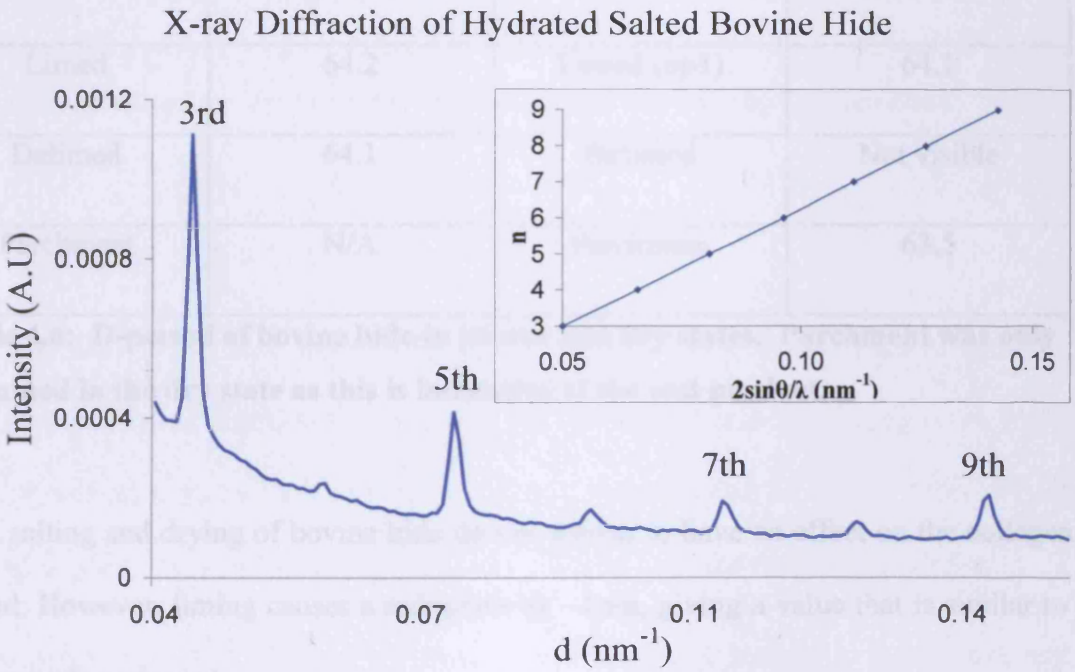

Figure 4.6: A linear intensity profile of the SAXS image of hydrated salted bovine hide represented in Figure 4.5. The orders of Bragg reflections due to the electron density distribution of the gap and overlap interactions of collagen molecules in the axial direction have been included. The positions of these orders with respect to each other, and calibration against a known standard were used to calculate the D-period of the axial gap and overlap. Insert plot is an example of n orders vs $2\sin\theta/\lambda$, where the slope is equal to the d- spacing.

Changes to the D-period have been listed in Table 4.6 for all sample treatments and also the effect of dehydration on bovine hide.

Bovine Hide (WET)	**D-period (nm) (± 0.283nm)**	**Bovine Hide (DRY)**	**D-period (nm) (± 0.141nm)**
Untreated	65.3	Untreated	65.3
Salted	65.0	Salted	64.9
Limed	64.2	Limed (npl)	64.1
Delimed	64.1	Delimed	Not visible
Parchment	N/A	Parchment	63.5

Table 4.6: D-period of bovine hide in its wet and dry states. Parchment was only examined in the dry state as this is indicative of the end product.

Both salting and drying of bovine hide do not appear to have an effect on the collagen D-period. However, liming causes a reduction by ~1nm, giving a value that is similar to the 63.5 nm of parchment.

The effects on the collagen D-period of ovine hide after processing can be seen in Table 4.7.

Ovine Hide (WET)	D-period (nm) (± 0.106nm)	Ovine Hide (DRY)	D-period (nm) (± 0.171nm)
Untreated	64.6	Untreated	64.7
Limed	63.8	Limed	Not visible
Split Limed	64.0	Split Limed	63.5
Parchment	N/A	Parchment	63.7

Table 4.7: D-period of ovine hide in its wet and dry states. The limed sample in the dry state did not give a clear diffraction image to allow for data analysis. Parchment was only examined in the dry state as this is indicative of the end product.

The untreated ovine hide samples have a D-period (Table 4.7), which is almost 1nm smaller than that of untreated bovine hide (Table 4.6). Again the liming of the hide has induced a shortening of the D-period by about 0.8nm, similar to bovine hide. Drying of the samples does not appear to have a significant effect on the collagen D-period.

As an in-house control, rat hide was processed in a similar manner to parchment, and the results of the D-period measurements can be seen in Table 4.8.

Rat Hide (WET)	D-period (nm) (± 0.170nm)	Rat Hide (DRY)	D-period (nm) (± 0.314nm)
Untreated	64.6	Untreated	64.6
Salted	64.8	Salted	64.9
Limed	62.9	Limed	63.6

Table 4.8: D-period of rat hide in its wet and dry states. Parchment of rat hide was not within the sample set.

Untreated rat hide has a D-period similar to that of ovine hide. The salting of the hide induces an increase of the D-period by 0.2nm. After liming there is a decrease in D-period length concurring with the results for both bovine and ovine hide. However, even though the untreated D-period is similar to ovine, which might be indicative of a looser weave, the D-period after liming is reduced more, possibly due to the thin hide allowing a deeper penetration of the lime solution.

4.3.5: Fibril Diameter and Packing

As shown in Figure 1.7, collagen forms into microfibrils and further into fibrils, which in skin are typically in the dimensions of 40-100 nm [44]. As with the principle that smaller X-ray scattering angles allowed for the determination of the larger dimensions of the D-period in comparison with wider angles being used to determine the smaller molecular dimensions of helical rise per residue, even smaller angles allow for the determination of these large collagen fibril diameters.

The scattering from a fibril is conveniently represented by the scattering of a solid cylinder with a given diameter (Subsection 2.8). The scattering function of such a cylinder is conveniently described as a first-order Bessel function (for example Eikenberry et al., 1982) [74]. The ultra small-angle X-ray scattering (USAXS) pattern of bovine hide (Figure 4.7), obtained at station ID02 of the ESRF, gave a sufficient resolution to determine scattering features due to the convolution of the Bessel function from the cylindrical nature of the collagen fibrils and the interference function due to the interactions between neighbouring fibrils [25, 28].

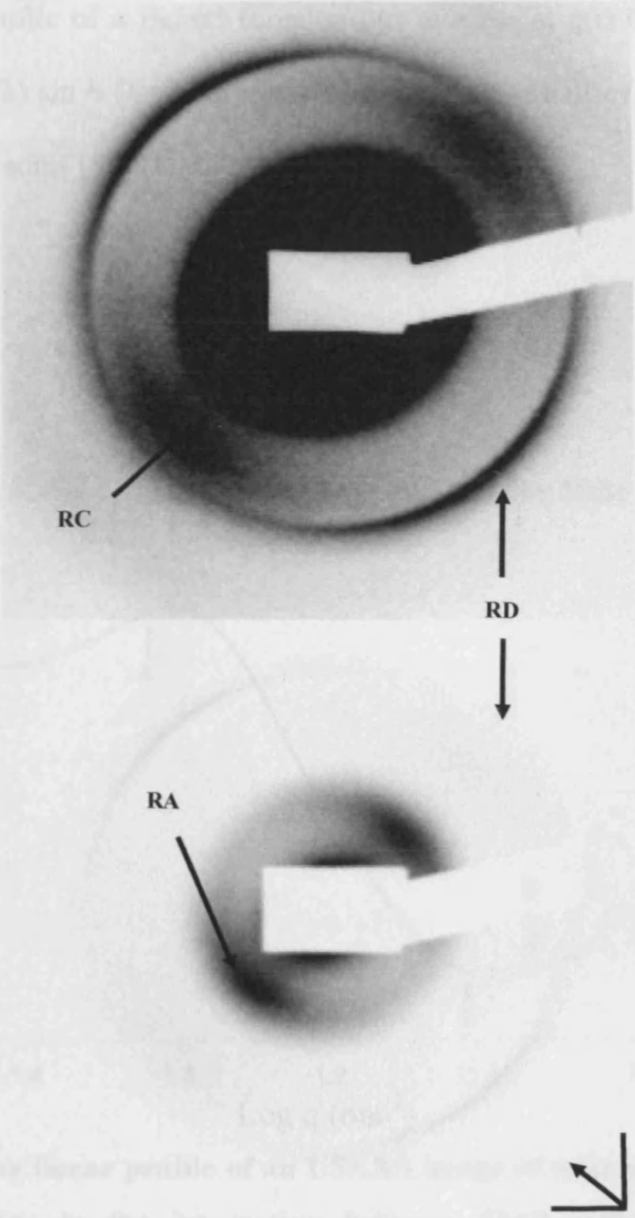

Figure 4.7: USAXS pattern of limed bovine skin obtained at ESRF station ID02. The top and bottom images are used to illustrate how adjusting the minimum and maximum intensity limits of the same image can highlight the features present within the diffraction pattern. The sample to detector distance was 10m, which was sufficient to observe: RA) The interference due to the interaction between fibril cylinders; RC) The 5.14 maxima of the fibril cylinder Bessel function; RD) The 1st order Bragg reflection due to the electron density distribution of the gap and overlap interactions of collagen molecules in the axial direction. Orientation of the long fibre axis is indicated by the arrow on the bottom right of the figure.

A linear intensity profile of a Bessel function has maxima at q(r) 0.0, 5.14. 8.42, 11.6, 14.8, where $q = (4\pi/\lambda) \sin \theta$ (λ= X-ray wavelength and θ = half of the scattering angle) and r is the cylinder radius [88] (Figure 4.8).

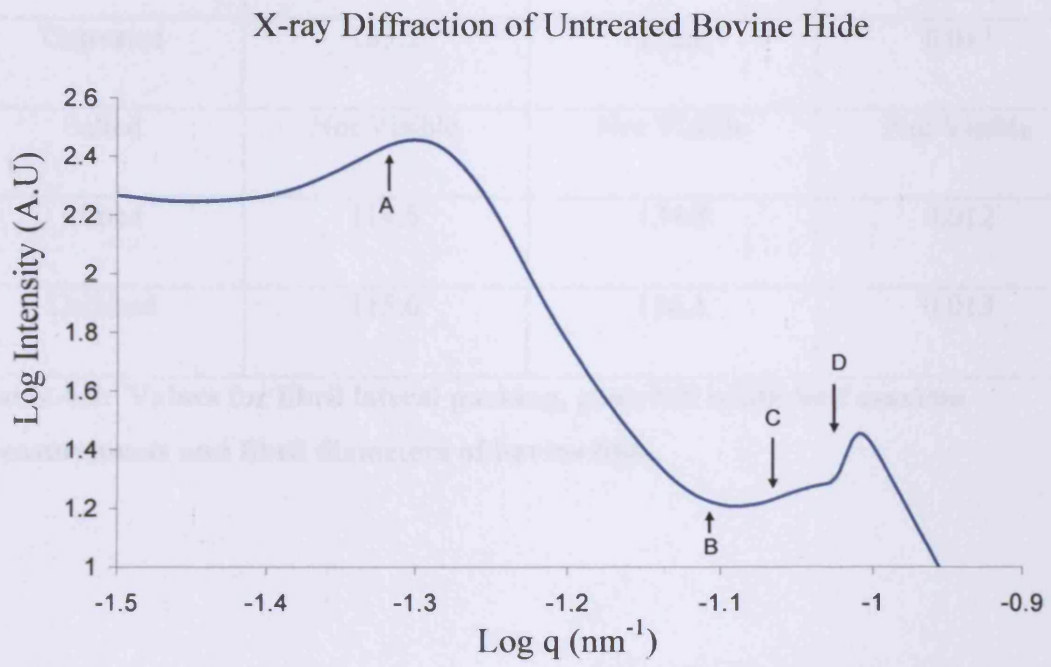

Figure 4.8: A log-log linear profile of an USAXS image of untreated bovine hide. A) The interference due to the interaction between fibril cylinders. B) The 3.83 minimum of the fibril cylinder Bessel function. C) The 5.14 maximum of the fibril cylinder Bessel function. D) The 1st order Bragg reflection due to the electron density distribution of the gap and overlap interactions of collagen molecules in the axial direction.

Plotting the normalized intensity from a cylindrical object against q (Figure 4.8), the collagen fibril radii were obtained from the position of these maxima in reciprocal space as shown in Table 4.9.

Bovine Hide Wet Samples	**Fibril Diameter (nm) (± 2.33nm)**	**Fibril Lateral Packing (nm) (± 1.13nm)**	**Full width half maxima (nm^{-1})**
Untreated	103.2	122.6	0.013
Salted	Not Visible	Not Visible	Not Visible
Limed	114.5	134.8	0.012
Delimed	115.6	136.1	0.013

Table 4.9: Values for fibril lateral packing, peak full width half maxima measurements and fibril diameters of bovine hide.

The interference function is dependent on the relative positions of the cylinders (fibrils), and a linear intensity profile against the scattering vector q can be used to determine the nearest neighbour centre-to-centre spacing [74]. Table 4.9 shows that after liming the fibril diameter increases by ~11 nm and that deliming of the sample does not appear to have an effect on the packing at the suprafibrillar level. The mean centre-to-centre distance from Table 4.9 shows that liming of the bovine hide increases the distance between the fibrils. The full width half maxima of the interference function (Figure 4.8) do not change, indicating that there is no change in the level of disorder or crystal size. Deliming seems not to have any effect on the collagen fibril packing.

4.3.6: Effects of processing at the molecular level – microfocus analysis

Previous X-ray images have been taken with the beam direction travelling from the grain side through the sample to the flesh side, giving average scattering of the sample depth. A microfocus beam at ESRF station ID13 made it possible to align the beam in a direction perpendicular to the grain/flesh, allowing a cross section scan to be obtained as shown in the light microscope image of bovine hide (Figure 4.9).

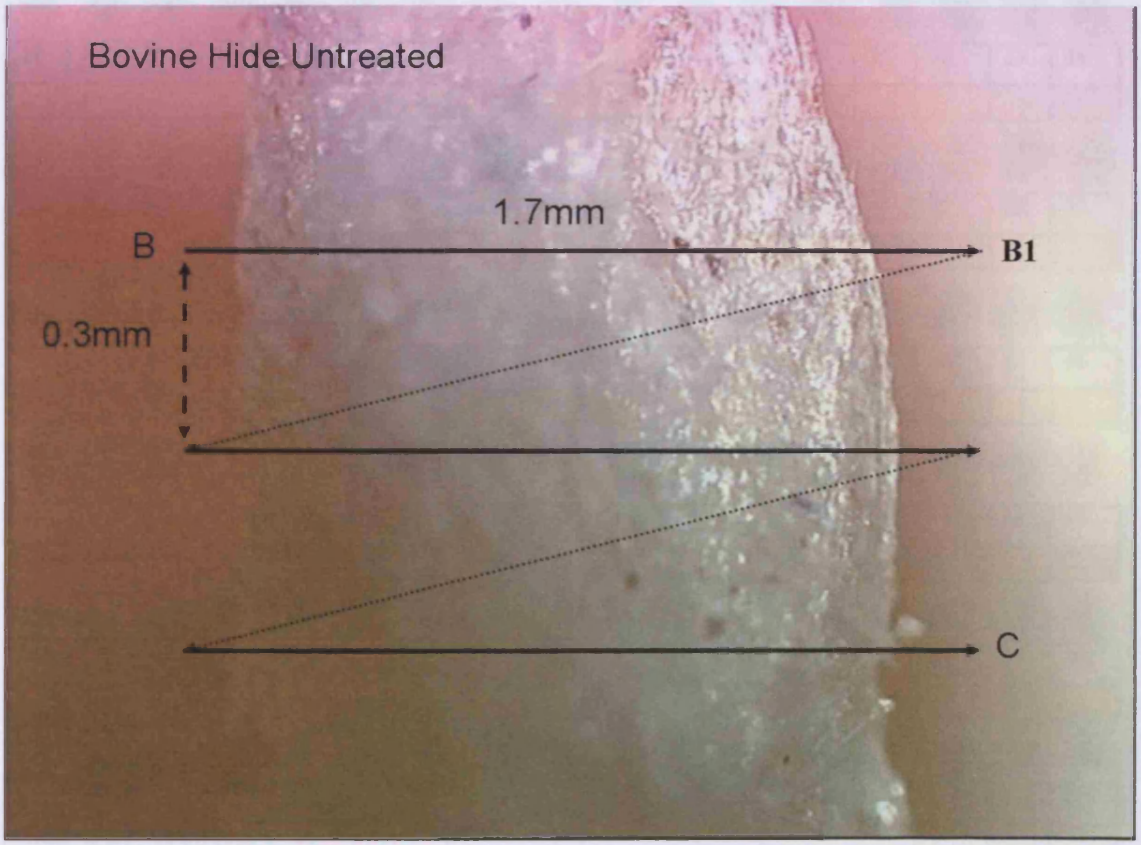

Figure 4.9: A light microscope image of bovine hide with the sample positioned in the direction of the microfocus beam. The scan started at a point before the grain side (B) and images were taken in 10 micron steps, across the sample to point B1, just after the flesh side. In the case of untreated bovine hide the scan distance was over 1.7mm, with 171 scans taken per row. Point C was the final end point. Image scale has been estimated.

Figure 4.10 is representative of the cross sectional scan from B to B1 of untreated bovine hide shown in Figure 4.9. At wide angles the collagen, lipid and mineral features were observed.

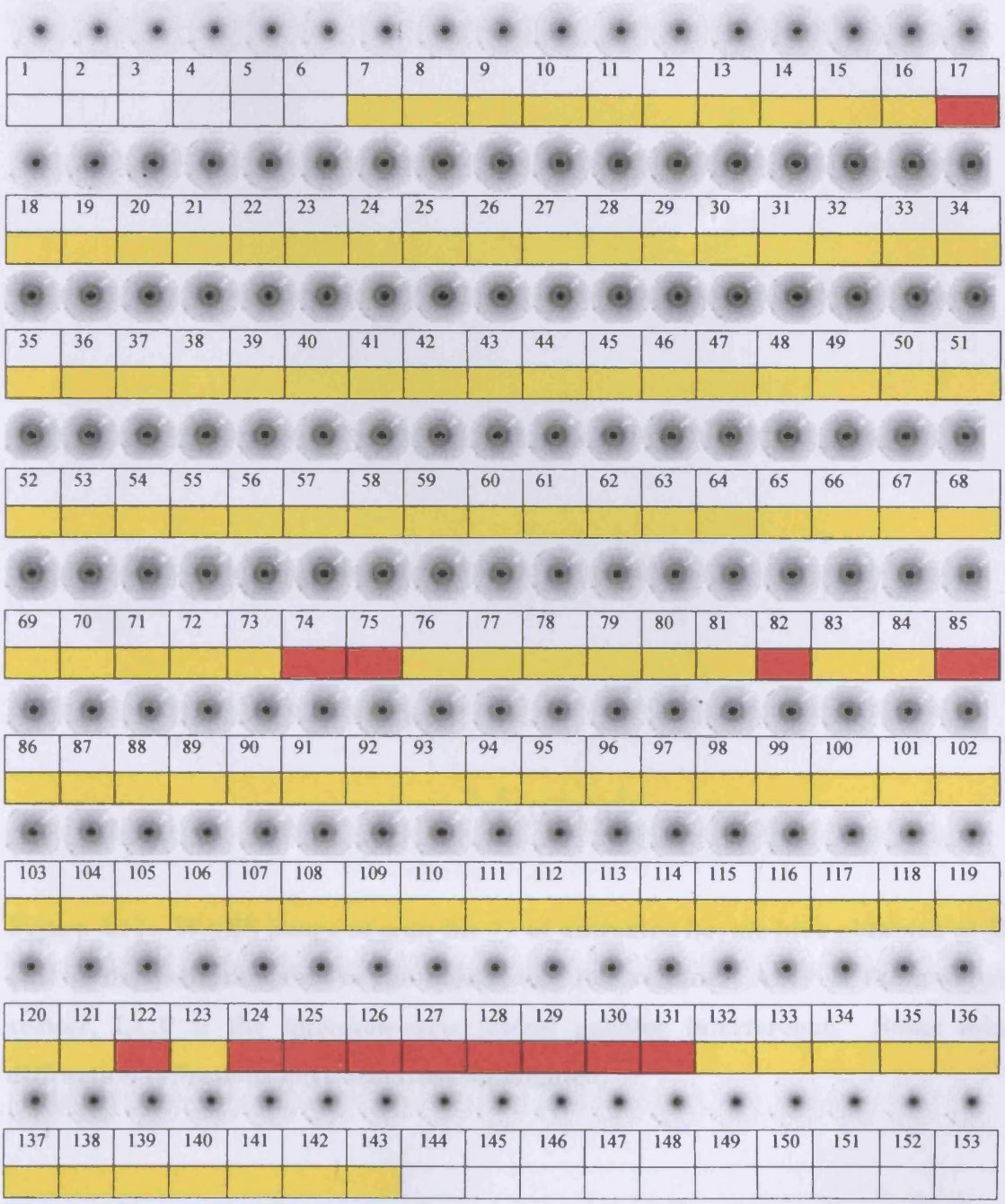

Figure 4.10: A microfocus scan of untreated bovine hide. Scan is from left (file 1) to right (file 153). Yellow blocks represents the presence of collagen molecules. Red blocks represent the presence of mineral reflections and collagen. White blocks indicate that there is no collagen, or mineral present at that position on scan.

The X-ray image for file 74 showing reflections from mineral and collagen has been expanded and are shown in figure 4.11.

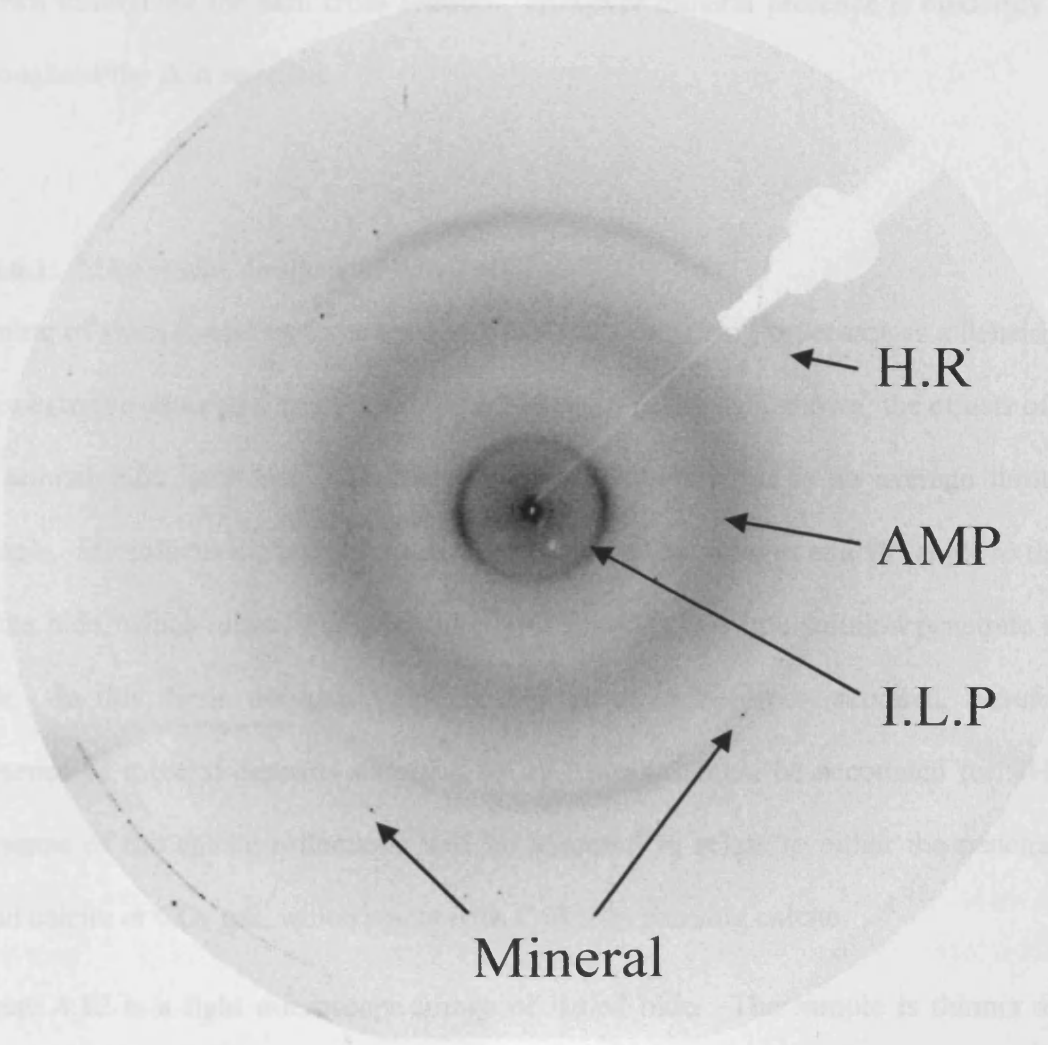

Figure 4.11: WAXS image of scan file 71 of untreated bovine hide obtained at ID13. H.R is the reflection due to the helical rise per residue. AMP is the amorphous scatter, I.L.P is the intermolecular lateral packing interference. Some mineral diffraction reflections have also been highlighted.

These are typical of collagen diffraction, showing the reflections due to collagen intermolecular lateral packing, helical rise per residue and amorphous scatter. File 74 also contains mineral diffraction spots. The presence of collagen and orientation is clearly shown throughout the skin cross section. However mineral presence is randomly spaced throughout the skin samples.

4.3.6.1: Microfocus analysis of limed skin

Liming of skins is known to be used in many manufacturing processes as a dehairing step or in extreme cases as a gelatinization process. As previously shown, the effects of liming on animal hide have been quantitatively measured, but this is an average through the sample. Microfocus diffraction makes it possible to take images at a 90° angle to the plane of the hide, which allows questions like how far does the lime solution penetrate into the hide. In this thesis the assumption is that the hide becomes saturated, therefore, the presence of mineral deposits observed by microfocus, must be accounted for. Here the presence of the calcite reflections will be assumed to relate to either the penetration of solid calcite or CO_2 gas, which reacts with $Ca(OH)_2$ forming calcite.

Figure 4.12 is a light microscope image of limed hide. The sample is thinner and less intact than that of untreated hide. The scan in this case was still 10 micron steps, but only 140 steps were required to scan the cross section of the hide.

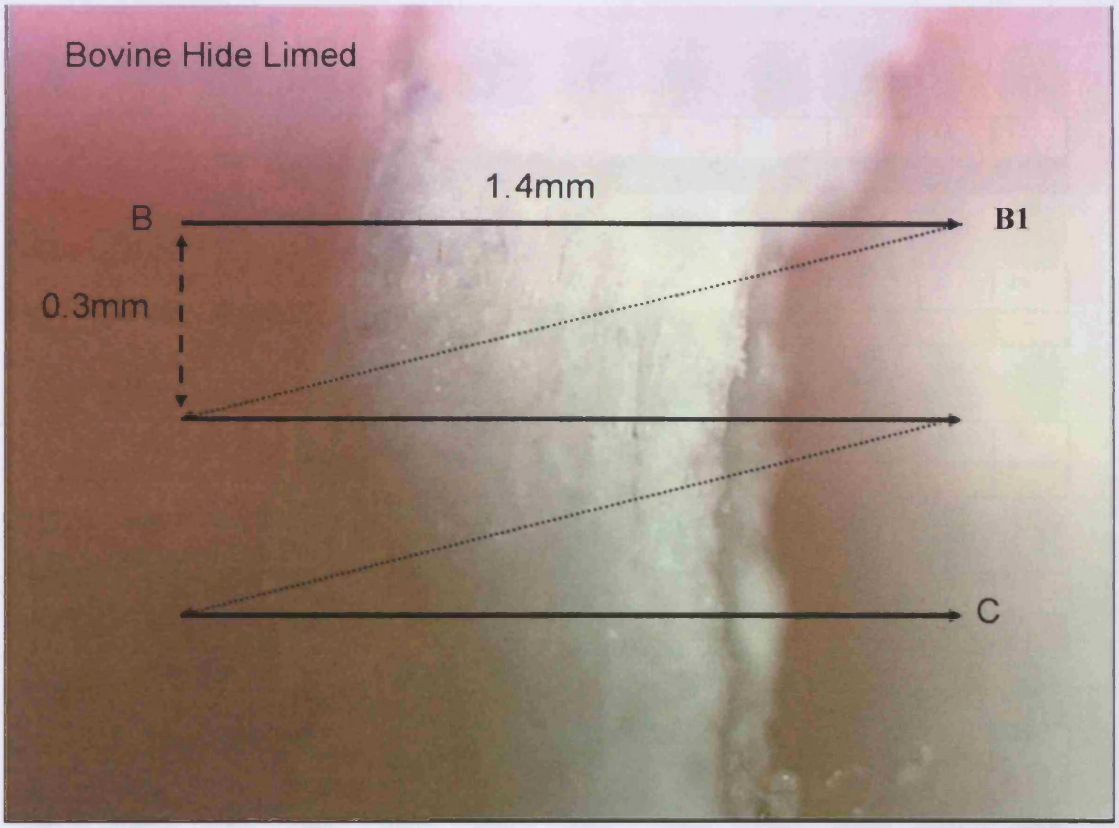

Figure 4.12: A light microscope image of limed bovine hide with the sample positioned in the direction of the microfocus beam. The scan started at a point before the grain side (B) and images were taken in 10 micron steps, across the sample to point B1, just after the flesh side. In the case of limed bovine hide the scan distance was over 1.4mm, with 141 scans taken per row. Point C was the final end point. Image scale has been estimated.

The complete scan of the limed hide is shown in figure 4.13, with the presence of collagen, lipid and mineral highlighted.

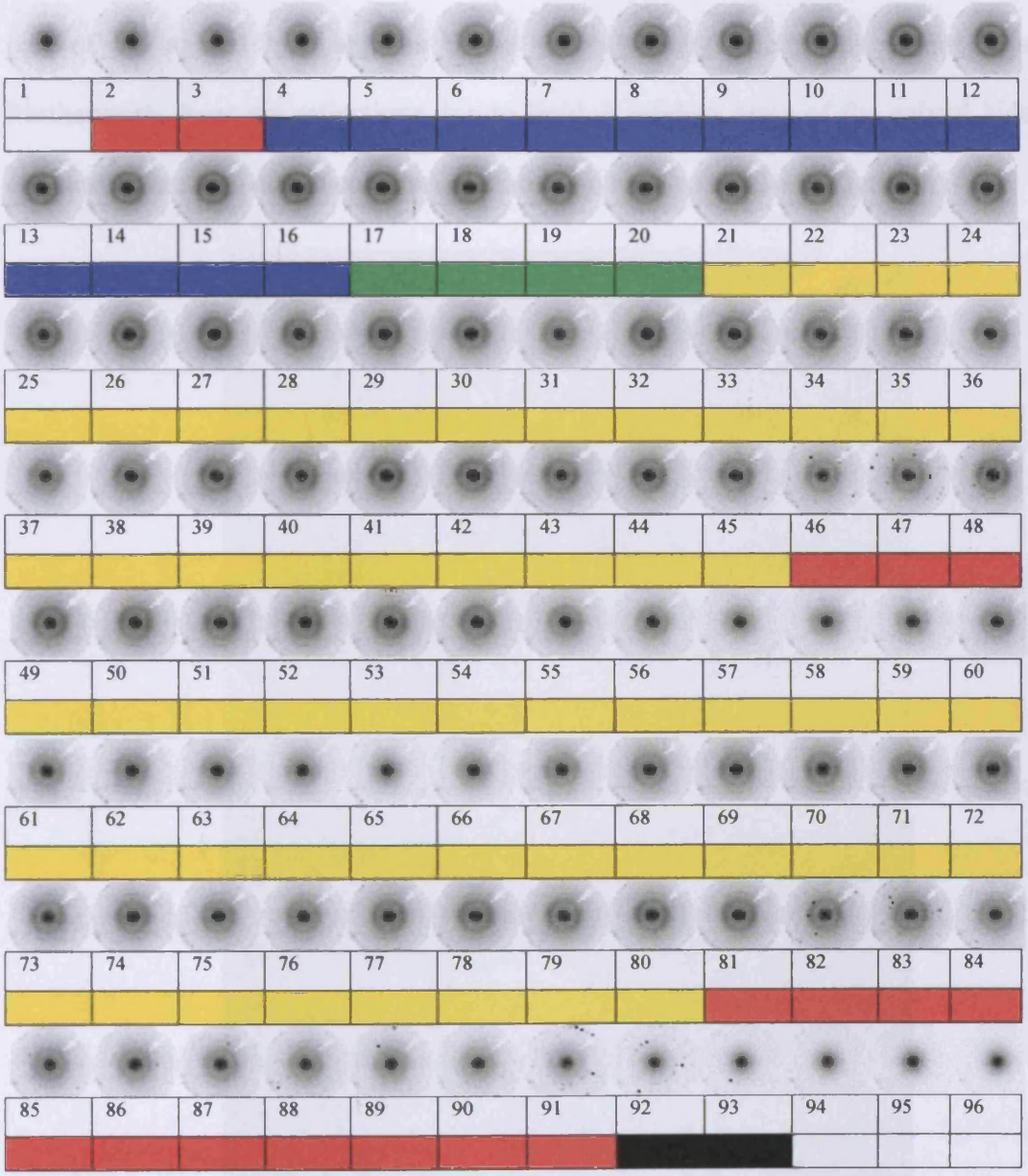

Figure 4.13: A microfocus scan of untreated bovine hide. Scan is from left (file 1) to right (file 96). Yellow blocks represent the presence of collagen molecules only. Red blocks represent the presence of collagen and mineral; blue blocks represent the presence of collagen, mineral and lipid; dark green blocks represent the presence of collagen and lipid; black represents mineral reflections; white blocks indicate that there is no collagen, lipid or mineral present at that position on scan.

As can be seen in figure 4.13 it is clear that mineral reflections indicate that there is limited penetration of solid calcite or CO_2 into the animal hide. This may indicate that the central part of the animal hide appears to be untouched by calcite that is not in solution. Furthermore, there are reflections due to lipid at random areas of the animal hide. File 9 contains reflections due to collagen, mineral and lipid as shown in Figure 4.14.

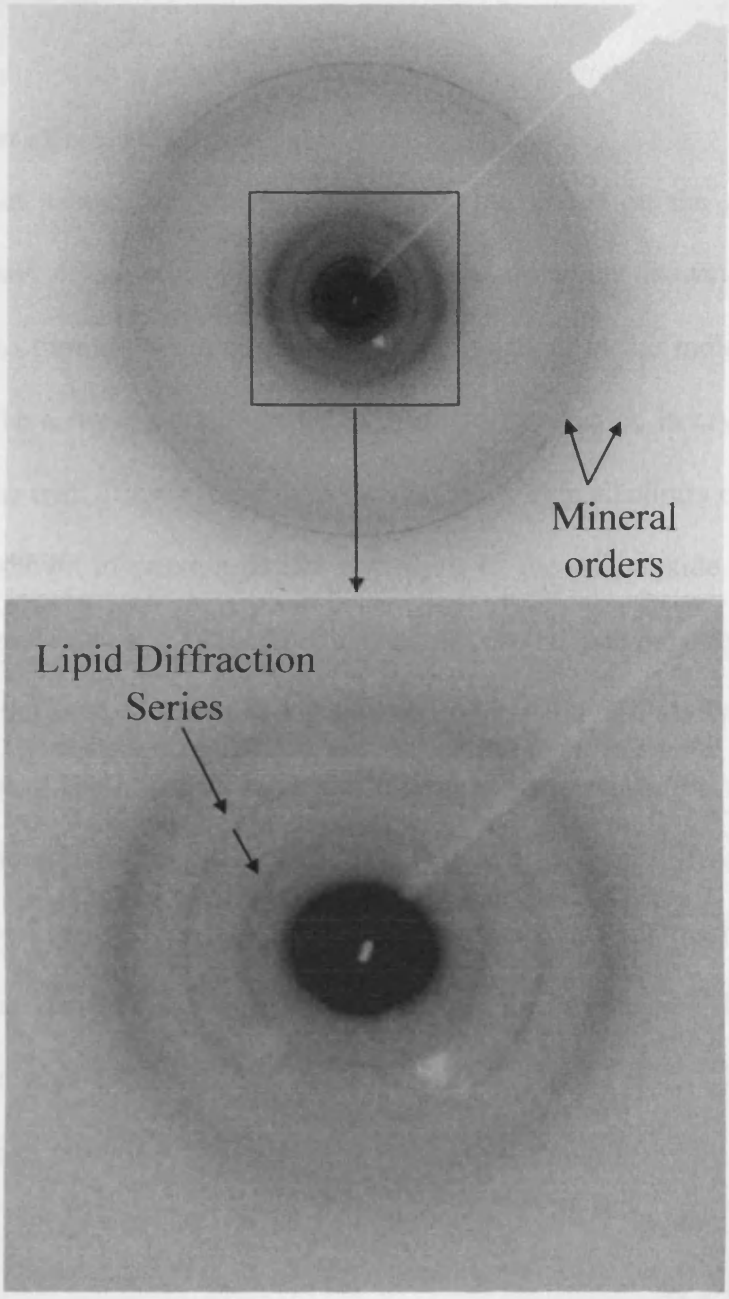

Figure 4.14: An X-ray pattern of limed bovine hide obtained on the microfocus beamline ID13. File 9 from the scans shown in Figure 4.13, highlighting the presence of lipid (zoomed excerpt from top image) and mineral reflections.

The expanded image of file 9 of the limed sample shows the ordered calcite mineral rings. The zoomed in image of the centre also shows the presence of lipid orders.

4.4: Discussion

4.4.1: Treatment effects at the molecular level

Results show that salting and liming do not have an effect on the distance between constituent residues of the collagen helix in the axial direction. However, the increased peak width due to liming gave a clear indication of changes at the molecular level. This broadening may be a result of an increase in disorder, a reduction in crystallite size, or a combination of the two. These effects could be due to the high alkalinity of the lime liquor, which has been shown to cause a partial hydrolysis of the polypeptide backbone and to hydrolyze the amide groups [93]. The hydrolysis of the polypeptide chains may be expected to alter the axial rise per residue distance at the point of hydrolysis; alternatively, several breakages in the collagen helix could lead to local relaxation of structure. The change of the amino acids from the L to D forms may have an effect on the distance between neighbouring residues [89, 94]. Results indicate that although there is not an overall change in axial rise per residue distance, after salting or liming there is a breakdown in the local order, which could be explained by local effects such as hydrolysis and racemisation.

4.4.2: Treatment effects on collagen to collagen molecule interactions

Salting of bovine hide increases the intermolecular lateral packing between collagen molecules and increases the level of disorder. This indicates that water or salt may be entering the spaces between the collagen molecules within the fibrils and that the fibrils are expanding. Following liming, the intermolecular lateral packing peak becomes narrower, indicating that there may be a reduction in local disorder. The results demonstrate that this is accompanied by a swelling at the molecular level. The presence of Ca^{2+} ions from the lime is thought to cause an influx of water molecules causing the fibres to swell [3]. The high alkalinity of the lime solution shifts the iso-electric point causing some of the charges along the molecule to change, altering the side chain interactions between the molecules. This, combined with hydrolysis of the side chains, which reduces the number of sites available for salt bridge cross linkages, may cause a lowering of stability [95]. Weakening of intermolecular collagen interactions and the influx of water may cause the loosening of the fibre network as found here.

4.4.3: Treatment effects on the quarter staggered array (D-period)

There was a reduction in D-period after liming, which is most likely due to a change in the fibrillar structure in the axial direction. The weakening of side chain interactions due to hydrolysis and the change in the isoelectric point induced by the high alkalinity of the lime liquor may allow the possibility of the collagen molecules to move past each other. Drying of the samples does not appear to have a further effect on the D-period indicating that the contraction is due to liming and not dehydration.

4.4.4: Treatment effects on fibril diameter and packing

Collagen interactions with proteoglycans are fundamental to fibril diameter and packing. Proteoglycans are involved in dissipating compression stresses in the skin and are also involved in alignment of collagen fibrils [96]. The polysaccharide hyaluronan connects the decorin protein cores associated with dermatan sulfate bridges, which act as a compression resistive bridge between the fibrils. Salting of skin has been shown to remove up to 100% of the hyaluronan [3], but it requires the liming stage to remove over 50% of dermatan sulfate. The removal of hyaluronan may release the pressure constraint on the fibrils, allowing the collagen fibrils to expand, and the "opening up" of the collagen fibres. The results here show that after salting there is an increase in the distance between the collagen molecules in the hydrated state, and even more expansion after liming, which is carried through the hierarchical levels up to fibril packing; deliming did not appear to reverse these increases, indicating that the effects of salting and liming are permanent. The removal of non-collagenous material due to the lime liquor is responsible for the increase in the collagen/amorphous ratio, indicating that there is less amorphous material in comparison to collagen. If the collagen ratio had decreased, this would have indicated that the collagen molecules had become denatured. However, our results imply that the collagen structure and hierarchy, although weakened, are still relatively stable.

4.4.5: Microfocus analysis on the liming of bovine hide

The penetration of solid calcite or CO_2 gas, which reacts with $Ca(OH)_2$ forming calcite into the animal hide has been shown to be limited to about 170 μm. If the hypothesis, that calcite reflections are an indicator of penetration into the animal hide, then it would be interesting to examine whether this could be related to how much liming solution and treatment is required to make the ideal parchment. The environmental impact of reducing

lime solutions is an important area for research. Also the duration of hide soaking in liming solution, can be fundamental in the predisposition of complete parchment to degradation. The presence of lipid in parchment as shown by Ghioni et al, (2005) [97] and their suggestion that its presence is possibly due to endogenous skin lipid, seems to be confirmed.

4.5: Publication

Parts of the work presented in this chapter appear in the publication:

Maxwell, C.A., T.J. Wess, and C.J. Kennedy, *X-ray diffraction study into the effects of liming on the structure of collagen.* Biomacromolecules, 2006. 7: p. 2321-2326.

Chapter 5: X-ray Diffraction Study into the Effects of Solvents on the Structure of Collagen

5.1: Introduction

In Chapter 4, the parchment-making process, specifically the effects of salting and liming on animal hides, and in particular their collagen structure [98] was described. Salting of parchment removed the non-collagenous components of the skin, whilst liming increased the lateral distance between neighbouring molecules and reduced the axial D-period of the collagen.

The steps in the parchment-making process are generic and representative of general hide treatments and finishing procedures, resulting in a variety of collagen-based products. It has been shown that the collagen stability is altered by not only the chemicals used to preserve and de-hair hides, but also the manner in which these steps are applied [53]. Harsh treatments of hides at the manufacturing stage can result in parchments with poorer hydrothermal stability, resulting in an accelerated degradation of parchment over time. The study presented in this chapter focussed on a set of historic parchment samples known to have been processed with the solvents acetone (propan-2-one) and 2-ethoxy ethanol with the aim of producing a higher quality writing material by degreasing the parchment.

To examine the effects of these treatments, this study utilised the techniques of small angle X-ray scattering (SAXS), wide angle X-ray scattering (WAXS) and Fourier transform infra-red spectroscopy (FT-IR) to describe the long and short range structural and chemical effects of these treatments respectively.

5.2: Experimental

5.2.1: Sample preparation

A variety of caprine (goat) and ovine (sheep) hide samples taken from different stages of a known and well recorded parchment-manufacturing process were gifted by Chris Clarkson. The two species of skin used for this trial were from Abyssinian hair sheep and Javanese goat. All hides had been soaked by the manufacturer in a 0.5% chloros antiseptic solution (sodium hypochlorite) before being processed. The oxidizing effects of chloros on the hierarchy of collagen have not been examined in this study. However, for the purposes of this study, the effects of the acetone and 2-ethoxy ethanol solutions have been compared to that of limed samples. Six different treatments had been used by the manufacturer on both caprine and ovine hides (Table 5.1).

Samples	Treatments					
1	2% Liming 8 days, Unhaired, Scudded, Fleshed	1hr 100% 2-ethoxy ethanol	Toggled, Dried, Finished			
2	2% Liming 8 days, Unhaired, Scudded, Fleshed	2 hrs 150% Acetone	Toggled, Dried, Finished			
3	2% Liming 8 days, Unhaired, Scudded, Fleshed	1 hr 80% Acetone, 1hr 80% 2-ethoxy ethanol	Toggled, Dried, Finished			
4	2% Liming 7 days, Unhaired, Scudded, Fleshed	1 hr 80% Acetone, 1hr 80% 2-ethoxy ethanol	Poor quality	Re-limed for 4 days	1 hr 80% Acetone, 1hr 80% 2-ethoxy ethanol	Toggled, Dried, Finished
5	2% Liming 8 days, Unhaired, Scudded, Fleshed	1 hr Acetone, 1hr 65% 2-ethoxy ethanol	Toggled, Dried	1% SUMAC tanning solution	1 hr 65% Acetone, 1hr 65% 2-ethoxy ethanol	Toggled, Dried, Finished
6	2% Liming 8 days, Unhaired, Scudded, Fleshed	1 hr Acetone, 1hr 65% 2-ethoxy ethanol	Toggled, Dried	Potash alum tanning	Finished	

Table 5.1: Sample list and process treatments applied to caprine (C goat) and ovine (O sheep) hide. Caprine samples will be labelled as C1-C6 and ovine samples O1-O6.

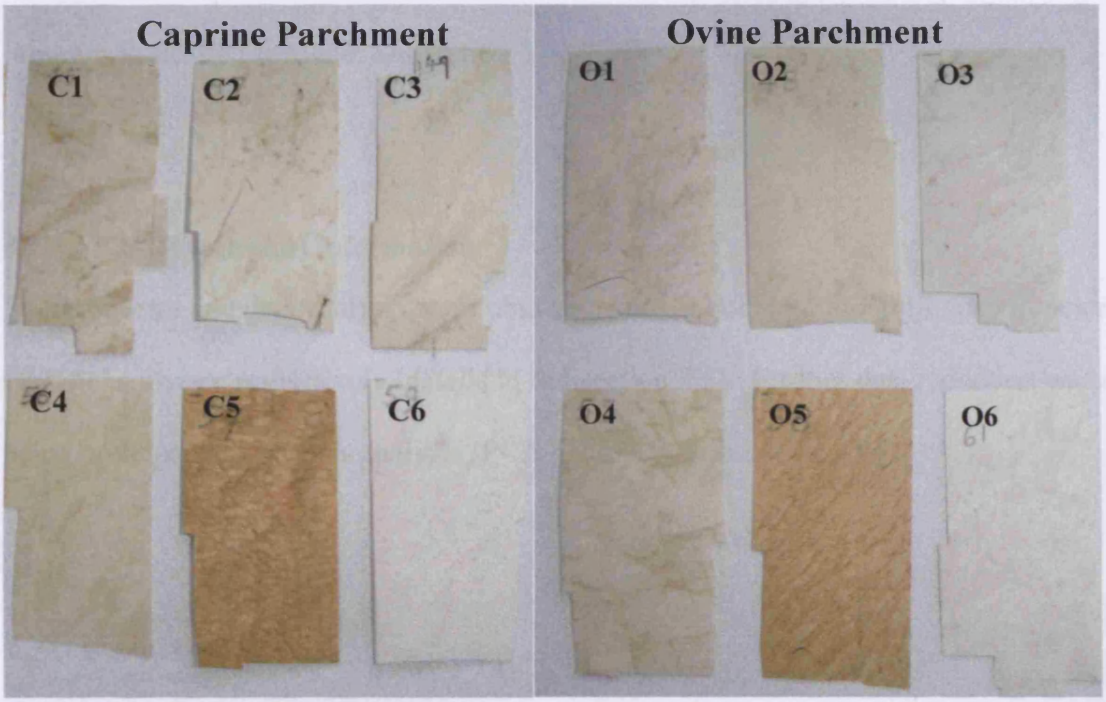

Figure 5.1: Image of samples of caprine and ovine hide treated with acetone (propan-2-one) and 2-ethoxy ethanol as per the protocol in Table 5.1. Samples gifted by Chris Clarkson.

5.2.2: X-ray technical detail

The ultra small angle X-ray scattering images (USAXS) patterns of bovine hide obtained at station ID02 of the European Synchrotron Radiation Facility (ESRF), Grenoble, France, (details Subsection 3.3.3) gave a sufficient resolution to determine scattering features due to the cylindrical nature of collagen fibrils and the interference between fibril structures. Hydrated rat tail tendon was used as a calibration standard.

WAXS images were collected on the Bruker NanoSTAR small angle X-ray scattering station at Cardiff University, (details in Subsection 3.2).

The two-dimensional diffraction images were converted into one dimensional linear intensity profiles using the CCP13 (Collaborative Computational Project 13) program

FibreFix. Analysis of the linear profiles was done using the AISL software, peak fitting program PeakFit4 (details in Subsection 3.4).

5.2.3: FT-IR technical information

FT-IR spectra and data analysis were obtained using a Nicolet 380FT-IR spectrometer and OMNIC software respectively (details in Subsection 3.5). Further data reduction was done using principal components analysis (PCA, details in Subsection 3.6).

5.3: Results

5.3.1: The effects of acetone and 2-ethoxy ethanol on the collagen D-period

As explained in Chapter 2, scattering by X-rays at small angles (<6° at $\lambda = 0.154$nm) gives information regarding the long range order of structures; it is a process that is experimentally similar to the better known X-ray diffraction; however, this technique uses a longer sample-to-detector distance that allows longer periodicities and particle sizes, up to several hundred nanometres in length, to be investigated. Collagen fibrils from skin display a fundamental axial periodicity of 65.5nm [99]which falls into the range of SAXS. The periodicity, or D-period, is a result of regular fluctuations in the electron density of collagen in the axial direction [12, 26]. This is manifested in SAXS as a series of sharp Bragg reflections on the meridian of the small angle scattering image (Fig. 5.1) [39].

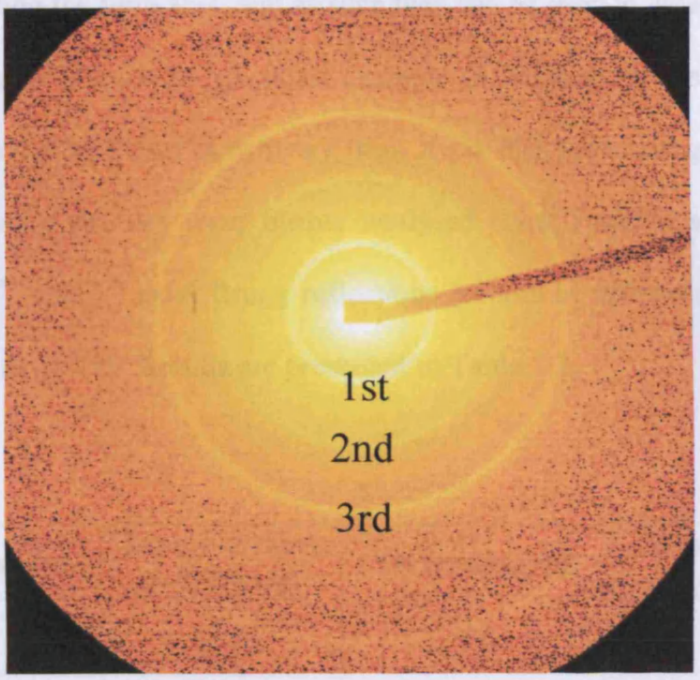

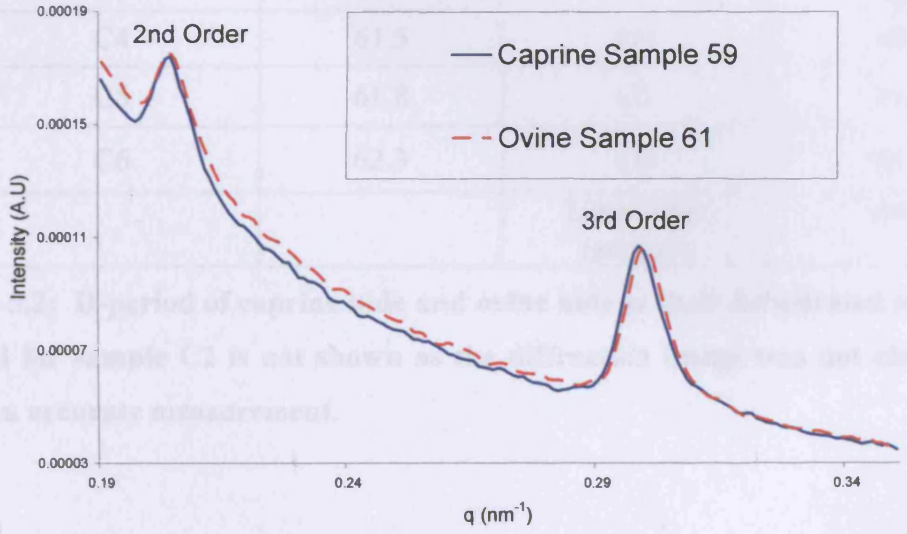

Figure 5.1: X-ray diffraction of ovine and caprine hide at station ID02 at ESRF. Top) Diffraction image of caprine hide sample. Sample to detector distance of 10m, was sufficient to observe the 1st, 2nd and 3rd order Bragg reflections due to the electron density distribution of the gap and overlap interactions of collagen molecules in the axial direction. Bottom) Linear intensity profile of caprine and ovine X-ray diffraction 2D images obtained using CCP13 FibreFix software.

The intensity and position of these Bragg peaks is a reflection of the alteration of the electron density along the fibre axis, and as such they can be used to determine changes in the collagen D-period. Figure 5.1 gives an example of intensity versus scattering angle linear profile generated by FibreFix software from X-ray diffraction images of caprine and ovine hide. The linear profiles were further analysed using Peakfit4 software, and the positions of the 2nd and 3rd axial Bragg reflections (orders of diffraction) were used to calculate the axial D-period. Results are presented in Table 5.2.

Caprine samples	D-period (nm) (± 0.698nm)	Ovine samples	D-period (nm) (± 0.722nm)
C1	61.5	O1	61.8
C2	Not observed	O2	62.4
C3	62.0	O3	62.2
C4	61.5	O4	60.9
C5	61.8	O5	61.9
C6	62.3	O6	61.7
		Limed skin (control)	64.1

Table 5.2: D-period of caprine hide and ovine hide in their dehydrated states. The D-period for sample C2 is not shown as the diffraction image was not clear enough to give an accurate measurement.

The D-period of collagen from the caprine and ovine hide samples were between 60.9 and 62.4nm, with the exception of the limed ovine hide control, which had not been treated with propan-2-one or 2-ethoxy ethanol and had a D-period of 64.1nm. The value for the limed sample had been extensively studied for other skin species and was typically in this range [98].

5.3.2: The effects of acetone and 2-ethoxy ethanol on the collagen intermolecular lateral packing

The lateral distance between neighbouring collagen molecules is approximately 1.2nm, and is observed using WAXD [24]. Figure 5.2, shows a peak from a WAXD image, which arises from the intermolecular lateral packing of the collagen molecules.

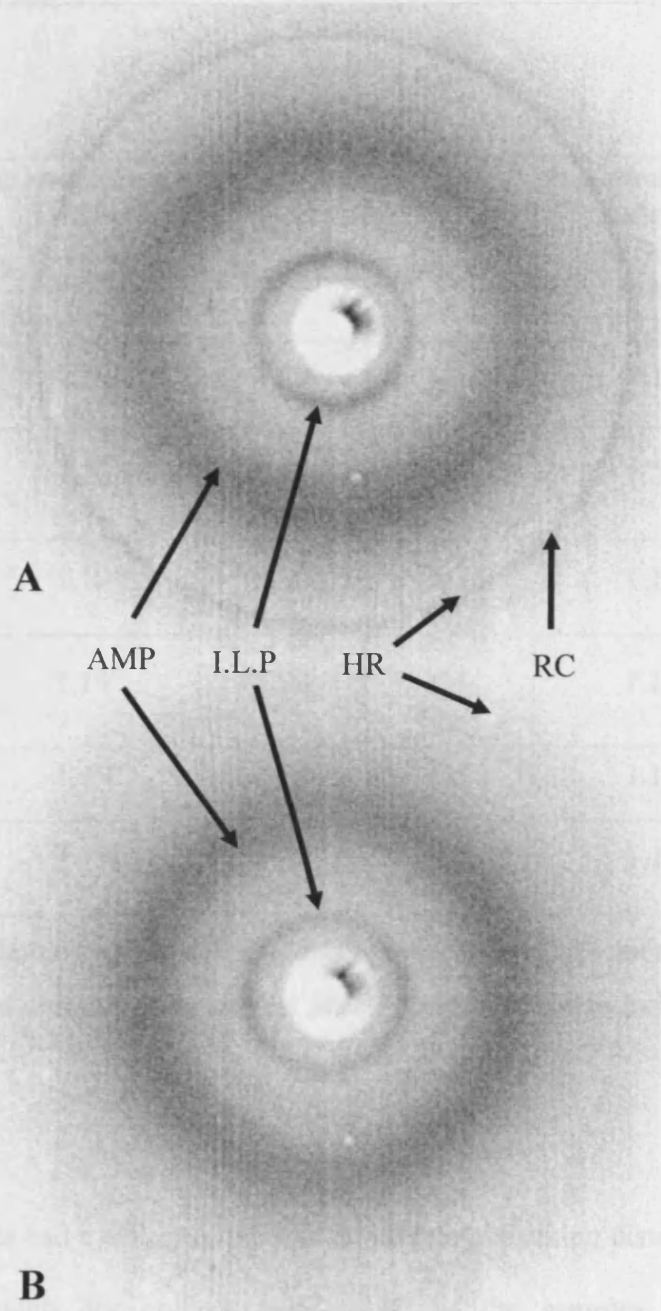

Figure 5.2: WAXD patterns obtained on the NanoSTAR at Cardiff University of A) caprine hide sample C4, and B) caprine hide sample C5 at a sample to detector distance of 4cm. ILP is representative of the scatter related to the helix to helix interactions between collagen molecules (Intermolecular lateral packing). AMP contains the amorphous scatter. RC relates to the scatter from the mineral calcite. HR is the scatter due to the helical rise per residue along the collagen molecule and in diffraction image A, the HR scatter is masked by the calcite scatter (RC).

Analysis of the intensity profiles obtained for the treated caprine and ovine hide samples are presented in Table 5.3.

Caprine samples	Intermolecular Lateral packing (nm) (± 0.07nm)	FWHM (nm^{-1})	Ovine samples	Intermolecular Lateral packing (nm) (± 0.017nm)	FWHM (nm^{-1})
C1	1.20	1.20	O1	1.19	1.14
C2	1.20	1.29	O2	1.20	1.11
C3	1.19	1.36	O3	1.18	1.13
C4	1.19	1.28	O4	1.18	1.21
C5	1.19	1.34	O5	1.17	1.15
C6	1.19	1.38	O6	1.18	1.22

Table 5.3: Collagen intermolecular lateral packing (ILP) measurements of treated caprine hide and ovine hide in its dry state. Peak full width half maximum (FWHM) is shown.

All of the samples had a collagen intermolecular lateral packing distance of ~1.2nm, which was consistent with dry collagen [100]. All of the samples were treated by the manufacturer with slaked lime as part of the dehairing process, which reacts with carbon dioxide in the atmosphere to form precipitated crystals of calcium carbonate. The presence of the calcite can be detected by X-ray diffraction at 0.3nm as shown in Figure 5.2 [90].

5.3.3: Fourier transform infrared spectroscopy

FT-IR spectra of collagen display bands at 3333, 3071, 1658, 1549 and 1240 cm^{-1}, which are characteristic of amide A, B, I, II and III bands of collagen, respectively [101]. The protein amide C=O stretching vibrations are the predominant cause of the amide I absorption. Amide II absorption is due to the combined effects of N-H bending vibrations (60%) and C-N stretching vibrations (40%). The absorption due to amide III is representative of a complex combination of C-N stretching and N-H bending from amide linkages and CH_2 wagging vibrations from proline side chains and backbone glycine residues [24]. The presence of calcium carbonate can also be determined using FT-IR, with known absorption peaks at 1429 and 877 cm^{-1} [102]. The peak at 877 cm^{-1} is present regardless of which calcium carbonate isomorph gives the signal (i.e. calcite or vaterite [103]). Both peaks may be attributed to Ca-O stretching vibrations [104]. The FT-IR spectra for caprine hide are shown in Figure 5.3, with an example of caprine hide containing calcium carbonate.

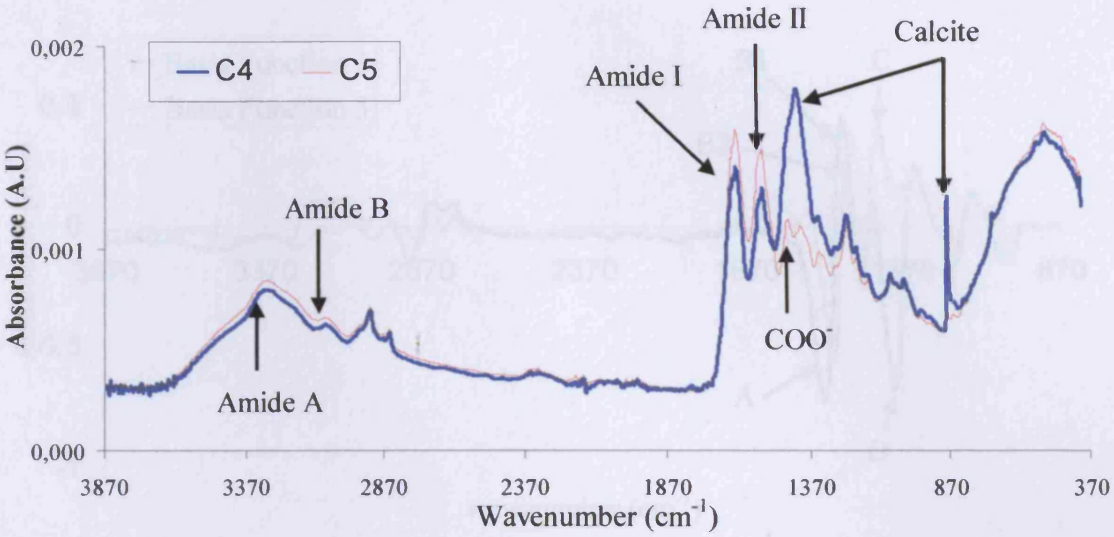

Figure 5.3: FT-IR spectra of solvent-treated caprine parchment. Both samples C4 and C5 exhibited a typical characteristic collagen spectrum with peak positions at 3333, 3071, 1658, 1549, 1240 cm^{-1} representing amide A, B, I, II and III. Sample C4 had peaks at 1429 and 877 cm^{-1}, which was due to calcium carbonate crystals from the manufacturing process.

Basis functions one and three produced from PCA analysis of FT-IR data of caprine and ovine hide are shown in Figure 5.4.

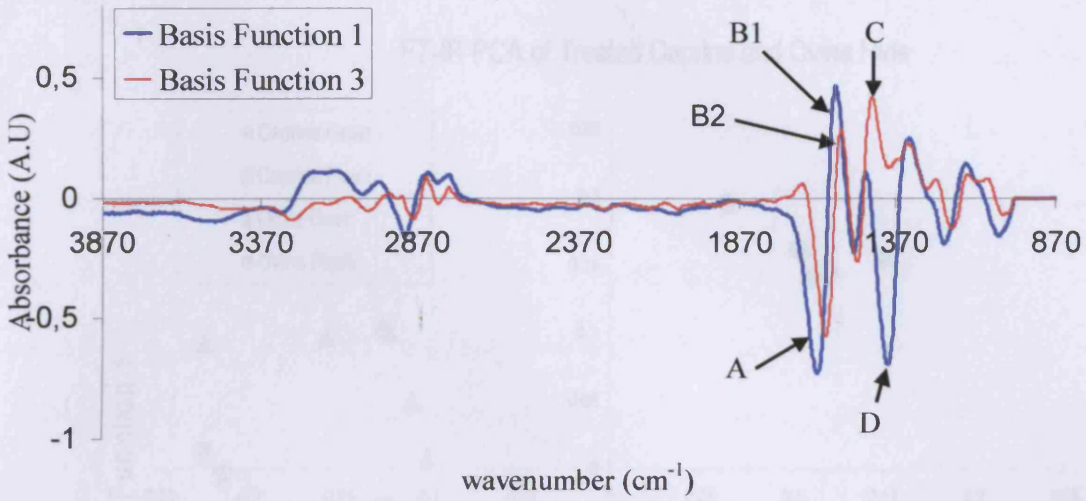

Figure 5.4: PCA basis functions 1 and 3 of FT-IR data for caprine and ovine hide. The most significant changes are highlighted by basis function one and are shown to occur as peaks at about A)1658, B1)1560 and D)1430 cm^{-1} ,which are representative of collagen amide I , amide II and calcite peaks. Basis function three, highlights more discrete changes at peak positions C)1450 and B2)1550 cm^{-1}. These peaks represent collagen carboxylic groups and amine II.

The most significant changes are highlighted by basis function one and are shown to occur as peaks at about 1430, 1560 and 1658 cm^{-1}, which are representative of calcite and collagen amide II and I peaks. Basis function three, which highlights the more discrete changes at peak positions 1450 and 1550, represents the collagen carboxylic groups and the amide II groups. Plots of the PCA coefficients for the FT-IR data of caprine and ovine hide are shown in Figure 5.5.

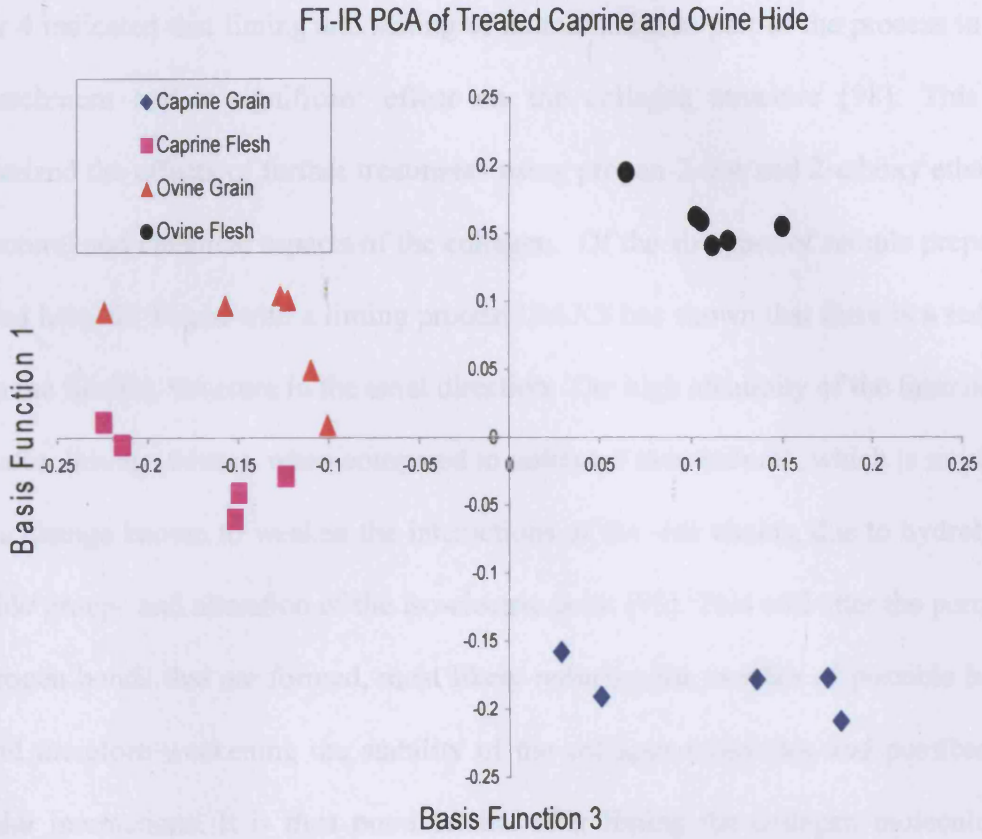

Figure 5.5: Scatter plot of the coefficients of PCA analysis of FT-IR data for treated caprine and ovine hides. There are clear separations across basis function 1 between caprine and ovine species. Basis function 3 represents a separation between skin sides (flesh versus grain).

PCA analysis was able to distinguish the flesh from the grain sides within the species type and, with the exception of possibly two outlying points; to a lesser extent it is possible to separate caprine from ovine hide, indicating that there are discrete variations in the chemical interactions within collagen between species and between skin layers. However, as there is no separation within a sample, it is clear that the treatment of the hides has little localised effect on the chemical characteristics of the hide collagen.

5.4: Discussion into the effects of acetone and 2-ethoxy ethanol on collagen structure

Chapter 4 indicated that liming and salting of animal hides as part of the process to create new parchment had a significant effect on the collagen structure [98]. This study characterized the effects of further treatments using propan-2-one and 2-ethoxy ethanol on the structural and chemical aspects of the collagen. Of the six types of sample preparation described here, all began with a liming process. SAXS has shown that there is a reduction in D- in the fibrillar structure in the axial direction. The high alkalinity of the lime liquor is period after liming (64nm), when compared to untreated hide (65nm), which is most likely due to a change known to weaken the interactions of the side chains, due to hydrolysis of the amide groups and alteration of the iso-electric point [93]. This will alter the percentage of hydrogen bonds that are formed, most likely reducing the number of possible bonding sites and therefore weakening the stability of the collagen molecules and possible inter-molecular interactions. It is thus possible that after liming the collagen molecules may move past each other, which would account for the reduction in D-period. However, finished parchment samples have been shown to have a D-period which is contracted more than that of limed skins [98]. Results from this study have shown that treating with propan-2-one or 2-ethoxy ethanol further reduces D-period. One possible explanation is that these solvent treatments may remove more tightly bound water, causing a tilt in the gap and overlap regions between the collagen molecules; dehydration is one cause of D-period reduction [91, 105]. Whilst SAXS details changes to the long range axial structure of the collagen fibrils, WAXS was employed to describe the interactions between neighbouring collagen molecules in the dehydrated state. As with previous studies, the packing distance between the collagen molecules was ~1.2nm; this is consistent with dehydrated collagen molecules [100]. The fact that there was no further reduction in the distance between

neighbouring molecules indicates that the solvent treatments have not induced the molecules to move closer together in the lateral direction.

The major differences between the FT-IR spectra, as indicated by PCA, are due to the presence of calcium carbonate. The ability of the PCA technique to analyse the FT-IR spectra and to distinguish between the samples based on skin type as well as on which side of the skin was used, demonstrates its effectiveness as a powerful analytical tool. It would, however, not be correct to assume from this data that identification of species type and skin side is possible for unknown samples using PCA of FT-IR data, as PCA describes the variance within the data set given. The presence of the calcite peak, which is at the position of greatest variance in regards to basis function 1, would indicate that the liming stage of parchment manufacture may have a fundamental impact.

An interesting characteristic of skin type is that the weave of the collagen fibres, varies between species. For example, caprine hide is known to have a more compact weave compared to ovine [3]. The skin type with the looser weave may be more susceptible to lime penetration and thus the effects that the liming solution has on the collagen fibres. Furthermore, the density of the collagen weave is different on the flesh and grain sides, which will affect the penetration of the liming solution into the fibre network. Another variable which can affect collagen-fibre orientation is the location from which the samples were taken from the skin, which again may have an effect on liming penetration. Liming solution is known to open up the collagen fibre network, and this may have an effect on the penetration of further chemical treatments, in this case alcohol and ketone solutions. It should be noted that the variance within the sample set detected by PCA comes from species and not from the ketone or alcohol treatments.

5.5: Publication

Parts of the work presented in this chapter appear in the publication:

Maxwell, C.A., N. Bell, C.J. Kennedy, and T.J. Wess, *X-ray diffraction and FT-IR study of caprine and ovine hide.* The Paper Conservator, 2006. 29: p. 55-62.

Chapter 6: X-ray Studies of a Collagen Material for Leather Production Treated with Chromium Salt

6.1: Introduction

Chapters 4 and 5 investigated the effects of parchment manufacture on the collagen structure. In this chapter efforts were made to investigate a treatment process that produces minimum effluents and is thus environmentally friendly, and yet significantly increases the quality and heat resistance of a fibrous collagen material for the leather industry. The structural properties of collagen fibrils in chrome tanned bovine leather were examined after chromium salts with varying concentrations were applied during the preparation process. X-ray diffraction study was carried out on dried treated samples to assess the influence of chromium ion concentration on collagen fibres.

6.2: Experimental

6.2.1: Sample preparation of tanned leather

Sample preparation of the chromium tanned leather was carried out at Radom Technical University and supplied by Krysztof Smiechowski [55].

The excess flesh and fatty tissue under the hide was removed by a fleshing machine before the hides were loaded into drums. The hides were washed to remove dirt and blood from the surface. After fleshing, the hides were weighed and washed. The washing procedure and the leather tanning protocol are outlined in Figure 6.1.

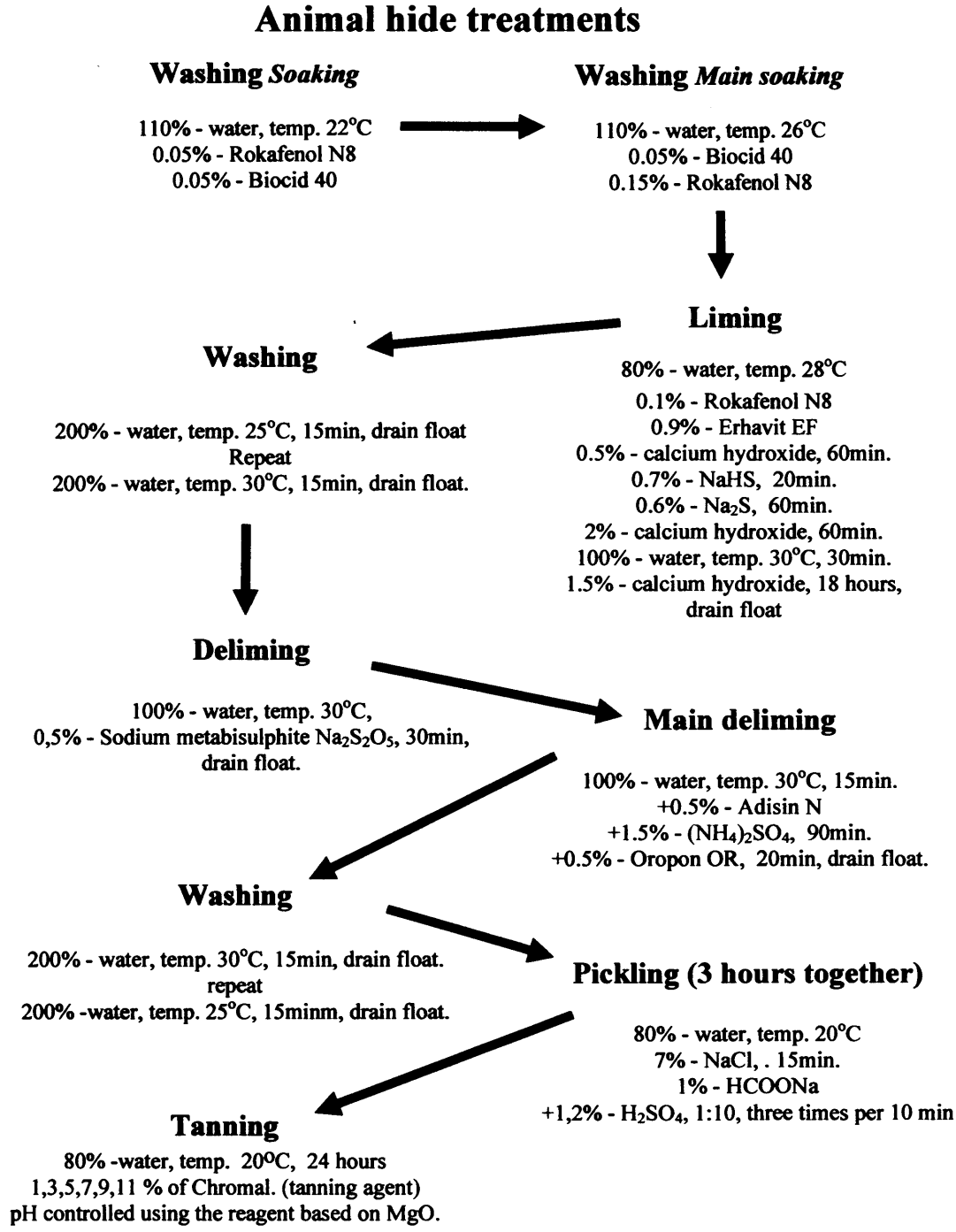

Figure 6.1: Steps of leather chrome tanning process (general flow diagram). The percentage expresses the amount of additive in comparison with the weight of hide (200% of water means that for 100 kg of hides, 200 kg of water was used, etc). Chemicals used are characterized in Table 6.1.

No.	Name, symbol and Source	Characteristic
1	Rokafenol N8, Rokita S.A. Poland	Nonionic agent (detergent) based on ether. polyoxyethylene(9)nonylphenol ether (99%); water (1%).
2	Biocid 40, Biokimica Italy	Bacteriocide Concentration 40-42%.
3	Erhavit EF, TFL Germany	Agent for increasing the rate of calcium diffusion into the hide. Regulation of swelling.
4	Adisin N, Adipol Chorzow, Poland	Mixture of weak aliphatic acids, for removal of calcium.
5	Oropon OR, TFL Germany	Agent based on pancreatin (enzymatic) 650-790LVE).Used at pH 6-8

Table.6.1: Specialized chemical names, sources and characteristics.

The soaking process, which has a pH of 8-9 due to the addition of Na_2CO_3, restores lost moisture to hides that have been salted and stored for long periods before processing. Hair removal using lime was followed by washing and deliming cycles before pickling. In the pickling process, water, sulfuric acid and sodium chloride are added. The acidic environment of this solution makes the hides ready to accept the tanning chemicals. The addition of sodium chloride prevents any swelling of the hide.

The 24 hour tanning process converts the hide into a stable material which will not putrefy and is less susceptible to attack by bacteria. The tanning agent Chromal (containing about 25% Cr_2O_3) was added, and the Cr_2O_3 penetrated (24 hours at 18 – 20 °C) into the hide structure and cross-linked with the collagen. Different amounts of Chromal were used (1,3,5,7,9,11%) and after tanning, the amount of Cr_2O_3 in the leather was measured by

titration with $KMnO_4$. Once adequate penetration of the chrome had occurred (24 hours), the hides were basified. A slightly alkaline chemical such as magnesium oxide was added and the pH was slowly raised to ~4. The parameters of the process are presented (Table 6.2).

Sample No	Chromal [%]	% Cr_2O_3 in leather	pH before	pH after tanning
0	Sample without tanning agent (control sample)			
1	1	0.9	3.7	4.6
2	3	2.0	3.5	4.6
3	5	3.4	3.2	4.4
4	7	3.7	3.0	4.2
5	9	4.3	3.1	4.2
6	11	5.2	3.0	4.1

Table 6.2: Parameters of the tanning process obtained for leather samples.

The samples were then dried at room temperature for 24 hours (Figure 6.2) and then submitted for analysis.

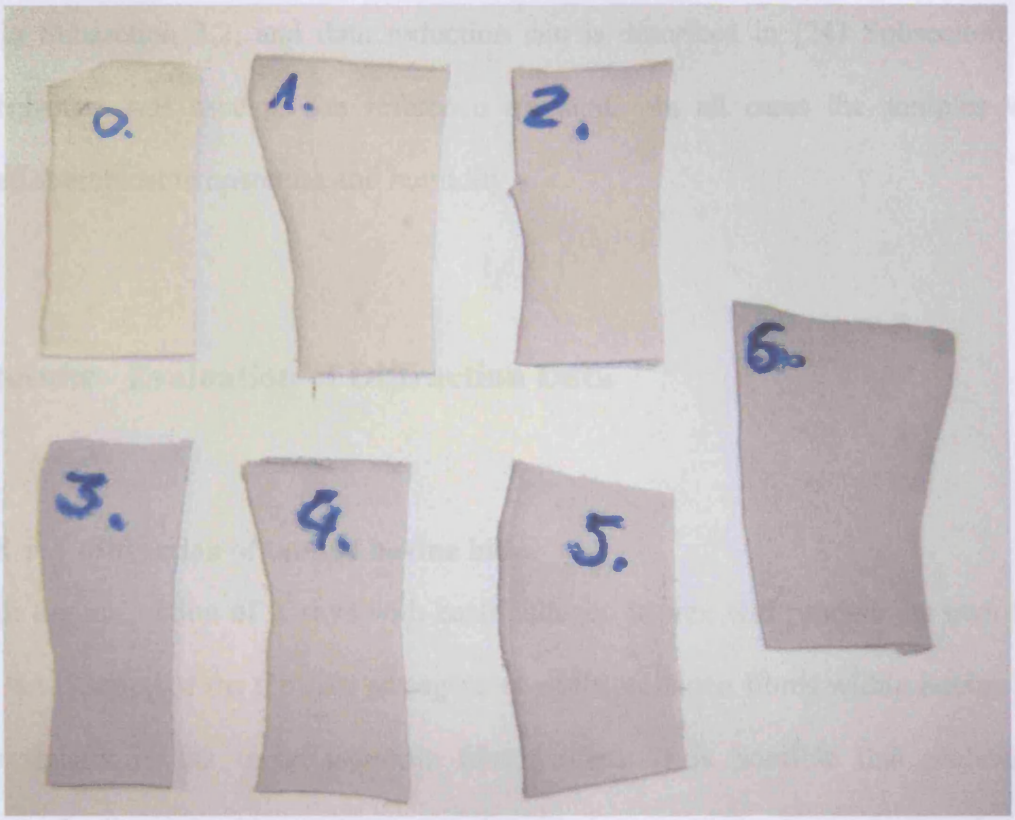

Figure 6.2: Image of leather samples treated with different concentrations of chromal solution. Parameters of leather samples after treatments are shown in Table 6.2.

6.2.2: X-ray diffraction parameters

The SAXS patterns of bovine hide obtained at station 2.1 of the Synchrotron Radiation Source (SRS), Daresbury, (details subsection 3.3.2), gave a sufficient resolution to determine Bragg orders due to electron density profile of the gap and overlap region of chromium tanned collagen fibrils. Hydrated rat tail tendon was used as a calibration standard.

WAXS patterns were obtained using a Bruker AXS NanoStar small angle scattering station with a camera length of 4.4cm, which allowed the wide angle diffraction features of

collagen to be observed to a resolution of 0.2nm. Details of the scattering system are shown in Subsection 3.2, and data reduction can is described in [24] Subsection 3.4. Silver behenate was used as the reference standard. In all cases the samples were examined at ambient temperature and humidity.

6.3: Results - Evaluation of Diffraction Data

6.3.1: X-ray diffraction of tanned bovine hide

Although the interaction of X-rays with each collagen triplex will produce its own fibre pattern, the isotropy of the felt-like arrangement of the collagen fibres within bovine hide samples usually results in an isotropic fibre pattern. It is possible that preferential alignment of collagen in skin can been seen, but this is most likely due to the location that the sample was taken from rather than the processing.

6.3.2: Wide angle X-ray scattering patterns of chromium bovine hide

Wide angle X-ray scattering fibre patterns of chromium bovine hide were obtained and used to analyse the effects of chromium tanning on collagen at the intra and inter molecular level. Quantitative measurements of the changes in the collagen axial rise per residue reflection, and the contribution of diffuse and helical scattering to the fibre pattern were obtained (Figure 6.3).

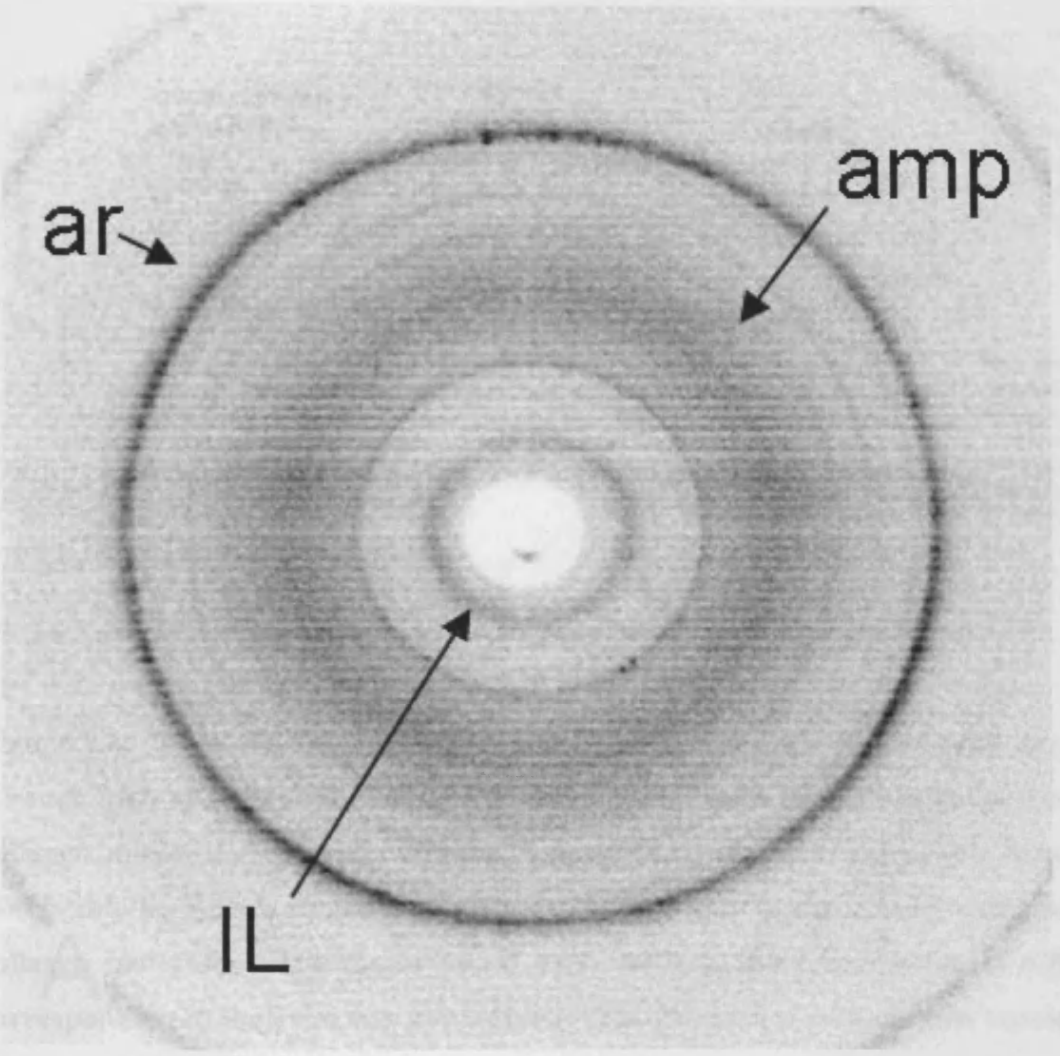

Figure 6.3: X–ray diffraction pattern of isotropic collagen from bovine hide representing packing characteristics of axial rise per residue (ar), amorphous region (amp) and intermolecular lateral distance (IL).

The helical rise per residue represents the mean axial step between the amino acid residues of collagen chains within the molecules. Linear traces of the radially averaged fibre diagrams are shown in figure 6.4.

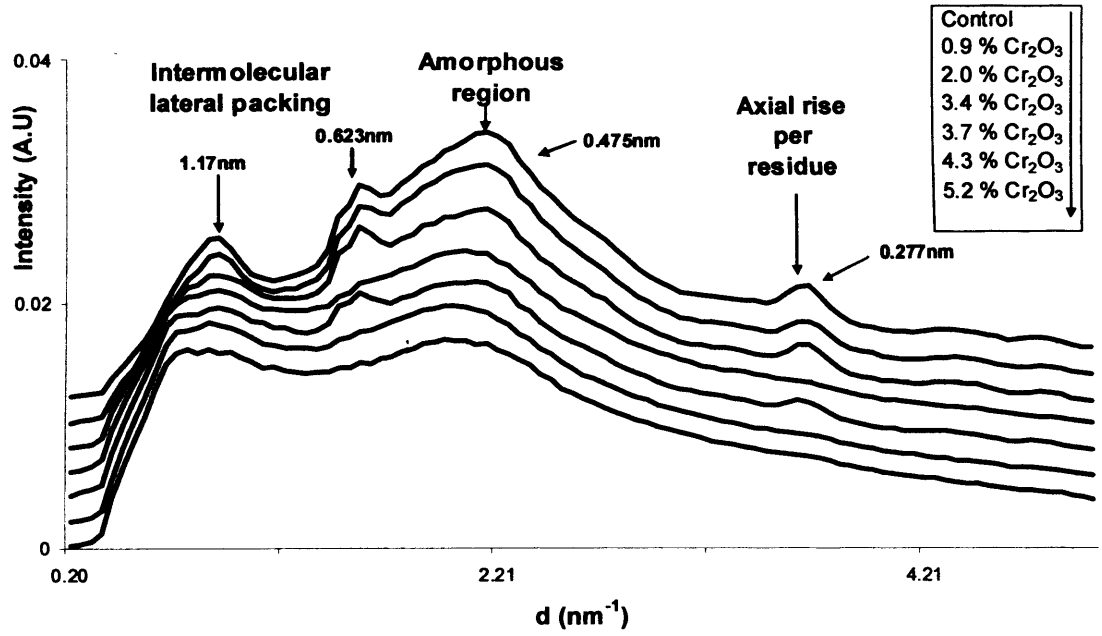

Figure 6.4: Linear X-ray scattering profile of bovine hide treated with chromium. At such high angles the diffraction results mainly from the helical properties of the collagen molecules. The amorphous halo present in most diffraction data is also observable here, as is the characteristic reflection due to the side by side packing of collagen molecules. The major trend observable is the contribution of diffraction corresponding to the axial rise per residue; this diminishes with chrome tanning. (All linear traces have been normalised and offset).

The data obtained for the linear profiles of Figure 6.4 is represented in Table 6.3.

Bovine hide	Axial rise per residue (nm) (± 0.032nm)	Peak height (intensity)	Full width half maxima d (nm^{-1})	Integrated intensity
0 % Cr_2O_3 (Control)	0.276	0.01334	0.733	0.065
0.9 % Cr_2O_3	0.276	0.00931	0.787	0.049
2.0 % Cr_2O_3	0.274	0.00619	0.873	0.036
3.4 % Cr_2O_3	0.278	0.00729	0.820	0.040
3.7 % Cr_2O_3	0.277	0.00311	1.585	0.033
4.3 % Cr_2O_3	0.276	0.00473	0.951	0.030
5.2 % Cr_2O_3	0.275	0.00395	0.902	0.024

Table 6.3: Helical rise per residue and peak characteristics as measured using PeakFit4 program.

Although not completely correlating with chromium salt levels, there is a decrease in peak height and an increase in full width half maxima, as concentrations of chromium salt increase. The peak height and full width half maxima values can be used to determine the integrated intensity, which is an indication of order within the collagen structure. The integrated intensity decreases, with the exception of sample 3 (although still decreasing) in a linear trend, as chromium salt concentrations increase. Therefore chromium salt seems to cause a loss of order within the collagen molecules at the molecular and helical level dependent on its concentration. The increase in full width half maxima can be interpreted as the distribution of axial rise per residue values in the sample. There is a link between chromium salt concentration and increasing helical rise per residue distribution, but a direct link with chromium salt concentration is not clear. The change in the mean value of the axial rise per residue as a function of chromium treatment is probably negligible.

6.3.3: Wide angle X-ray scattering of chromium bovine hide

X-ray diffraction to a real space resolution of 0.9nm allows a more accurate evaluation of the intermolecular lateral packing of the collagen molecules, which occurs in the region of ~1 nm for the dehydrated state. The treatment of bovine skin with chromium has an effect on the peak profiles (Figure 6.4 and Figure 6.6) which seems to be directly related to concentration.

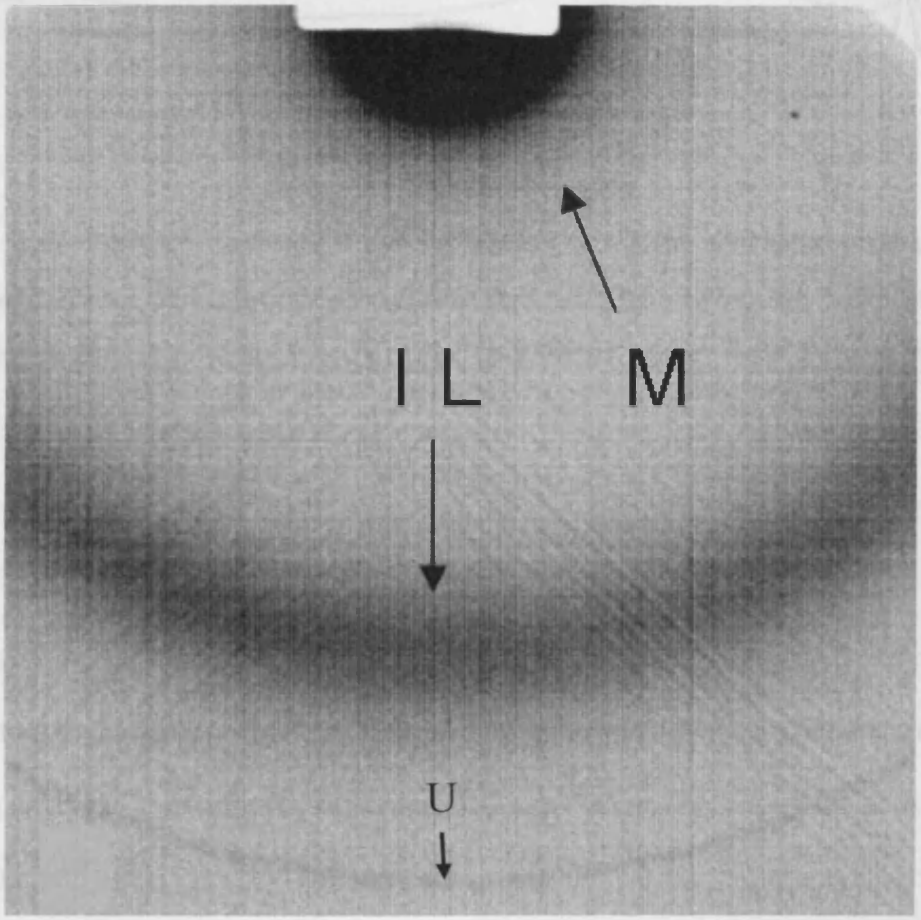

Figure 6.5: WAXS pattern of isotropic collagen from bovine hide representing packing characteristics of intermolecular lateral packing (IL) and meridional Bragg orders (M). Unknown reflection (U).

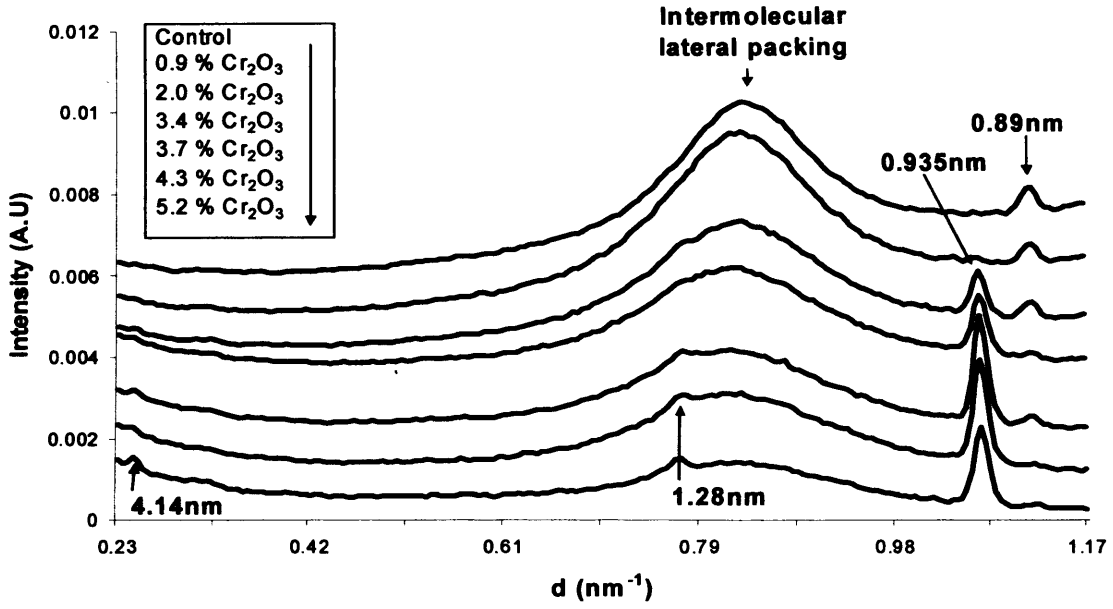

Figure 6.6: WAXS data obtained at station 2.1 SRS Daresbury at a sample to detector distance of 1.25m of bovine hide treated with chromium was analysed using PeakFit4 to obtain a linear trace profile. (All linear traces have been normalised and offset).

Although it is not a completely linear relationship, increasing chromium salt concentration relates to a reduction in height of the peak that represents the characteristic intermolecular lateral packing of the collagen molecules. There is also a reduction of the peak occurring at d = 1.07 nm^{-1} (0.935nm real lattice space), with increasing chromium salt concentration and also an appearance of another peak at d = 1.12 nm^{-1} (0.89nm real lattice space) possibly a diffraction series of lipid bilayer interactions with Cr^{3+} ions. The linear traces of Figure 6.6 were further analysed using PeakFit4 to give values concerning peak profiles (Tables 6.4, 6.5, and 6.6). The intermolecular lateral packing distance between the collagen molecules increases slightly after the addition of chromal to the bovine hide (Table 6.4).

Bovine hide Samples at 1.25m	Intermolecular lateral packing (nm) (± 0.027 nm)	Peak Height (Intensity)	Full width half maxima d (nm^{-1})
0 % Cr_2O_3 (Control)	1.19	0.003044	5.379
0.9 % Cr_2O_3	1.20	0.003414	5.893
2.0 % Cr_2O_3	1.20	0.002377	6.331
3.4 % Cr_2O_3	1.21	0.001927	6.076
3.7 % Cr_2O_3	1.23	0.001612	5.990
4.3 % Cr_2O_3	1.22	0.001545	5.936
5.2 % Cr_2O_3	1.22	0.000864	5.703

Table 6.4: Intermolecular lateral packing and peak characteristics of chromal treated bovine hide as measured using PeakFit4 program.

The FWHM of the peaks increase on the addition of chromal, indicating an increase in the distribution of packing distances represented by the I.L.P. of collagen molecules. At 3% chromal concentration (2% chromium salt), the increase in distributions of packing distances seems to be at a maximum level with subsequent increases in concentration causing a reduction in packing distribution, possibly due to chemical penetration being more even.

The reduction in order associated with the I.L.P. distance of collagen seems to correlate with the loss of the peak at 0.89nm (Table 6.5).

Bovine hide Samples at 1.25m (0.9nm Resolution)	Peak at 1.13 d Real space (nm)	Peak Height (Intensity)	Full width half maxima d (nm^{-1})	Integrated Intensity
0 % Cr_2O_3 (Control)	0.889	0.00057	0.614	0.00232
0.9 % Cr_2O_3	0.889	0.00044	0.562	0.00167
2.0 % Cr_2O_3	0.889	0.00038	0.527	0.00134
3.4 % Cr_2O_3	0.888	0.00012	0.451	0.00037
3.7 % Cr_2O_3	0.889	0.00021	0.486	0.00070
4.3 % Cr_2O_3	0.889	0.00005	0.244	0.00009
5.2 % Cr_2O_3	0.887	0.00009	0.508	0.00031

Table 6.5: Unknown peak (0.89nm) characteristics of chromal treated bovine hide, as measured using PeakFit4 program.

This peak is not due to chromium salt concentration as it is found in the control sample, but its integrated intensity does appear to reduce as chromium salt concentration increases. There is a variation in the distribution of the repeating unit responsible for this peak; this small sample run of chromium salt treated leather indicates that there is a possible link between chromium salt concentration and collagen packing and hierarchy.

The peak that occurs at d = 1.07 nm^{-1} is not present in the control sample and therefore is a diffraction characteristic of the addition of chromal. The cumulative effect of the repeating unit at this peak only appears to be significant at chromal concentrations of 3% or more. The peak position does not change with increasing chromium concentration Table 6.6, but the peak height does.

Bovine hide Samples at 1.25m (0.9nm Resolution)	Peak at 1.07 d Real space (nm)	Peak Height (Intensity)	Full width half maxima d (nm^{-1})	Integrated Intensity (A.U)
0 % Cr_2O_3 (Control)	No peak			
0.9 % Cr_2O_3	No peak			
2.0 % Cr_2O_3	0.931	0.00102	0.527	0.00381
3.4 % Cr_2O_3	0.930	0.00138	0.583	0.00540
3.7 % Cr_2O_3	0.931	0.00253	0.553	0.00937
4.3 % Cr_2O_3	0.931	0.00245	0.565	0.00927
5.2 % Cr_2O_3	0.931	0.00184	0.587	0.00723

Table 6.6: Unknown peak (0.93nm) characteristics as measured using PeakFit4 program. A.U = arbitrary units.

Subsequently there is an increase of order within the structure as chromium salt concentration increases, possibly indicating that this peak is due to the local structure of chromium salt crystallinity and not collagen chromium interactions.

6.3.4: Small angle X-ray scattering of chromium tanned bovine hide

Collagen is known to contain a number of long range interactions resulting from axial order and substructures within the fibril. Observation of these features by X-ray diffraction requires long camera geometries in order to resolve closely spaced features in reciprocal space. Meridional peak positions can be determined accurately at a geometry that allows observation of diffraction from structural features to a real space resolution of 6nm. In particular, this can reveal the 6th order up to the 11th order, with more intense 6th order indicating a lower level of sample hydration. The peak profiles (Figure 6.7 and 6.8)

are characteristic diffraction reflections of the gap and overlap regions between the collagen molecules in the axial direction.

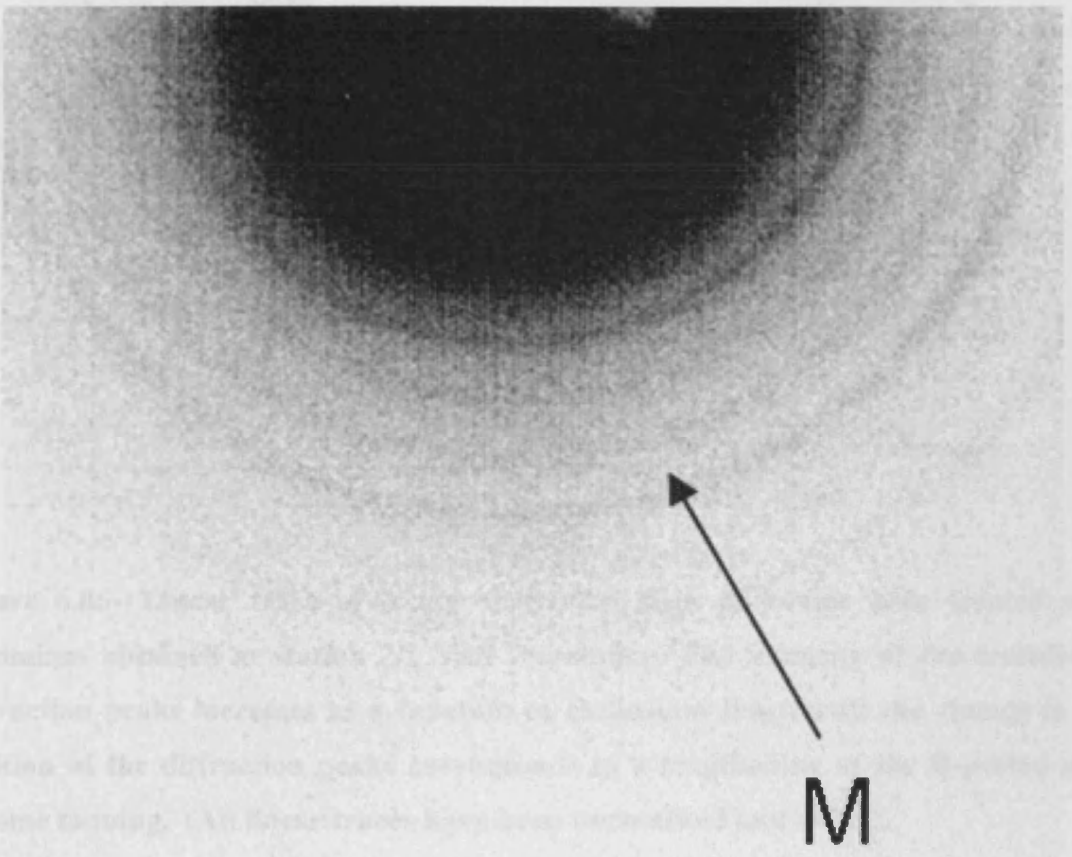

Figure 6.7: X–ray diffraction pattern of isotropic collagen from bovine hide at sample to detector distances representing packing characteristics of the meridional diffraction series (M) of collagen structure corresponding to the 65nm repeat.

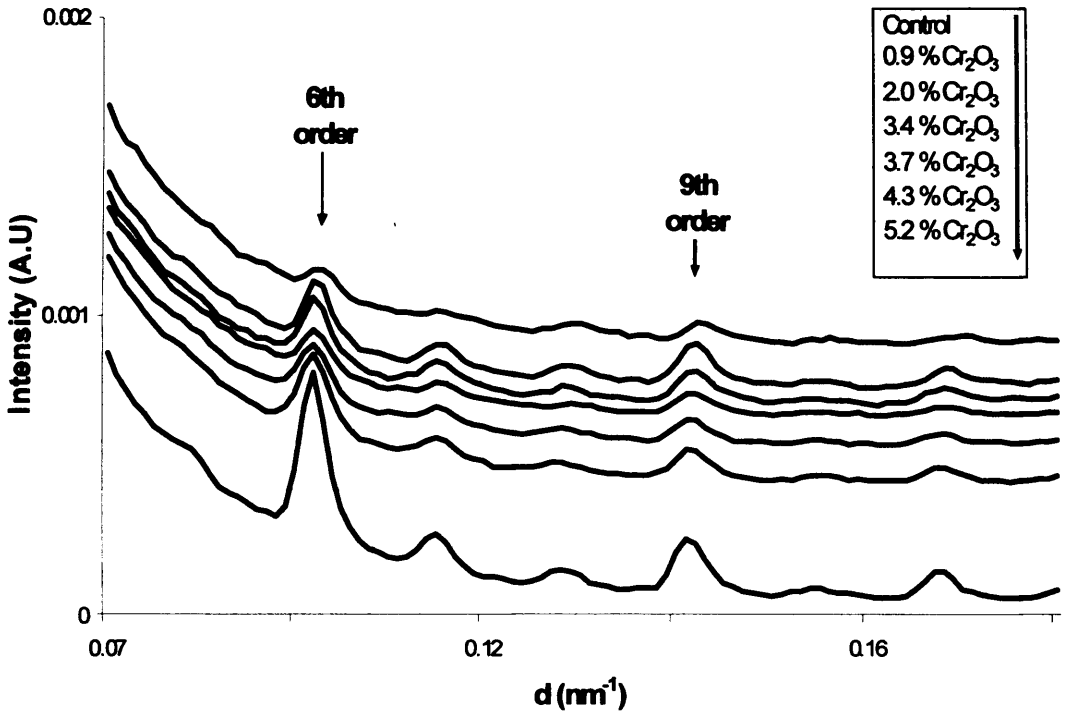

Figure 6.8: Linear trace of X-ray scattering data of bovine hide treated with chromium obtained at station 2.1 SRS Daresbury. The intensity of the meridional diffraction peaks increases as a function of chromium treatment; the change in the position of the diffraction peaks corresponds to a lengthening of the D-period with chrome tanning. (All linear traces have been normalised and offset).

The relative intensities of the large 6^{th} order, in comparison with the 7^{th} and 8^{th} for example, is typical of a dry collagen sample. The spacing between the orders is very similar for all the samples, with the exception of the control sample indicating chromium salt effect on the gap and overlap region of the collagen molecules. The PeakFit4 program was used to give a more detailed interpretation of the peak profiles representing the characteristic axial staggered array (D-period) of the collagen molecules in Table 6.7.

Bovine hide	D-period (nm) (± 0.582 nm)	Peak Height (Intensity)	Full width half maxima d (nm^{-1})
0 % Cr_2O_3 (Control)	62.7	0.000173	1.192
0.9 % Cr_2O_3	64.4	0.000274	0.893
2.0 % Cr_2O_3	64.0	0.000276	0.899
3.4 % Cr_2O_3	63.8	0.000226	0.945
3.7 % Cr_2O_3	64.0	0.000269	0.900
4.3 % Cr_2O_3	64.0	0.000356	0.877
5.2 % Cr_2O_3	64.3	0.000627	0.680

Table 6.7: Peak profile data of bovine hide samples analysed, from X-ray scattering data obtained from SRS Daresbury station 2.1 at a sample to detector distance of 8m (6nm resolution).

The decrease in the breadth of the meridional diffraction peaks is indicative of the D-period structure of the collagen fibrils becoming regular or indeed the overall length of the coherent crystallites becoming longer.

6.4: Discussion

The effect of chrome tanning to different extents has been observed here as a function of structural order over a range of length scales. The data shown here suggests that the axial rise per residue of the collagen helix is altered by tanning; however, this does not correspond to a concomitant increase in the contribution of the amorphous region of the fibre pattern, indicating that the degree of gelatinization is not increased. It may therefore be possible that significant alterations are made to the collagen helical backbone without total disruption. This will have a cumulative effect on the side by side molecular packing within the collagen fibril that leads to an increase in the intermolecular distances, as well as the variance of helical interactions. This may be due to deviations from the standard helix geometry that allows molecules to pack on a simple quasi-hexagonal lattice with a ~1nm spacing [106]. The nanometre length scale also reveals structural features that are altered by the tanning process; the evolution and change of sharp Bragg reflections at 4.4, 0.89 and 0.835 nm correspond to reflections observed to result from lipid diffraction. The interaction of Cr (III) ions with lipid bilayers will not only increase fundamental spacing but also increase the contrast between bilayers resulting in enhanced diffraction peaks.

The long range interactions of collagen are dominated by the axial repeating structure due to molecular staggering along the collagen fibril. This showed that the axial periodicity of the stagger between collagen molecules is increased upon tanning. The main change observed in these samples, however, is the increase in diffraction signal of Bragg peaks above the continuous background. This indicates that the overall long range crystallinity of the collagen molecules and the specificity of the axial order may be increased. It also may result in part from the enhanced electron density contrast made by the addition of Cr (III) ions to the structure. If the latter is the predominant effect, an important feature to note is that the intensity distribution amongst meridional reflections of the enhanced signal is the

same as that of an untanned sample. This would imply that the labelling of Cr (III) along the length of the collagen molecule is relatively even and if specific to certain amino acids, must indicate that their distribution is even through the collagen molecule. Specific heavy atom staining by a number of metal species is known to occur and alter the intensity of meridional reflections in both wet and dry samples [107].

In relation to the increased measurements of shrinkage temperature as a function of chromal addition, this may be reflected in the broadening of the peak at approximately 1nm spacing which is characteristic of the side by side interactions of collagen molecules. Here the possible changes in conformation brought about by intermolecular cross-links may be producing a less locally ordered lattice structure.

6.5: Publication

Parts of the work presented in this chapter appear in the publication:

Maxwell, C.A., K. Smiechowski, J. Zarlok, A. Sionkowska, and T.J. Wess, *X-ray studies of a collagen material for leather production treated with chromium salt.* Journal of American Leather Chemists Association, 2005. 100: p. 9-17.

Chapter 7: Discussion and conclusions

7.1: X-ray diffraction/scattering as a tool to examine effects of animal hides processing on collagen structure.

This work examined how the processing of animal hide (*post mortem*) into a useable material affects the structural hierarchy of collagen, and as a consequence the integrity of the finished material. Many previous studies have generated detailed information on the processes without measuring quantitatively the changes that have occurred to the collagen structure. Here X-ray studies were carried out, first as this technique can be used safely to examine materials of significant value, whether it is monetary or historical without the need for the cutting of the sample. Second X-ray studies of collagen materials have been used for many years and as such are a well tested technique, which is capable of making these types of measurements.

This thesis examined the preservation stage of salting and the primary dehairing treatment of liming, which was used in both the manufacture of parchment and leather. The application of ketone and alcohol as a finishing treatment of parchment, which was used to produce a better (purely a subjective term depending on the manufacturer) writing material, was also assessed.

The significant deviation between leather and parchment was the cross linking tanning stage using chromium. This was studied to measure the changes in collagen hierarchy due to the tanning solution. Moreover, the amount of chromium used to achieve the desired end product was measured, to see if the environmental impact of chromium could be limited by reducing concentrations of chromium used.

7.2: Liming of animal hide

A general statement that the collagen fibres within the animal hide "open up" due to processing stages has been widely accepted. The X-ray diffraction studies detailed in this thesis now quantitatively describe a swelling in fibre structure at the molecular level, which is observed through the hierarchical levels of collagen. Altering the amino acid side chains of the collagen molecules is likely to reduce stability between the molecules. This, combined with the influx of water and the removal of proteoglycans from between the fibrils, is most likely to be the cause of about 20% "opening up" of the collagen fibres. Therefore, further swelling of the animal hide, which accounts for the remaining 80% of the "opening up", must be occurring between the collagen fibres. This would be observed at the mesoscopic level, which is beyond the limits of the techniques used, and the scope of this thesis. However, the most noticeable structural change due to liming is the reduction in the D-period. When combined with the axial rise per residue distance being unaffected, this indicates that most of the changes are due to intermolecular interactions of collagen molecules as opposed to intramolecular.

However, the penetration of solid calcite or CO_2 gas, which reacts with $Ca(OH)_2$ forming calcite, based on the hypothesis that the presence of calcite mineral peaks is an indication of how deep penetration into the hide occurs, has been shown to be limited to about 170 microns. This implies that the integrity of the collagen fibres that are deeper than this penetration level, remain unaffected by solid calcite deposits and as such may be responsible for the durability of parchment, which has been observed from historical materials.

7.3: Treatment with propan-2-one and 2-ethoxy ethanol

The effects of the propan-2-one and 2-ethoxy ethanol treatments are apparent on the fibrillar level, where they cause a reduction in the axial D-period, indicating a dehydration process. This may indicate that conservation treatments of historic parchment objects, in which solvents are used, may be causing changes at the molecular level. Whether these changes are irreversible or not will require further study. However, the treatments have no effect on the collagen molecule-to-molecule interactions or chemical characteristics. This may be due to the degree of penetration of the treatments into the collagen structure. An unexpected result is that FT-IR data can distinguish between species and skin layer, and that the key difference arises from calcite. This indicates a difference in the uptake of calcite by the different layers during the liming process.

7.4: Treatment with chromium (tanning)

A major part of animal processing into leather is the addition of cross-linking between the collagen molecules by the tanning solution. In this particular study chromium salt was used to form these crosslinks and the subsequent changes were observed using X-ray diffraction. The concentration of the chromal solution was controlled, as chromium is known to be an environmentally hazardous substance. It was observed that there was a slight increase in the lateral packing between the collagen molecules, which would be expected if there was crosslinking occurring between the chromium salt and the collagen molecules. The maximum level of disorder achieved at the molecular level (I.L.P.) was at 2% chromal, which indicates that chromium penetration is not completely even. An even penetration of chromal solution was seen to be achieved at 3% chromium salt. Therefore, subsequent additions of chromium salt seem to have little impact on collagen structure at the molecular level.

The effect of chromium salt on the supramolecular level (D-period) occurs at very low levels (0.9% chromium), indicating little requirement for increased chromium concentrations. However, the stabilising effect of crosslinking between the collagen molecules indicates that concentrations of 3% chromium salt are required to make the structural changes to the collagen molecules. Further additions may lead to increased stability, possibly due to increased interactions between the chromium salt and the collagen.

7.5: Summary and potential future projects

The results presented in this thesis, show that X-ray scattering techniques can be used to give quantitative measurements of collagen structure before and after some of the most common treatments on animal hide. However, the processing of animal hides into useable materials can involve a wide variety of treatments and also many different types of animal species. The preservation stage, examined here was salting, but this could be extended to the freezing method for example, which does not aid the release of the hyaluronic acid from the hide. How this affects collagen structurally compared to the effect of salting on animal hide (collagen) could be measured using X-ray scattering techniques.

This thesis also examined the liming process as a method of dehairing animal hide, and confirmed the swelling of the fibres by quantitatively measuring collagen packing changes. An extension to this would be to measure changes due to exposure time to the liming solution, temperature, and to extend the range of animal species and ages.

Liming of course is not the only method of dehairing animal hide. Historical methods can vary, depending on regions and religion; a similar investigation to the one carried out in this thesis on different de-hairing processes for example, the use of enzymes may give an

insight into differences between finished parchments. This in turn may be a useful indicator of region of manufacture and religious significance. FT-IR spectroscopy could be a powerful technique, when combined with X-ray scattering to determine this.

Tanning methods in leather production vary depending on the purpose of the finished product. This thesis investigated the chromium tanning of animal hide and measured changes in collagen structure over a gradient of concentrations. The outcome was to determine how much chromium was required to make a suitable end product with minimal environmental impact; at least from a structural perspective. This study could be extended to the other mineral tannages of zirconium and aluminium, the vegetable tans, the synthetic tans or aldehyde tannages [8]. Furthermore, the applications of fat-liquoring agents, which are used to introduce some flexibility to the leather, are known to have an effect on mechanical strength and durability of material.

These are just a few examples of where the techniques used in this thesis to examine the processing of animal hide could be extended into further projects.

Bibliography

1. De Clercq, M., *Review; photographic gelatin production.* Journal of Imaging Science and Technology, 1995. 39: p. 367-372.
2. Oates, J.A.H., *Lime and limestone: chemistry and technology, production and uses.* 1st ed. 1998: Wiley- vch. 455.
3. Haines, B.M., *Parchment, the physical and chemical characteristics of parchment and the materials used in its conservation.* 1999, Northampton: The Leather Conservation Centre. 1-32.
4. Menon, G.K., *New insights into skin structure: scratching the surface.* Advanced Drug Delivery Reviews, 2002. 54: p. S3-S17.
5. Gustauson, K.H., *The structure of skin and the chemistry of collagen*, in *Chemistry and Reactivity of Collagen.* 1956, Academic Press: New York. p. 30-52.
6. Horie, C.V., *Deterioration of skin in museum collections.* Polymer Degradation and Stability, 1990. 29: p. 109-133.
7. Beanes, S.T., C. Dang, C. Soo, and K. Ting, *Skin repair and scar formation:the central role of TGF-beta.* Expert Reviews in Molecular Medicine, 2003. 5: p. 1-11.
8. Sharphouse, J.H., *Leather technician's handbook.* 1st ed. 1971, London: Vernon Lock Ltd. 575.
9. Dale, B.A., K.A. Holbrook, and P.M. Steinert, *Assembly of stratum corneum basic protein and keratin filaments in macrofibrils.* Nature, 1978. 276: p. 729-731.
10. Hijazy., M., *Principles of pediatric dermatology.* 1971, J & A Churchill: London. p. Chapter 1.
11. Monteiro-Riviera, N.A., A.O. Inman, T.H. Snider, J.A. Blank, and D.W. Hobson, *Comparisons of an in vitro skin model to normal human skin for dermatological research.* Microscopy Research and techniques, 1997. 37: p. 172-179.
12. Kennedy, C.J. and T.J. Wess, *The structure of collagen within parchment - a review.* Restaurator-International Journal for the Preservation of Library and Archival Material, 2003. 24: p. 61-80.
13. Alberts, B., D. Bray, K. Hopkin, A. Johnson, J. Lewis, M. Raff, K. Roberts, and P. Walter, *Essential Cell Biology.* 2nd ed. 2003: Garland Science Textbooks. 896.
14. Gelse, K., E. Poschl, and T. Aigner, *Collagens-structure, function and biosynthesis.* Advanced Drug Delivery Reviews, 2003. 55: p. 1531-1546.
15. Usha, R. and T. Ramasami, *The effects of urea and n-propanol on collagen denaturation: using DSC, circular dicroism and viscosity.* Thermochimica Acta, 2004. 409: p. 201-206.
16. Fratzl, P., K. Misof, I. Zizak, G. Rapp, H. Amenitsch, and S. Bernstorff, *Fibrillar structure and mechanical properties of collagen.* Journal of Structural Biology, 1998. 122: p. 119-122.
17. Kronick, P.L. and P.R. Beuchler, *Fiber orientation in calfskin by laser light scattering or X-ray diffraction and quantitative relation to mechanical properties.* Journal of American Leather Chemists Association, 1986. 81: p. 221.
18. Purslow, P.P., T.J. Wess, and D.W.L. Hukins, *Collagen orientation and molecular spacing during creep and stress-relaxation in soft connective tissues.* The journal of Experimental Biology, 1998. 201: p. 135-142.

19. Hanson, E.F., S.N. Lee, and H. Sobel, *The effects of relative humidity on some physical properties of modern vellum.* Journal of the American Institute for Conservation, 1992. 31: p. 325-342.
20. Woo, S.L., G.A. Johnson, and B.A. Smith, *Mathematical modelling of ligaments and tendons.* Journal of Biomedical Engineering, 1993. 115: p. 468-473.
21. Henkel, W. and R.W. Glanville, *Covalent crosslinking between molecules of type I and type III collagen.* European journal of biochemistry, 1982. 122: p. 205-213.
22. Henkel, W., *Cross-link analysis of the C-telopeptide domain from type III collagen.* Journal of Biochemistry, 1996. 318: p. 497-503.
23. Obrink, B., *A study of the interactions between monomeric tropocollagen and glycosaminoglycans.* European journal of biochemistry, 1973. 33: p. 387-400.
24. Sionkowska, A., M. Wisniewski, J. Skopinska, C.J. Kennedy, and T.J. Wess, *Molecular interactions in collagen and chitosan blends.* Biomaterials, 2004. 25: p. 795-801.
25. Goh, K.L., J. Hiller, J.L. Haston, D.F. Holmes, K.E. Kadler, A. Murdoch, J.R. Meakin, and T.J. Wess, *Analysis of collagen fibril diameter distribution in connective tissues using small-angle X-ray scattering.* Biochimica et Biophysica Acta, 2005. 1722: p. 183-188.
26. Hodge, A.J. and J.A. Petruska, *Recent studies with the electron microscope on ordered aggregates of the tropocollagen molecule*. 1st ed. Aspects of Protein Chemistry, ed. G.N. Ramachandran. 1963, London: Academic Press. 289-300.
27. Hodge, A.J. and J.A. Petruska, *Electron Microscopy*, ed. S.S. Breese. Vol. 1. 1962, New York: Academic Press.
28. Quantock, A.J., K.M. Meek, and S. Chakravarti, *An X-ray diffraction Investigation of corneal Structure in lumican-deficient mice.* Investigative Ophthalmology & Visual Science, 2001. 42: p. 1750-1756.
29. Orgel, J.P., T.J. Wess, and A. Miller, *The in situ conformation and axial location of the intermolecular cross-linked non-helical telopeptides of type I collagen.* Structure with Folding and Design, 2000. 8: p. 137-142.
30. Burgeson, R.E., *The junction zone and the dermis.* Current Problems in Dermatology, 1987. 17: p. 61-75.
31. Venturoni, M., T. Gutsmann, G.E. Fantner, J.H. Kindt, and P.K. Hansma, *Investigations into the polymorphism of rat tail tendon fibrils using atomic force microscopy.* Biochemical and Biophysical Research Communications, 2003. 303: p. 508-513.
32. Bozec, L. and M. Horton, *Topography and mechanical properties of single molecules of type I collagen using atomic force microscopy.* Biophysical Journal, 2005. 88: p. 4223-4231.
33. Rich, A. and F.H.C. Crick, *The structure of collagen.* Nature, 1955. 176: p. 915-916.
34. Fraser, R.D.B., T.P. MacRae, and E. Suzuki, *Chain conformation in the collagen molecule.* Journal of Molecular Biology, 1979. 129: p. 463-481.
35. Ramachandran, G.N. and G. Kartha, *Structure of collagen.* Nature, 1955. 176: p. 593-595.
36. Bella, J., M. Eaton, D.B. Brodsky, and H.M. Berman, *Crystal and molecular structure of a collagen-like peptide at 1.9 Angstroms resolution.* Science, 1994. 266: p. 75-81.
37. Bella, J., D.B. Brodsky, and H.M. Berman, *Hydration structure of a collagen peptide.* Structure, 1995. 3: p. 893-906.

38. Brodsky, D.B. and J.A.M. Ramshaw, *The collagen triple-helix structure.* Matrix Biology, 1997. 15: p. 545-554.
39. Orgel, J.P.R.O., A. Miller, T.C. Irving, R.F. Fischetti, A.P. Hammersley, and T.J. Wess, *The In situ supermolecular structure of type I collagen.* Structure, 2001. 9: p. 1061-1069.
40. Buehler, M.J., *Nature designs tough collagen: explaining the nanostructure of collagen fibrils.* Proceedings of the National Academy of Sciences of the United States of America, 2006. 103: p. 12285-12290.
41. Kadler, K.E., D.F. Holmes, J.A. Trotter, and J.A. Chapman, *Collagen fibril formation.* Journal of Biochemistry, 1996. 316: p. 1-11.
42. Pinnell, S.R. and G.R: Martin, *The cross-linking of collagen and elastin: enzymatic conversion of lysine in peptide linkage to alpha-aminoadipic-delta-semialdehyde (allysine) by an extract from bone.* Biochemistry, 1958. 61: p. 708-716.
43. Eyre, D.R., M.A. Paz, and P.M. Gallop, *Cross-linking in collagen and elastin.* Annual Reviews of Biochemistry, 1984. 53: p. 717-748.
44. Kielty, C.M., I. Hopkinson, and M.E. Grant, *Collagen, the collagen familly:structure, assembly and organisation in extracellular matrix*, in *Connective Tissue and its Heritable Disorders*, P.M. Royce and B. Steinmann, Editors. 1993, Wiley-Liss: New York. p. 103-147.
45. Hay, E.D., *Cell biology of extracellular matrix*, ed. E.D. Hay. 1991, New York: Plenum Press. 468.
46. Kjellen, L. and U. Lindahl, *Proteoglycans: structures and interactions.* Annual Reviews of Biochemistry, 1991. 60: p. 443-475.
47. Scott, J.E., M. Ritchie, R.W. Glanville, and A.D. Cronshaw, *Peptide sequences in gluteraldehyde-linked proteodermatan sulphate: collagen fragments from rat tail tendon locate the proteoglycan binding sites.* Biochemical Society Transaction, 1997. 25: p. 663.
48. Scott, J.E., C.R. Orford, and E.W. Hughes, *Proteoglycan-collagen arrangements in developing rat tail tendon.* Biochemical Journal, 1981. 195: p. 573-581.
49. Krusius, T. and E. Ruoslahtl, *Primary structure of an extracellular matrix proteoglycan core protein deduced from cloned cDNA.* Proceedings of the National Academy of Sciences of the United States of America, 1986. 83: p. 7683-7687.
50. Tajima, S., T. Nishikawa, H. Hatano, and Y. Nagai, *Distribution of macromolecular components in human dermal connective tissue.* Archives of Dermatological Research, 1981. 273: p. 115-120.
51. Woods, C.S., *From skin to parchment; a short description of the nature of skin, the chemical and physical changes brought about when turning skin into parchment and their implications for conservation.* Papier Restaurierung, 2002. 3: p. 13-18.
52. Poole, J.B. and R. Reed, *The preparation of leather and parchment by the dead sea scrolls community.* Technology and Culture3, 1962. 1: p. 1-26.
53. Chahine, C., *Changes in hydrothermal stability of leather and parchment with deterioration: a DSC study.* Thermochimica Acta, 2000. 365: p. 101-110.
54. Derrick, M., *Evaluation of the state of degradation of dead sea scroll samples using FT-IR spectroscopy.* The American Institute for Conservation, 1991. 10.
55. Bienkiewicz, K., *Physical chemistry of leathermaking*, ed. F.L. Malabar. 1983: Krieger Publishing Co.
56. Rao, R., P. Thanikaivelan, and U.N. Balachandran, *An eco-friendly option for less-chrome and dye-free leather processing: in situ generation of natural colours in leathers tanned with Cr–Fe complex.* Clean technology Environment Policy, 2002. 4: p. 115-121.

57. Rajaram, R., U.N. Balachandran, and T. Ramasami, *Chromium(III) induced abnormalities in human lymphocyte cell proliferation: evidence for apoptosis.* Biochemical and Biophysical Research Communications, 1995. 210: p. 434-440.
58. Costa, M. and C.B. Klein, *Toxicity and carcinogenicity of chromium compounds in humans.* Critical Reviews in Toxicology, 2006. 36: p. 155-163.
59. Langard, S., *One hundred years of chromium and cancer: a review of epidemiological evidence and selected case reports.* American Journal of Industrial Medicine, 1990. 17: p. 189-215.
60. Cabeza, L.F., M.M. Taylor, G.L. DiMaio, E.M. Brown, W.N. Marmer, R. Carrio, P.J. Celma, and J. Cot, *Processing of leather waste: pilot scale studies on chrome shavings. Isolation of potentially valuable protein products and chromium.* Waste Management, 1998. 18: p. 211-218.
61. Walawska, B. and Z. Kowalski, *Model of technological alternatives of production of sodium chromate (VI) with the use of chromic wastes.* Waste Management, 2000. 20: p. 711-723.
62. Brown, E.M., *Effects of neutral salts on collagen structure and chromium-collagen interactions.* Journal of American Leather Chemists Association, 1999. 94: p. 59-68.
63. Brown, E.M., R.L. Dudley, and A.R. Elsetinow, *A conformational study of collagen as affected by tanning procedures.* Journal of American Leather Chemists Association, 1997. 92: p. 225-233.
64. Brown, E.M., G. King, and J.M. Chen, *Model of the helical portion of a type I collagen microfibril.* Journal of American Leather Chemists Association, 1997. 92: p. 1-7.
65. Maeser, M., *The effect of hide location and cutting direction on the tensile properties of upper leather.* Journal of American Leather Chemists Association, 1960. 55: p. 501.
66. Sturrock, E.J., C. Boote, G.E. Attenburrow, and K.M. Meek, *The effects of the biaxial stretching of leather on fibre orientation and tensile modulus.* Journal of Materials Science, 2004. 39(7): p. 2481-2486.
67. Sturrock, E.J., G.E. Attenburrow, C. Boote, and K.M. Meek, *The effect on bending stiffness of drying leather under strain.* Journal of the Society of Leather Technologists and Chemists, 2001. 86: p. 6-10.
68. Boote, C., E.J. Sturrock, G.E. Attenburrow, and K.M. Meek, *Pseudo-affine behaviour of collagen fibres during the axial deformation of leather.* Journal of Materials Science, 2002. 37: p. 3651-3656.
69. Wright, D.M. and G.E. Attenburrow, *The set and mechanical behaviour of partially processed leather dried under strain.* Journal of Materials Science, 2000. 35: p. 1353-1357.
70. Newton, R.H. and K.M. Meek, *Circumcorneal annulus of collagen fibrils in the human limbus.* Investigative Ophthalmology & Visual Science, 1998. 39: p. 1125-1134.
71. Hukins, D.W.L., *X-ray diffraction by disordered and ordered systems.* 1st ed. 1981: Pergamon Press.
72. Cullity, B.D., *Elements of X-ray diffraction.* 2nd ed, ed. M. Cohen. 1978: Addison Wesley. 545.
73. Glazer, A.M., *The structure of crystals.* Student monographs in physics. 1987, Bristol: IOP Publishing Limited. 55.

74. Eikenberry, E.F., B. Brodsky, and D.A.D. Parry, *Collagen fibril morphology in developing chick metatasal tendons: 1. X-ray diffraction studies.* International Journal of Biological Macromolecules, 1982. 4: p. 322-328.
75. Oster, G. and D.P. Riley, *Scattering from cylindrically symmetric systems.* Acta Crystallographica, 1952. 5: p. 272-276.
76. Worthington, C.R. and H. Inouye, *X-ray diffraction study of the cornea.* International Journal of Biological Macromolecules, 1985. 7: p. 2-8.
77. Ramachandra, G.N., *Structure of collagen at the molecular level.* Treatise on Collagen, ed. G.N. Ramachandra. 1967, London: Academic Press. 103-183.
78. Squire, J., *The structural basis of muscular contraction.* 1st ed. 1981, New York: Plenum Press. 716.
79. Pavia, D.L., G.M. Lampman, and G.S. Kriz, *Introduction to spectroscopy.* 3rd ed. 2001: Harcourt. 593.
80. Hollas, J.M., *Modern spectroscopy.* 3rd ed. 1996: Wiley. 393.
81. Grossmann, J.G., *Shape determination of biomolecules in solution from synchrotron X-ray scattering.* Scattering, ed. P.S.E.R. Pike. 2002: Academic Press. 1123-1139.
82. Narayanan, T., O. Diat, and P. Bosecke, *SAXS and USAXS on the high brilliance beamline at the ESRF.* Nuclear Instruments and Methods in Physics Research Section A: Accelerators, Spectrometers, Detectors and Associated Equipment, 2001. 467-468: p. 1005-1009.
83. Kirkpatrick, P. and A.V. Baez, *Formation of optical images by X-rays.* Journal of the Optical Society of America, 1948. 38: p. 766-774.
84. Basilevsky, A., *Statistical factor analysis and related methods, theory and applications.* 1994, New York: John Wiley and Sons.
85. Everitt, B.S. and G. Dunn, *Applied multivariate data analysis.* 1992, New York: Oxford University Press.
86. Haines, B.M., *Shrinkage temperature in collagen fibres.* Leather Conservation News, 1987. 3: p. 1-5.
87. Kolomaznik, K., A. Blaha, T. Dedrle, D.G. Bailey, and M.M. Taylor, *Non-ammonia deliming of cattle hides with magnesium lactate.* Journal of American Leather Chemists Association, 1996. 91: p. 18-20.
88. Meek, K.M. and A.J. Quantock, *The use of X-ray scattering techniques to determine corneal ultrastructure.* Progress in Retinal and Eye Research, 2001. 20: p. 95-137.
89. Weiner, S., Z. Kustanovich, E. Gil-Av, and W. Traub, *Dead sea scroll parchments:unfolding of the collagen molecules and racemization of aspartic acid.* Nature, 1980. 287: p. 820-823.
90. Kennedy, C.J., J. Hiller, D. Lammie, M. Drakopoulos, M. Vest, M. Cooper, W.P. Adderley, and T.J. Wess, *Microfocus X-ray diffraction of historical parchment reveals variations in structural features through parchment cross sections.* Nanoletters, 2004. 4: p. 1373-1380.
91. Wess, T.J. and J.P. Orgel, *Changes in collagen structure: drying, dehydrothermal treatment and relation to long term deterioration.* Thermochimica Acta, 2000. 365: p. 119-128.
92. Stinson, R.H. and P.R. Sweeney, *Skin collagen has an unusual d-spacing.* Biochimica et Biophysica Acta, 1980. 621: p. 158-161.
93. Menderes, O., A.D. Covington, E.R. Waite, and M.J. Collins, *The mechanism and effects of collagen amide group hydrolysis during liming.* Journal of the Society of Leather technologists and Chemists, 1998. 83: p. 107-110.

94. Ritz-Timme, S. and M. Collins, *Racemisation of aspartic acid in human proteins.* Ageing Research Reviews, 2002. 1: p. 43-59.
95. Cameron, G.J., I.L. Alberts, J.H. Laing, and T.J. Wess, *Structure of type I and type III heterotypic collagen fibrils: an X-ray diffraction study.* Journal of Structural Biology, 2002. 137: p. 15-22.
96. Scott, J.E., *Structure and function in extracellular matrices depend on interactions between anionic glycosaminoglycans.* Pathologie Biologie, 2001. 49: p. 284-289.
97. Ghioni, C., J. Hiller, C.J. Kennedy, A.E. Aliev, M. Odlyha, M. Boulton, and T.J. Wess, *Evidence of a distinct lipid fraction in historical parchments: a potential role in degradation?* Journal of Lipid Research, 2005. 46: p. 2726-2734.
98. Maxwell, C.A., T.J. Wess, and C.J. Kennedy, *X-ray diffraction study into the effects of liming on the structure of collagen.* Biomacromolecules, 2006. 7: p. 2321-2326.
99. Brodsky, B., E.F. Eikenberry, and K. Cassidy, *An unusual collagen periodicity in skin.* Biochimica et Biophysica Acta, 1980. 621: p. 162-166.
100. Wray, J., *Structural studies on biological fibres.* 1971, University of Oxford: Oxford. p. 26-27.
101. Renugopalakrishnan, V., G. Chandrakasan, S. Moore, T.B. Hutson, C.V. Berney, and R.S. Bhatnagar, *Bound water in collagen. Evidence from Fourier transform Infrared and Fourier transform Infrared photoacoustic spectroscopic study.* Macromolecules, 1989. 22.
102. Long, D.G.F., B. Silveira, and P. Julig, *Chert analysis by Infrared spectroscopy.* A Collection of Papers Presented at the 33rd Annual Meeting of the Canadian Archaeological Association, 2001.
103. Xie, A.J., Y.H. Shen, C.Y. Zhang, Z.W. Yuan, X.M. Zhu, and Y.M. Yang, *Crystal growth of calcium carbonate with various morphologies in different amino acid systems.* Journal of Crystal Growth, 2005. 285: p. 436-443.
104. Kim, D.S. and C.K. Lee, *Surface modification of precipitated calcium carbonate using aqueous fluosilicic acid.* Applied Surface Science, 2002. 202: p. 15-23.
105. Fratzl, P. and A. Daxer, *Structural transformation of collagen fibrils in corneal stroma during drying: An X-ray scattering study.* Biophysical Journal, 1993. 64: p. 1210-1214.
106. Miller, A. and D. Tocchetti, *Calculated X-ray diffraction pattern from quasi-hexagonal model for the molecular arrangement in collagen.* International Journal of Biological Macromolecules, 1980. 3: p. 9-18.
107. Wess, T.J., A. Miller, and J.P. Bradshaw, *Cross-link sites in type I collagen fibrils studied by neutron diffraction.* Journal of Molecular Biology, 1990. 213: p. 1-5.

Appendix 1 - Publications

X-ray Diffraction Study into the Effects of Liming on the Structure of Collagen

Clark A. Maxwell,* Tim J. Wess, and Craig J. Kennedy

Biophysics Division, School of Optometry and Vision Sciences, University of Cardiff, Redwood Building, King Edward VII Avenue, Cathays Park, Cardiff, Wales, United Kingdom CF10 3NB

Received March 17, 2006; Revised Manuscript Received May 26, 2006

The manufacture of parchment from animal skin involves processes that remove hair, fats, and other macromolecules. Although it is well understood that the collagen fibers "open up" during processing, this study uses small and wide-angle X-ray diffraction to measure quantitatively the changes induced at the nanoscopic and microscopic levels. The axial rise per residue distance within the collagen molecules is unaffected by salt and lime treatments. Salting of the hides appears to remove noncollagenous materials. The intermolecular lateral packing distance between the hydrated collagen molecules (1.4 nm) increases after salting (~1.5 nm) and liming (~1.55 nm); drying is responsible for a reduction to ~1.2 nm in all samples. The axial staggered array (*d* spacing) is reduced by 1 nm after liming and is unaffected by drying. The average fibril diameter increases from 103.2 to 114.5 nm following liming, and the fibril-to-fibril distance increases from 122.6 to 136.1 nm.

Introduction

A major byproduct of the meat industry is animal hides, which provides a valuable source of collagen based materials. Collagen products include leather and parchment, and as gelatin, it is used in the food industry, photographic industry,[1] and pharmaceutical industry for capsules to aid oral drug delivery. Collagen is the major extra cellular matrix protein and forms naturally into polymers that associate together into specific hierarchical structures. The formation of these structures and their association with noncollagenous macromolecules such as the proteoglycans chrondroitin sulfate and dermatan sulfate[2−4] is fundamental to the high level of tensile strength and flexibility that collagen gives to tissues, such as tendon, ligaments, and skin.[5]

Hides usually undergo a series of primary treatments such as salting, liming, and mechanical abrasion in order to partially preserve, remove hair (and other noncollagenous macromolecules), and alter the overall mechanical properties of the tissue.[5] Parchment manufacture is a well established use of hide where the steps in manufacture are representative of general hide treatments and finishing processes resulting in a variety of products. For example, the use of tanning agents in the manufacture of leather and not in parchment is the fundamental difference between both manufacturing processes. Liming and salting have remained key steps in parchment production for at least the last millennia and is a relatively modern method compared to that used to make the Dead Sea Scrolls. Examining the molecular alterations engendered in the tissue by salting and liming protocols will therefore give useful information applicable to many different collagen based manufacturing processes.

To date the changes in collagen and associated molecules at the molecular, nanoscopic, and microscopic levels brought about by hide treatments are not well described in the literature. Terms such as "opening up" of the collagen fibers is often used to describe the effects of the processes such as liming and salting without a firm structural basis.[6] The purpose of the data presented here is to describe quantitatively the alterations to collagen structure in the processes of salting, liming, and drying that are used in parchment manufacture but are also representative of many other collagen treatments.

Collagen based tissues such as skin are hierarchically organized materials where there is an intimate relationship and connectivity between the molecular structure relating to the helical organization within individual collagen molecules. The well-defined nanoscopic axial and lateral organization of locally associated collagen molecules and thence the organization of discrete fibrillar structures as shown in Figure 1 produce a functional tissue.

Collagen molecules are composed of three polypeptide chains that form a triple helix. The collagen molecules are staggered axially relative to their neighboring molecules by *d*, ~67 nm in tendon or ~65.5 nm in skin. This arrangement is known as the Hodge−Petruska model.[2,7,8]

The *d* repeat is a characteristic feature of collagen. The stagger leaves a gap between linearly adjacent molecules as the molecular length (300 nm) is not an exact multiple of the *d* period, which results in a gap region and an overlap region within each *d* repeat. The gap region comprises 0.54 of *d*, and the overlap subsequently comprises 0.46 of *d*.[9] Of the 29 known collagen types, types I, II, III, V, and XI are capable of forming fibrils. The collagen molecules are orientated forming cylindrical objects with diameters ranging between 10 and 500 nm.

X-ray diffraction was used quantitatively to measure changes at different levels of the collagen structural hierarchy, from intra- and intermolecular interactions to analysis of the size of the collagen fibrils in the hydrated and dehydrated states that comprise fundamental elements of the parchment making process. Due to its minimal sample preparation requirements, X-ray diffraction has great potential when analyzing parchments that should not be damaged, as they can be valuable historical materials. It is therefore an important technique, which can be used to analyze and compare both historical and modern materials.

* Corresponding author. Tel: +44 29 2087 0203. Fax: +44 29 2087 4859. E-mail: MaxwellCA@cardiff.ac.uk.

10.1021/bm060250t CCC: $33.50
Published on Web 07/22/2006

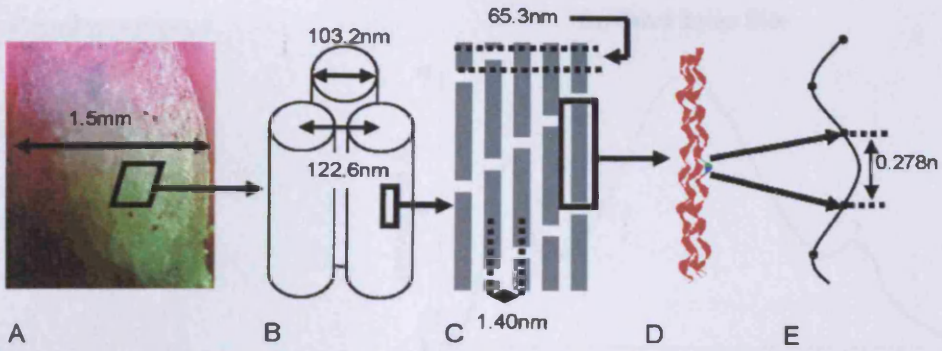

Figure 1. Collagen hierarchy from the microscopic down to the molecular. (A) An image of untreated bovine hide. (B) Fibril packing. (C) Microfibril packing. (D) Collagen triple helix. (E) Helical rise per residue distance. Diagram is for hydrated untreated bovine hide and is not to scale.

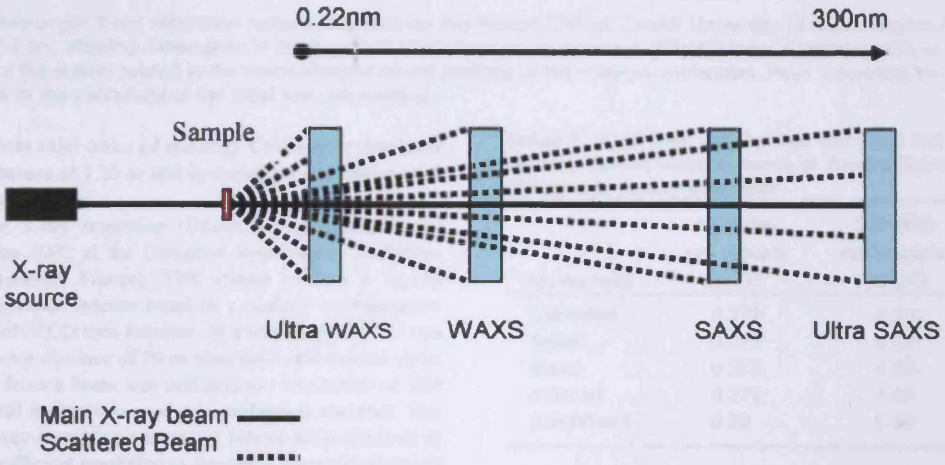

Figure 2. Illustration of sample to detector distances covering UWAXS to USAXS scattering angles. The range of structural features that can be obtained is in the region of 0.22 up to 300 nm.

Table 1. List of Bovine Hide Samples ($n = 3$ for Each Process Stage) Supplied by W. Visscher from William Cowley, Parchment and Vellum Works, Newport Pagnell, U.K.[a]

bovine hide wet	bovine hide dry
untreated (control)	untreated
salted	salted
limed	limed
delimed	delimed
n/a	parchment (control)

[a] Hydrated untreated hide was used as a control. Completed parchment is in a dehydrated state and was therefore used only as a control for the dried samples.

Materials And Methods

Treated Skin Samples. The treated animal skins were supplied by W. Visscher from William Cowley, parchment and vellum works, Newport Pagnell, U.K. The samples selected were calfskin which had been treated in a traditional parchment liming manufacturing process. Due to exact methods being subject to proprietary, a detailed description of the manufacturing process will not be disclosed, but typically salting is used for preservation before processing, followed by soaking the skin in slaked lime for up to 2 weeks for dehairing and removal of proteoglycans and other noncollagenous macromolecules. Deliming of skins involves the use of washing in water and the addition of neutralizing salts.[10]

The control samples used were untreated, mechanically dehaired skin (scraped using a blunt knife; the presence of hair keratin was not observed in X-ray diffraction images and therefore discounted as a possible cause of interference) and parchment representing the start and end products of the process. Table 1 contains a list of the samples used including the dry samples, which were obtained by slowly air-drying a portion of the hydrated samples at room temperature over a 7 day period.

X-ray Scattering Technical Details. X-ray scattering images were obtained and used to analyze the effects of selected stages of the parchment manufacturing process on collagen. By using a series of camera lengths (Figure 2) information was obtained regarding the intra- and intermolecular and intra- and interfibrilar interactions.

The NanoSTAR facility at Cardiff University, with a sample to detector distance of 4 cm, gives ultra wide-angle X-ray scattering (UWAXS) patterns allowing features of collagen structures of between 0.22 and 3.0 nm to be observed. A 0.154 nm X-ray beam is generated by a Kristalloflex 760 X-ray generator (Bruker AXS, Germany) and focused using cross-coupled Göbel mirrors and a 3-pinhole collimation system. A HI−STAR 2d detector is used for data collection. The NanoSTAR was used to measure the changes in the axial rise per residue distance of the collagen helix and the contributions of collagen and amorphous matter to the X-ray diffraction image. Calibration standard was calcite.

Wide and small-angle X-ray scattering (WAXS and SAXS) data were obtained from experiments carried out at SRS Daresbury, U.K., beam line station 2.1, which has a fixed X-ray wavelength of 0.154 nm and a variable sample to camera (multiwire detector) length of 0.9 to 8.0 m giving information on structures in the range from 1 to 200 nm. The sample holder has a computer controlled X−Y elevation stage for movement of the sample in specific and measurable directions.[11] A 1.25 m sample to detector distance was used to obtain WAXS data to evaluate accurately the intermolecular lateral packing of the collagen molecules, which occurs in real space, in the region of ~1 nm in the dehydrated state. The sample to detector distance was increased to 8 m to allow SAXS experiments to observe long-range interactions of

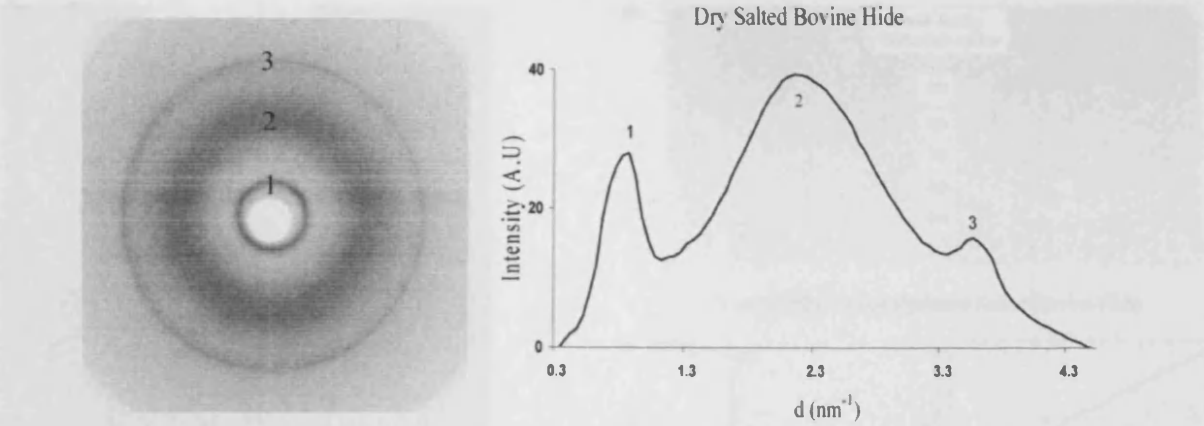

Figure 3. (Left) Wide-angle X-ray diffraction pattern obtained on the NanoSTAR at Cardiff University of salted bovine hide at a sample to detector distance of 4 cm, allowing dimensions in the region of 10−0.2 nm to be resolved. (Right) Linear intensity profile of the 2D image. Peak 1 is representative of the scatter related to the intermolecular lateral packing of the collagen molecules. Peak 2 contains the amorphous scatter. Peak 3 corresponds to the periodicity of the axial rise per residue.

collagen resulting from axial order (*d* spacing). Calibration standards used were silver behenate at 1.25 m and hydrated rat tail tendon at 8 m sample to detector distance.

Ultra small-angle X-ray scattering (USAXS) experiments were carried out on station ID02 at the European Synchrotron Radiation Facility (ESRF, Grenoble, France). This station utilizes a highly collimated, monochromatic intense beam in a pinhole configuration on to a XRII−FReLoN CCD area detector. At a wavelength of 0.1 nm and a sample to detector distance of 10 m, structural information up to 300 nm is obtained from a beam size and detector resolution of 100 μm.[12] Hydrated rat tail tendon was used as a calibration standard. The ultra small-angle X-ray scattering patterns of bovine hide obtained at station ID02 gave a sufficient resolution to determine scattering features due to the cylindrical nature of collagen fibrils and the interference between fibril structures.

The 2-D diffraction patterns were converted into 1-D linear intensity profiles using CCP13 software without significant loss of data.[13] PeakFit4 (AISL software) the one-dimensional peak fitting program was used to determine the peak size shapes and integrated intensity of the linear profiles.

Collagen in both skin and parchment is arranged in a felt-like network; the isotropy of the felt-like arrangement of the collagen fibers[14] within animal hide samples usually results in a radially averaged diffraction image. Preferential alignment of collagen in skin is occasionally seen, but this is most likely due to the location that the sample was taken from, such as collagen fibers taken from the neck and spinal areas.[6]

Results

Evaluation of the Diffraction Data. X-ray scattering patterns of collagen obtained by UWAXS display diffraction series corresponding to axial repeating structures. The position of the strong reflection at approximately 0.29 nm[15] relates to the axial rise distance (helical rise per residue) between the amino acid residues along collagen molecular triple helices. The typical isotropy of a wide angle diffraction pattern from bovine hide and its linear trace of intensity versus scattering angle are shown in Figure 3.

Further analyses using Peakfit4 software of the linear profiles are given in Table 2. The helical rise per residue value of the collagen molecules appears to be relatively unchanged following different treatments. The full width half-maximum of the axial rise per residue peak in Figure 3 increases from untreated skin through to parchment where the greatest change is observed due to the liming of bovine hide.

Table 2. Axial Rise per Residue and Peak Full Width Half Maxima (fwhm) Measurements of Treated Bovine Hide, and the Collagen to Amorphous Ratio

bovine hide	axial rise per residue (nm)	full width half maxima (nm^{-1})	collagen/ amorphous ratio
untreated	0.278	3.23	0.14
salted	0.277	3.95	0.17
limed	0.279	4.89	0.18
delimed	0.279	4.08	0.17
parchment	0.29	5.96	0.18

Collagen/Amorphous Ratio. Gelatinization is caused by a loss of structural order within collagen due to unfolding of the molecules forming gelatin.[16] Dividing the integrated intensity of the peak that accounts for the intermolecular lateral packing of the collagen molecules by the peak arising from the amorphous scatter that result from gelatin and other noncollagenous materials, it is possible to determine a ratio of collagen to amorphous content within the samples.[16,17] Table 2 shows that the ratio of collagen to amorphous material increases as the untreated skin is treated with sodium chloride and then calcium hydroxide.

Changes in Intermolecular Lateral Packing. An X-ray diffraction image displaying the collagen molecule−molecule interactions (intermolecular lateral packing) observable at 1.2 nm[7] is shown in Figure 4. The X-ray diffraction patterns obtained were plotted as linear traces of intensity versus scattering angle, which were analyzed using Peakfit4 software, and the structural information obtained is shown in Table 3.

Salting of bovine hide induces an increase from 1.4 to ~1.5 nm in the intermolecular lateral packing distance between the collagen molecules in the hydrated state compared to untreated skin. The full width half-maximum of the intermolecular lateral packing reflection of the diffraction pattern in Figure 4 is reduced slightly by salting. These results show that salting induces a greater average distance between collagen molecules but has a minimal effect on the collagen crystallinity.

Liming of the bovine hide increases the distance between the collagen molecules by ~0.15 nm compared to untreated skin. The full width half-maximum of the peak at ~1.55 nm is reduced after liming.

Deliming of the sample does not appear to have an effect on the intermolecular lateral packing distance indicating that the

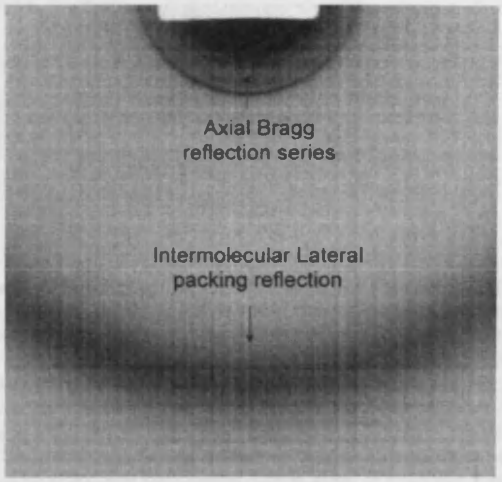

Figure 4. X-ray diffraction pattern obtained at SRS Daresbury station 2.1 of limed bovine hide at a sample to detector distance of 1.25 m, allowing dimensions in the region of 1 nm to be resolved.

liming stage has induced a permanent change in the collagen hierarchical stability. Table 3 shows that after dehydration the collagen molecule-to-molecule distance reduces to ~1.2 nm for all samples and that there is little variation in the full width half-maxima of the intermolecular lateral packing peak.

***d* Spacing.** Collagen exhibits a number of long-range interactions resulting from axial order and possible substructures within the fibril. To observe large-scale features by X-ray diffraction, small angle scattering is used.

The electron density profile of the *d* spacing produces a diffraction series of sharp reflections on the small angle scattering image as shown in Figure 5, panels a and b.[14] These sharp reflections can be used to determine a change in the *d* spacing of the collagen molecules as the alteration in electron density along the fiber axis are reflected in changes to the intensity of these peaks. A useful indicator of sample hydration can be obtained from the reflection intensities, where a strong 5th order of diffraction indicates high levels of hydration and a strong 6th order of diffraction indicates dehydration[3] as shown in Figure 5. Changes to the *d* spacing have been listed in Table 4 for all sample treatments and also the effect of dehydration. Both salting and drying of bovine hide do not appear to have an effect on the collagen *d* spacing. However, liming of bovine hide causes a reduction by ~1 nm giving a value that is similar to the 63.5 nm of parchment.

Fibril Diameter and Packing. The scattering from a fibril is conveniently represented by the scattering of a solid cylinder with a given diameter. The scattering function of such a cylinder is conveniently described as a first-order Bessel function (for example Eikenberry et al., 1982).[18] The ultra small-angle X-ray scattering (USAXS) pattern of bovine hide (Figure 6) obtained at station ID02 of the ESRF gave a sufficient resolution to

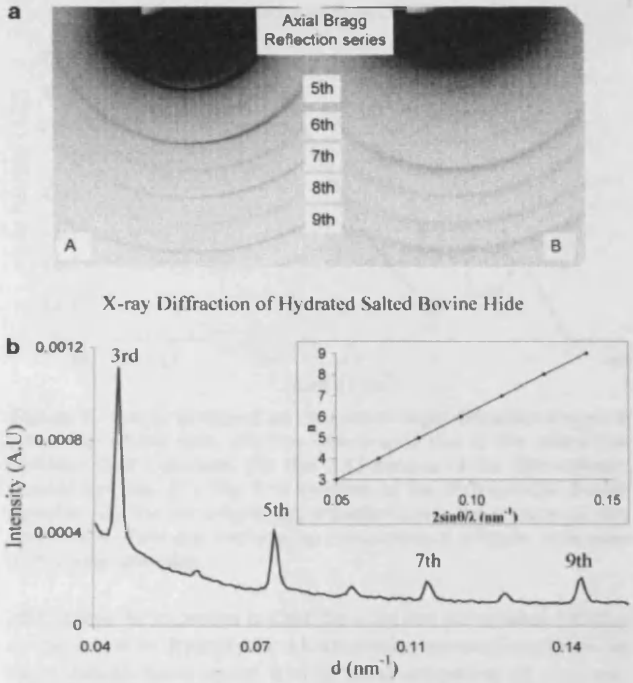

Figure 5. (a) X-ray diffraction pattern obtained at SRS Daresbury station 2.1 of bovine hide at a sample to detector distance of 8 m, allowing dimensions in the region of 200 nm to be resolved. (A) Wet salted hide. (B) Dry salted hide. (b) A linear intensity profile of the small angle diffraction image of hydrated salted bovine hide represented in Figure 5. The orders of Bragg reflections due to the electron density distribution of the gap and overlap interactions of collagen molecules in the axial direction have been included. The positions of these orders with respect to each other, and calibration against a known standard were used to calculate the *d* spacing of the axial gap and overlap. Insert plot is an example of n orders vs 2 sin θ/λ, where the slope is equal to the *d* spacing.

determine scattering features due to the convolution of the Bessel function from the cylindrical nature of the collagen fibrils and the interference function due to the interactions between neighboring fibrils.[8,9]

A linear intensity profile of a Bessel function has maxima at $qr = 0.0, 5.14, 8.42, 11.6, 14.8$, where $q = (4\pi/\lambda) \sin\theta$ (λ = X-ray wavelength and θ = half of the scattering angle) and r is the cylinder radius.[15] Plotting the normalized intensity from a cylindrical object against q, the collagen fibril radii were obtained from the position of these maxima in reciprocal space as shown in Table 5.

The interference function is dependent on the relative positions of the cylinders (fibrils), and a linear intensity profile against the scattering vector q can be used to determine the nearest neighbor center-to-center spacing.[18] Table 5 shows that after liming the fibril diameter increases by ~11 nm and that

Table 3. Collagen Intermolecular Lateral Packing and Peak Full Width Half Maxima (fwhm) Measurements of Bovine Hide in Its Wet and Dry States

bovine hide (wet)	intermolecular lateral packing (nm) (± 0.012 nm)	full width half maxima (nm^{-1})	bovine hide (dry)	intermolecular lateral packing (nm) (± 0.251 nm)	full width half maxima (nm^{-1})
untreated	1.40	1.83	untreated	1.20	1.01
salted	1.49	1.70	salted	1.20	1.05
limed	1.55	1.57	limed	1.17	1.01
delimed	1.57	1.61	delimed	1.18	1.02
			parchment	1.16	1.04

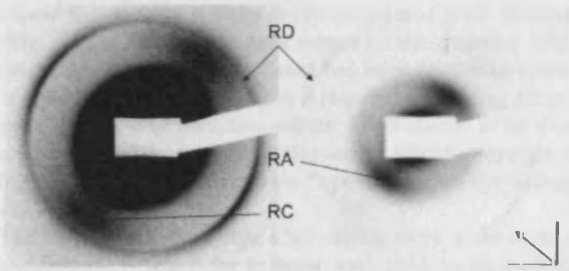

Figure 6. Diffraction pattern of limed bovine skin obtained at ESRF station ID02. The left and right images are used to illustrate how adjusting the minimum and maximum intensity limits of the same image can highlight the features present within the diffraction pattern. The sample to detector distance was 10 m, which was sufficient to observe; (RA) the interference due to the interaction between fibril cylinders, (RC) the 5.14 maxima of the fibril cylinder Bessel function. (RD) The 1st order Bragg reflection due to the electron density distribution of the gap and overlap interactions of collagen molecules in the axial direction. Orientation of the long fiber axis is indicated by the arrow on the bottom right of figure.

Table 4. *d* Spacing of Bovine Hide in Its Wet and Dry States

bovine hide (wet)	d spacing (nm) (± 0.283 nm)	bovine hide (dry)	d spacing (nm) (± 0.141 nm)
untreated	65.3	untreated	65.3
salted	65.0	salted	64.9
limed	64.2	limed (np1)	64.1
delimed	64.1	delimed	not visible
parchment	n/a	parchment	63.5

Table 5. Values for Fibril Lateral Packing, Peak Full Width Half Maxima Measurements and Fibril Diameters of Bovine Hide

bovine hide wet samples	fibril diameter (nm) (± 2.33 nm)	fibril lateral packing (nm) (± 1.13 nm)	full width half maxima (nm^{-1})
untreated	103.2	122.6	0.013
salted	not visible	not visible	not visible
limed	114.5	134.8	0.012
delimed	115.6	136.1	0.013

deliming of the sample does not appear to have an effect on the packing at the suprafibriller level.

The mean center-to-center distance from Table 5 shows that liming of the bovine hide increases the distance between the fibrils. The full width half-maxima of the interference function from Figure 7 does not change, indicating that there is no change in the level of disorder or crystal size. Deliming seems not to have any effect on the collagen fibril packing.

Discussion

The effects of processing hides on the structure of collagen, from the molecular to the fibrillar structures, have been evaluated by X-ray diffraction.

UWAXS described the effects of treatments at the molecular level. Results show that salting and liming do not have an effect on the distance between residues in the axial direction. However, the increased peak width due to liming gave a clear indication of changes at the molecular level. This broadening may be a result of an increase in disorder, a reduction in crystallite size, or a combination of the two. These effects could be due to the high alkalinity of the lime liquor which has been shown to cause a partial hydrolysis of the polypeptide backbone and to hydrolyze the amide groups.[19] The hydrolysis of the polypeptide

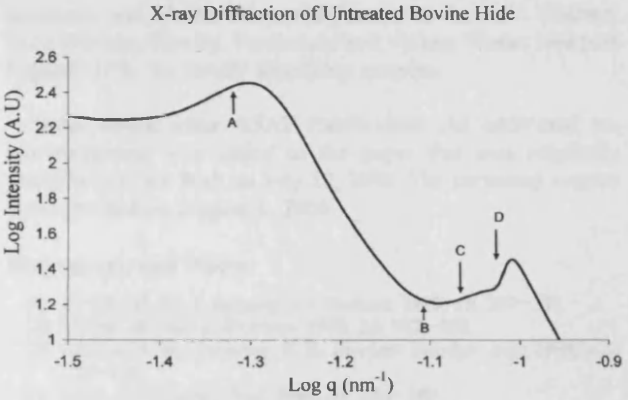

Figure 7. Linear profile of an ultra small angle diffraction image of untreated bovine hide. (A) The interference due to the interaction between fibril cylinders. (B) The 3.83 minima of the fibril cylinder Bessel function. (C) The 5.14 maxima of the fibril cylinder Bessel function. (D) The 1st order Bragg reflection due to the electron density distribution of the gap and overlap interactions of collagen molecules in the axial direction.

chains may be expected to alter the axial rise per residue distance at the point of hydrolysis; alternatively, several breakages in the collagen helix could lead to local relaxation of structure. The change of the amino acids from the L to D forms may have an effect on the distance between neighboring residues. Results indicate that although there is not an overall change in axial rise per residue distance, after salting or liming there is a breakdown in the local crystallinity, which could be explained by local effects such as hydrolysis and racemisation.

WAXS was employed to describe the interactions between neighboring collagen molecules. Salting of bovine hide increases the intermolecular lateral packing between collagen molecules and increases the level of disorder. This indicates that water or salt may be entering the spaces between the collagen molecules within the fibrils and that the fibrils are expanding.

Following liming, the intermolecular lateral packing peak becomes narrower, indicating that there may be a reduction in local disorder. The results demonstrate that this is accompanied by a swelling at the molecular level. The presence of Ca^{2+} ions from the lime is thought to cause an influx of water molecules causing the fibers to swell.[6] The high alkalinity of the lime solution shifts the iso-electric point causing some of the charges along the molecule to change, altering the side chain interactions between the molecules. This combined with hydrolysis of the side chains, which reduces the number of sites available for salt bridge cross linkages, may cause a lowering of stability.[5] Weakening of intermolecular collagen interactions and the influx of water may cause the loosening of the fiber network as found here.

SAXS showed that there was a reduction in *d* spacing after liming, which is most likely due to a change in the fibrillar structure in the axial direction. The weakening of side chain interactions due to hydrolysis and the change in the isoelectric point induced by the high alkalinity of the lime liquor may allow the possibility of the collagen molecules to move past each other, particularly if there was a reduction in intermolecular cross-links. Drying of the samples does not appear to have an effect on the *d* spacing indicating that the contraction is due to liming and not dehydration.

Collagen interactions with proteoglycans are fundamental to fibril diameter and packing. Proteoglycans are involved in dissipating compression stresses in the skin and are also involved in alignment of collagen fibrils.[4] The polysaccharide hyaluron

connects the decorin protein cores associated with dermatan sulfate bridges, which act as a compression resistive bridge between the fibrils. Salting of skin has been shown to remove up to 100% of the hyaluron,[6] but it requires the liming stage to remove over 50% of dermatan sulfate. The removal of hyaluron may release the pressure constraint on the fibrils, allowing the collagen fibrils to expand, and the "opening up" of the collagen fibers.

The results here show that after salting there is an increase in the distance between the collagen molecules in the hydrated state, and even more expansion after liming, which is carried through the hierarchical levels up to fibril packing; deliming did not appear to reverse these increases, indicating that the effects of salting and liming are permanent.

The removal of noncollagenous material due to the lime liquor is responsible for the increase in the collagen/amorphous ratio indicating that there is less amorphous material in comparison to collagen. If the collagen ratio had decreased, this would have indicated that the collagen molecules had become denatured. However, our results imply that the collagen structure and hierarchy although weakened are still relatively stable.

Conclusions

A general statement that the collagen fibers within the animal hide "open up" due to processing stages has been widely accepted. Our X-ray diffraction studies now quantitatively describe a swelling in fiber structure at the molecular level, which is observed through the hierarchical levels of collagen. Altering the amino acid side chains of the collagen molecules is likely to reduce stability between the molecules. This combined with the influx of water and the removal of proteoglycans from between the fibrils is most likely to be the cause of the "opening up" of the collagen fibers. However, the most noticeable structural change due to liming is the reduction in the *d* spacing. This combined with the helical rise per residue distance being unaffected is an indication that most of the changes are due to intermolecular interactions of collagen molecules as opposed to intramolecular.

Acknowledgment. We wish to thank Gunter Grossman, Station Manager of Beamline 2.1, Daresbury, U.K. and Thomas Weiss, Beamline ID02, ESRF, Grenoble, France for technical assistance and advice. We would also like to thank W. Visscher from William Cowley, Parchment and Vellum Works Newport Pagnell, U.K. for kindly supplying samples.

Note Added after ASAP Publication. An additional acknowledgment was added to the paper that was originally published on the Web on July 22, 2006. The corrected version was reposted on August 4, 2006.

References and Notes

(1) De Clercq, M. *J. Imaging Sci. Technol.* **1995**, *39*, 367−372.
(2) Obrink, B. *Eur. J. Biochem.* **1973**, *33*, 387−400.
(3) Stinson, R. H.; Sweeney, P. R. *Biochim. Biophys. Acta* **1980**, *621*, 158−161.
(4) Scott, J. E. *Pathol. Biol.* **2001**, 49, 284−289.
(5) Cameron, G. J.; Alberts, I. L.; Laing, J. H.; Wess, T. J. *J. Struct. Biol.* **2002**, *137*, 15−22.
(6) Haines, B. M. *Parchment, The physical and chemical characteristics of parchment and the materials used in its conservation*; The Leather Conservation Centre: Northampton, 1999.
(7) Sionkowska, A.; Wisniewski, M.; Skopinska, J.; Kennedy, C. J.; Wess, T. J. *Biomaterials* **2004**, *25*, 795−801.
(8) Goh, K. L.; Hiller, J. L.; Haston, D. F.; Holmes, K. E.; Kadler, A.; Murdoch, Meakin, J. R.; Wess, T. J. *Biochim. Biophys. Acta* **2005**, *1722*, 183−188.
(9) Quantock, A. J.; Meek, K. M.; Chakravarti, S. *Invest. Ophthalmol. Vision Sci.* **2001**, *42*, 1750−1756.
(10) Kolomaznik, K.; Blaha, A.; Dedrle, T.; Bailey, D. G.; Taylor, M. M. *J. Am. Leather Chem. Assoc.* **1996**, *91*, 18−20.
(11) Grossmann, J. G. In *Scattering*; Pike, P. S. E. R., Ed.; Academic Press: London, 2002; pp 1123−1139.
(12) Narayanan, T.; Diat, O.; Bosecke, P. *Nucl. Instrum. Methods A* **2001**, *467−468*, 1005−1009.
(13) Wess, T. J.; Drakopoulos, M.; Snigirev, A.; Wouters, J.; Paris, O.; Fratzl, P.; Collins, M.; Hiller, J.; Nielsen, K. *Archaeometry* **2001**, *43*, 117−129.
(14) Wess, T. J.; Orgel, J. P. *Thermochim. Acta* **2000**, *365*, 119−128.
(15) Meek, K. M.; Quantock, A. J. *Prog. Retin. Eye Res.* **2001**, *20*, 95−137.
(16) Weiner, S.; Kustanovich, Z.; Gil-Av, E.; Traub, W. *Nature* **1980**, *287*, 820−823.
(17) Kennedy, C. J.; Hiller, J.; Lammie, D.; Drakopoulos, M.; Vest, M.; Cooper, M.; Adderley, W. P.; Wess, T. J. *Nano Lett.* **2004**, *4*, 1373−1380.
(18) Eikenberry, E. F.; Brodsky, B.; Parry D. A. D. *Int. J. Biol. Macromol.* **1982**, *4*, 322−328.
(19) Menderes, O.; Covington, A. D.; Waite, E. R.; Collins, M. J. *J. Soc. Leather Tech. Chem.* **1998**, *83*, 107−110.

BM060250T

Clark A. Maxwell, Nancy Bell, Craig J. Kennedy and Tim J. Wess

X-ray diffraction and FT-IR study of caprine and ovine hide

Parchment is a historically important writing medium, based on the processed hides of animals. Many studies have been conducted on the deterioration of historical parchment in order to describe the molecular and fibrillar changes that may be occurring over time, which may help develop new methods to prevent deterioration or to restore parchments.[1,2]

In our previous study, we described the parchment-making process, specifically the effects of salting and liming on animal hides, and in particular their collagen structure.[3] It was demonstrated that a major influence on the future degradation of parchment is the method used to create parchment from animal hides. Salting of parchment removed the non-collagenous components of the skin, whilst liming increased the lateral distance between neighbouring molecules and reduced the axial d-spacing of the collagen (Fig. 1).

The interactions of collagen with other macromolecules, for example proteoglycans, are fundamental to collagen packing. Proteoglycans are involved in dissipating compression stresses in the skin and are also involved in alignment of collagen fibrils.[4] These proteoglycans are composed of a polysaccharide, hyaluron, which connects the decorin protein cores associated with dermatan sulphate bridges, which act as a compression resistive bridge between the fibrils. Salting of skin has been shown to remove up to 100% of the hyaluron, but it requires the liming stage to remove over 50% of dermatan sulphate.[5,6] The removal of hyaluron may release the pressure constraint on the fibrils, allowing the collagen fibrils to expand, thus 'opening up' the collagen fibres.

A property of collagen that can infer stability changes is that of shrinkage temperature. Collagen when heated in water gives a sudden shrinkage in length. Mammalian skin that has not been processed has a shrinkage temperature of 65°C and the limed samples have a shrinkage temperature of 60°C or less.[7] This shrinkage is due to breaking of hydrogen bonds, which are partly responsible for collagen helical stability. Changes in the collagen amino acid side chains will

Fig. 1 Representation of collagen molecule arrangement within a fibril. A) Each block represents a collagen molecule in the staggered array conformation found within a fibril. The intermolecular lateral packing distance between the collagen molecules is shown by I.L.P. B) The d-spacing of the collagen molecules represented by a gap and overlap area within the staggered array. This is representative of the electron density profile, which gives the characteristic step function of the collagen fibril.

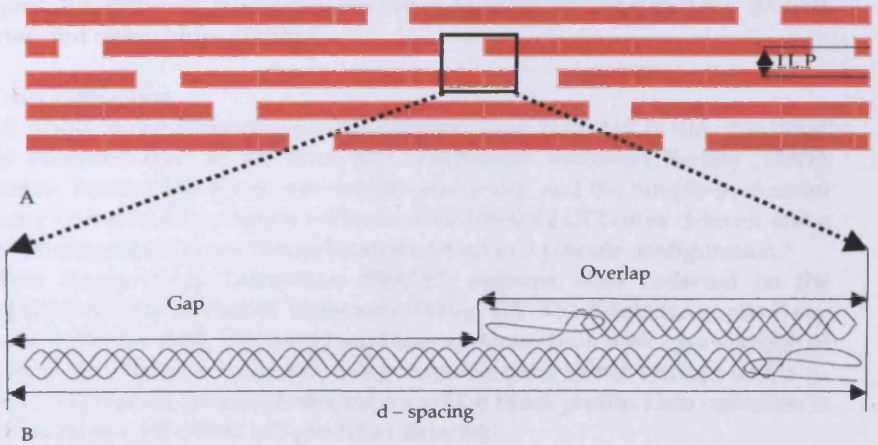

1 Larsen, R., ed., *Microanalysis of Parchment* (London: Archetype, 2002);

2 Fessas D., Schiraldi A., Tenni R., Vitellaro Zuccarello, L., Bairati A., and A. Facchini, 'Calorimetric, biochemical and morphological investigations to validate a restoration method of fire injured ancient parchment', *Thermochimica Acta* 348 (2000):129–137.

3 Maxwell, C.A., Wess, T.J., and C.J. Kennedy, 'An X-ray diffraction study into the effects of liming on the structure of collagen', *Biomacromolecules* 7 (2006): 2321–2326.

4 Scott, J.E., 'Structure and function in extracellular matrices depend on interactions between anionic glycosaminoglycans', *Pathology Biology* 49 (2001): 284–289.

5 Haines, B. M., 'Parchment; the physical and chemical characteristics of parchment and the materials used in its conservation', *(Northampton: The Leather Conservation Centre,* 1999). 1–32.

6 Alexander, K.T.W., Haines, B.M., and M.P Walker, 'Influence of proteoglycan removal on opening up in the beamhouse', *Journal of the American Leather Chemists Association* 81 (1986): 85–102.

7 Haines, B. M., 'Shrinkage temperature in collagen fibres', *Leather Conservation News* 3 (1987): 1–5

Samples	Treatments					
1	2% Liming 8 days, Unhaired, Scudded, Fleshed	1hr 100% 2-ethoxy ethanol	Toggled, Dried, Finished			
2	2% Liming 8 days, Unhaired, Scudded, Fleshed	2 hrs 150% Propan-2-one	Toggled, Dried, Finished			
3	2% Liming 8 days, Unhaired, Scudded, Fleshed	1 hr 80% Propan-2-one, 1hr 80% 2-ethoxy ethanol	Toggled, Dried, Finished			
4	2% Liming 7 days, Unhaired, Scudded, Fleshed	1 hr 80% Propan-2-one, 1hr 80% 2-ethoxy ethanol	Poor quality	Re-limed for 4 days	1 hr 80% Propan-2-one, 1hr 80% 2-ethoxy ethanol	Toggled, Dried, Finished
5	2% Liming 8 days, Unhaired, Scudded, Fleshed	1 hr Propan-2-one, 1hr 65% 2-ethoxy ethanol	Toggled, Dried	1% SUMAC tanning solution	1 hr 65% Propan-2-one, 1hr 65% 2-ethoxy ethanol	Toggled, Dried, Finished
6	2% Liming 8 days, Unhaired, Scudded, Fleshed	1 hr Propan-2-one, 1hr 65% 2-ethoxy ethanol	Toggled, Dried	Potash-alum tanning	Finished	

Table 1 Sample list and process treatments applied to historic caprine (C goat) and ovine (O sheep) hide. Caprine samples will be labelled as C1-C6 and Ovine samples O1-O6.

alter the proportion of hydrogen bonds that are formed. As shown in our previous study this will also have an effect on the d-spacing. Therefore a reduction in d-spacing could infer a reduction in collagen stability.

The steps in the parchment-making process are generic processing steps representative of general hide treatments and finishing processes resulting in a variety of collagen-based products. It has been shown that not only the chemicals used to preserve and de-hair hides can alter the collagen stability, but also the manner in which these steps are applied.[8] Harsh treatments of hides at the manufacturing stage can result in parchments with poorer hydrothermal stability, resulting in an accelerated degradation of parchment over time.

The current study focussed on a set of historic parchment samples known to have been processed with the solvents propan-2-one and 2-ethoxy ethanol with the aim of producing a higher quality writing material by degreasing the parchment.

To examine the effects of these treatments, we utilised the techniques of Small Angle X-ray Scattering (SAXS), Wide Angle X-ray Diffraction (WAXD) and Fourier Transform Infra-Red Spectroscopy (FT-IR) to describe the long- and short- range structural and chemical effects of these treatments respectively.

Materials and methods

1. Samples

A variety of caprine (goatskin) and ovine (sheepskin) samples taken from different stages of a known and well recorded parchment-manufacturing process were gifted by Chris Clarkson. The two species of skin used for this trial were from Abyssinian hair sheep and Javanese goat. All hides had been soaked by the manufacturer in a 0.5% Chloros antiseptic solution before being processed. The oxidizing effects of chloros on the hierarchy of collagen have not been examined in this study. However, for the purposes of this study, the effects of the propan-2-one and 2-ethoxy ethanol solutions have been compared to that of limed samples. Six different treatments had been used by the manufacturer on both caprine and ovine hides (Table 1).

2. X-ray diffraction

Small Angle X-ray Scattering (SAXS) patterns were collected at the ultra small angle beamline ID02 at the European Synchrotron Radiation Facility (ESRF), Grenoble, France. The X-ray wavelength was 0.1nm, and the sample-to-detector distance was 10m. This station utilizes a XRII-FReLoN CCD area detector and a highly collimated, intense monochromatic beam in a pinhole configuration.[9]

Wide Angle X-ray Diffraction (WAXD) patterns were collected on the NanoSTAR facility at Cardiff University, Wales, UK. The Kristalloflex 760 X-ray generator (Bruker AXS, Germany) produces an X-ray beam with a wavelength of 0.154nm. The beam is focussed using cross-coupled Göbel mirrors and a 3-pinhole collimation system producing a 100¶Ãm beam profile. Data collection is obtained from a HI-STAR 2-D gas-filled detector.

8 Chahine C., 'Changes in hydrothermal stability of leather and parchment with deterioration: a DSC study', *Thermochimica Acta* 365 (2000): 101–110.

9 Narayanan T., Diat O. and Boesecke P., 'SAXS and USAXS on the high brilliance beamline at the ESRF', *Nuclear Instruments and Methods in Physics Research section A: Accelerators, Spectometers, Detectors and Associated Equipment 467–468 (2001): 1005–1009.*

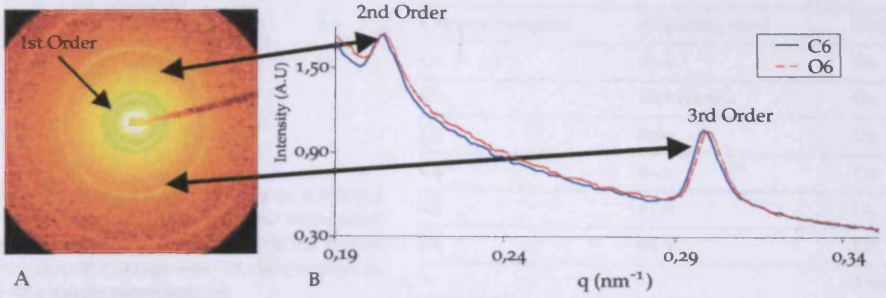

Fig. 2 A) Diffraction image of caprine parchment sample C6 obtained at ESRF station ID02. Sample to detector distance of 10m was sufficient to observe the 1st, 2nd and 3rd order Bragg reflections due to the electron density distribution of the gap and overlap interactions of collagen molecules in the axial direction. B) Linear intensity profile of the X-ray diffraction 2D image obtained using CCP13 FibreFix software.

The two-dimensional diffraction patterns were converted into one-dimensional linear intensity profiles[10] using the CCP13 (Collaborative Computational Project 13) program FibreFix. Analysis of the linear profiles was done using the peak fitting program PeakFit4 (AISL software).

3. FT-IR Spectroscopy

FT-IR spectra were obtained using a Nicolet 380FT-IR spectrometer at The National Archives, London. All spectra were recorded by absorption mode at $4cm^{-1}$ intervals and 32-times scanning over a wavelength range from $400cm^{-1}$ up to $4000cm^{-1}$. Data reduction was obtained by OMNIC software.

To better explain the differences present in the FT-IR spectra between samples, principal components analysis (PCA) was performed using in-house software. PCA is a data reduction technique that aims to reduce the dimensionality of any given data set, and to identify new underlying variables in the data set. The mathematical basis for PCA has been well documented.[11,12] PCA rotates the original data into a new set of axes, such that the first few axes reflect most of the variations within the data. By plotting the data on these axes, major underlying structures may be spotted automatically. PCA generates basis functions that explain the nature of the variance in the data. There are as many basis functions as there are initial variables, and they are sorted in decreasing order of importance, as dictated by their associated eigenvalues.

For each original variable, PCA generates coefficients that describe how much that variable contributes to the basis functions. Plotting the coefficients can determine if there is any correlation or trend in the variables.

Results

1. Small Angle X-ray Scattering

Scattering by X-rays at small angles ($<6^{\circ}$ at $\lambda = 1.54nm$) gives information regarding the long-range order of structures; it is a process that is experimentally similar to the better known X-ray diffraction, however, this technique uses a longer sample-to-detector distance that allows longer periodicities and particle sizes, up to several hundred nanometres in length, to be investigated. Collagen fibrils from skin display a fundamental axial periodicity of 65.5nm which falls into the range of SAXS.[13] The periodicity, or d-spacing, is a result of regular fluctuations in the electron density of collagen in the axial direction.[14,15] This is manifested in SAXS as a series of sharp Bragg reflections on the meridian of the small angle scattering image (Fig. 2).[16] The intensity and position of these Bragg peaks is a reflection of the alteration of the electron density along the fibre axis, and as such they can be used to determine changes in the collagen d-spacing. Figure 2 gives an example of an intensity versus scattering angle linear profile generated by FibreFix software from X-ray diffraction images of caprine and ovine hide. The linear profiles were further analysed using Peakfit4 software, and the positions of the 2nd and 3rd axial Bragg reflections (orders of diffraction)

10 Wess TJ., Wess L and Hocking PM., 'The structure of avian cartilage', *Journal of Comparative Pathology* (1997): 116, 145-155.

11 Basilevsky, A., *Statistical Factor Analysis and Related Methods, Theory and Applications* (New York: Wiley, 1994);

12 Everitt, B.S. and G. Dunn, *Applied Multivariate Data Analysis* (Oxford; New York: Oxford University Press. 1992).

13 Brodsky, B., Eikenberry E.F. and K. Cassidy., 'An unusual collagen periodicity in skin', *Biochimica et Biophysica Acta* 621 (1980): 162-166

14 Kennedy CJ., and T.J. Wess., 'The structure of collagen within parchment: A review', *Restaurator* 24:2 (2003): 61-80;

15 Hodge, A. J., and J.A. Petruska, *'Aspects of Protein Chemistry'* (Ramachandran, G. N, 1963).

16 Orgel JP., Miller A., Irving TC., Fischetti RF., Hammersley., and TJ Wess.,The in situ supermolecular structure of type I collagen' *Structure* 9 (2001): 1061-1069.

Caprine samples	d-spacing (nm)	Ovine samples	d-spacing (nm)
C1	61.5	O1	61.8
C2	Not shown	O2	62.4
C3	62.0	O3	62.2
C4	61.5	O4	60.9
C5	61.8	O5	61.9
C6	62.3	O6	61.7
		Limed skin (control)	64.1

Table 2 d-spacing of caprine hide (± 0.698nm) and ovine hide (± 0.722nm) in their rehydrated states. The d-spacing for sample C2 is not shown as the diffraction image was not clear enough to give an accurate measurement.

were used to calculate the axial d-spacing and are presented in Table 2. The d-spacing of collagen from the caprine and ovine hide samples were between 60.9 and 62.4nm, with the exception of the limed ovine hide control, which had not been treated with propan-2-one or 2-ethoxy ethanol and had a d-spacing of 64.1nm. The value for the limed sample had been extensively studied for other skin species and was typically in this range.[3]

2. Wide Angle X-ray Diffraction

The lateral distance between neighbouring collagen molecules is approximately 1.2nm, and is observed using WAXD.[17] Figure 3 shows a peak from a WAXD image, which arises from the intermolecular lateral packing of the collagen molecules. Analysis of the intensity profiles obtained for the treated caprine and ovine hide samples are presented in Table 3. All of the samples had a collagen intermolecular lateral packing distance of ~1.2nm, which was consistent with dry collagen.[18]

All of the samples were treated by the manufacturer with slaked lime as part of the dehairing process, which reacts with carbon dioxide in the atmosphere to form precipitated crystals of calcium carbonate. The presence of the calcite can be detected by X-ray diffraction at 0.3nm as shown in figure 3.[19]

3. Fourier Transform Infrared Spectroscopy

FT-IR spectra of collagen displays bands at 3333, 3071, 1658, 1549 and 1240cm^{-1}, which are characteristic of amide A, B, I, II and III bands of collagen, respectively.[20] The protein amide C=o stretching vibrations are the predominant cause of the amide I absorption. Amide II absorption is due to the combined effects of N-H bending vibrations (60%) and C-N stretching vibrations (40%). The

Fig. 3 Wide-angle diffraction patterns obtained on the NanoSTAR at Cardiff University of A) Caprine parchment sample C4, and B) Caprine parchment sample C5 at a sample to detector distance of 4cm. ILP is representative of the scatter related to the helix-to-helix interactions between collagen molecules (Intermolecular lateral packing). AMP contains the amorphous scatter. RC relates to the scatter from the mineral calcite. HR is the scatter due to the helical rise per residue along the collagen molecule and in diffraction image A, the HR scatter is masked by the calcite scatter (RC).

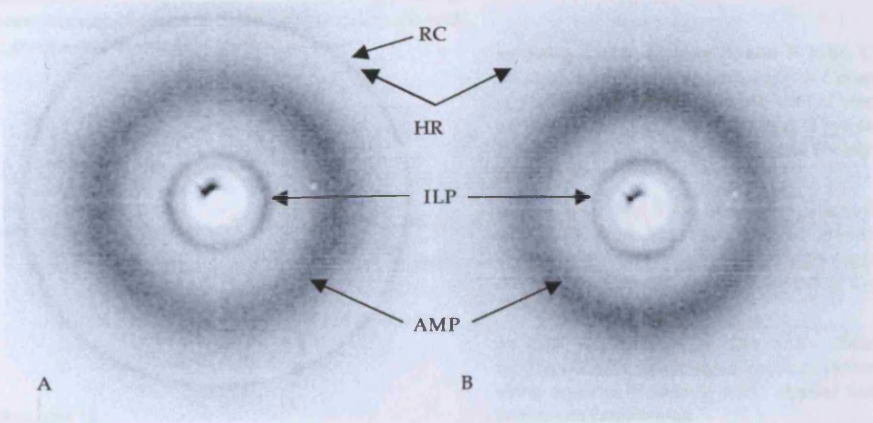

17 Sionkowska A., Wisniewski., Skopinska J., Kennedy CJ., and TJ Wess.,'Molecular interactions in collagen and chitosan blends', *Biomaterials* 25.5 (2004): 795-801.

18 Wray, J., *'Structural Studies on Biological Fibres'*, PhD thesis, University of Oxford (1971) 26-27.

19 Kennedy CJ., Hiller J., Lammie D., Drakopoulos M., Vest M., Cooper M., Adderley W.P., and T.J. Wess., 'Microfocus x-ray diffraction of historical parchment reveals variations in structural features through parchment cross sections', *Nano Letters* 4 (2004):1373-1380.

20 Renugopalakrishnan VG., Chandrakasan SM., Hutson TB., Berney CV., and RS Bhatnagar.,'Bound water in collagen. Evidence from fourier transform infrared and fourier transform infrared photoacoustic spectroscopic study', *Macromolecules* (1989): 10.

Caprine samples	Intermolecular Lateral packing (nm)	FWHM (nm-1)	Ovine samples	Intermolecular Lateral packing (nm)	FWHM (nm-1)
C1	1.20	1.20	O1	1.19	1.14
C2	1.20	1.29	O2	1.20	1.11
C3	1.19	1.36	O3	1.18	1.13
C4	1.19	1.28	O4	1.18	1.21
C5	1.19	1.34	O5	1.17	1.15
C6	1.19	1.38	O6	1.18	1.22

Table 3 Collagen intermolecular lateral packing (ILP) measurements of treated caprine hide (± 0.007nm) and ovine hide (± 0.007nm) in its dry state. The full width maxima (FWHM) of these peaks are given for caprine hide (± 0.13nm^{-1}) and for ovine hide (± 0.07nm^{-1}).

absorption due to amide III is representative of a complex combination of C-N stretching and N-H bending from amide linkages and CH_2 wagging vibrations from proline side chains and backbone glycine residues.[17] The presence of calcium carbonate can also be determined using FT-IR, with known absorption peaks at 1429 and 877cm^{-1}.[21] The peak at 877cm^{-1} is present regardless of which calcium carbonate isomorph gives the signal (i.e. calcite or vaterite; Xie et al, 2005). Both peaks may be attributed to Ca-O stretching vibrations.[23] The FT-IR spectra for caprine hide are shown in Figure 4, with an example of caprine hide containing calcium carbonate.

Basis functions one and three produced from PCA analysis of FT-IR data of caprine and ovine hide are shown in Figure 5. The most significant changes are

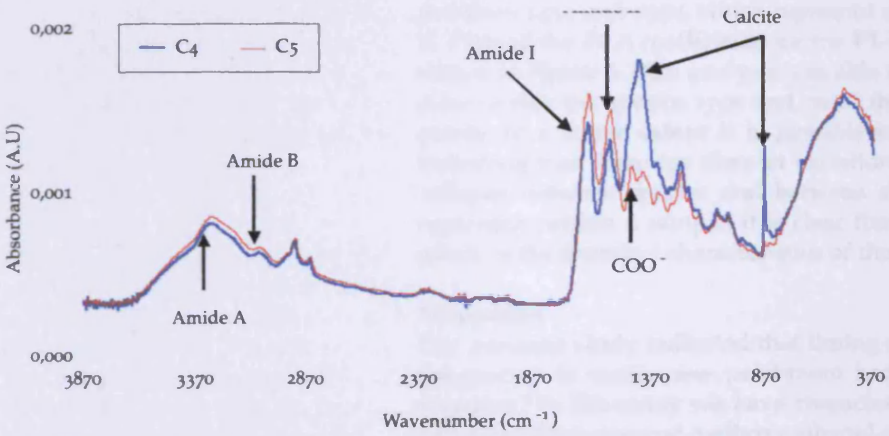

Fig. 4 FT-IR spectra of solvent-treated caprine parchment. Both samples C4 and C5 exhibited a typical characteristic collagen spectrum with peak positions at 3333, 3071, 1658, 1549, 1240cm^{-1} representing amide A, B, I, II and III. Sample C4 had peaks at 1429 and 877cm^{-1}, which was due to calcium carbonate crystals from the manufacturing process.

Fig. 5 PCA basis functions one and three of FT-IR data for caprine and ovine parchment. The most significant changes are highlighted by basis function one and are shown to occur as peaks at about A)1658, B1)1560 and D)1430cm^{-1}, which are representative of collagen amide I , amide II and calcite peaks. Basis function three, which highlights more discreet changes at peak positions C)1450 and B2)1550cm^{-1}, which represent collagen carboxylic groups and amine II.

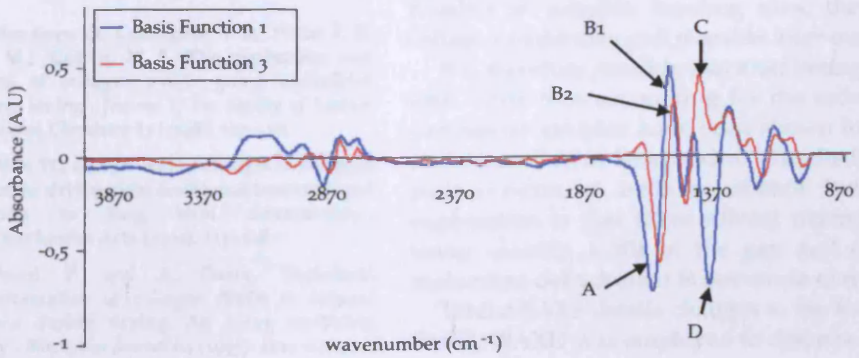

21 Long, D.G.F., Silveira B. and P. Julig, Chert Analysis by Infrared Spectroscopy. A Collection of Papers Presented at the 33rd Annual Meeting of the Canadian Archaeological Association (Ontario: The Ontario archaeological Society inc, 2001) 255-267.

22 Xie A-J., Shen Y-H., Zhang C-Y., Yuan Z-W, Zhu X-M., and YM Yang.,'Crystal growth of calcium carbonate with various morphologies in different amino acid systems. *Journal of Crystal Growth* 285 (2005): 436-443.

23 Kim D.S. and C.K. Lee C.K., 'Surface modification of precipitated calcium carbonate using aqueous fluosilicic acid', *Applied Surface Science* 202 (2002):15-23.

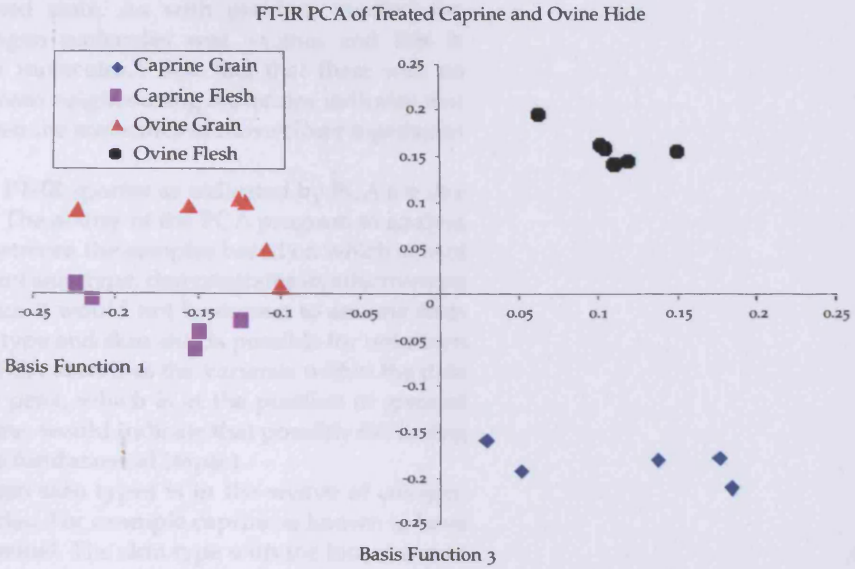

Fig. 6 Scatter plot of the coefficients of PCA analysis of FT-IR data for solvent-treated caprine and ovine parchment. There are clear separations across basis functions one between caprine and ovine species. Basis function three represents a separation between skin side (flesh to grain).

highlighted by basis function one and are shown to occur as peaks at about 1430, 1560 and 1658cm^{-1}, which are representative of calcite and collagen amide II and I peaks. Basis function three, which highlights more discreet changes at peak positions 1450 and 1550, which represent collagen carboxylic groups and amine II. Plots of the PCA coefficients for the FT-IR data of caprine and ovine hide are shown in Figure 6. PCA analysis was able to distinguish the flesh from the grain sides within the species type and, with the exception of possibly two outlying points, to a lesser extent it is possible to separate caprine from ovine hide, indicating that there are discreet variations in the chemical interactions within collagen between species and between skin layers. However, as there is no separation within a sample, it is clear that the treatment of the hides has little effect on the chemical characteristics of the hide collagen.

Discussion

Our previous study indicated that liming and salting of animal hides as part of the process to create new parchment had a significant effect on the collagen structure.[3] In this study we have characterized the effects of further treatments using propan-2-one and 2-ethoxy ethanol on the structural and chemical aspects of the collagen.

Of the six types of sample preparation described here, all began with a liming process. SAXS has shown that there is reduction in d-spacing after liming (64nm), when compared to untreated hide (65nm), which is most likely due to a change in the fibrillar structure in the axial direction. The high alkalinity of the lime liquor is known to weaken the interactions of the side chains, due to hydrolysis of the amide groups and alteration of the iso-electric point.[24] This will alter the percentage of hydrogen bonds that are formed, most likely reducing the number of possible bonding sites, therefore weakening the stability of the collagen molecules and possible inter-molecular interactions.

It is therefore possible that after liming the collagen molecules may move past each other thus accounting for the reduction in d-spacing. However, finished parchment samples have been shown to have a d-spacing which is contracted more than that of limed skins.[3] Results from this study show that treating with propan-2-one or 2-ethoxy ethanol further reduces d-spacing. One possible explanation is that these solvent treatments may remove more tightly bound water causing a tilt in the gap and overlap regions between the collagen molecules; dehydration is one cause of d-spacing reduction.[25,26]

Whilst SAXS details changes to the long-range axial structure of the collagen fibrils, WAXD was employed to describe the interactions between neighbouring

24 Menderes, O., Covington, A. D., Waite, E. R. and M.J. Collins, M. J. 'The mechanism and effects of collagen amide group hydrolysis during liming', *Journal of the Society of Leather Technician Chemistry* 83 (1998): 107–110.

25 Wess TJ., and JP Orgel.,'Changes in collagen structure: drying, dehydrothermal treatment and relation to long term deterioration', Thermochimica Acta (2000), 119–128.

26 Fratzl P. and A. Daxer, 'Structural transformation of collagen fibrils in corneal stroma during drying: An X-ray scattering study', *Biophysics Journal* 64 (1993): 1210–1214.

collagen molecules in the dehydrated state. As with previous studies, the packing distance between the collagen molecules was ~1.2nm and this is consistent with dehydrated collagen molecules.[18] The fact that there was no further reduction in the distance between neighbouring molecules indicates that the solvent treatments have not induced the molecules to move closer together in the lateral direction.

The major differences between the FT-IR spectra as indicated by PCA are due to the presence of calcium carbonate. The ability of the PCA program to analyse the FT-IR spectra and to distinguish between the samples based on which side of the skin was tested and to a lesser extent skin type, demonstrates its effectiveness as a powerful analytical tool. However, it would not be correct to assume from this data that identification of species type and skin side is possible for unknown samples using PCA of FT-IR data, as PCA describes the variance within the data set given. The presence of the calcite peak, which is at the position of greatest variance in regards to basis function one, would indicate that possibly the liming stage of parchment manufacture has a fundamental impact.

An interesting characteristic between skin types is in the weave of collagen fibres, which is different between species. For example caprine is known to have a more compact weave compared to ovine[5]. The skin type with the looser weave may be more susceptible to lime penetration and thus the effects that the liming solution has on the collagen fibres. Furthermore, the density of the collagen weave is different on the flesh and grain sides, thus affecting the penetration of the lime solution into the fibre network. Another variable which can affect collagen-fibre orientation, is the location from which the samples were taken from the skin, which again may have an effect on lime penetration. The presence of lime solution is known to open up the collagen fibre network and the level of this opening up may have an effect on the level of penetration of further chemical treatments, in this case alcohol and ketone solutions. It should be noted that the variance within the sample set detected by PCA comes not from the ketone or alcohol treatments.

Conclusions

The effects of the propan-2-one and 2-ethoxy ethanol treatments are apparent on the fibrillar level, where they cause a reduction in the axial d-spacing, indicating a dehydration process. This may indicate that conservation treatments of historic parchment objects in which solvents are used may be causing changes at the molecular level. Whether these changes are irreversible or not will require further study. However, the treatments have no effect on the collagen molecule to molecule interactions or chemical characteristics. This may be due to the degree of penetration of the treatments into the collagen structure. An unexpected result is that FT-IR data can distinguish between species and skin layer, and that the key difference arises from calcite. This indicates a difference in the uptake of calcite by the different layers during the liming process.

Acknowledgements

We thank Chris Clarkson for providing samples for analysis. We also thank the staff at beamline ID02, ESRF, for technical assistance and advice.

Summary

The processing of animal hides to create parchment involves several steps. Our previous study characterized the effects of salting and liming on the structure of collagen, the predominant component of hides and parchment. The current study investigates the effects on collagen structure of the use of solvents propan-2-one and 2-ethoxy ethanol, treatments used historically to produce parchments of a high quality. It was found by small angle X-ray scattering (SAXS) that the axial d-spacing of collagen was reduced in samples treated with these solvents as compared to control samples, indicating that the treatments have induced further dehydration and rearrangement of the molecules. However, wide angle X-ray diffraction (WAXD) indicated that, in the lateral direction, the distance between neighbouring molecules was not altered. WAXD also displayed clear peaks brought about by the presence of calcite in the samples, residual from the liming process. The presence of calcium carbonate was confirmed by Fourier Transform-Infra-red spectroscopy (FT-IR). FT-IR was shown to differentiate between caprine and ovine samples, and the flesh and grain layers of the hide. The main difference, as inferred by principal components analysis (PCA) arises from the calcite peaks, indicating that the different layers from the different skins take up calcium carbonate in a different way during the liming process. The solvent treatments did not appear to affect the FT-IR spectra in any way.

Résumé

Röntgendiffraktionsanalyse und FT-IR Analyse von Ziegen- und Schafshäuten

Die Behandlung von Tierhäuten zur Herstellung von Pergament beinhaltet eine Reihe von Schritten. Unsere vorherige Untersuchung charakterisierte die Effekte des Salzens und Kälkens auf die Kollagenstrukturen, die Hauptbestandteile von Häuten und Pergament. In dieser Untersuchung analysieren wir die Effekte von propan-2-on und 2-ethoxy-ethanol auf die Kollagenstruktur, zwei Lösungsmittel, die historisch angewandt wurden, um Pergament von besserer Qualität herzustellen. Durch den Gebrauch von SAXS (*small angle x-ray scattering*) wird festgestellt, dass die axiale d-Platzierung des Kollagens gegenüber der Kontrolle durch die Behandlung mit den Lösungsmitteln reduziert wurde, was eine weitere Dehydrierung und ein neues Arrangement der Moleküle nahelegt. WAXD (*wide angle x-ray diffraction*) zeigt jedoch, dass die Distanz in lateraler Richtung zwischen benachbarten Molekülen sich nicht geändert hat. WAXD gibt auch eine klare Indikation für die Präsenz von Kalzit in den Proben, welches als Rest des Kälkungsprozesses zurückgeblieben war. Die Präsenz von Kalziumcarbonat wird durch Fouriertransforminfrarotspektroskopie bestätigt. FT-IR kann, wie gezeigt wird, zwischen Proben von Ziegen- und Schafshäuten und zwischen Haar- und Fleischseite der Häute unterscheiden. Der Hauptunterschied liegt, wie mit PCA (*principal compound analysis*) angedeutet wird, in den Peaks für Kalzit, was nahelegt dass verschiedene Lagen verschiedener Häute das Kalziumcarbonat während des Kälkungsprozesses verschieden aufnehmen. Die Behandlung durch Lösungsmittel scheint die FT-IR Spektra nicht zu beeinflussen.

Zusammenfassung

Röntgendiffraktionsanalyse und FT-IR Analyse von Ziegen- und Schafshäuten

Die Behandlung von Tierhäuten zur Herstellung von Pergament beinhaltet eine Reihe von Schritten. Unsere vorherige Untersuchung charakterisierte die Effekte des Salzens und Kälkens auf die Kollagenstrukturen, die Hauptbestandteile von Häuten und Pergament. In dieser Untersuchung analysieren wir die Effekte von propan-2-on und 2-ethoxy-ethanol auf die Kollagenstruktur, zwei Lösungsmittel, die historisch angewandt wurden, um Pergament von besserer Qualität herzustellen. Durch den Gebrauch von SAXS (*small angle x-ray scattering*) wird festgestellt, dass die axiale d-Platzierung des Kollagens gegenüber der Kontrolle durch die Behandlung mit den Lösungsmitteln reduziert wurde, was eine weitere Dehydrierung und ein neues Arrangement der Moleküle nahelegt. WAXD (*wide angle x-ray diffraction*) zeigt jedoch, dass die Distanz in lateraler Richtung zwischen benachbarten Molekülen sich nicht geändert hat. WAXD gibt auch eine klare Indikation für die Präsenz von Kalzit in den Proben, welches als Rest des Kälkungsprozesses zurückgeblieben war. Die Präsenz von Kalziumcarbonat wird durch Fouriertransforminfrarotspektroskopie bestätigt. FT-IR kann, wie gezeigt wird, zwischen Proben von Ziegen- und Schafshäuten und zwischen Haar- und Fleischseite der Häute unterscheiden. Der Hauptunterschied liegt, wie mit PCA (*principal compound analysis*) angedeutet wird, in den Peaks für Kalzit, was nahelegt dass verschiedene Lagen verschiedener Häute das Kalziumcarbonat während des Kälkungsprozesses verschieden aufnehmen. Die Behandlung durch Lösungsmittel scheint die FT-IR Spektra nicht zu beeinflussen.

Resumen

Röntgendiffraktionsanalyse und FT-IR Analyse von Ziegen- und Schafshäuten

Die Behandlung von Tierhäuten zur Herstellung von Pergament beinhaltet eine Reihe von Schritten. Unsere vorherige Untersuchung charakterisierte die Effekte des Salzens und Kälkens auf die Kollagenstrukturen, die Hauptbestandteile von Häuten und Pergament. In dieser Untersuchung analysieren wir die Effekte von propan-2-on und 2-ethoxy-ethanol auf die Kollagenstruktur, zwei Lösungsmittel, die historisch angewandt wurden, um Pergament von besserer Qualität herzustellen. Durch den Gebrauch von SAXS (*small angle x-ray scattering*) wird festgestellt, dass die axiale d-Platzierung des Kollagens gegenüber der Kontrolle durch die Behandlung mit den Lösungsmitteln reduziert wurde, was eine weitere Dehydrierung und ein neues Arrangement der Moleküle nahelegt. WAXD (*wide angle x-ray diffraction*) zeigt jedoch, dass die Distanz in lateraler Richtung zwischen benachbarten Molekülen sich nicht geändert hat. WAXD gibt auch eine klare Indikation für die Präsenz von Kalzit in den Proben, welches als Rest des Kälkungsprozesses zurückgeblieben war. Die Präsenz von Kalziumcarbonat wird durch Fouriertransforminfrarotspektroskopie bestätigt. FT-IR kann, wie gezeigt wird, zwischen Proben von Ziegen- und Schafshäuten und zwischen Haar- und Fleischseite der Häute unterscheiden. Der Hauptunterschied liegt, wie mit PCA (*principal compound analysis*) angedeutet wird, in den Peaks für Kalzit, was nahelegt dass verschiedene Lagen verschiedener Häute das Kalziumcarbonat während des Kälkungsprozesses verschieden aufnehmen. Die Behandlung durch Lösungsmittel scheint die FT-IR Spektra nicht zu beeinflussen.

Contact addresses

Clark A. Maxwell, Craig J. Kennedy, Tim J. Wess
Biophysics Division
School of Optometry and Vision Sciences
University of Cardiff
Redwood Building
King Edward VII Avenue
Cathays Park
Cardiff
Wales CF10 3NB
UK
email: MaxwellCA@cardiff.ac.uk

Nancy Bell
The National Archives
Kew
Richmond
Surrey TW9 4DU
UK
email: nancy.bell@thenationalarchives.org.uk

X-RAY STUDIES OF A COLLAGEN MATERIAL FOR LEATHER PRODUCTION TREATED WITH CHROMIUM SALT

by

Clark A. Maxwell[1*], Krzysztof Smiechowski[2], Jan Zarlok[2], Alina Sionkowska[3], Timothy J. Wess[1]

[1]*Structural Biophysics Group*
School of Optometry and Vision Sciences
CARDIFF UNIVERSITY, CARDIFF, UK

[2]*Faculty of Materials Science and Footwear Technology*
Radom Technical University
CHROBREGO 27, 26-600 RADOM, POLAND

[3]*Faculty of Chemistry*
Nicholas Copernicus University
GAGARIN 7, 87-100 TORUN, POLAND

ABSTRACT

Efforts have been made to investigate a treatment process that produces minimum effluents (i.e., environmentally friendly), and yet significantly increases the quality and heat resistance of a fibrous collagen material for the leather industry. The structural properties of collagen fibrils in chrome tanned bovine leather have been examined when chromium salts with different concentrations were applied to treat bovine skin collagen to obtain a leather product. The treated samples were dried and an X-ray diffraction study was carried out to assess the influence of chromium ion concentration on collagen fibres.

Observations showed that molecular arrangement in collagen depends on concentration of chromium ions used in the tanning process. Bovine collagen treated with tanning agents at Chrome concentrations of (1,3,5,7,9,11%), resulted in changes in the molecular packing within the collagen fibrils. The shrinkage temperature of fibers cross-linked with chromium salt increases compared to the control.

INTRODUCTION

Collagen products are components in a great variety of important goods: parchment, leather, gelatin for pharmaceutical and food applications, hydrolysates and glues. Collagen is a natural polymer, the main component of skin and connective tissue. It has great tensile strength, and is the primary constituent of ligaments and tendons. It is responsible for skin strength, and its degradation leads to wrinkles that accompany aging. The native tropocollagen molecule (molecular mass 300 kDa) consists of three polypeptide chains of about 1000 amino acid residues each, wound round one another to form a strong triple helix.[1] The atoms in the individual chains are held together with covalent bonds, while the helix is stabilised by weaker bonds.[2] Collagen is a fibrous protein composed mostly of glycine, alanine, proline, and hydroxyproline. The spatial configurations of repeated triple amino acid sequences are responsible for the helical conformation between the strands. Water molecules are intimately connected with the hydrogen bonding, holding the triple helix together. The collagen molecules align together forming microfibrils, which pack together forming fibrils and then fibres.

Leather is made from animal skins or hides which have been chemically treated to preserve quality and natural beauty. During tanning the collagen in the rawhide is cross-linked to make it stronger, more durable, and to keep it from rotting. Raw animal skins go through several steps during the process. Dependent on the type of hide used and the desired end-product, the steps taken during tanning can vary greatly. Tanning is essentially the reaction of collagen fibres in the hide with the tanning agent. The use of chromium salts as the tanning agent has dominated the tanning industry in recent decades and this remains the most widespread method of tanning today, although there is growing pressure in many countries for replacement by materials with a lower environmental impact.[3,4] Leather waste usually contains 3-7% Cr(III), obtained in the chromic tanning and production of shoes and leather goods.

Research has been dedicated to the improvement of leather quality, and to extend leather durability by developing new

*Corresponding author: maxwellca@cf.ac.uk
Manuscript received February 7, 2005, accepted for publication May 11, 2005

technology for the tanning of collagenous materials. This can be achieved by judicious selection of parameters for leather drying to promote retention of the proper content of water, by improving the UV and heat resistance of automotive upholstery leather, and by developing in-line monitoring of the mechanical properties of leather during its manufacture. Research programs are aiming to minimize the environmental impact of leather production, through the development of new tanning processes and the utilization of solid tannery waste.[4,5,6] Central to the success of leather production is the degree of modification to the hierarchical structures formed by collagen molecules, fibrils and fibres during the conversion from rawhide to leather.[7,8,9]

Processed leather consists of an interwoven matrix of fibres composed of a chemically cross-linked form of the triple-helical protein collagen. A study by Maeser[10] indicated that intra-hide variability of tensile stiffness depended upon the preferred direction of fibres in different regions of the hide. Kronick and Beuchler[11] showed that stretching untanned hide can produce changes in the orientation and distribution of its collagen fibres.

Although there have been studies on the structural order of collagen fibres, relatively few have investigated the structural changes of collagen molecular packing within a fibril that are central to the success of the tanning process. A broad objective of research in leather technology is to provide knowledge of collagen fibril and molecular integrity necessary for the development of effective low chromium tanning systems. Approaches are generally through a correlation of biophysical experiments[7,8] of bovine skin treatment with different concentrations of chromium salt. X-ray diffraction studies covering length scales from ~100 to 0.2nm spacing enables rapid assessment of interactions between amino acid residues in the helix and inter-helical interactions within the fibrils[12] The synchrotron EXAFS study of Reich and co-workers[13] into binuclear chromium-collagen complexes addresses the nearest neighbour atomic environment of chromium in leather. Our work is complementary to this as we are examining how chromium binding alters collagen structure at different hierarchical levels from the atomic to the nanoscopic.

EXPERIMENTAL

Sample preparation:[3,14,15]

The excess flesh and fatty tissue under the hide was removed by a fleshing machine before the hides were loaded into drums. The hides were washed to remove dirt and blood from the surface. After fleshing, the hides were weighed and washed. The washing procedure and the

Washing procedure:
Soaking:
110% - water, temp. 22°C
0.05% - Rokafenol N8
0.05% - Biocid 40,
0.2% - Na_2CO_3, stir 90 min, drain float.
Main soaking:
110% - water temp. 26°C
0.05% - Biocid 40
0.15% - Rokafenol N8
.,1% - Na_2CO_3,
+150% - water, temp. 20°C, (14 hours)
Liming:
80% - water, temp. 28°C
0,1% - Rokafenol N8
0,9% - Erhavit EF
0.5% - calcium hydroxide, 60min.
0.7% - NaHS, 20min.
0.6% - Na_2S, 60min.
2% - calcium hydroxide, 60min.
100% - water, temp. 30°C, 30min.
1.5% - calcium hydroxide, 18 hours, drain float
Washing:
200% - water, temp. 25°C, 15min, drain float
Washing:
200% - water, temp. 30°C, 15min, drain float.
Deliming):
100% - water, temp. 30°C,
0.5% - Sodium metabisulphite $Na_2S_2O_5$,
30min, drain float.
Main deliming:
100% - water, temp. 30°C, 15min.
+0.5% - Adisin N
+1.5% - $(NH_4)_2SO_4$, 90min.
+0.5% - Oropon OR, 20min, drain float.
Washing:
200% - water, temp. 30°C, 15min, drain float.
200% -water, temp. 25°C, 15minm, drain float.
Pickling (3 hours together)
80% - water, temp. 20°C
7% - NaCl, 15min.
1% - HCOONa
+1.2% - H_2SO_4, 1:10, three times per 10 min.
Tanning:
80% -water, temp. 20°C, 24 hours
1,3,5,7,9,11 % of Chromal. (tanning agent)
pH controlled using the reagent based on MgO.

Figure 1. - Steps of leather chrome tanning process (general flow diagram). Chemicals used are described in Table I.

TABLE I
Process Chemicals, Sources and Characteristics

Chemical Name and Source	Characteristic
Rokafenol N8, Rokita S.A.Poland	Nonionic agent (detergent) based on ether. polyoxyethylene(9)nonylphenol ether (99%); water (1%).
Biocid 40, Biokimica Italy	Bacteriocide Concentration 40-42%.
Erhavit EF, TFL Germany	Agent for increasing the rate of calcium diffusion into the hide. Regulation of swelling.
Adisin N, Adipol Chorzow, Poland	Mixture of weak aliphatic acids, for removal of calcium.
Oropon OR, TFL Germany	Agent based on pancreatin (enzymatic) 650-790LVE).Used at pH 6-8

leather tanning protocol are outlined in figure 1. The chemicals used in these processes are characterized in Table I. The percentages in figure 1 express the amount of additive in comparison with the weight of hide (200% of water means that for 100 kg of hides, 200 kg of water was used, etc). The soaking process, which has a pH of 8-9 due to the addition of Na_2CO_3, restored lost moisture to hides that had been salted and stored for long periods before processing. Hair removal using lime was followed by washing and deliming cycles before pickling. In the pickling process: water, sulphuric acid and sodium chloride are added. The acidic environment of this solution made the hides ready to accept the tanning chemicals. The addition of sodium chloride prevented any swelling of the hide.

The 24 hour tanning process converts the hide into a stable material which will not putrefy and be less susceptible to attack by bacteria. The tanning agent Chromal (containing about 25% of Cr_2O_3) was added and the Cr_2O_3 penetrated (24 hours at 18 - 20 °C) into the hide structure and cross-linked with the collagen. Different amounts of Chromal were used (1,3,5,7,9,11%) and after tanning, the amount of Cr_2O_3 in the leather was measured by titration with $KMnO_4$. Once adequate penetration of the chrome had occurred (2 hours), the hides were basified. A slightly alkaline chemical such as magnesium oxide was added and the pH was slowly raised to ~4. The parameters of the process are presented in Table II. The samples were dried at room temperature for 24 hours and then submitted for analysis.

X-ray diffraction studies

High-angle X-ray diffraction patterns were obtained using a Bruker AXS Nanostar small angle scattering station with a camera length of 4.4cm, which allowed the wide angle diffraction features of collagen to be observed to a resolution of 0.2nm. Details of the scattering system and data reduction can be obtained in.[16]

Small angle X-ray diffraction studies were made at the SRS Daresbury on beamline 2.1. This allowed long range features of collagen in the tanned material to be investigated over length scales of up to 100nm. (For full details of the experimental set up see Kennedy *et al.*[17] All diffraction patterns were converted using in-house software into linear profiles of scattered intensity (I) vs scattering angle d (where $d = (2/\lambda)\mathrm{Sin}\theta$), where λ is the x-ray wavelength and θ is half of the scattering angle. The linear profiles were further analysed using XFIT the one-dimensional peak - fitting program (Collaborative Computational Project 13)[18] In all cases the samples were examined at ambient temperature and humidity.

Fibril shrinkage temperature experiments

The shrinkage temperature of leather was measured according to the Polish Norm PN-92/P-22152. Temperature was measured at the moment when the sample started to shrink in water/glycerol liquid (1:1) during heating with the rate 1°C per minute. The experimental setup used to determine

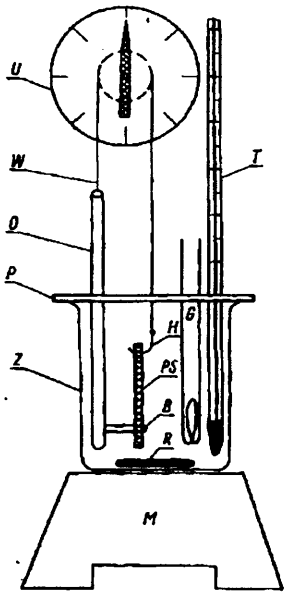

Figure 2. - The experimental set up for shrinkage temperature measurements (M- magnetic stirrer, R- magnetic rod, Z- beaker, P- cover, G- heater, T- thermometer, B- handler, H- hook, O- pipe (tube), PS- sample of leather, W- rope (fibre), U- indicating device). Temperature was measured at the moment when the sample began to contract (shrink). During the measurement the sample of leather was soaked in a beaker containing water and glycerol (1:1). The heating increment was 1° per minute (starting from 20°C).

TABLE II
Parameters of the Tanning Process and Shrinkage Temperature of Obtained Leather

Sample No.	Chromal [%]	% Cr_2O_3 in leather	pH before tanning	pH after tanning	Shrinkage temperature[°C]
0	Sample without tanning agent (control sample)				68
1	1	0.9	3.7	4.6	83
2	3	2.0	3.5	4.6	93
3	5	3.4	3.2	4.4	97
4	7	3.7	3.0	4.2	107
5	9	4.3	3.1	4.2	119
6	11	5.2	3.0	4.1	119

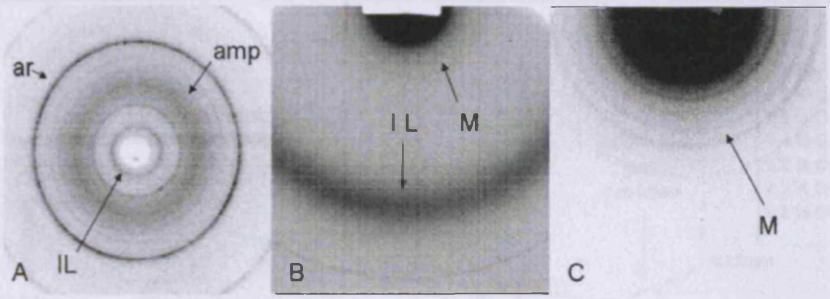

Figure 3. - X - ray diffraction pattern of isotropic collagen from bovine hide at different sample to detector distances representing packing characteristics of A) Axial rise per residue (ar) and amorphous region (amp), B) Intermolecular lateral packing (IL), C) Meridional diffraction series (M) of collagen structure corresponding to the 65nm repeat.

shrinkage temperature is shown in figure 2.

RESULTS

Thermal stability

Collagen fibres exhibit a sudden shrinkage in length when heated. Fibres in leather have had chemical cross-links introduced which raise the temperature at which the fibres shrink. If wet leather is heated, there is a point when it begins to change radically. This is the shrinkage temperature which for vegetable tanned leather this occurs between 75 and 85°C. The amount of shrinkage can range from 5% to 40%, depending on the characteristics of the leather. The shrinkage temperature is a test that identifies hydrothermal stability, and therefore requires the presence of excess water (and occasionally added glycerine) for it to be carried out. A high shrinkage temperature is one of the parameters demanded of good leather. The thermal behaviour of fibrillar collagens is rather complex and depends on amongst other factors, water content, age of collagen, and sample preparation.[19-23] The shrinkage temperature of raw hide is between 50-60 °C, while for tanned leather, it is much higher. The complex cross-links between Cr(III) salt and collagen makes leather more stable thermally.[24,25] The shrinkage temperature for leather that contains different % of chromium was investigated, and the results are presented in Table II. Shrinkage temperatures of cross-linked fibres with chromium salt, shows increases when compared to the control sample. Shrinkage temperature for hide without tanning agent (control sample) was 68 °C, hide with 2% of Cr_2O_3 was 93 °C, and 5% was 119 °C.

X-ray diffraction

Although the interaction of X-rays with each collagen triplex will produce its own fibre diagram, the isotropy of the felt like arrangement of the collagen fibres within bovine hide samples usually result in an isotropic fibre diagram. It is possible that preferential alignment of collagen in skin can be seen, but this is most likely due to the location that the sample was taken from rather than the processing. Collagen fibres taken from the neck and spinal areas are known to be preferentially aligned.[26] The typical isotropy of collagen X - ray diffraction patterns from bovine hide are shown in figure 3.

High angle X-ray diffraction

High angle x-ray fibre diagrams were obtained and used to analyse the effects of chromium tanning on collagen at the intra and inter molecular level by measuring quantitatively, the changes in the axial rise per residue reflection position of the collagen helix, and the contribution of diffuse and helical scattering to the fibre diagram. The term helical rise per residue represents the mean axial step between the amino acid residues of collagen chains within the molecules. Linear traces of the radially averaged fibre dia-

TABLE III
Helical Rise per Residue and Peak Characteristics as Measured Using XFIT Program

Bovine hide Samples at 0.4m (0.02nm resolution)	Axial rise per residue (nm)	Peak Height (Intensity)	Full Width half maxima d (nm^{-1})	Integrated Intensity
0 % Cr_2O_3 (Control)	0.276	0.01334	0.733	0.065
0.9 % Cr_2O_3	0.276	0.00931	0.787	0.049
2.0 % Cr_2O_3	0.274	0.00619	0.873	0.036
3.4 % Cr_2O_3	0.278	0.00729	0.820	0.040
3.7 % Cr_2O_3	0.277	0.00311	1.585	0.033
4.3 % Cr_2O_3	0.276	0.00473	0.951	0.030
5.2 % Cr_2O_3	0.275	0.00395	0.902	0.024

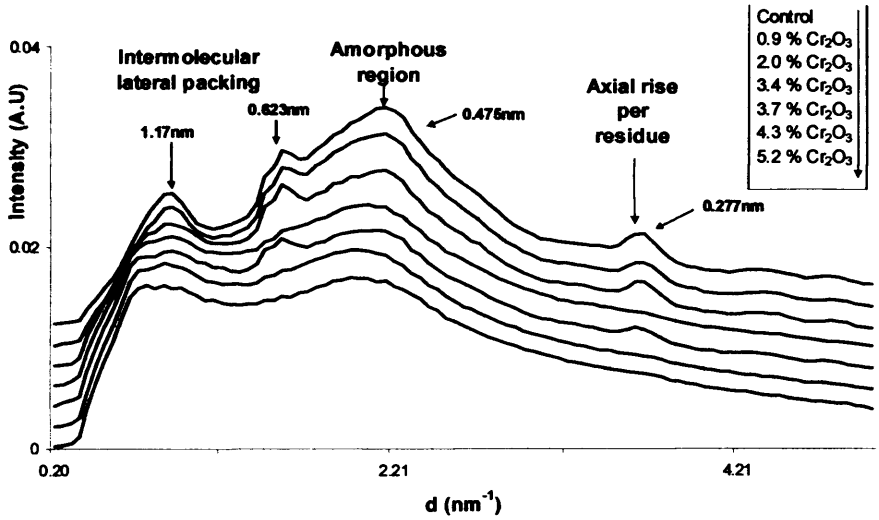

Figure 4. - Linear X-ray scattering profile of bovine hide treated with chromium. At such high angles the diffraction results mainly from the helical properties of the collagen molecules. The amorphous halo present in most diffraction data is also observable here as is the characteristic reflection due to the side by side packing of collagen molecules. The major trend observable is the contribution of diffraction corresponding to the axial rise per residue, this diminishes with chrome tanning. (All linear traces have been normalised and offset).

grams are shown in figure 4. The data obtained for the linear profiles of figure 4 is represented in table III.

Although not completely correlating with chromium salt levels, there is a decrease in peak height and an increase in half width maxima, as concentrations of chromium salt increase. The peak height and half width maxima values can be used to determine the integrated intensity, which is an indication of order within the collagen structure. The integrated intensity decreases with the exception of sample 3 (although still decreasing) linearly as chromium salt concentration increases. Therefore chromium salt seems to cause a loss of order within the collagen molecules at the molecular and helical level dependent on its concentration. The increase in half width maxima can be interpreted as the distribution of axial rise per residue values in the sample. There is a link between chromium salt concentration and increasing helical rise per residue distribution, but a direct link with chromium salt concentration is not clear. The change in the mean value of the axial rise per residue as a function of chromium treatment is probably negligible.

Wide angle x-ray diffraction with a resolution of 0.9nm
X-ray diffraction to a real space resolution of 0.9nm allows a more accurate evaluation of the intermolecular lateral packing of the collagen molecules, which occurs in the region of ~1 nm for the dehydrated state. The treatment of bovine skin with chromium has an effect on the peak profiles (figure 5), which seems to be directly related to concentration. Although not a completely linear relationship, increasing chromium salt concentration relates to a reduction in height of the peak that represents the characteristic intermolecular lateral packing of the collagen molecules. There is also a reduction of the peak occurring at d = 1.07 nm^{-1} (0.935nm real lattice space), with increasing chromium salt concentration and also an appearance of another peak at

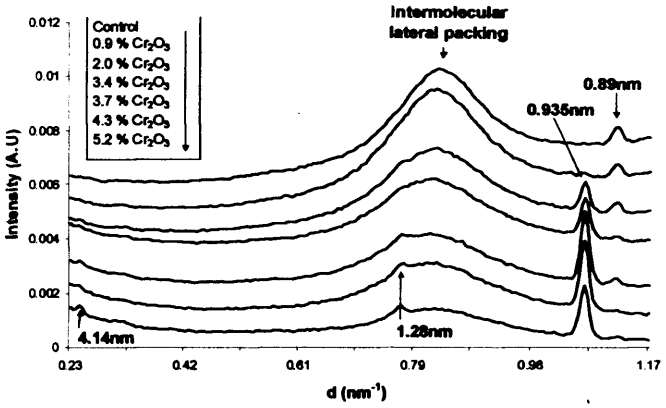

Figure 5 - X-ray scattering data obtained at station 2.1 SRS Daresbury at a sample to detector distance of 1.25m of bovine hide treated with chromium was analysed using XFIT to obtain a linear trace profile. (All linear traces have been normalised and offset).

d = 1.12 nm^{-1} (0.89nm real lattice space) possibly a diffraction order of lipid bilayer interactions with Cr^{3+} ions. The linear traces of figure 5 were further analysed using XFIT to give values concerning peak profiles (tables IV, V, and VI). The intermolecular lateral packing distance between the collagen molecules increases slightly after the addition of chromal to the bovine hide (table IV). The full width half maxima of the peaks increase on the addition of chromal, indicating an increase in the distribution of packing distances represented by the intermolecular lateral packing of collagen molecules. At 3% chromal concentration (2% chromium salt), the increase in distributions of packing distances seems to be at a maximum level with subsequent increases in concentration causing a reduction in packing distribution, possibly due to chemical penetration being more even. The integrated intensity, which represents the level of order within the structure, reduces with increasing chromium salt concentration.

The reduction in order associated with the intermolecular lateral packing distance of collagen seems to correlate with the loss of the peak at 0.89nm (table V). This peak is not due to chromium salt concentration as it is found in the control sample, but its integrated intensity does appear to reduce as chromium salt concentration increases. There is a variation in the distribution of the repeating unit responsible for this peak; this small sample run of chromium salt treated leather indicates that there is a possible link between chromium salt concentration and structural order.

TABLE IV

Intermolecular Lateral Packing and Peak Characteristics as Measured Using XFIT Program

Bovine hide Samples at 1.25m (0.9nm resolution)	Intermolecular lateral packing	Peak Height (Intensity) (nm)	Full Width half maxima d (nm^{-1})	Integrated Intensity
0 % Cr_2O_3 (Control)	1.19	0.003044	5.379	0.10949
0.9 % Cr_2O_3	1.20	0.003414	5.893	0.13458
2.0 % Cr_2O_3	1.20	0.002377	6.331	0.10068
3.4 % Cr_2O_3	1.21	0.001927	6.076	0.07831
3.7 % Cr_2O_3	1.23	0.001612	5.990	0.06461
4.3 % Cr_2O_3	1.22	0.001545	5.936	0.06137
5.2 % Cr_2O_3	1.22	0.000864	5.703	0.03297

TABLE V

Unknown Peak (0.89nm) Characteristics as Measured Using XFIT Program

Bovine hide Samples at 1.25m (0.9nm Resolution)	Peak at 1.13 d Real space (nm)	Peak Height (Intensity)	Full Width half maxima d (nm^{-1})	Integrated Intensity
0 % Cr_2O_3 (Control)	0.889	0.00057	0.614	0.00232
0.9 % Cr_2O_3	0.889	0.00044	0.562	0.00167
2.0 % Cr_2O_3	0.889	0.00038	0.527	0.00134
3.4 % Cr_2O_3	0.888	0.00012	0.451	0.00037
3.7 % Cr_2O_3	0.889	0.00021	0.486	0.00070
4.3 % Cr_2O_3	0.889	0.00005	0.244	0.00009
5.2 % Cr_2O_3	0.887	0.00009	0.508	0.00031

TABLE VI
Unknown Peak (0.93nm) Characteristics as Measured Using XFIT Program.

Bovine hide Samples at 1.25m (0.9nm Resolution)	Peak at 1.07 d Real space (nm)	Peak Height (Intensity)	Full Width half maxima d (nm^{-1})	Integrated Intensity
0 % Cr_2O_3 (Control)	No peak			
0.9 % Cr_2O_3	No peak			
2.0 % Cr_2O_3	0.931	0.00102	0.527	0.00381
3.4 % Cr_2O_3	0.930	0.00138	0.583	0.00540
3.7 % Cr_2O_3	0.931	0.00253	0.553	0.00937
4.3 % Cr_2O_3	0.931	0.00245	0.565	0.00927
5.2 % Cr_2O_3	0.931	0.00184	0.587	0.00723

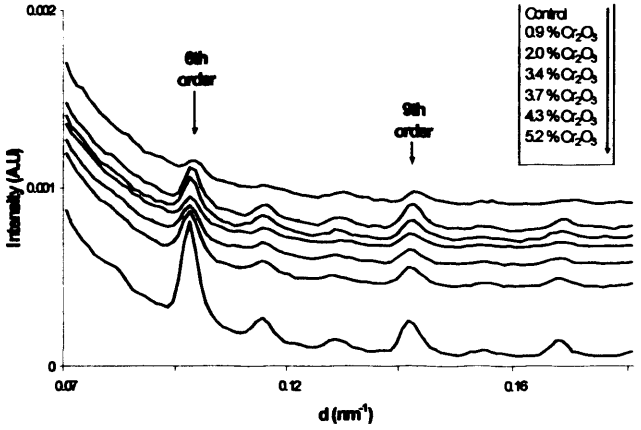

Figure 6. - X-ray scattering data of bovine hide treated with chromium obtained at station 2.1 SRS Daresbury at a sample to detector distance of 4m was used to obtain a linear trace. The intensity of the meridional diffraction peaks increases as a function of chromium treatment, the change in the position of the diffraction peaks corresponds to a lengthening of the D period with chrome tanning. (All linear traces have been normalised and offset).

The peak that occurs at d = 1.07 nm^{-1} is not present in the control sample and therefore is a diffraction characteristic of the addition of chromal. The cumulative effect of the repeating unit at this peak only appears to be significant at chromal concentrations of 3% or more. The peak position does not change with increasing chromium concentration (table VI), but the peak height does. Subsequently there is an increase of order within the structure as chromium salt concentration increases, possibly indicating that this peak is due to the local structure of chromium salt crystallinity and not collagen chromium interactions.

Small angle x-ray diffraction with a resolution of 6nm

Collagen is known to contain a number of long range interactions resulting from axial order and substructures within the fibril. Observation of these features by X-ray diffraction requires long camera geometries in order to resolve closely spaced features in reciprocal space. Meridional peak positions can be determined accurately at a geometry that allows observation of diffraction from structural features to a real space resolution of 6nm. In particular the 6th order up to the 11th order, and a more intense 6th order indicating a lower level of sample hydration. The peak profiles (figure 6) are characteristic diffraction reflections of the gap and overlap regions between the collagen molecules in the axial direction. The relative intensities of the large 6th order in

TABLE VII
Xfit Software Used to Determine Peak Profile Data of Bovine Hide Samples Analysed from X-ray Scattering Data Obtained from SRS Daresbury Station 2.1 at a Sample to Detector Distance of 8m (6nm Resolution).

Bovine hide on 8m camera, giving a resolution of 6nm	Quarter staggered array spacing (nm)	Peak Height (Intensity)	Full Width half maxima d (nm^{-1})	Integrated Intensity
0 % Cr_2O_3 (Control)	62.7	0.000173	1.192	0.001377
0.9 % Cr_2O_3	64.4	0.000274	0.893	0.001638
2.0 % Cr_2O_3	64.0	0.000276	0.899	0.001659
3.4 % Cr_2O_3	63.8	0.000226	0.945	0.001429
3.7 % Cr_2O_3	64.0	0.000269	0.900	0.001618
4.3 % Cr_2O_3	64.0	0.000356	0.877	0.002086
5.2 % Cr_2O_3	64.3	0.000627	0.680	0.002854

comparison with the 7th and 8th for example is typical of a dry collagen sample. The spacing between the orders is very similar for all the samples, with the exception of the control sample indicating chromium salt effect on the gap and overlap region of the collagen molecules. The XFIT program was used to give a more detailed interpretation of the peak profiles representing the characteristic axial staggered array (d-spacing) of the collagen molecules in table VII. The decrease in the breadth of the meridional diffraction peaks is indicative of the D periodic structure of the collagen fibrils becoming regular or indeed the overall length of the coherent crystallites becoming longer.

CONCLUSIONS

The effect of chrome tanning to different extents has been observed here as a function of structural order over a range of length scales. The data shown here suggests that the axial rise per residue of the collagen helix is altered by tanning; however this does not correspond to a concomitant increase in the contribution of the amorphous region of the fibre diagram indicating that the degree of gelatinisation is not increased. It may therefore be possible that significant alterations are made to the collagen helical backbone without total disruption. This will have a cumulative effect on the side by side molecular packing within the collagen fibril that leads to an increase in the intermolecular distances, as well as the variance of helical interactions. This may be due to deviations from the standard helix geometry that allows molecules to pack on a simple quasi-hexagonal lattice with a ~1nm spacing.[27] The nm length scale also reveals structural features that are altered by the tanning process; the evolution and change of sharp Bragg reflections at 4.4, 0.89 and 0.835 nm correspond to reflections observed to result from lipid diffraction, the interaction of Cr(III) ions with lipid bilayers will not only increase fundamental spacing but also increase the contrast between bilayers resulting in enhanced diffraction peaks.

The long range interactions of collagen are dominated by the axial repeating structure due to molecular staggering along the collagen fibril. This showed that the axial periodicity of the stagger between collagen molecules is increased upon tanning. The main change observed in these samples however is the increase in diffraction signal of Bragg peaks above the continuous background. This indicates that the overall long range crystallinity of the collagen molecules and the specificity of the axial order may be increased. It also may result in part from the enhanced electron density contrast made by the addition of Cr(III) ions to the structure. If the latter is the predominant effect, an important feature to note is that the intensity distribution amongst meridional reflections of the enhanced signal is the same as that of an untanned sample. This would imply that the labelling of Cr (III) along the length of the collagen molecule is relatively even and if specific to certain amino acids, must indicate that their distribution is even through the collagen molecule. Specific heavy atom staining by a number of metal species is known to occur and alter the intensity of meridional reflections in both the wet and dry samples.[28]

In relation to the increased measurements of shrinkage temperature as a function of chromal addition, this may be reflected in the broadening of the peak at approximately 1nm spacing which is characteristic of the side by side interactions of collagen molecules. Here the possible changes in conformation brought about by intermolecular cross-links may be producing a less locally ordered lattice structure.

ACKNOWLEDGEMENTS

We wish to thank Gunter Grossmann, Station Manager of Beamline 2.1, Daresbury, UK for technical assistance and advice.

REFERENCES

1. Rich, A. and Crick, F. H. C.; The molecular structure of collagen. *J. Mol. Biol.* **3**, 483-506, 1961
2. Bailey, A. J. and Paul, R. G; Collagen- a not so simple protein. *JSLTC* **82**,104-110,1998
3. Bienkiewicz K.; Physical Chemistry of Leathermaking. Krieger Publishing Co., Malabar, FL (1983).
4. Rao, R., Thanikaivelan, P., and Nair, B. U.; An eco-friendly option for less-chrome and dye-free leather processing: in situ generation of natural colours in leathers tanned with Cr-Fe complex. *Clean Techn Environ Policy* **4**, 115-121, 2002
5. Walawska, B. and Kowalski, Z.; Model of technological alternatives of production of sodium chromate(VI) with the use of chromic wastes. *Waste Management* **20**, 711-723, 2000
6. Cabeza, L. F., Taylor, M. M., DiMaio, G. L., Brown, E. M., Marmer, W. N., Carrio, R., Celma, P. J., and Cot, J.; Processing of Leather Waste: Pilot Scale Studies on Chrome Shavings. Isolation of Potentially Valuable Protein Products and Chromium. *Waste Management* **18**, 211-218, 1998
7. Brown, E. M.; Effects of neutral salts on collagen structure and chromium-collagen interactions. *JALCA* **94**, 59-68, 1999
8. Brown, E. M., Dudley, R. L., and Elsetinow, A. R.; A Conformational Study of Collagen as Affected by Tanning Procedures. *JALCA* **92**, 225-233, 1997

9. Brown E. M., King, G, and Chen, J. M.; Model of the helical portion of a type I collagen microfibril. *JALCA* **92**, 1-7, 1997
10. Maeser, M.; The effect of hide location and cutting direction on the tensile properties of upper leather. *JALCA* **55**, 501, 1960
11. Kronick, P. L. and Buechler, P. R.; Fiber orientation in calfskin by laser light scattering or X - ray diffraction and quantitative relation to mechanical properties. *JALCA* 81, 221, 1986
12. Newton, R. H. and Meek, K. M.; Circumcorneal annulus of collagen fibrils in the human limbus. *Inv. Opth. Vis Sci.* **39**, 1125-1134, 1998
13. Reich, T., Rossberg, A., Hennig, C., and Reich, G.; Characterization of Chromium Complexes in Chrome Tannins, Leather, and Gelatin Using Extended X-ray Absorption Fine Structure (EXAFS) Spectroscopy. *JALCA* **96**, 133, 1986
14. Lasek, W.; *Kolagen. PWB, Warszawa*, 222, 1978
15. Smiechowski, K. and Zarlok, J.; Projektowanie zakladu w przemysle lekkim na przykladzie garbarni. Organizacja procesu produkcji-maszyny-urzadzenia-technologie. Wydawnictwo Politechniki Radomskiej, (Polish book), (2000).
16. Sionkowska, A., Wisniewski, M., Skopinska, J., Kennedy, C. J., and Wess, T. J.; Molecular interactions in collagen and chitosan blends. *Biomaterials* 25, 795-801, 2004
17. Kennedy, C. J., Vest, M., Cooper, M., and Wess, T. J.; Laser cleaning of parchment: structural, thermal and biochemical studies into the effect of wavelength and fluence. *Applied Surface Science* **227**, 151-163 (2004).
18. Squire, J., AL-Khayat, H., Arnott, S., Crawshaw, J., Denny, R., Diakun G, Dover D, ForsythT, He A, Knupp C, Mant G, Rajkumar, G., Rodman, M., Shotton, M., Windle, A.; New CCP13 Software and the Strategy behind Further Developments: Stripping and Modelling of Fibre Diffraction Data. *Fibre Diffraction Review* **11**, 7-19, 2003
19. Flory, P. J. and Garrett, R. R.; Phase transition in collagen and gelatin systems. *J. Am. Chem. Soc.* **80**, 4836-4845, 1958
20. Luescher, M., Ruegg, M., and Schindler, P.; Effect of hydration on thermal stability of tropocollagen and its dependence on the presents of neutral salts. *Biopolymers* **13**, 2489-2503, 1974
21. Sionkowska, A. and Kaminska, A.; Thermal helix-coil transition in UV irradiated collagen from rat tail tendon. *Int. J. Biol. Macromol.* **24**, 337-340, 1999
22. Usha, R. and Ramasami, T.; The effects of urea and n-propanol on collagen denaturation: using DSC, circular dichroism and viscosity. *Thermochimica Acta* **409**, 201-206, 2004
23. Miles, C. A., Burjanadze, T. V., and Bailey, A. J.; The kinetics of the thermal denaturation of unrestrained rat tail tendon determined by differential scanning calorimetry. *J. Mol. Biol.* **245**, 437-446, 1995
24. Haines, B.; Shrinkage temperature in collagen fibres. *Leather Conservation News* **3**, 1-5, 1987
25. Rajini, K. H., Usha, R,, Arumugam, V., and Sanjeevi, R.; Fracture behaviour of cross-linked collagen fibres. *Journal of Material Science* **36**, 5589-5592, 2001
26. Haines, B. M.; Parchment, The physical and chemical characteristics of parchment and the materials used in its conservation. Northampton. *The Leather Conservation Centre*, 1-33, 1999
27. Miller, A. and Tocchetti, D.; Calculated X-ray diffraction pattern from a quasi-hexagonal model for the molecular arrangement in collagen. *Int. J. Biol. Macromol.* **3**, 9-18, 1981
28. Wess, T. J., Miller, A., and Bradshaw, J. P.; Cross-link sites in Type I collagen fibrils studied by neutron diffraction. *J. Mol. Biol.* **213**, 1-5, 1990